Selected Papers in the Hydrologic Sciences 1986

January 1986

Limnology of West Point Reservoir, Georgia and Alabama
By D.B. Radtke

Aqueous geochemistry of the Bradys Hot Springs geothermal area, Churchill County, Nevada
By A.H. Welch and A.M. Preissler

Investigation of the possible formation of diethylnitrosamine resulting from the use of rhodamine WT dye as a tracer in river waters
By T.R. Steinheimer and S.M. Johnson

Estimating stream-aquifer interactions in coal areas of eastern Kansas by using streamflow records
By H.E. Bevans

Investigations of organic contaminants derived from wood-treatment processes in a sand and gravel aquifer near Pensacola, Florida
By W.E. Pereira and C.E. Rostad

Evaluating strategies for ground-water contaminant plume stabilization and removal
By S.M. Gorelick and B.J. Wagner

Recent growth of Gulkana Glacier, Alaska Range, and its relation to glacier-fed river runoff
By L.R. Mayo and D.C. Trabant

Extension of the unsteady one-dimensional open-channel flow equations for flow simulation in meandering channels with flood plains
By L.L. DeLong

Comparison of two stream-discharge record reconstruction techniques for eight gaging stations in Maine
By R.A. Fontaine

Channel widening characteristics and bank slope development along a reach of Cane Creek, west Tennessee
By Andrew Simon and C.R. Hupp

Evaluation of a suggested sequence for the chemical extraction of soluble amorphous phases from clays
By S.L. Rettig and B.F. Jones

Comparison of velocity interpolation methods for computing open-channel discharge
By J.M. Fulford and V.B. Sauer

A preliminary evaluation of a discharge computation technique that uses a small number of velocity observations
By L.R. Bohman and W.J. Carswell, Jr.

United States Geological Survey Water-Supply Paper 2290

Selected Papers in the Hydrologic Sciences 1986

Edited by Seymour Subitzky

January 1986

Limnology of West Point Reservoir, Georgia and Alabama
By D.B. Radtke

Aqueous geochemistry of the Bradys Hot Springs geothermal area, Churchill County, Nevada
By A.H. Welch and A.M. Preissler

Investigation of the possible formation of diethylnitrosamine resulting from the use of rhodamine WT dye as a tracer in river waters
By T.R. Steinheimer and S.M. Johnson

Estimating stream-aquifer interactions in coal areas of eastern Kansas by using streamflow records
By H.E. Bevans

Investigations of organic contaminants derived from wood-treatment processes in a sand and gravel aquifer near Pensacola, Florida
By W.E. Pereira and C.E. Rostad

Evaluating strategies for ground-water contaminant plume stabilization and removal
By S.M. Gorelick and B.J. Wagner

Recent growth of Gulkana Glacier, Alaska Range, and its relation to glacier-fed river runoff
By L.R. Mayo and D.C. Trabant

Extension of the unsteady one-dimensional open-channel flow equations for flow simulation in meandering channels with flood plains
By L.L. DeLong

Comparison of two stream-discharge record reconstruction techniques for eight gaging stations in Maine
By R.A. Fontaine

Channel widening characteristics and bank slope development along a reach of Cane Creek, west Tennessee
By Andrew Simon and C.R. Hupp

Evaluation of a suggested sequence for the chemical extraction of soluble amorphous phases from clays
By S.L. Rettig and B.F. Jones

Comparison of velocity interpolation methods for computing open-channel discharge
By J.M. Fulford and V.B. Sauer

A preliminary evaluation of a discharge computation technique that uses a small number of velocity observations
By L.R. Bohman and W.J. Carswell, Jr.

U.S. GEOLOGICAL SURVEY WATER-SUPPLY PAPER 2290

DEPARTMENT OF THE INTERIOR
DONALD PAUL HODEL, Secretary

U.S. GEOLOGICAL SURVEY
Dallas L. Peck, Director

UNITED STATES GOVERNMENT PRINTING OFFICE: 1986

For sale by the Superintendent of Documents,
U.S. Government Printing Office,
Washington, DC 20402

Library of Congress Catalog card No. 85-600358

PREFACE

Selected Papers in the Hydrologic Sciences is a new journal-type publication presenting timely results on hydrologic studies derived from the Federal research program and the Federal-State cooperative program of the U.S. Geological Survey, which is aimed at meeting widespread public and professional interests of the hydroscience community. Also included may be results of some studies done on behalf of other Federal agencies.

This third issue of the *Selected Papers* series, comprising 13 topical papers, addresses a range of topics including model simulation of ground- and surface-water systems, hydrogeochemistry, limnology, and selected physical and chemical techniques for hydrologic studies.

As a journal-type publication, *Selected Papers* is intended to serve as a forum that encourages dialogue between readers and authors. Discussion from *all* members of the hydroscience community is welcomed. A discussion section for readers' comments and authors' replies is included in each issue. Such dialogue for this issue will be open until June 1986. Address comments to Editor, *Selected Papers in the Hydrologic Sciences*, U.S. Geological Survey, 444 National Center, Reston, Virginia 22092.

Seymour Subitzky
Editor

SI and Inch-Pound Unit Equivalents

International System of Units (SI), a modernized metric system of measurement. All values have been rounded to four significant digits. Use of hectare (ha) as an alternative name for square hectometer (hm^2) is restricted to measurement of land or water areas. Use of liter (L) as a special name for cubic decimeter (dm^3) is restricted to the measurement of liquids and gases.

Multiply SI units	By	To obtain inch-pound units
Length		
micrometer (μm)	0.000 039 37	inch (in)
millimeter (mm)	0.039 37	inch (in)
centimeter (cm)	0.393 7	inch (in)
meter (m)	3.281	foot (ft)
	1.094	yard (yd)
kilometer (km)	0.621 4	mile (mi)
Area		
centimeter^2 (cm^2)	0.155 0	inch^2 (in^2)
meter^2 (m^2)	10.76	foot^2 (ft^2)
	1.196	yard^2 (yd^2)
	0.000 247 1	acre
hectometer^2 (hm^2)	2.471	acre
kilometer^2 (km^2)	0.386 1	mile^2 (mi^2)
Volume		
centimeter^3 (cm^3)	0.061 02	inch^3 (in^3)
milliliter (mL)	0.061 02	inch^3 (in^3)
liter (L)	61.02	inch^3 (in^3)
	0.035 31	foot^3 (ft^3)
	33.82	ounce, fluid (oz)
	2.113	pint (pt)
	1.057	quart (qt)
	0.264 2	gallon (gal)
meter^3 (m^3)	35.31	foot^3 (ft^3)
	1.308	yard^3 (yd^3)
	264.2	gallon (gal)
	0.000 810 7	acre-foot (acre-ft)
kilometer^3 (km^3)	0.239 9	mile^3 (mi^3)
Mass		
microgram (μg)	0.000 015 43	grain (gr)
gram (g)	0.035 27	ounce, avoirdupois (oz avdp)
kilogram (kg)	0.002 205	pound, avoirdupois (lb avdp)

Multiply SI units	By	To obtain inch-pound units
Mass per unit volume		
microgram per liter (μg/L)	0.000 058 41	grain per gallon (gr/gal)
milligram per liter (mg/L)	0.058 41	grain per gallon (gr/gal)
Mass or volume per unit time (includes flow)		
gram per minute (g/min)	0.035 27	ounce (avoirdupois) per minute (oz/min)
milliliter per minute (mL/m)	0.033 82	ounce (fluid) per minute (oz/min)
	0.035 31	foot^3 per second (ft^3/s)
liter per second (L/s)	15.85	gallon per minute (gal/min)
meter^3 per second (m^3/s)	35.31	foot^3 per second (ft^3/s)
	15 850	gallon per minute (gal/min)
meter per second (m/s)	3.281	foot per second (ft/s)
meter per day (m/d)	3.281	foot per day (ft/d)
Transmissivity		
meter^2 per day (m^2/d)	10.76	foot^2 per day (ft^2/d)
Force per unit area		
kilopascal (kPa)	0.145 03	pound-force per inch^2 (lbf/in^2)
kilogram per meter^2 (kg/m^2)	0.204 8	pound-force per foot^2 (lbf/ft^2)
kilogram per meter^3 (kg/m^3)	0.624 6	pound-force per foot^3 (lbf/ft^3)
Temperature		
degree Celsius (°C)	Temp °F=1.8 temp °C+32	degree Fahrenheit (°F)
Specific conductance		
microsiemens per centimeter at 25 degrees Celsius (μS/cm at 25 °C)	1.000	micromho per centimeter at 25 degrees Celsius (μmho/cm at 25 °C)
millisiemens per meter at 25 degrees Celsius (mS/m at 25 °C)	1.000	millimho per meter at 25 degrees Celsius (mmho/m at 25 °C)

CONTENTS

Preface **iii**

SI units and inch-pound unit equivalents **iv**

Limnology of West Point Reservoir, Georgia and Alabama
By D.B. Radtke **1**

Aqueous geochemistry of the Bradys Hot Springs geothermal area, Churchill County, Nevada
By A.H. Welch and A.M. Preissler **17**

Investigation of the possible formation of diethylnitrosamine resulting from the use of rhodamine WT dye as a tracer in river waters
By T.R. Steinheimer and S.M. Johnson **37**

Estimating stream-aquifer interactions in coal areas of eastern Kansas by using stream-flow records
By H.E. Bevans **51**

Investigations of organic contaminants derived from wood-treatment processes in a sand and gravel aquifer near Pensacola, Florida
By W.E. Pereira and C.E. Rostad **65**

Evaluating strategies for ground-water contaminant plume stabilization and removal
By S.M. Gorelick and B.J. Wagner **81**

Recent growth of Gulkana Glacier, Alaska Range, and its relation to glacier-fed river runoff
By L.R. Mayo and D.C. Trabant **91**

Extension of the unsteady one-dimensional open-channel flow equations for flow simulation in meandering channels with flood plains
By L.L. DeLong **101**

Comparison of two stream-discharge record reconstruction techniques for eight gaging stations in Maine
By R.A. Fontaine **107**

Channel widening characteristics and bank slope development along a reach of Cane Creek, west Tennessee
By Andrew Simon and C.R. Hupp **113**

Evaluation of a suggested sequence for the chemical extraction of soluble amorphous phases from clays
By S.L. Rettig and B.F. Jones **127**

Comparison of velocity interpolation methods for computing open-channel discharge
By J.M. Fulford and V.B. Sauer **139**

A preliminary evaluation of a discharge computation technique that uses a small number of velocity observations
By L.R. Bohman and W.J. Carswell, Jr. **145**

Limnology of West Point Reservoir, Georgia and Alabama

By Dean B. Radtke

Abstract

West Point Reservoir is a multiple-purpose project on the Chattahoochee River about 112 river kilometers downstream from Atlanta on the Alabama-Georgia border. Urbanization has placed large demands on the Chattahoochee River, and water quality below Atlanta was degraded even before impoundment. Water-quality, bottom-sediment, and fish-tissue samples were collected from the reservoir to determine whether water-quality problems have occurred subsequent to impoundment.

Severe hypolimnetic oxygen deficiency occurred in the reservoir following thermal stratification in the spring of 1978 and 1979. During stratified periods, concentrations of dissolved iron and manganese in the hypolimnion at the dam pool ranged from 0 to 7,700 and 30 to 2,000 micrograms per liter, respectively.

During thermally stratified periods, phytoplankton standing crops in the upper lentic section of the reservoir ranged from 39,000 to 670,000 cells per milliliter. A maximum algal growth potential value (U.S. Geological Survey method) of 48.0 milligrams per liter was obtained at the uppermost data-collection station. The primary growth-limiting nutrients were nitrogen in the lotic section and phosphorus in the lentic section.

The highest measured concentrations of volatile solids and total iron, manganese, phosphorus, and organic carbon in sediments occurred in the lentic section of the reservoir, where bottom sediments consist mainly of silt and clay. Polychlorinated biphenyls and chlordane concentrations in the bottom sediments were as high as 740 and 210 micrograms per kilogram, respectively. Concentrations of polychlorinated biphenyls and chlordane in fish tissue ranged from 19 to 3,800 and 6.0 to 280 micrograms per kilogram, respectively.

INTRODUCTION

West Point Reservoir, in west-central Georgia, is in an 8,944-km^2 drainage basin of the upper Chattahoochee River (fig. 1). The study area encompassed the Chattahoochee River from Franklin, Georgia, to Langdale, Alabama, approximately 69 km in river length. West Point Reservoir is impounded by a U.S. Army Corps of Engineers gravity-type dam 2,211 m long and 29.6 m high, 5.1 km north of West Point, and 112 river km downstream from Atlanta, Georgia. The reservoir has a surface area of 10,360 ha, a volume of 605 hm^3, and a shoreline of 840 km at normal pool elevation of 194 m above sea level (U.S. Army Corps of Engineers, 1975).

West Point Reservoir is designed to provide flood control, power, recreation, fish and wildlife enhancement, and streamflow regulation for downstream navigation. Construction of the reservoir was authorized by the United States Flood Control Act of 1962. The reservoir filled to normal pool elevation in June of 1975.

The problems associated with water quality in the study area, as pointed out by Cherry and others (1978), are for the most part related to urbanization in the Atlanta and LaGrange metropolitan areas. This urbanization has created large demands on the Chattahoochee River, not only as a major water supply but as a transporter of municipal and industrial wastes. As a result, the water quality in the river below Atlanta was in a degraded condition, even before impoundment. Excessive organic, nutrient, and pathogenic organism loadings could cause accelerated eutrophication and could spoil the recreational potential of the proposed reservoir. For this reason concern was expressed even before the dam's closure about the potential effect of these metropolitan areas on the reservoir.

Purpose and Scope

The objectives of this study were to (1) document general postimpoundment water-quality conditions of the reservoir, (2) identify water-quality problems, (3) collect data to develop guidance for reservoir water elevation control and reservoir-release water-quality relations, (4) study special problems and collect data necessary to develop criteria for solutions of such problems, and (5) collect data that would provide an adequate data base and understanding of project conditions to facilitate coordination with State agencies in implementing watershed pollution control.

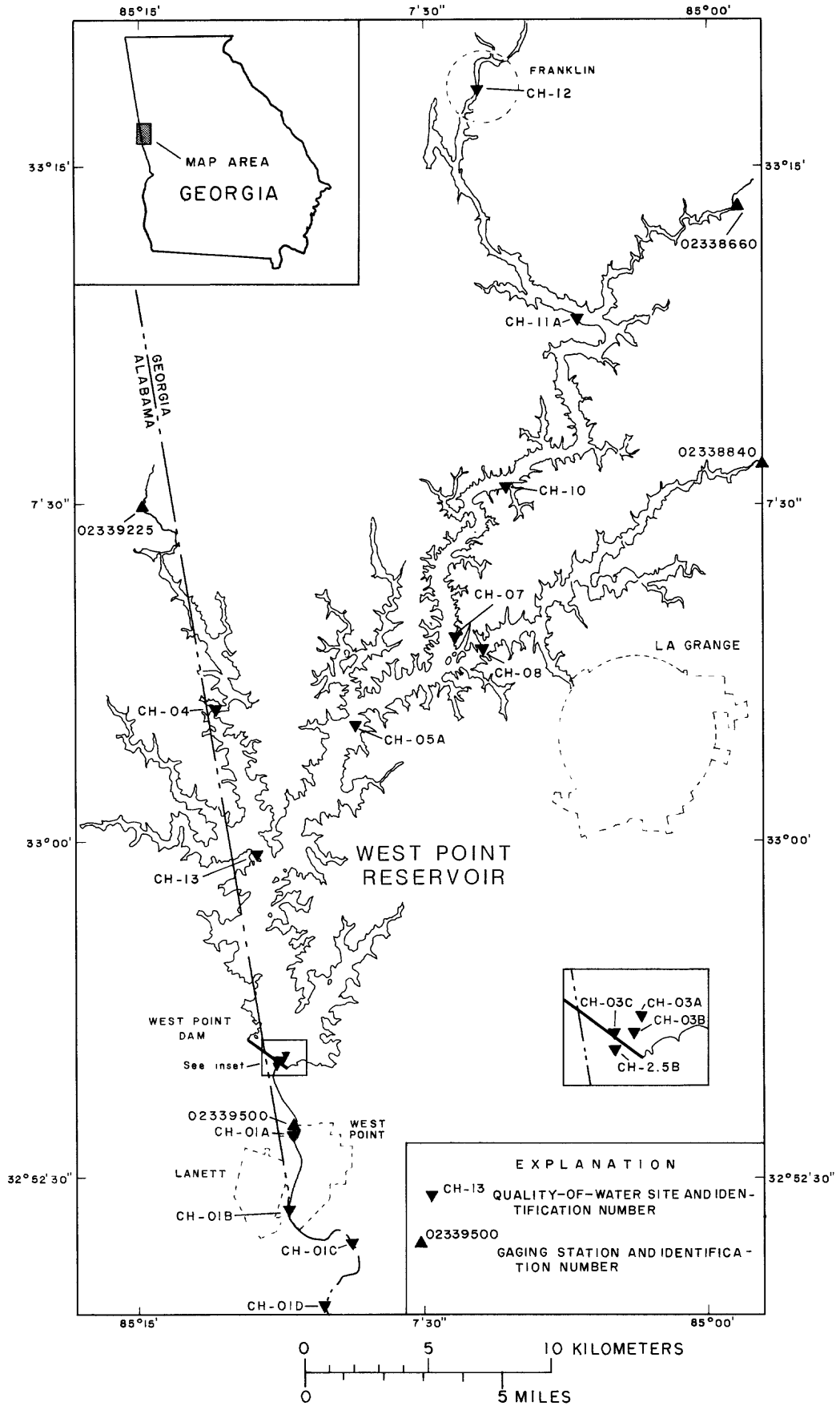
85°15'
7'30"
85°00'
33°15'
7'30"
33°00'
32°52'30"
MAP AREA
GEORGIA
GEORGIA
ALABAMA
FRANKLIN
CH-12
02338660
CH-11A
02338840
CH-10
02339225
CH-07
CH-08
LA GRANGE
CH-04
CH-05A
WEST POINT
RESERVOIR
CH-13
CH-03C
CH-03A
CH-03B
CH-2.5B
WEST POINT
DAM
See inset
02339500
CH-01A
WEST
POINT
LANETT
CH-01B
CH-01C
CH-01D
EXPLANATION
CH-13 QUALITY-OF-WATER SITE AND IDENTIFICATION NUMBER
02339500 GAGING STATION AND IDENTIFICATION NUMBER
0 5 10 KILOMETERS
0 5 MILES

The purpose of this report is to provide an abbreviated and timely version of a very large earlier report, which was prepared in cooperation with the U.S. Army Corps of Engineers Mobile District. This report provides significant information about reservoir limnology, which is transferable to other reservoir studies. Included are significant contributions concerning the limitations of phosphorus-based models for predicting the eutrophication status of reservoirs, ecologic information related to the distribution of plankton populations and communities in lotic and lentic habitats within a reservoir, and information demonstrating the relation of sediment distribution in reservoirs to the occurrence of potentially harmful chemical constituents and the potential bioaccumulation of these chemicals through the food chain.

Data analyzed included the physical properties and chemical constituents of both water and sediment, the bacteriology and biology (standing stock and biomass) of the reservoir, and the chemical constituents of fish tissue. In order to determine river and reservoir water-quality conditions during thermally stratified and unstratified periods, water quality of the reservoir and the river downstream from the dam was sampled 17 times between April 1978 and December 1979.

RESERVOIR STRATIFICATION AND THE EFFECTS ON WATER QUALITY

Thermal Stratification

West Point Reservoir is a monomictic system that undergoes an annual thermal stratification-destratification cycle in four distinct stages: (1) the onset of stratification (thermal density layering) in the spring, (2) a stratified period during the summer, (3) a fall mixing period or turnover, and (4) a winter unstratified period. The reservoir is weakly stratified during the summer. The stability and duration of summer stratification depend on inflow water discharge, inflow water temperature relative to reservoir water temperature, air temperature, wind velocity, cloud cover, reservoir morphometry, and residence time.

Field measurements of water temperature provide a qualitative picture of stratification and mixing patterns. The four stages of the stratification-destratification cycle in the main channel of West Point Reservoir are shown in figure 2. Each line represents a constant water temperature with respect to depth and distance along the reservoir reach. Each individual graph represents the spatial (longitudinal) change in water temperature from Franklin, Ga. (station CH–12), to the dam pool area (station CH–03C). Stratification during the summer was typified by horizontal temperature isopleths (July 1978). Under these circumstances, inflow water from the Chattahoochee River seems to follow an intermediate horizontal flow plane of similar density. During the stratification period, the depth of this interflow probably fluctuates vertically with periodic changes in river temperature. Rapid fluctuations in river temperature at CH–12 are caused by the release of cool water from upstream reservoirs during daily flow regulation. The fall mixing period is illustrated by the nearly vertical temperature isopleths shown in the graph for October 1978. Mixing usually does not occur until the fall, when cooling of the surface water and wind-generated thermal convection currents have lessened the temperature difference between the surface and bottom waters. After complete mixing, the entire reservoir is essentially the same temperature, as shown by the graph for January 1979. In the springtime, thermal stratification occurs, as illustrated by the graph for April-May 1979. The progressive warming of the water at the surface of the reservoir allowed the reestablishment of a vertical density gradient.

Data indicate that West Point Reservoir affected downstream water quality primarily as a result of changes in the chemical nature of the water column at the dam pool, brought on by seasonal stratification and dissolved-oxygen depletion. Withdrawal depths at West Point Dam cannot be altered to control downstream water quality, because the intakes for both the main and the service penstocks are fixed near the reservoir bottom and differ by only 1.52 m in altitude. Thus, the quality of the released water is fairly constant during periods of maximum and minimum flow through the penstocks.

Observed water temperatures in the Chattahoochee River downstream from West Point Dam were dependent on the temperature of the bottom water at the dam pool and on the ambient air temperature. Observed temperatures at station CH–2.5B were similar to those measured in the bottom water of the dam pool. Since water was always withdrawn from the same level, temperature differences between minimum and maximum daily release periods were generally small. However, these temperature differences were greater during periods when there was a substantial difference between the ambient air temperature and the water temperature of hypolimnion at the dam pool. River water was more rapidly warmed by the atmosphere during minimum daily release periods than during maximum daily release periods.

Dissolved-Oxygen Enrichment-Depletion Cycle

The distribution of dissolved oxygen (DO) in West Point Reservoir was strongly influenced by stratification and mixing. During the study period, severe hypolimnetic oxygen deficits occurred in the spring and summer months because stratification curtailed vertical mixing.

Figure 1. West Point Reservoir study area and locations of the principal data-collection stations.

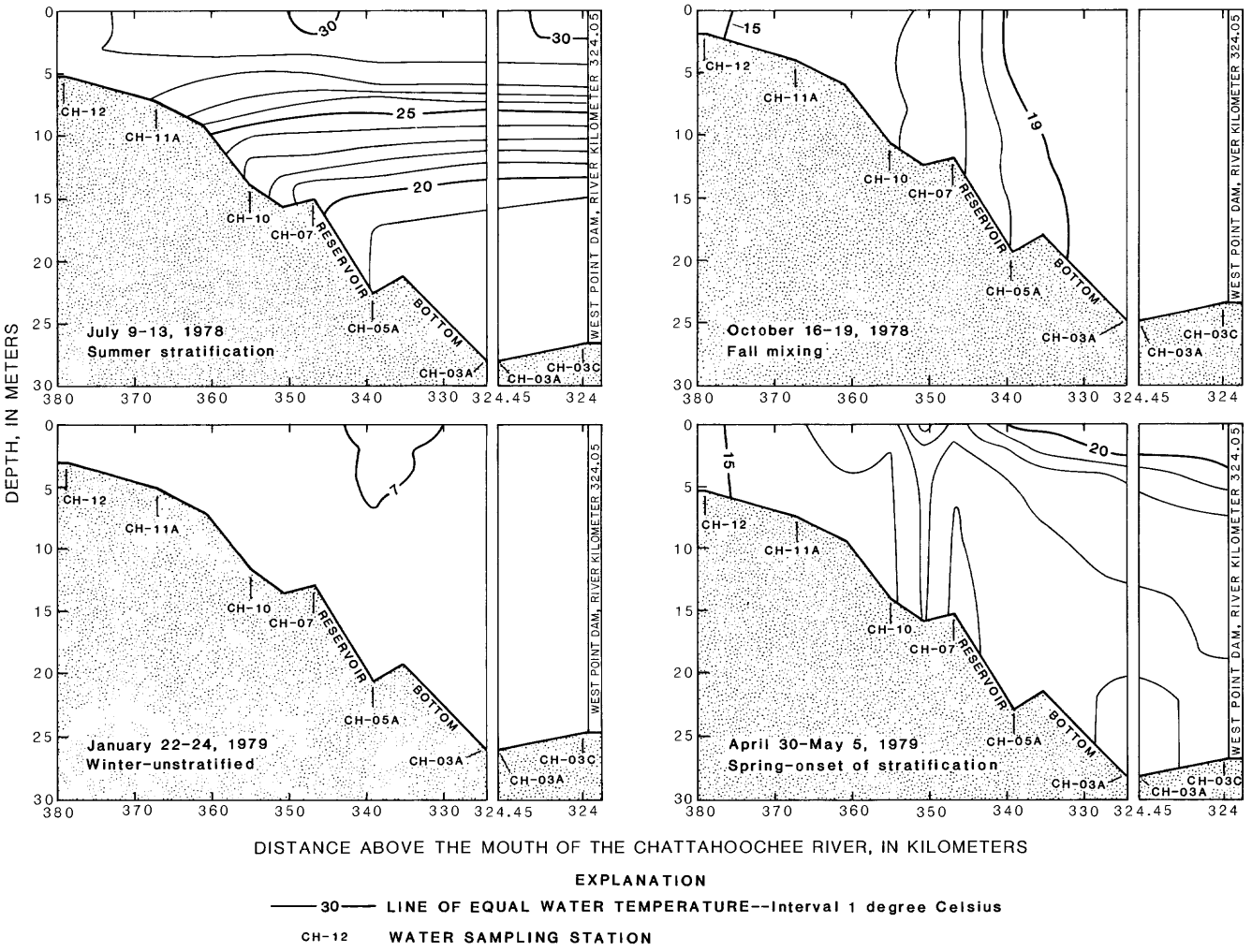

Figure 2. Patterns of water temperature in West Point Reservoir for selected data-collection trips.

The oxygen demand in the hypolimnion was high, owing to decomposition of settled particulate organic matter and benthic biological and chemical oxygen demand.

The seasonal aspects of the dissolved-oxygen cycle in the main channel of the reservoir are shown in figure 3. Marked metalimnial concentration gradients, as evidenced by the compressed horizontal dissolved-oxygen isopleths seen in the July graph, indicate a highly stratified system.

For both 1978 and 1979 stratified periods, the highest DO concentration in the epilimnion was in the reach between stations CH–10 and CH–07. The supersaturated conditions were the result of phytoplankton production. The effects of high concentrations of phytoplankton, as measured by chlorophyll *a*, on the pH and DO concentrations at the surface of the lentic section of the reservoir are illustrated in figure 4. Because the photosynthetic process requires carbon dioxide, a decrease in carbon dioxide produces a decrease in the hydrogen ion concentration and an increase in pH. The subsequent release of dissolved oxygen during photosynthesis accounts for the high DO concentrations in the euphotic zone.

In contrast, hypolimnetic anoxia is partly a result of downward migration of autochthonous organic matter when plankton production is high. The oxidation and respiration process in the hypolimnion consume the available oxygen and thus, without adequate mixing, create low DO concentrations (fig. 3). During July 1978, the main channel was anoxic below a depth of about 10 m from station CH–10 downstream to the dam pool (station CH–03C). It is likely that relatively large amounts of particulate cellular material settled to the hypolimnion in the reach between CH–10 and CH–05 and exerted a high oxygen demand. Conditions were not as severe during July 1979, when the anoxic part of the hypolimnion extended below a depth of about 10 m from about halfway between stations CH–07 and CH–05A to the dam pool (station CH–03C).

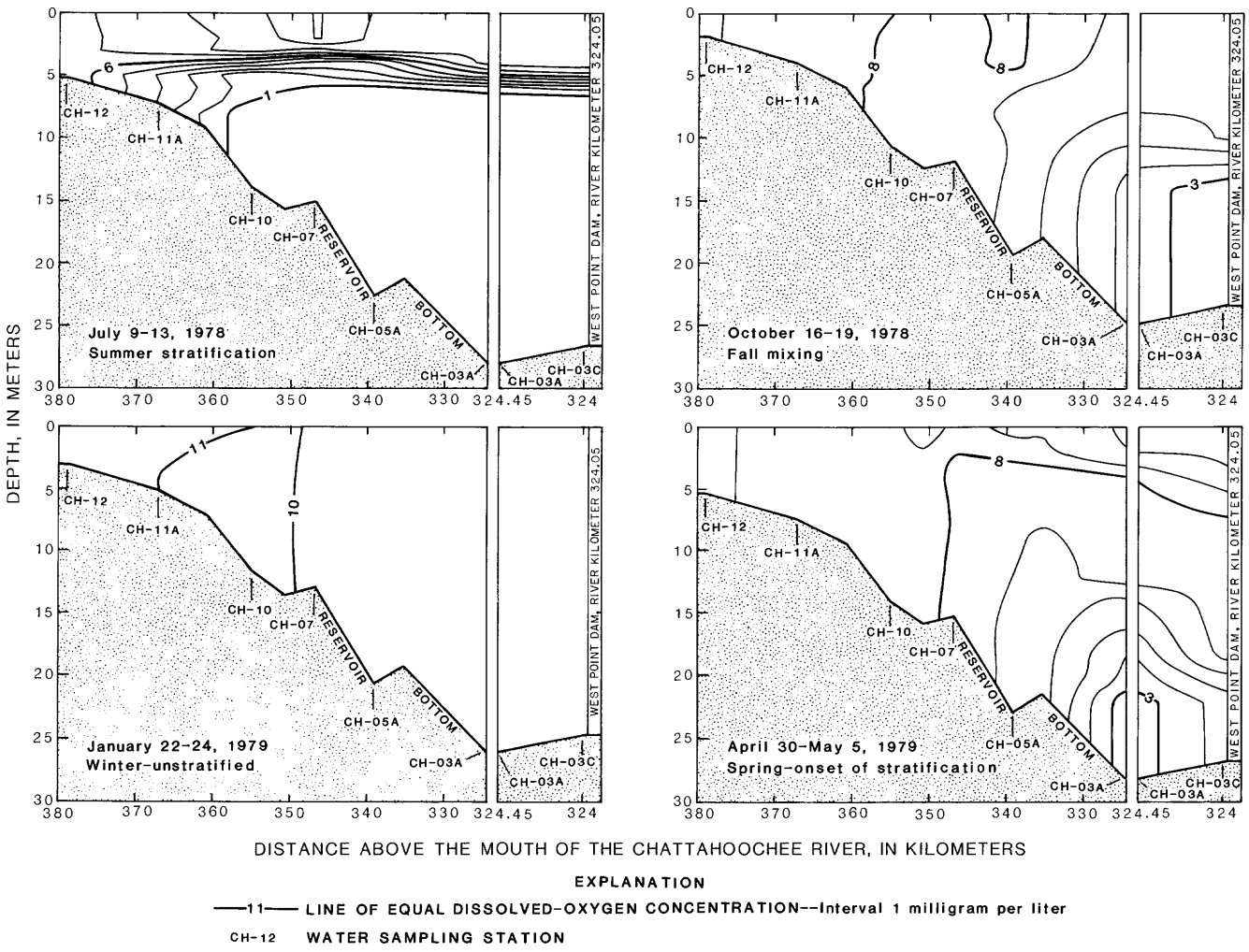

Figure 3. Patterns of dissolved-oxygen concentrations in West Point Reservoir for selected data-collection trips.

Hypolimnetic dissolved-oxygen deficits persisted until vertical mixing occurred in the fall. The October 1978 graph in figure 3 shows the dissolved-oxygen conditions in the main channel of West Point Reservoir during the mixing period. Epilimnial cooling just before October 1978 disrupted the thermocline and allowed vertical mixing to occur throughout most of the main channel reach. Only the bottom water near the dam pool (station CH–03C) remained near anoxia during October 16–19, 1978. In January 1979, the entire main channel was well mixed. The April-May 1979 graph shows the distribution of dissolved oxygen during the initial stages of the 1979 stratification period, which occurred in the springtime.

Hypolimnetic dissolved-oxygen depletion was more pronounced in Yellowjacket (CH–08) and Wehadkee Creeks (CH–04) tributaries than in the main channel, partly because thermal stratification persisted longer in the two tributaries. These tributaries received small inflows and, therefore, were more lacustrine than the main channel because the metalimnion was not subjected to the destabilizing influence of higher velocity inflow and short-term temperature fluctuation caused by regulation of the Chattahoochee River. This observation suggests that water-quality problems associated with dissolved-oxygen depletion could have been more pronounced in the tributaries than in the main channel.

One of the more critical degradations in water quality that occurred downstream from West Point Dam was the lower DO concentration caused by discharge of anoxic water during periods of stratification. The bottom water at the dam pool (station CH–03C) was anoxic from the end of May through the middle of September 1978 and during June and July 1979. Discharge of this anoxic water resulted in DO concentrations that reached a summertime minimum of 2.5 mg/L at station CH–2.5B (fig. 5). During the summer, DO concentrations during maximum daily releases were lower than concentrations during minimum daily releases because reaeration of

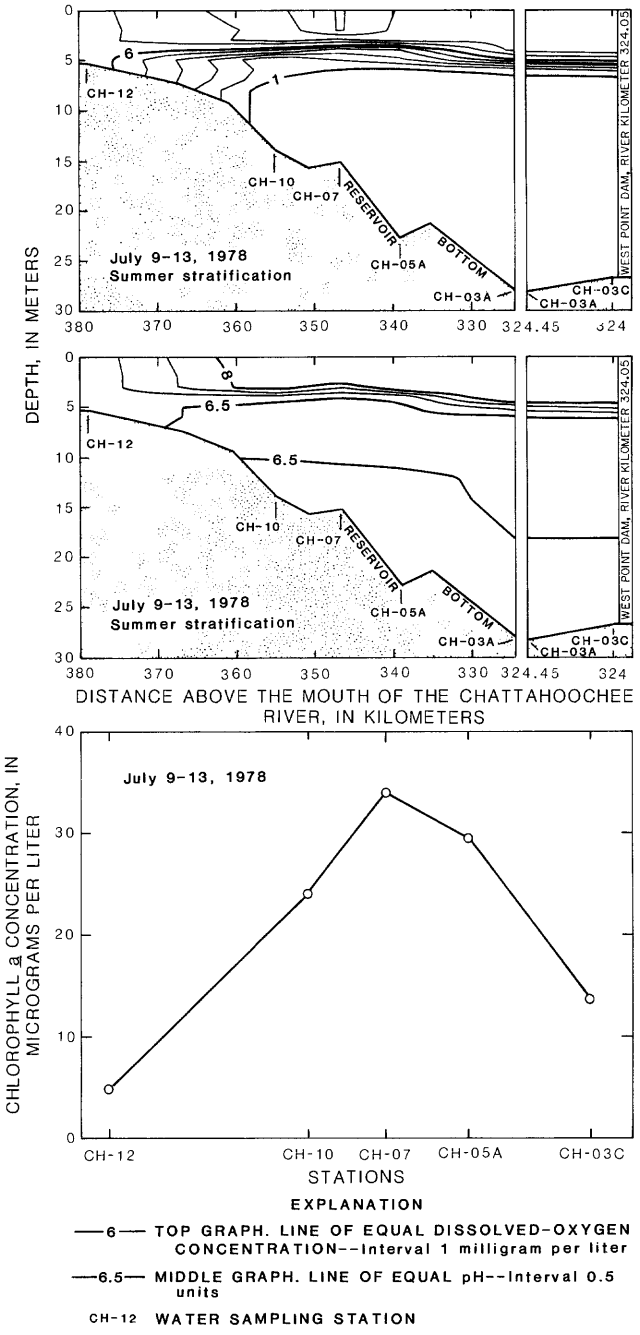

Figure 4. Relation of dissolved-oxygen concentrations and pH values to chlorophyll a concentrations in the euphotic zone of West Point Reservoir, July 9–13, 1978.

minimum daily release discharge was more rapid than reaeration of maximum daily release discharge.

Iron and Manganese Cycling

Clays prevalent in the Piedmont province of Georgia contain appreciable quantities of iron and manganese (Cherry, 1961) and are probably the main source of metal loading to West Point Reservoir. During an assessment of the river quality of the Upper Chattahoochee River basin, Faye and others (1978) demonstrated the role of silt-clay particulates as carriers for the suspended phases of a number of metals. The seasonal and longitudinal aspects of the metals cycle in this system are illustrated by a series of depth-reservoir reach isopleths (fig. 6). These graphs represent total iron distribution in the main channel during different times of the year and show the effects of upstream channel erosion, sedimentation, and thermal stratification. Because manganese behaves much like iron, these illustrations will be used to explain the distribution of both metals.

Thermal stratification and the ensuing hypolimnetic dissolved-oxygen depletion resulted in the high total iron concentrations at station CH–07 in July 1978 (fig. 6). The extent of ferric-iron reduction and subsequent release of soluble ferrous iron from bottom materials was found to vary spatially and temporally with the extent of dissolved-oxygen depletion, as can be seen in figures 3 and 6. Fall mixing and reaeration of the bottom water in the reservoir lowered iron and manganese concentrations in the water column. For example, observed concentrations of total iron were much lower and more uniform throughout the water column in October 1978 (fig. 6).

Most of the total iron in the upper reaches (lotic section) of the reservoir was in the suspended phase, as little ferrous iron was present in the water column in this section. Loading and sedimentation of particulate iron depend on flow conditions in the Chattahoochee River, the reservoir pool elevation, and other factors. At higher flows the river inflow generally carries more suspended material. The data collected, however, are insufficient to quantify this complex relation.

In contrast to conditions in the upper reaches of the main channel, the large increases in total iron in the bottom water of West Point Reservoir during stratified periods were due primarily to the dissolved iron. Extended periods of hypolimnetic anoxia and low oxidation-reduction potentials resulted in higher dissolved-iron concentrations.

Increases in the iron and manganese content of release water from West Point Reservoir were attributed primarily to the solubility of these sediment-bound metals in the anoxic hypolimnion during summer months. Solubility of these substances during anoxic conditions in the dam pool resulted in their objectionable concentrations in downstream public water supplies. The increases during minimum and maximum daily release periods generally mostly coincided with increases in the dissolved metals at the dam pool. During stratified periods, dissolved-metal concentrations accounted for most of the total constituent concentrations in the reservoir. During unstratified periods, most of the total constituent concentrations were composed of suspended constituents. No appreciable

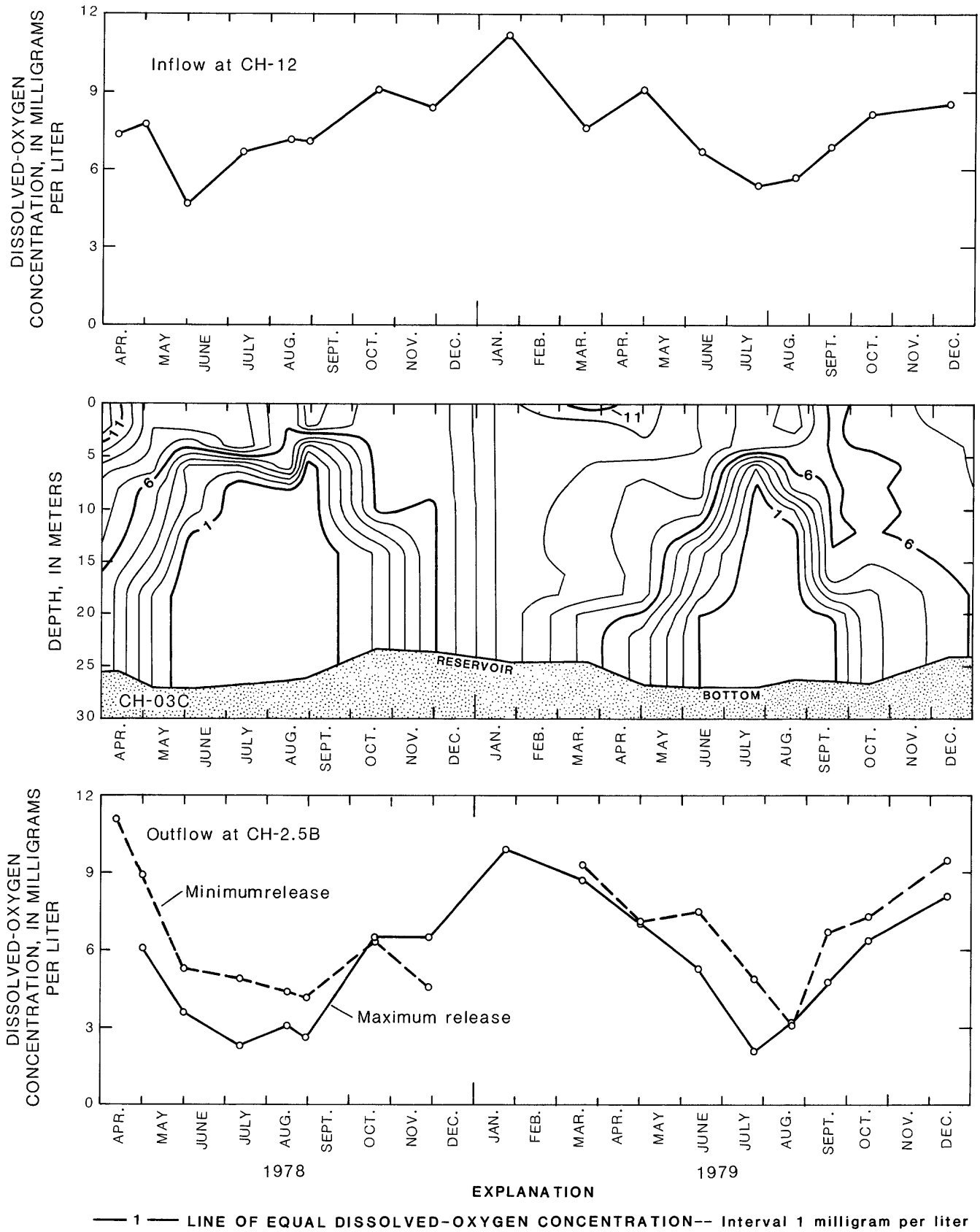

Figure 5. Seasonal patterns of dissolved-oxygen concentrations in inflow to West Point Reservoir, in waters at the dam pool, and in minimum and maximum daily release waters from the reservoir, April 1978 to December 1979.

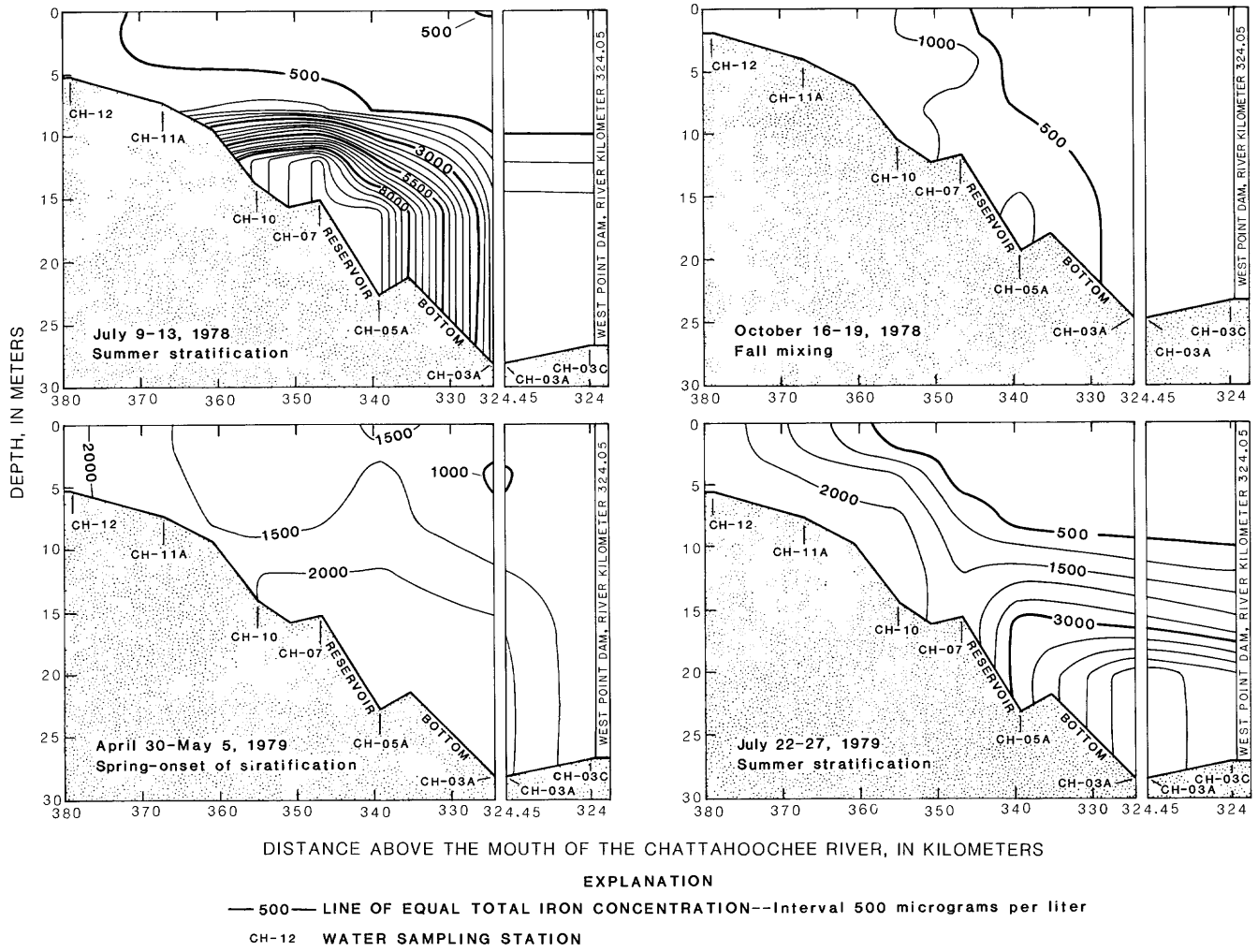

Figure 6. Patterns of total iron concentrations in West Point Reservoir for selected data-collection trips.

difference in the total constituent metal concentrations was observed between minimum and maximum daily release periods and between downstream river stations CH–2.5B and CH–01D.

Nutrient Cycling

Nutrient input to an aquatic system is important in terms of its impact on phytoplankton growth and eutrophication. Excluding Yellowjacket and Wehadkee Creeks, point- and nonpoint-source loading to the Chattahoochee River are the primary nutrient input to West Point Reservoir. Point-source contributions from metropolitan Atlanta dominate during low-flow periods; nonpoint runoff predominates during high-flow periods and storm events (Stamer and others, 1978). This alternation produces a balance between river discharge and nutrient concentration such that the nutrient load is fairly uniform year-round. Treated sewage and urban runoff are the primary input to Yellowjacket Creek, and agricultural runoff is the primary input to Wehadkee Creek. Inflow water discharge, thermal stratification, biologic activity, and interflow affected the distribution of nutrients in West Point Reservoir.

Inflow concentrations of total phosphorus and dissolved orthophosphate were high (0.42 and 0.28 mg/L, respectively) during the stratified periods. An appreciable amount of this incoming load, however, was removed from the epilimnion by the time water reached the middle of the reservoir. Between stations CH–11A and CH–10, the reservoir quickly deepens, flow velocities decrease, and vertical mixing decreases, thereby facilitating deposition. Removal of phosphorus from the upper water column was probably a result of two factors: (1) settling of particulate phosphorus associated with inorganic suspended sediment and plankton and (2) phytoplankton uptake, which depleted the dissolved phosphorus. Hypolimnial concentrations of suspended and dissolved phosphorus were relatively high as far downstream as station CH–05A. The suspended phosphorus was most

likely derived from sestonic settling and from material carried by interflow, whereas the dissolved phosphorus was probably derived from sestonic decomposition and the release of phosphorus from the sediments. The mobilization of sediment-bound phosphorus is most prevalent during severe stratification, when hypolimnial waters are anoxic and have a low oxidation-reduction potential. Once the water column mixes in the fall, reaeration, higher oxidation-reduction potentials, and increased inflow could allow much of the hypolimnial dissolved phosphorus to be removed from the water column by coprecipitation with ferric iron and by flushing from the reservoir.

During unstratified periods, vertical concentration gradients of total phosphorus and dissolved orthophosphate concentrations in the reservoir were negligible, and horizontal downstream gradients were much shallower than during thermal stratification.

Phosphorus data collected at the tributary stations in the reservoir during 1978 and 1979 indicate that Yellowjacket Creek (CH–08) had much greater concentrations of phosphorus than Wehadkee Creek (CH–13). Appreciable hypolimnial concentrations of total phosphorus and dissolved orthophosphate were observed at station CH–08 during the summer months. The particulate phosphorus probably represents a combination of particulates from sestonic settling and from point and nonpoint sources from the city of LaGrange, Ga. By comparison, the Wehadkee Creek station (CH–13) did not show appreciable concentrations of phosphorus even through anoxic conditions were present in the hypolimnion.

Phosphorus concentrations in the downstream reaches of the Chattahoochee River were affected by the seasonal chemical stratification and biological activity occurring in the reservoir. Outflow concentrations of phosphorus from the reservoir generally were low in relation to inflow concentrations.

Nitrite plus nitrate nitrogen and ammonia nitrogen concentrations during the nonstratified periods are illustrated by the April 30–May 5, 1979, isopleth in figure 7. For most of the reservoir reach, the water column was well mixed, as indicated by the nearly vertical isopleths of nitrite plus nitrate. The concentrations did show a steady decrease in the downstream direction. Very little ammonia nitrogen was present in the water column at this time, as would be expected in a strongly oxidizing environment.

Concentrations of nitrite plus nitrate and ammonia nitrogen were quite different during the stratified periods (fig. 7). Nitrite plus nitrate concentrations in the epilimnion and hypolimnion in the lentic section were lower than concentrations in the inflow at CH–12. The lower concentrations in the lentic section of the epilimnion were probably due to nitrogen uptake by phytoplankton, followed by plankton settling. The lower concentrations of nitrite plus nitrate in the lentic section of the hypolimnion were probably due to denitrification that occurred during the bacterial reduction of sestonic organic nitrogen to ammonia. Relatively high concentrations of nitrite plus nitrate, however, persisted in the metalimnion as far downstream as the dam pool (station CH–03A) as a result of interflow. The maximum concentration of total ammonia nitrogen (0.84 mg/L) occurred near hypolimnion in the vicinity of river kilometer 340, where dissolved-oxygen depletion was severe and oxidation-reduction potential was low. This ammonia probably originated from decomposition of organic detritus in the underlying sediment layers, from decomposition of settling particulate detrital material, and from denitrification.

Concentrations of nitrite plus nitrate nitrogen were much higher than ammonia nitrogen concentrations at the dam pool and in the river at station CH–2.5B during the winter, when reservoir waters were well oxygenated. However, concentrations of ammonia nitrogen were much higher than concentrations of nitrite plus nitrate nitrogen at these two sites during summer stratification periods, because of decomposition of organic material and denitrification in the anoxic hypolimnetic waters.

High ammonia concentrations in the Chattahoochee River measured at station CH–2.5B coincide with the occurrence of anoxic conditions and high ammonia concentrations at the dam pool (station CH–03C). No appreciable differences between ammonia concentrations during minimum and maximum daily release periods were observed except during periods of high ammonia concentrations at the dam pool. Nitrite plus nitrate concentrations at station CH–2.5B were nearly identical to those in the bottom water at the dam pool. Low concentrations of nitrite plus nitrate and high concentrations of ammonia nitrogen coincided with the occurrence of anoxic conditions at the dam pool.

BIOLOGIC CHARACTERISTICS AND RESPONSES TO NUTRIENT ENRICHMENT

The lentic section of the reservoir (stations CH–10 to CH–03C) showed the greatest zooplankton activity, ranging from 1,000 to 284,160 organisms/m^3. The largest concentrations of zooplankton were reported during early summer and autumn. During stratified periods, the highest concentrations of zooplankton were in the midsection of the reservoir (stations CH–07 and CH–05A); station CH–05A had the highest reported concentrations (284,160 organisms/m^3) in June 1979.

The zooplankton communities in West Point Reservoir consisted primarily of rotifers, cladocerans, and copepods. Rotifers were the predominant animal plankters both spatially and temporally. Cladocerans and copepods were more abundant at the dam pool (station CH–03C)

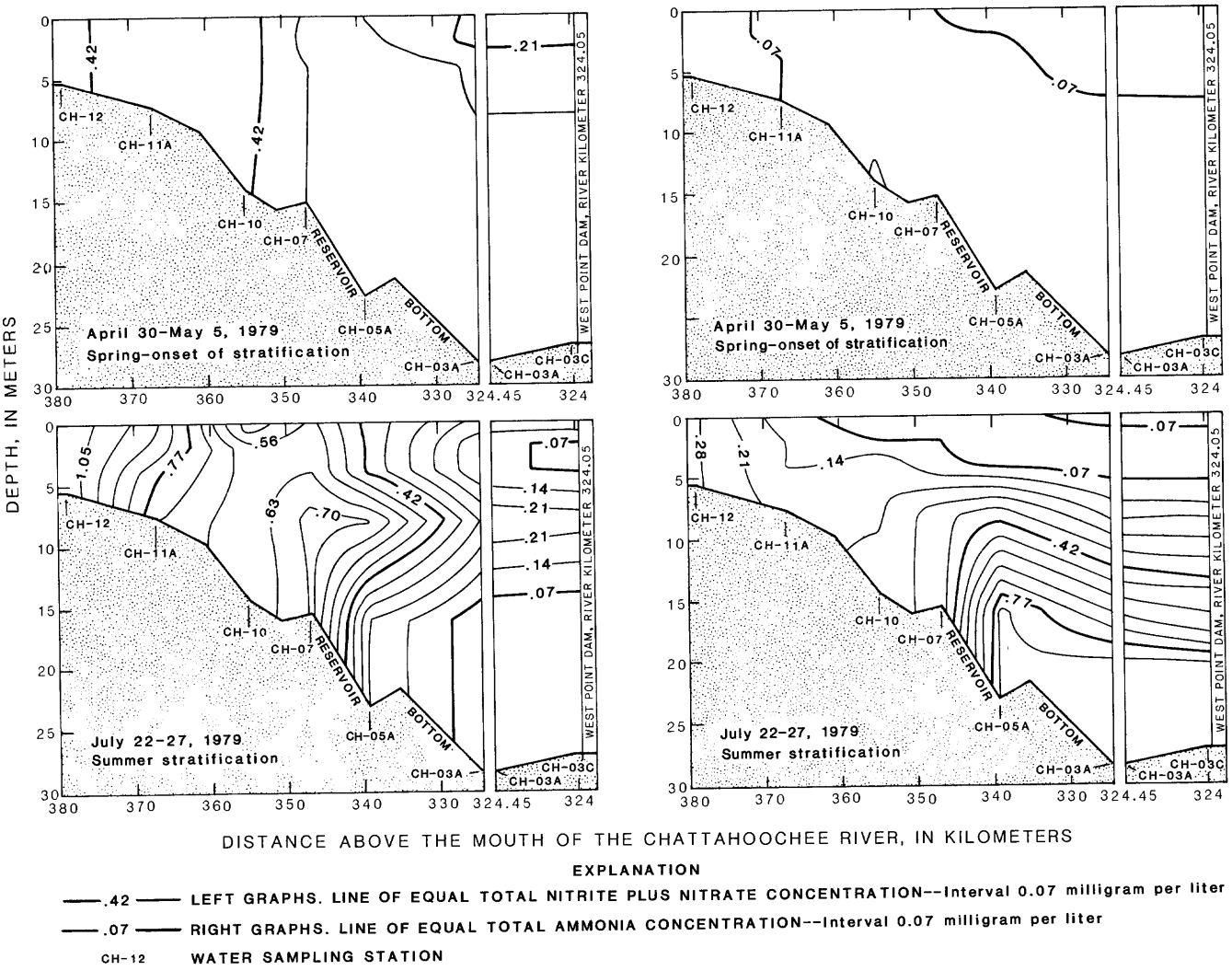

Figure 7. Patterns of total nitrite plus nitrate and total ammonia concentration in West Point Reservoir for selected data-collection trips.

than at upstream stations and, at all stations, were more abundant during spring and autumn.

For the sampling period, *Conochilus unicornis* and *Keratella crassa* were the most abundant rotifers, and *Bosmina longirostris* and *Diaphanosoma brachyurum* were the most abundant cladocerans. The fauna of the lotic section was low in species richness and was represented by forms characteristic of benthic riverine communities, for example, the *Bdelloid* rotifers. Species richness and true plankters making up the populations increased as the distance to the dam decreased.

Certain generalizations about the temporal and longitudinal variation of the major groups of phytoplankton can be made.

1. During stratified periods, the dominant group in terms of numbers per unit volume was the blue-green algae (Cyanophyta). *Agmenellum quadruplicatum*, *Anacystis incerta*, and *Lyngbya contorta* were the most prevalent.
2. The lotic section (vicinity of CH–12) was represented by forms characteristic of benthic riverine communities, for example *Gomphonema parvulum* and *Nitzschia palea.*
3. The ecotone between lotic and lentic environments (vicinity of CH–11A) was characterized by high species richness as a result of having representative species from both environments.
4. True plankters in the communities increased as the distance to the dam pool decreased.
5. Diatoms (Bacillariophyta) and green algae (Chlorophyta) are more common during spring and autumn than summer.

In the lotic environment, autotrophic production was probably limited by one or a combination of the following:

1. Water velocities were too great for plankton community development.
2. Large concentrations of nonfilterable-residue loading reduced the depth of the euphotic zone.

3. Growth was limited by nutrient deficiencies.

The upper lentic section or middle section of the reservoir (stations CH–10 to CH–05A) had the highest autotrophic production. This was in response to nutrient availability, a corresponding reduction in water velocity, and an increase in the euphotic zone depth as the reservoir became more lentic in nature. Station CH–07 had the highest estimated standing stock concentration (670,000 cells/mL) in June 1978. Zooplankton grazing and the uptake, utilization, and subsequent depletion of dissolved orthophosphate appeared to be the principal factors in the decline in autotrophic production in the dam pool area during summer stratified periods (fig. 8). In West Point Reservoir during stratified periods, zooplankton pulses generally coincided with or immediately followed phytoplankton pulses. No single factor (physical, chemical, or biological) can be designated the cause of the temporal and longitudinal succession of the phytoplankton.

AGP–USGS assay (Shoaf and Lium, 1979) data showed that the availability of nutrients decreased in response to increases in phytoplankton concentrations from the upper to the lower reaches of the reservoir (fig. 8). A maximum algal growth potential value of 48.0 mg/L was obtained at the uppermost station (CH–12) at Franklin, Ga., on July 13, 1978, whereas a minimum value of 0.4 mg/L was recorded at the dam pool station (CH–03C) in August 1978.

The Algal Assay Procedure: Bottle Test (U.S. Environmental Protection Agency, 1971) procedure was used to define possible nutrient limitation in West Point Reservoir and specifically to determine whether this limitation could be due to nitrogen, phosphorus, or trace-element deficiency. The determination was accomplished by measuring the growth response of *Selenastrum capricornutum* to singular and combined additions of 0.05 mg/L phosphorus as K_2HPO_4, 0.01 mg/L nitrogen as $NaNO_3$, and 0.01 mg/L ethlenediamine tetraacetate (EDTA) as Na_2EDTA to the test waters.

Figure 9 shows the effects of nutrient additions to the test water from West Point Reservoir. Growth responses of *Selenastrum capricornutum* due to nutrient additions were compared to growth responses in inoculated control flasks. The responses obtained in the control plus nitrogen and nitrogen plus EDTA additions identified nitrogen as the primary growth-limiting nutrient during the stratified period in the lotic section of the reservoir. In the lentic section, the growth response indicated that during the stratified periods, phosphorus was the primary growth-limiting nutrient. The effects of uptake and utilization of nutrients in autotrophic production and the subsequent depletion of these nutrients as demonstrated by the AGP response are shown in figure 9. Phosphorus addition in the presence of excess nitrogen plus EDTA seemed to support growth to its maximum.

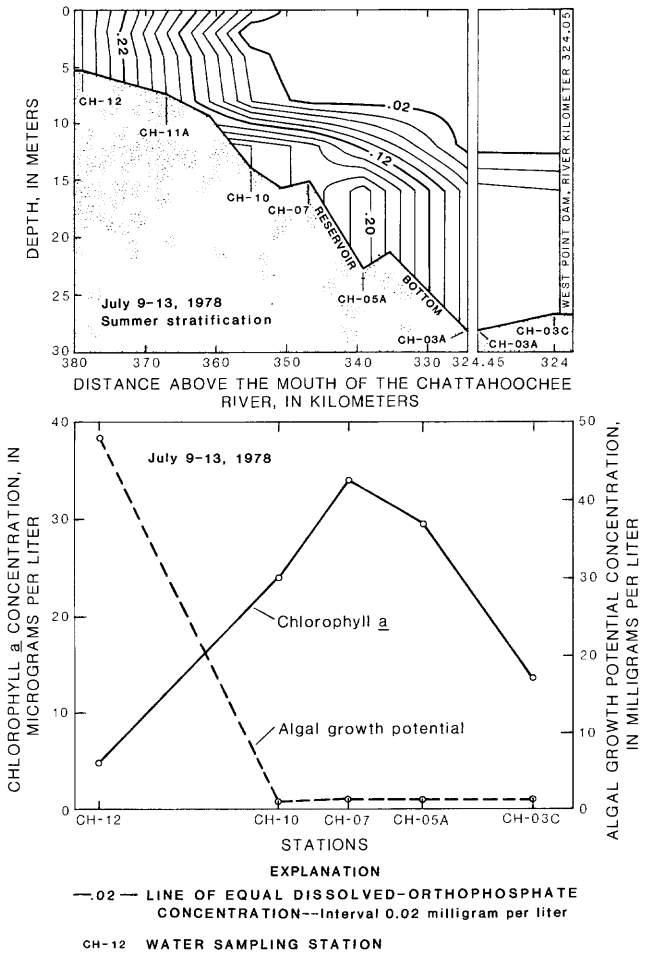

Figure 8. Relation of dissolved-orthophosphate concentrations to chlorophyll *a* concentrations and algal growth potential concentrations in the euphotic zone of West Point Reservoir, July 9–13, 1978.

Synthetic organic ligands such as Na_2EDTA are added to culture media to make sure trace elements are available to support algal growth. The growth responses attained with the addition of EDTA, however, were not conclusive. The algal response to EDTA addition could have been a result of secondary growth-regulating nutrient deficiencies and (or) the ability of *S. capricornutum* to metabolize the nitrogen contained in the Na_2EDTA complex.

BOTTOM MATERIAL CHARACTERISTICS

Data on particle size and constituent concentration of bottom material were collected from West Point Reservoir to provide information on the presence, concentration, and distribution of potentially harmful substances in the bottom sediments of the reservoir and the river below the dam.

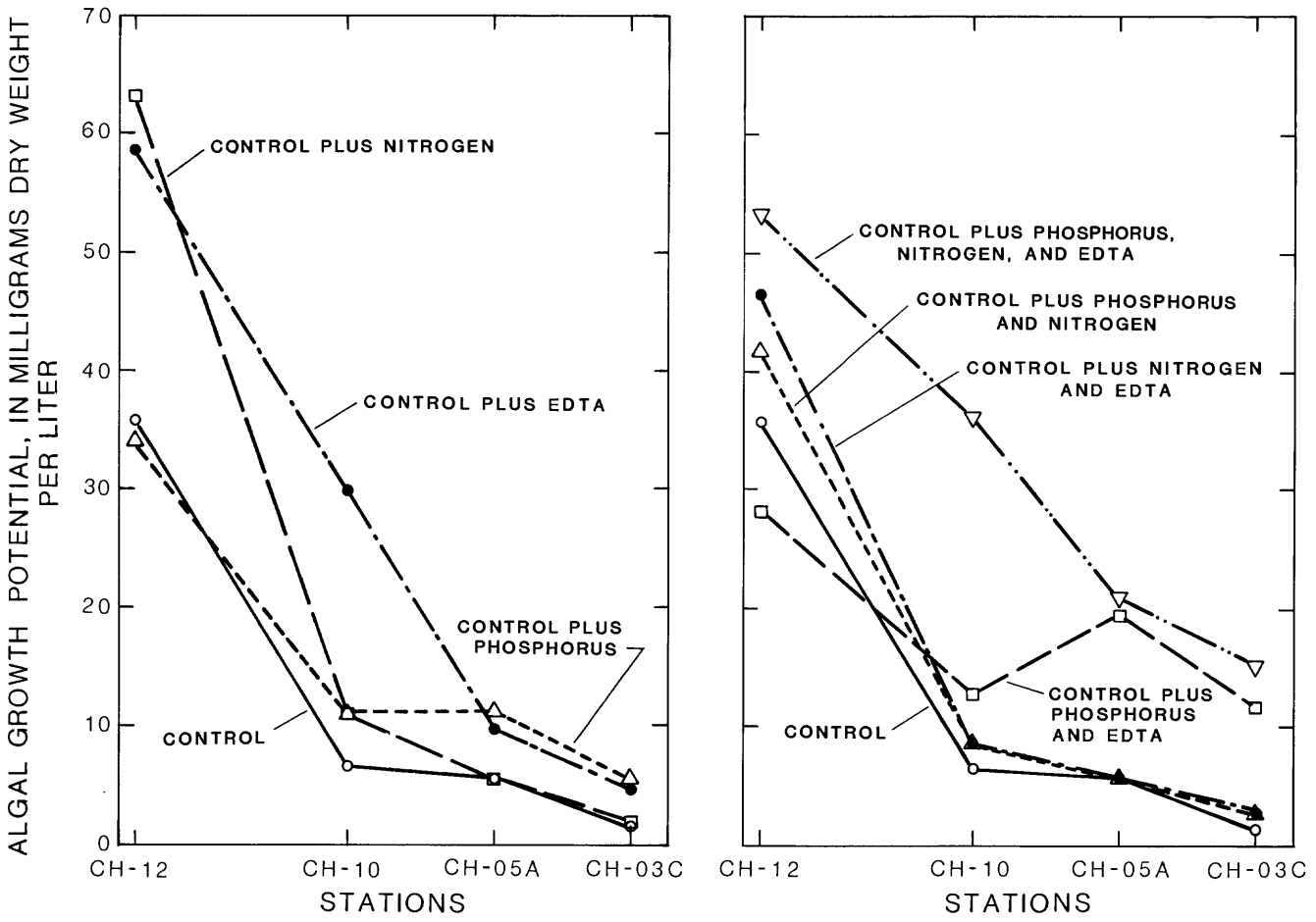

Figure 9. Effect of nutrient addition to water from West Point Reservoir on the growth of *Selenastrum capricornutum*, August 14–17, 1978.

The downstream gradation of bottom material particle size, from sand to silt plus clay, between the headwaters of the reservoir and the dam pool indicates decreasing velocities through the reservoir. Sand-size particles carried as suspended and bed load by the Chattahoochee River are retained in the upper section of the reservoir as the flow begins to decrease. Suspended particles finer than sand continue to settle out as the downstream velocities progressively decrease. The particle size of bottom material from tributary stations was more characteristic of mainstem reservoir stations than of the river stations below West Point Dam.

The streambed at the stations below West Point Dam was constantly being scoured by high-velocity water during release periods. This fact, along with the probable absence of silt and clay in the release water, accounts for the scarcity of fine materials in the bottom materials at these stations.

Within the reservoir, measurable concentrations of certain chemical constituents occurred where silt and clay particles made up most of the bottom material. The relation of these chemical constituents to particle size is illustrated in figures 10 and 11. Many of these substances (especially the chlorinated hydrocarbons) have low solubility in water, which favors their rapid sorption on suspended or sedimented materials.

FISH TISSUE QUALITY

In order to document and substantiate contaminant residue bioaccumulation in West Point Reservoir, whole and, during 1979 only, fillet fish tissue samples from two tributary reservoir sites were analyzed for a select number of chlorinated hydrocarbons and trace metals in 1978 and 1979. Results of the fish tissue analyses for these substances, which form persistent and toxic residues in the environment, are presented in table 1. Most tissue samples contained measurable amounts of chlorinated hydrocarbons and trace metals. Polychlorinated biphenyls (PCB's), chlordane, and DDT are especially notable because of their concern to human health.

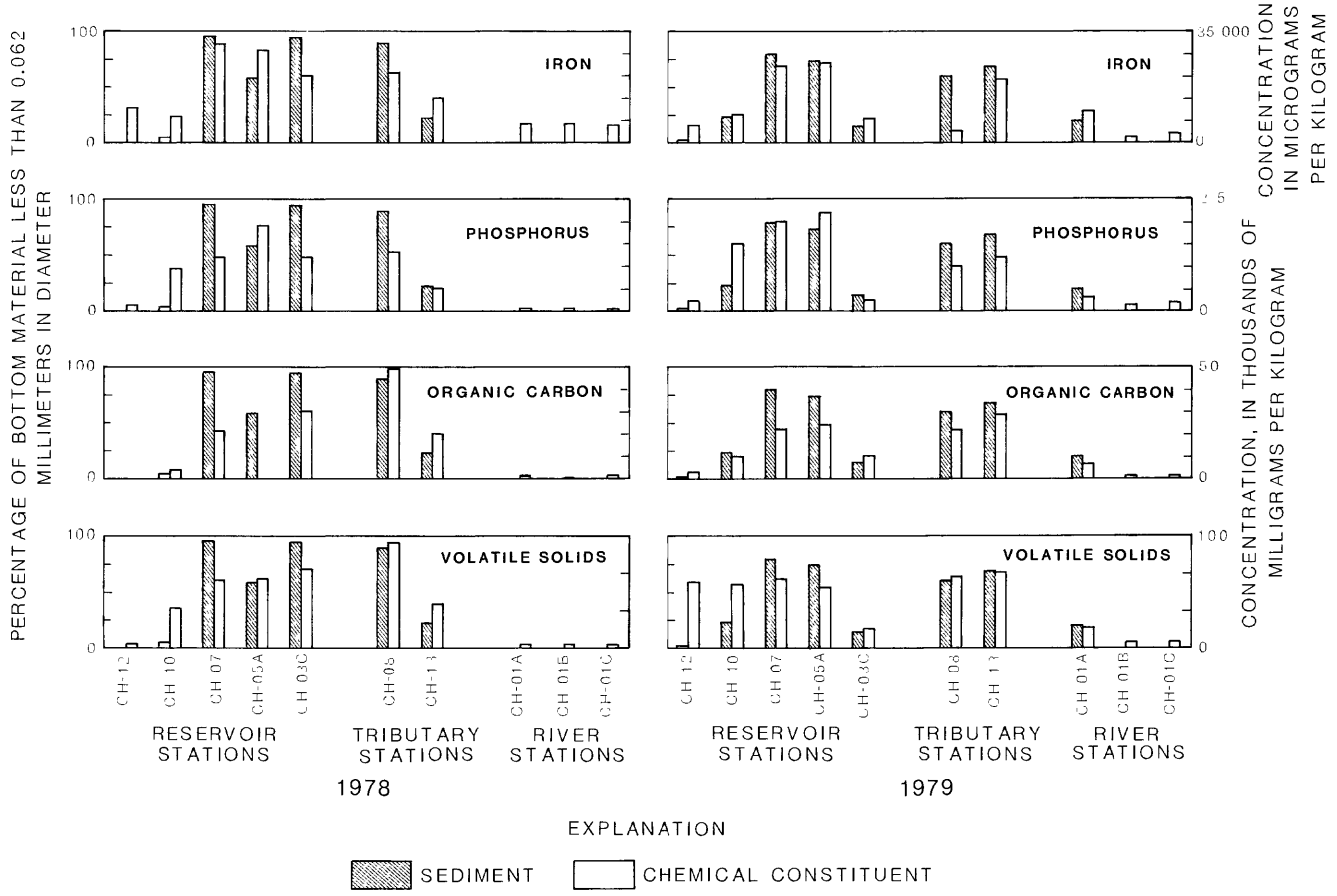

Figure 10. Percentage of silt and clay (particles less than 0.062 mm in diameter) in bottom material and concentrations of iron, phosphorus, organic carbon, and volatile solids in bottom material from West Point Reservoir and downstream river sites.

PCB's, which were found in high concentrations (3,800 μg/kg in one sample), are highly persistent and can accumulate in the environment. The National Academy of Sciences (1974) recommended that aquatic organisms should be protected so that the maximum residues in general body tissues will not exceed 500 μg/kg. Several whole fish samples from West Point Reservoir contained concentrations far exceeding this maximum recommended concentration.

The cyclodiene pesticides (chlordane, dieldrin, endrin, aldrin, heptachlor, and heptachlor epoxide) present the greatest hazards of all residual pesticides. Chlorinated hydrocarbon and metal concentrations in fish tissue in West Point Reservoir are given in table 1. These substances are highly persistent biologically and readily accumulate in the lipids of terrestrial and aquatic organisms. Even at low dosages, they are highly active carcinogens and affect the central nervous system of higher animals and humans, leading to irreversible changes in encephalographic and behavioral patterns (National Research Council, 1977).

DDT and its degradation products are of moderately acute toxicity to most organisms, including humans. Low water solubility, high lipid solubility, and subsequent bioaccumulation make these substances extremely persistent in living organisms. The major concern about DDT and its derivatives, therefore, is not their acute toxicity but their long-term chronic effects. DDT and its degradation products are still present (1978–79) in measurable amounts (<0.1 to 49 μg/kg) in fish tissue samples in West Point Reservoir, even though DDT was banned in the United States on January 1, 1973.

The selected trace metals were not present in high concentrations. However, the need exists for expanded monitoring of trace metals through the entire food chain.

The results of fish tissue analyses during 1978 should not be compared with those during 1979 because of the difference in sampling between 1978 and 1979. The important point is that measurable concentrations of potentially hazardous chlorinated hydrocarbons were found in whole and fillet fish samples of specimens that

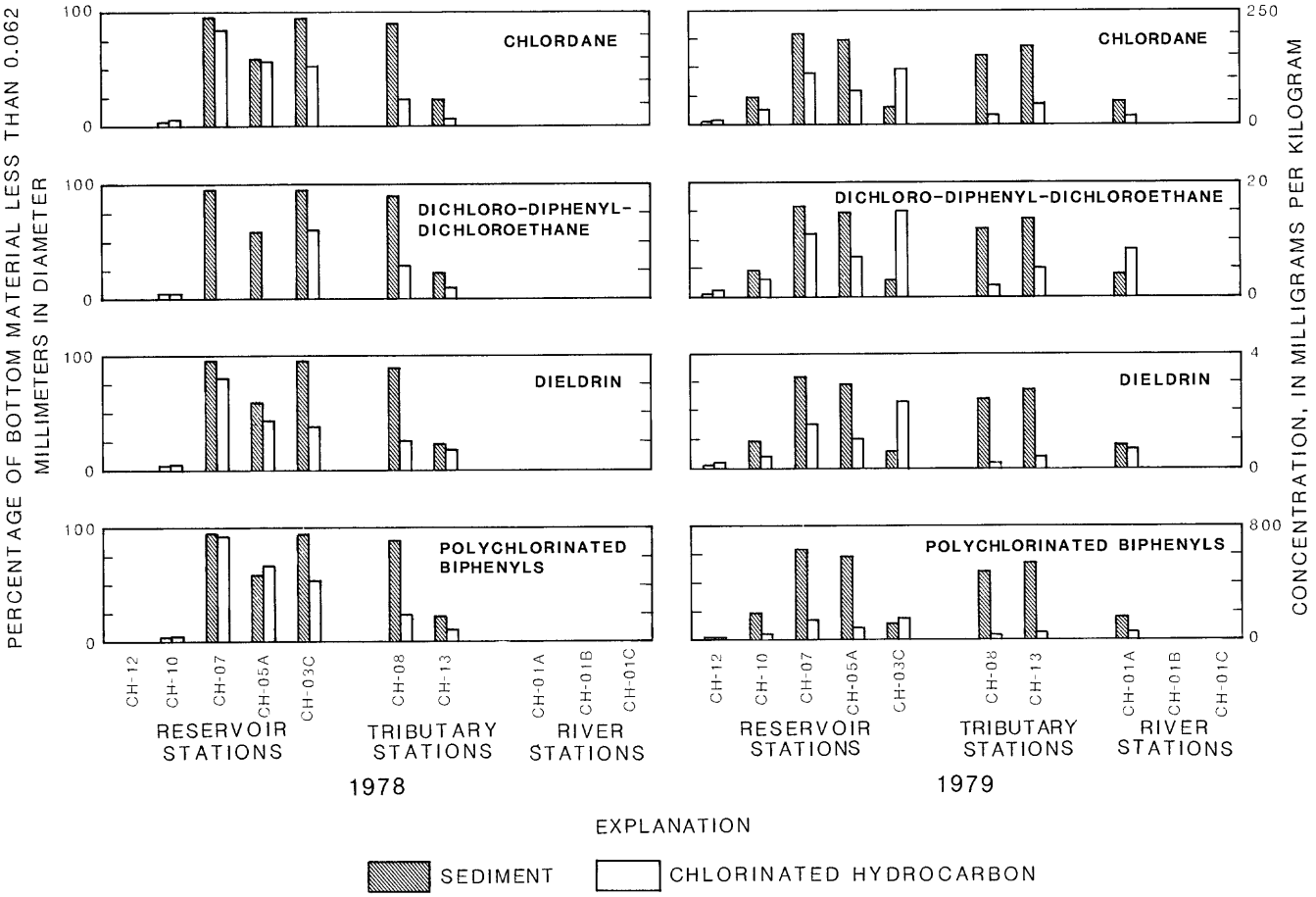

Figure 11. Percentage of silt and clay (particles less than 0.062 mm in diameter) in bottom material and concentrations of selected chlorinated hydrocarbons in bottom material from West Point Reservoir and downstream river sites.

were substantially smaller than the minimum size permitted for legal possession. If legal or larger than legal sized fish had been collected, it is probable that greater concentrations of these hazardous substances would have been found in the tissues.

SUMMARY AND CONCLUSIONS

Water-quality, bottom-material, and fish-tissue samples were collected from West Point Reservoir to determine whether water-quality problems have resulted from subsequent impoundment. Water-quality and bottom-material samples were also collected in the Chattahoochee River downstream from the dam to determine the impact of impoundment on river-quality conditions during thermally stratified and unstratified periods.

Significant concentrations of total iron, total manganese, total phosphorus, total organic carbon, and volatile solids in bottom material occurred in the lentic section of the reservoir and at the tributary stations, where silts and clays constitute most of the bottom material. PCB's and chlordane concentrations in the bottom material were also relatively high in this section of the reservoir.

Young bullhead catfish and largemouth bass tissue samples (both whole fish and fillet) analyzed for chlorinated hydrocarbons showed significant amounts of chlordane and PCB's. Concentrations in several of the whole-fish samples far exceeded the maximum recommended PCB limit of 500 μg/kg. It is important to note, however, that these samples were from fish substantially smaller than the minimum size permitted for legal possession. Because these substances are highly persistent, larger fish would probably contain even greater concentrations.

The lentic section of the reservoir showed the greatest biological activity in terms of plankton standing stock, adenosine triphosphate concentration, and chlorophyll production. The dominant plankton groups, in terms of numbers per unit volume, were blue-green algae and rotifers.

Algal-growth-potential assay data showed that the availability of nutrients decreased in response to increases in phytoplankton concentrations from the upper to the lower reaches of the reservoir. For example, the maxi-

Table 1. Chlorinated hydrocarbon and metals concentrations in fish tissues from tributaries in West Point Reservoir, 1978 and 1979

[Chlorinated hydrocarbon concentrations in micrograms per kilogram; metal concentrations in micrograms per gram; *, no recommended maximum concentration; < (combined with number), less than the detection limit; +, insufficient sample for analysis]

	Wehadkee Creek					Yellowjacket Creek					Recommended maximum concentration[1]
	Whole bass	Whole catfish		Bass fillet	Catfish fillet	Whole bass	Whole catfish		Bass fillet	Catfish fillet	
	1979	1978	1979	1979	1979	1979	1978	1979	1979	1979	
Chlorinated hydrocarbons											
Aldrin	<0.1	<0.1	<0.1	<0.1	<0.1	<0.1	<0.1	<0.1	<0.1	<0.1	100
BHC, total	<.1	<.1	<.1	<.1	<.1	<.1	<.1	<.1	<.1	<.1	100
Chlordane	7.0	15	220	<.1	6.0	21	210	280	26	220	100
DDD	<.1	8.5	20	<.1	1.7	3.4	34	21	.5	18	1,000
DDE	6.5	8.5	20	<.1	5.7	8.9	15	49	.8	36	1,000
DDT	<.1	<.1	<.1	<.1	<.1	1.0	<.1	8.3	.4	1.5	1,000
Dieldrin	<.1	.4	3.6	<.1	<.1	.8	2.9	13	1.0	5.8	100
Endosulfan	<.1	<.1	<.1	<.1	<.1	<.1	<.1	<.1	<.1	<.1	100
Endrin	<.1	<.1	<.1	<.1	<.1	<.1	<.1	1.0	<.1	.7	100
Heptachlor	<.1	<.1	<.1	<.1	<.1	<.1	<.1	1.6	<.1	1.7	100
Heptachlor epoxide	<.1	.5	1.3	<.1	<.1	<.1	<.1	<.1	<.1	<.1	100
Polychlorinated biphenyls (PCB)	37	2,600	290	<.1	19	46	3,800	340	39	170	500
Polychlorinated naphthalenes (PCN)	<1	<1	<1	<1	<1	<1	<1	<1	<1	<1	*
Perthane	<.1	<.1	<.1	<.1	<.1	<.1	<.1	<.1	<.1	<.1	100
Toxaphene	<.1	<.1	<.1	<.1	<.1	<.1	<.1	<.1	<.1	<.1	100
Metals											
Arsenic, total	+	.2	<.1	+	+	<.1	.1	<.1	<.1	<.1	*
Cadmium, total	+	.05	<.01	+	+	<.01	.05	<.01	<.01	<.01	200
Chromium, total	+	.5	.3	+	+	.8	.5	.4	<.1	.3	*
Lead, total	+	.38	.20	+	+	.20	.35	.20	10	.10	*
Mercury, total	+	<.1	<.1	+	+	<.1	<.1	<.1	<.1	<.1	*
Selenium, total	+	<1	<1	+	+	<1	<1	<1	<1	<1	*
Zinc, total	+	12	22	+	+	16	15	180	2	10	*

[1]National Academy of Sciences (1974).

mum algal growth potential value was obtained at the uppermost data-collection station at Franklin, Ga., whereas the minimum value was recorded at the dam pool station. The Algal Assay Procedure: Bottle Test identified nitrogen as the primary growth-limiting nutrient in the lotic section and phosphorus as the primary growth-limiting nutrient in the lentic section during stratified periods. Addition of phosphorus in the presence of excess nitrogen appeared to support growth to its maximum. Even though the AGP assay identified nitrogen as the limiting nutrient in the lotic section, light limitation and relatively rapid water movement are probably the primary causes for limited algal biomass in this section of the reservoir.

Water-quality data show that severe hypolimnetic oxygen deficiency developed in the reservoir after thermal stratification was established in the spring of both 1978 and 1979. This environment favored the release of iron, manganese, phosphorus, and other constituents from the sediments. During periods of thermal stratification, the release water from West Point Reservoir consistently exceeded the limits of water-quality standards and (or) criteria for iron, manganese, and dissolved-oxygen concentrations at the data-collection stations immediately downstream from the reservoir. The primary influence of the reservoir on downstream river water quality could be attributed to seasonal changes in the chemical nature of the water column at the dam pool, resulting from thermal stratification and dissolved-oxygen depletion.

Physical and chemical differences between minimum and maximum daily release water were, for the most part, negligible because the difference in altitude of the intakes for the main and service turbines is only 1.52 m. Most of the differences that were found resulted from physical and chemical changes of the water occurring immediately after release from the reservoir.

REFERENCES CITED

Cherry, R.N., 1961, Chemical quality of water of Georgia streams, 1957–58: Georgia Geological Survey Bulletin 69, 100 p.

Cherry, R.N., Faye, R.E., Stamer, J.K., and Kleckner, R.L., 1978, Summary report of the intensive river-quality assessment, upper Chattahoochee River basin: U.S. Geological Survey Circular 811, 47 p.

Faye, R.E., Carey, W.P., Stamer, J.K., and Kleckner, R.L., 1978, Erosion, sediment discharge, and channel morphology in the upper Chattahoochee River basin, Georgia: U.S. Geological Survey Open-File Report 78–576, 133 p.

National Academy of Sciences, National Academy of Engineering, 1974, Water-quality criteria, 1972: Washington, D.C., U.S. Government Printing Office, 549 p.

National Research Council, 1977, Drinking water and health: Washington, D.C., National Academy of Sciences, 939 p.

Shoaf, W.T., and Lium, B.W., 1979, Phytoplankton, seston, cellular contents and bioassay methods, *in* Greeson, P.E., Ehlke, T.A., Irwin, G.A., Lium, B.W., and Slack, K.V., eds., A supplement to—Methods for collection and analysis of aquatic biological and microbiological samples: U.S. Geological Survey Techniques of Water-Resources Investigations, Book 5, Chapter A4, 332 p.

Stamer, J.K., Cherry, R.N., Faye, R.E., and Kleckner, R.L., 1978, Magnitudes, nature, and effects of point and nonpoint discharges in the Chattahoochee River basin, Atlanta to West Point Dam, Georgia: U.S. Geological Survey Open-File Report 78–577, 105 p.

U.S. Army Corps of Engineers, 1975, Water resources development by the U.S. Army Corps of Engineers in Georgia: Atlanta, Ga., U.S. Army Corps of Engineers, South Atlantic Division, 105 p.

U.S. Environmental Protection Agency, 1971, Algal assay procedure—Bottle test: Corvallis, Oreg., National Eutrophication Research Program, 82 p.

Aqueous Geochemistry of the Bradys Hot Springs Geothermal Area, Churchill County, Nevada

By Alan H. Welch *and* Alan M. Preissler

Abstract

The aqueous geochemistry of the Bradys Hot Springs geothermal system has been examined to evaluate the source of recharge to the system, the thermal aquifer temperature, and the geochemical controls on the major and selected minor constituents in the thermal water.

The Bradys Hot Springs geothermal area is associated with a typical mountain-bounding fault in the Basin and Range province. The area is the discharge part of a thermal system that currently (1985) supplies heat for a commercial food-dehydration plant. The hottest water sampled at Bradys Hot Springs contains about 2,600 milligrams per liter of dissolved solids dominated by sodium, chloride, and sulfate. Chemical geothermometer data indicate thermal-aquifer temperatures ranging from 137 to 184 °C, although a measured down-hole temperature of 212 °C has been reported. Local meteoric water that has been concentrated by evaporation is the likely source of recharge to the thermal system. The primary controls on the dissolved-solids content of the thermal water (heated, deeply circulating ground water) apparently are evaporative concentration before recharge to the thermal aquifer and an increase in silica during passage through the thermal aquifer. Evaporative concentration and mineral solubility appear to be the primary controls on the minor constituents. Bromide is controlled primarily by evaporative concentration. Barium, fluoride, lead, and manganese concentrations may be controlled by mineral solubility. Lithium and, to a lesser extent, boron and strontium are more concentrated in the thermal water than in the local nonthermal water with the same chloride concentrations; these elements thus may be useful indicators of thermal water in the vicinity of Bradys Hot Springs when used in conjunction with chloride data.

INTRODUCTION

Objectives and Scope

This report considers the aqueous geochemistry of the Bradys Hot Springs geothermal area; it is an extension of a reconnaissance study (1981) of the Bradys area and several other geothermal areas in northern Nevada by Olmsted and others (1975). The overall objective of this effort is to analyze geochemical data to gain a better understanding of the nature of the Bradys Hot Springs geothermal system. Specific objectives include an attempt to determine the source and general chemical character of recharge to the system, the aquifer temperature, and the geochemical controls on major and minor constituents of the thermal water.

Previous Studies

Sources of data on the geothermal resources of Bradys Hot Springs are presented in Olmsted and others (1973, p. 14, 15) and Garside and Schilling (1979, p. 6, 7). Development and history of the geothermal resource is discussed by Olmsted and others (1975, p. 206–227), Rudisill (1978), and Garside and Schilling (1979, p. 6–11). Chemical analyses of water samples collected in the Bradys Hot Springs area are published in Clarke and Chatard (1884, 1 analysis, p. 24), Harrill (1970, 6 analyses, p. 27), Garside and Schilling (1979, 10 analyses, p. 83), Nehring and others (1979, 1 partial analysis along with isotopic data), and Benoit and others (1982, 4 analyses, p. 55). Evaluations of the chemical data include estimations of the aquifer temperatures (Nehring and Mariner, 1979; Nehring and others, 1979; Olmsted and others, 1975, p. 217) and a comparison between the Bradys Hot Springs and Desert Peak thermal systems (Benoit and others, 1982, p. 56). The geology of the adjacent Hot Springs Mountains is presented by Hiner (1979), Voegtly (1981), and Benoit and others (1982, p. 54–57). An evaluation of the energy available from the Bradys Hot Springs system has been made by Brook and others (1979, p. 52, 53).

Methods of Investigation

Ground-water sampling for geochemical characterization was the primary field activity during this study. Complementary geologic, geophysical, and hydrologic data also were collected as part of a broader U.S. Geological Survey evaluation of the geothermal system (1981). Much of these data were derived from wells drilled specifically for the hydrologic study. Table 1 presents records of selected wells in the Bradys Hot Springs and nearby Desert Peak areas.

Table 1. Records of selected wells in the Bradys Hot Springs and Desert Peak areas
[--, no data]

Well[1]	Land-surface altitude (ft)	Height of measuring point above land surface (ft)	Depth of screen[2] (ft below land surface)	Casing diameter (in)	Water-level depth below land surface (ft)	
					Jan. 1975	Feb.-April 1981
Bradys Hot Springs area						
AH–1	4,073	2.3	69.5–71.5	1.5	6.40	8.18
AH–2	4,076	1.9	139.8–141.8	1.5	7.84	9.55
AH–4	4,058	2.0	68.6–70.1	1.5	9.65	9.05
AH–5	4,104	2.0	101.6–103.1	1.5	44.50	45.16
AH–8	4,081	.8	116.1–117.8	1.5	27.59	28.04
AH–9	4,052	2.0	59.5–61.0	1.5	5.94	5.12
DH–15	4,121	3.8	58.5–60.0	1.5	17.09	34.47
DH–16	4,101	5.0	44.7–46.2	1.5	11.75	29.60
DH–17	4,075	2.8	143.8–145.3	1.5	10.93	11.79
AH–18	4,087	3.0	47.6–49.1	1.5	22.51	23.43
AH–20	4,101	2.5	86.7–88.2	1.5	36.42	43.66
M–8	[3]4,110	—	[4]610–800	—	—	—
B–1	[3]4,140	—	(1,758)	—	—	—
B–4	[3]4,120	—	(723)	—	—	—
Desert Peak area						
DH–31	4,091	2.5	133.2–134.7	2.0	30.45	31.70
B21–2[5]	[3]4,600	—	—	—	—	—

[1]Wells with AH and DH prefixes were augered (AH) or drilled by the mud-rotary technique (DH) by the U.S. Geological Survey. Private well M–8 is a production well at Bradys Hot Springs. Wells B–1 and B–4 are located in the general vicinity of B–8. Well B21–2 was drilled by Phillips Petroleum Company in the Desert Peak geothermal area.

[2]Values in parentheses represent the total depth of the well.

[3]Approximate altitude.

[4]Production depth from Rudisill (1978, p. 219).

[5]Benoit and others (1982, p. 50) indicate that the production is largely from zones more than 2,894 ft below land surface. Total well depth is 3,192 ft.

Geochemical data were collected by obtaining water samples from wells and measuring selected unstable constituents and properties (temperature, pH, carbonate, and bicarbonate) in the field. Before sampling, the wells were pumped or bailed in an attempt to assure that the water samples were representative of the native ground water. Very slow flow to several of the wells did not allow bailing immediately before sampling. These wells (AH–1, –9, and –31) were sampled as much as one month after bailing. The silica values for wells AH–1, –9, and –31 (table 2) may be low as a result of chemical changes within the well during the period between bailing and sampling. The overall conclusions presented here, however, do not depend solely on the analyses from wells AH–1, –9, and –31.

Temperature, pH, and alkalinity were measured in the field. Alkalinity (reported as bicarbonate and carbonate) and pH were measured by using the methods described by Wood (1976, p. 12–18). Bicarbonate and carbonate were determined on filtered samples (0.45-μm pore size). The pH measurements were made on unfiltered samples. Filtered, acidified samples were collected for cation analysis, whereas filtered but unacidified samples were collected for anion and isotopic analysis. Samples for silica analysis were filtered and then diluted with deionized water to prevent polymerization where oversaturation with respect to silica was indicated by preliminary field measurements. Samples collected for determination of major and minor constituents were placed in plastic bottles, whereas the isotope samples were placed in glass bottles. Records of selected wells (table 1) and chemical and isotopic data (table 2) for the Bradys Hot Springs area are in the U.S. Geological Survey computer-based storage system WATSTORE. These data, along with

other chemical analyses and ground-water information, may be retrieved by using a latitude/longitude polygon that includes the area represented in figure 5.

Acknowledgments

We thank Robert H. Mariner of the U.S. Geological Survey for allowing the use of previously unpublished geochemical data and Marvin Dommer of Geothermal Food Processors, Inc., for information on the operation of the facility at Bradys Hot Springs. Yousif K. Kharaka of the U.S. Geological Survey graciously supplied a modified version of the program SOLMNEQ and ideas on its use. Franklin H. Olmsted of the U.S. Geological Survey contributed ideas, information, and encouragement—all of which are greatly appreciated.

GEOLOGIC AND HYDROLOGIC SETTING

Bradys Hot Springs is in the western Basin and Range province, on the northwest flank of the Hot Springs Mountains about 50 mi east of Reno, Nev. (fig. 1). The Basin and Range province is characterized by east-west crustal extension; this structural activity has caused normal faulting along with siliceous and basaltic volcanism throughout much of the Hot Springs Mountains and adjacent areas. The surface distribution of geologic units is shown in figure 2. Tertiary sedimentary rocks in the area include sandstone, shale, tuff, diatomite, and limestone (Olmsted and others, 1975, p. 207). Deposits associated with the late Pleistocene Lake Lahontan consist primarily of clay, silt, and sand. Coarse-grained alluvial-fan deposits, stream gravels, and fine-grained playa deposits of Holocene age are all present in the Bradys Hot Springs area (Olmsted and others, 1975, p. 208, 209).

The geothermal activity, localized along a north-trending fault zone of unknown displacement (figs. 2, 3), has affected the surficial geology. Hot-spring and fumarole activity has resulted in the formation of predominately opaline sinter along a main fault and a smaller, subsidiary fault (W.A. Oesterling and R.J. Anctil, Southern Pacific Co., written commun., 1983). Geothermal alteration products consist of "tufa, sinter, salts, silification of rocks, oxidation of metallic elements to orange, yellow, and white deposits, [and] formation of kaolinite" (Olmsted and others, 1975, p. 211). Cinnabar and sulfur deposits have been reported by Bailey and Phoenix (1944, p. 51), and anomalously high mercury concentrations have been found around active steam vents (Garside, 1979).

The climate in the study area and vicinity is arid with diurnal and seasonal temperature extremes. Precipitation, in the form of rain and snow falling directly on the valley floors, generally provides little or no recharge to local ground-water systems. Ground-water recharge to nonthermal ground-water systems in the area is generally attributed to direct infiltration in mountain blocks and to infiltration from streams as they debouch onto alluvial fans. Recharge mechanisms have generally not been well defined for geothermal systems in northwestern Nevada. Recharge to geothermal systems has been attributed to direct infiltration in mountains and recharge to range-bounding faults (Welch and others, 1981). Recent work by Olmsted and others (1984) suggests that recharge to the Soda Lakes and Upsal Hogback geothermal systems in the western Carson Desert (fig. 1) can also be derived from shallow ground water in valley-fill deposits.

Ground water generally moves southwestward in valley-fill deposits of the Bradys Hot Springs area (Harrill, 1970, p. 10). Underflow from the north supplies much of the ground water to the study area (Harrill, 1970, p. 10, pl. 1). This underflow presumably is supplemented by small amounts of recharge from local precipitation in the surrounding mountains. Natural outflow in the valley-fill deposits occurs as underflow to the southwest and evaporation from the surface of the alkali flat (or playa) located to the northwest of Bradys Hot Springs and as transpiration from phreatophytes that surround the playa (Harrill, 1970, p. 10, 19, pl. 1). In the consolidated sedimentary and volcanic rocks, ground water moves primarily through fractures. Vertical fractures locally may allow significant recharge to the geothermal system from overlying valley-fill deposits. Unfortunately, the sites of such recharge cannot be ascertained from the limited hydrologic information available.

The general directions of shallow ground-water movement in the vicinity of Bradys Hot Springs are indicated by the configuration of the water table (fig. 4). Westward movement of thermal ground water that has risen from depth along the thermal fault zone is indicated by the steeply sloping water-table surface west of the fault.

Enhanced vertical permeability due to fracturing is indicated by the correlation between (1) the location of fumarole and spring deposits along the fault and (2) changes in water levels along the fault caused by fluid withdrawal (fig. 5). The decline in water levels is believed to have resulted primarily from the combined discharge from production and flow tests between late 1978 and early 1981. Discharge from one production well began in October 1978 for dehydration of vegetables, and two other wells underwent long-term production tests (9 months and 3 months) in 1980 and early 1981 (Marvin Dommer, Geothermal Food Processors, Inc., oral commun., 1981). According to Dommer, the combined flow during the tests was 1,500 gal/min, as compared to a normal production rate of 750 gal/min. The control of the upflow portion of the system by the local faults was also

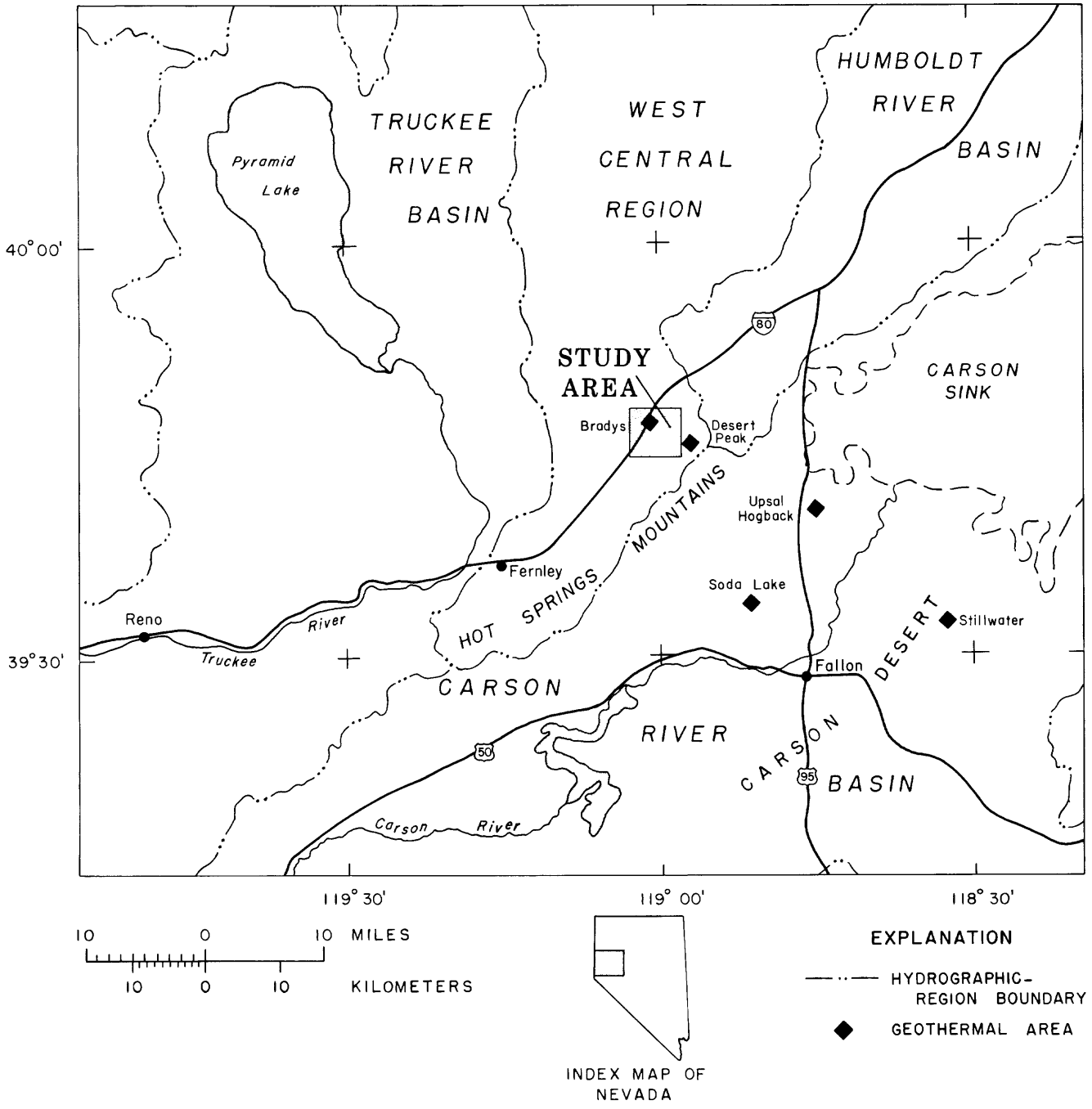

Figure 1. Location of the Bradys Hot Springs and other nearby geothermal areas.

noted by Rudisill (1978), on the basis of hydraulic data collected at wells B–1 and B–4 during a production test in 1977.

The hydrologic relationship between the Bradys Hot Springs area and the Desert Peak geothermal system, about 3 mi to the southeast, is not well understood. Although the water level in one thermal well in the Desert Peak system is more than 200 ft higher than the water level measured in Bradys thermal well DH–16, the equivalent cold-water head in the Desert Peak system is lower than the 3,900-ft altitude of the western Carson Desert (Frank Yeamans, Phillips Petroleum Co., oral commun., 1983; the equivalent cold-water head was calculated by using a temperature log and adjusting for the density differences caused by temperature). Thus, recharge to either system could be supplied by a system with a hydraulic head of less than 3,900 ft. As discussed later, geochemical considerations imply that saline water (which is commonly present in association with playas) could be the source of recharge to both systems.

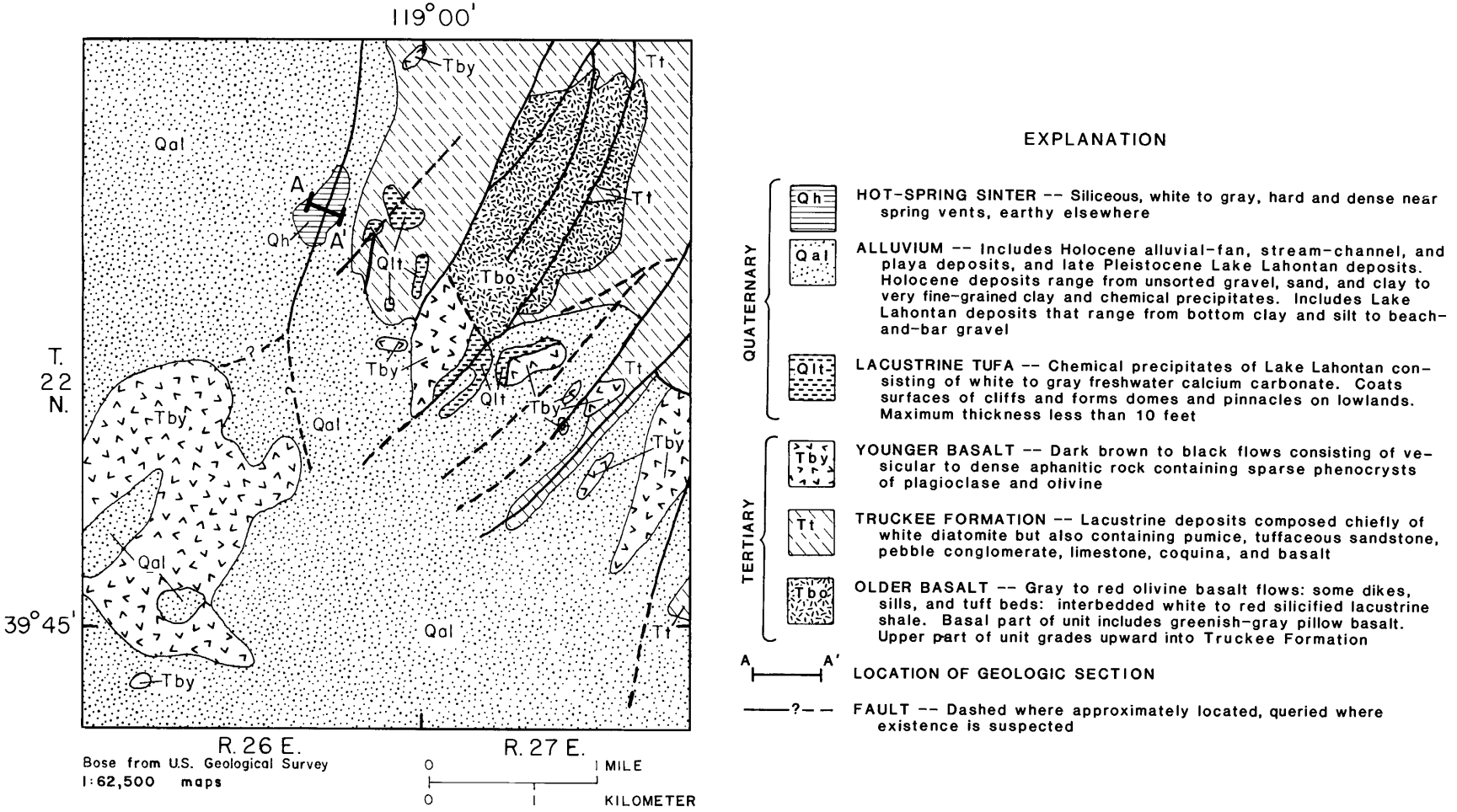

Figure 2. Generalized geology of the Bradys Hot Springs area. Modified from Voegtly (1981).

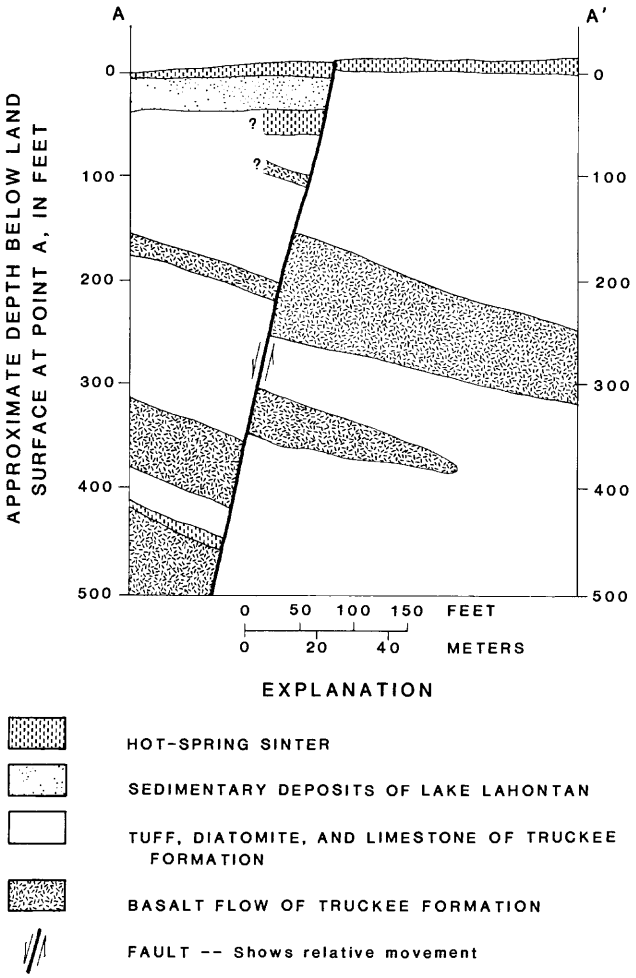

Figure 3. Geologic section across the unnamed fault at Bradys Hot Springs. Modified from Garside and Schilling (1979). Lateral extent of geologic units queried where uncertain.

AQUEOUS GEOCHEMISTRY

Major Constituents

Thermal water at Bradys Hot Springs contains about 2,600 mg/L of dissolved solids dominated by sodium, chloride, and sulfate, as indicated by the analyses of water from well M–8 (table 2). Chloride and sodium concentrations in the vicinity of Bradys Hot Springs[1] have narrow ranges of 910–1,100 mg/L and 660–850 mg/L, respectively, excluding the data for well AH–9. The higher values at well AH–9 (1,600 and 1,100 mg/L, respectively) may be a result of evaporative concentration of water moving downgradient from the hot area (fig. 4).

[1]Among wells listed in table 2, all but DH–31 and B21–2 are considered to be in the immediate vicinity of the hot-spring area (see fig. 4).

A modified version of the mineral-solution equilibrium program SOLMNEQ (Kharaka and Barnes, 1973) was used to evaluate the possible control exerted by mineral solubility on aqueous species in ground water of the study area. The program, which was supplied by Yousif K. Kharaka (U.S. Geological Survey, written commun., 1980) allows the user to calculate a pH at an elevated temperature by using a mass-balance assumption for the total H^+, as described by Kharaka and Mariner (1977, p. 72). The program also incorporates more recently developed methods for estimating aquifer temperatures. The mass-balance option was used to calculate the solution-mineral equilibria for each analysis at the measured down-hole temperature (this was required because the pH was measured at a lower temperature at land surface) and at the aquifer temperature indicated by the magnesium-corrected sodium-potassium-calcium geothermometer of Fournier and Potter (1979). [This geothermometer was selected because it is the least sensitive to mixing with nonthermal water (Fournier, 1977, p. 46).] However, some of the calculated temperatures (particularly at well AH–9) are probably too high. The results are included, nonetheless, because the calculations are useful in evaluating the effect of changes in temperature on mineral solubility. Following the suggestion of Paces (1972, p. 225, 226), if the value of log (AP/K) [the logarithm of the ratio of the activity product (AP) to the equilibrium constant (K) for a particular mineral] is between −0.5 and +0.5, then the water is regarded as being in equilibrium with the mineral considered. The activity product is obtained by multiplying the activities of the chemical species that form a particular mineral. For instance, the activity product for calcite ($CaCO_3$) is $[Ca^{2+}] \times [CO_3^{2-}]$, where the square brackets signify the activities of the component species.

The water in the vicinity of Bradys Hot Springs appears to be saturated with respect to calcite. As shown in figure 6, the samples are either near saturation [log (AP/K) between −0.5 and +0.5] or slightly oversaturated (greater than +0.5) with respect to calcite. A possible contributor to the total carbonate ($H_2CO_3 + HCO_3^- + CO_3^{2-}$) is CO_2 derived from the deep crust or upper mantle, as proposed for many tectonically active areas of the world by Barnes and others (1978). Part of the difference in pH between the water at producing well M–8 and at the other wells may be the result of greater CO_2 outgassing at the other wells. The pH of the water from well M–8 is probably affected by CO_2 outgassing before sampling as calcite precipitation occurs in the well (Garside and Schilling, 1979, p. 7).

The sulfate data show a wide range of values, but no mineral-equilibrium control is obvious. The sulfate concentration in the thermal water, as represented by the analysis for M–8, may be due in part to oxidation of sulfide minerals—a process that can generate hydrogen ions

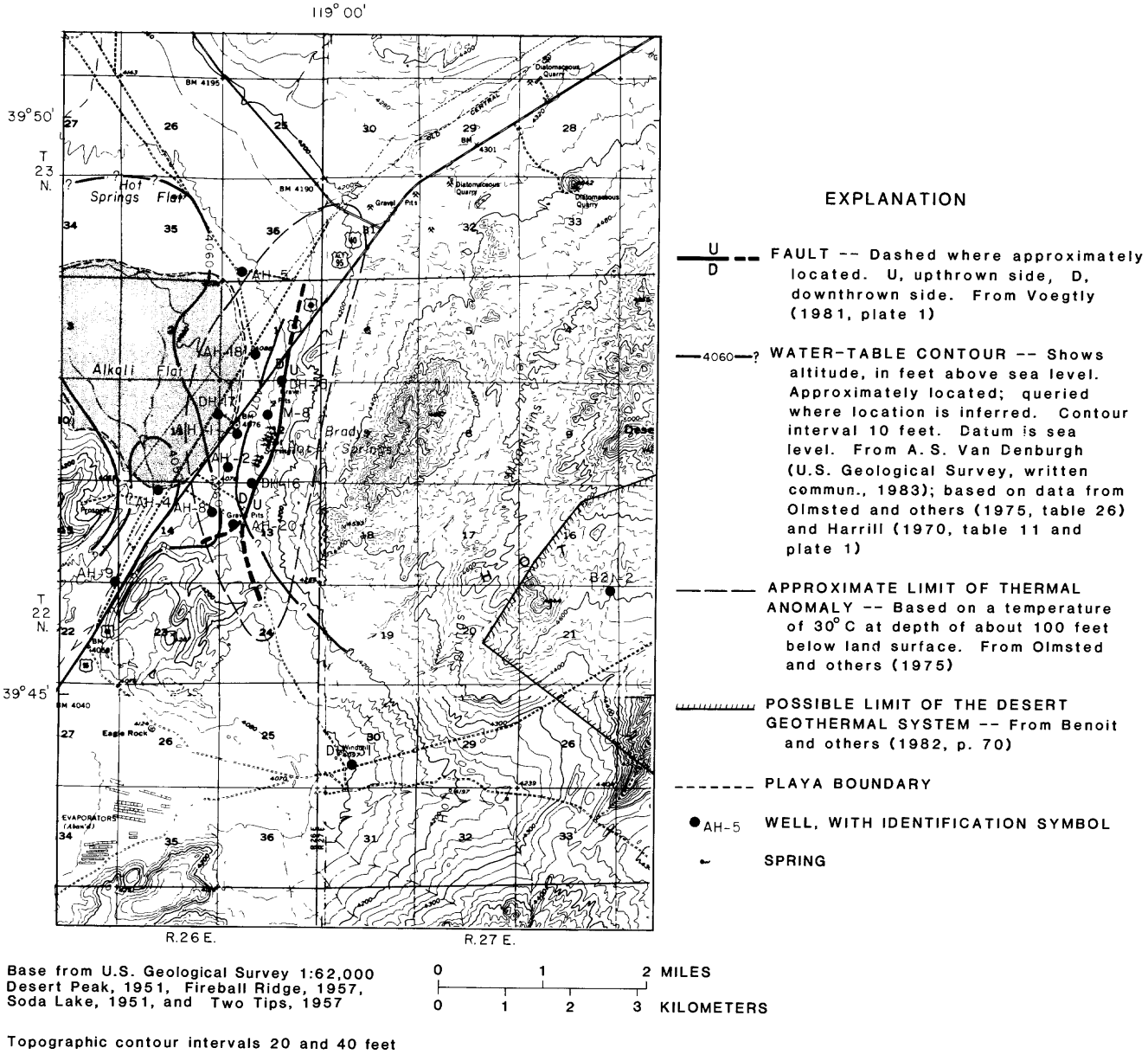

Figure 4. Approximate water-table altitude, 1969–73, and locations of wells.

(Hem, 1970, p. 162)—or to dissolution of gypsum in valley-fill or playa deposits.

The relationship between the Bradys Hot Springs and Desert Peak geothermal systems is considered by Benoit and others (1982). The thermal water of the Desert Peak system, as represented by the analysis of a sample from well B21–2, has a much higher chloride concentration than water of the Bradys Hot Springs system. [Data for well B21–2 are used for comparison because the sampling technique at this well was superior to that at the other two deep production wells in the Desert Peak system (Benoit and others, 1982, p. 54).] The difference in chloride concentrations indicates that the two systems do not have a common deep source of water unless it is modified in one or both systems.

The chloride concentration (4,200 mg/L) in water from well DH–31 is consistent with the proposal by Benoit and others (1982, p. 56) that some of the flow from the Desert Peak system moves to the west, with eventual discharge in the vicinity of a non-flowing dug well (well S34, T22N, R26E in table 5 of Benoit and others, 1982). At well DH–31, which is located between well B21–2 and the dug well discussed by Benoit and others (1982), the chloride concentration (4,200 mg/L) is

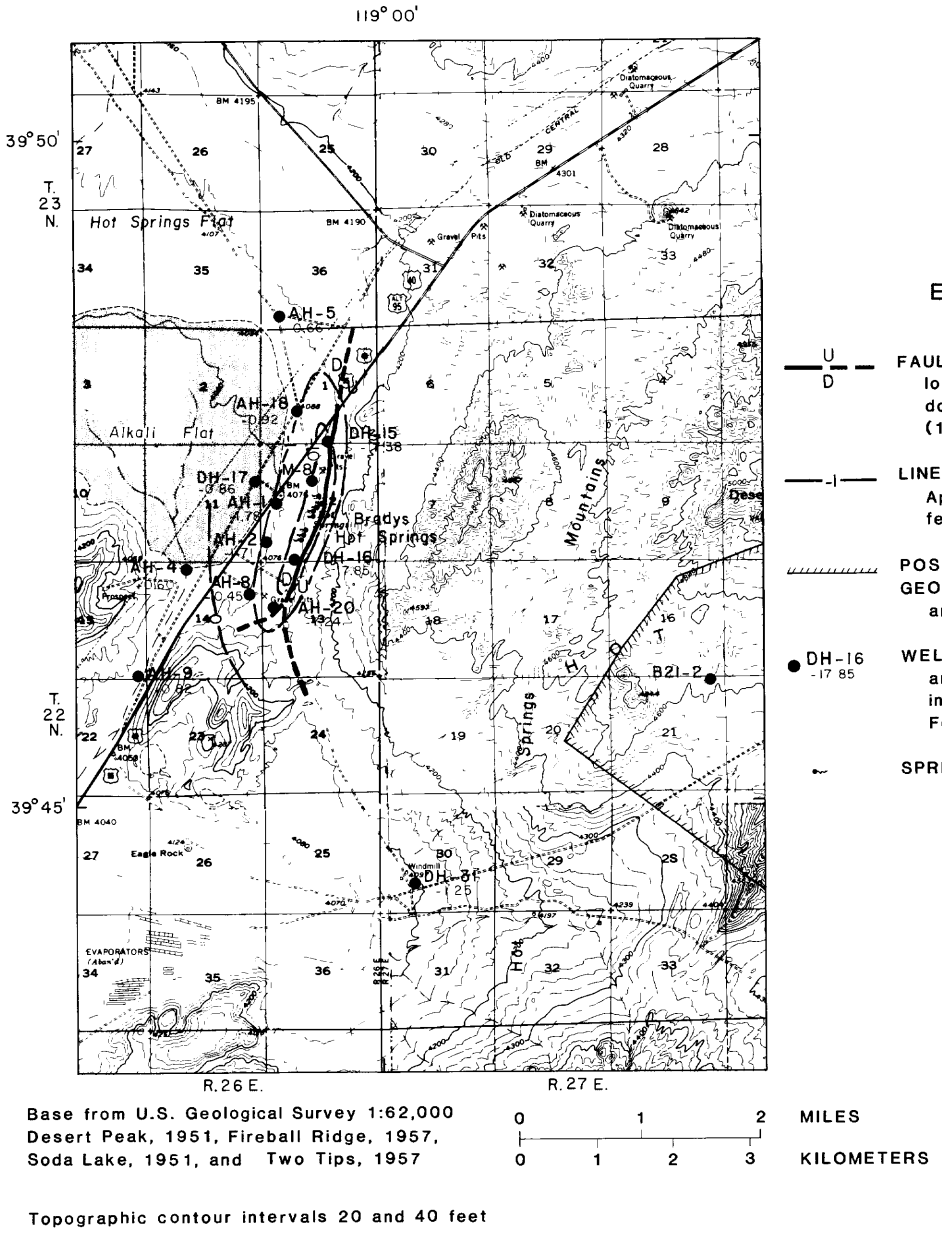

Figure 5. Changes in ground-water level between January 1975 and February 1981.

greater than that in water from well B21–2 (about 3,600 mg/L) and is therefore consistent with some vapor loss from the rising hot water in the Desert Peak system. The low silica at well DH–31 (17 mg/L) in comparison to B21–2 (350 mg/L) is presumably a result of silica precipitation due to cooling. The difference in sulfate of 7.0 mg/L at DH–31 compared to 90 mg/L at B21–2 is more difficult to explain but may, at least in part, be due to loss of H_2S after conversion of sulfate to sulfide. The ground-water flow direction indicated by water-level contours presented by Hiner (1979, p. 64) is also consistent with some of the outflow from the Desert Peak system moving to and past well DH–31.

Minor Constituents

Some minor constituents can be used as indicators of thermal fluids or are of environmental concern. Minor constituents examined in this study are barium, boron, bromide, fluoride, lead, lithium, manganese, and strontium. The concentrations of some of these constituents in the Bradys system appear to be controlled primarily by either evaporative concentration or the solubility of a solid phase (mineral). Bromide is largely controlled by evaporative concentration, whereas barium, fluoride, lead, and manganese appear to be controlled by solubility

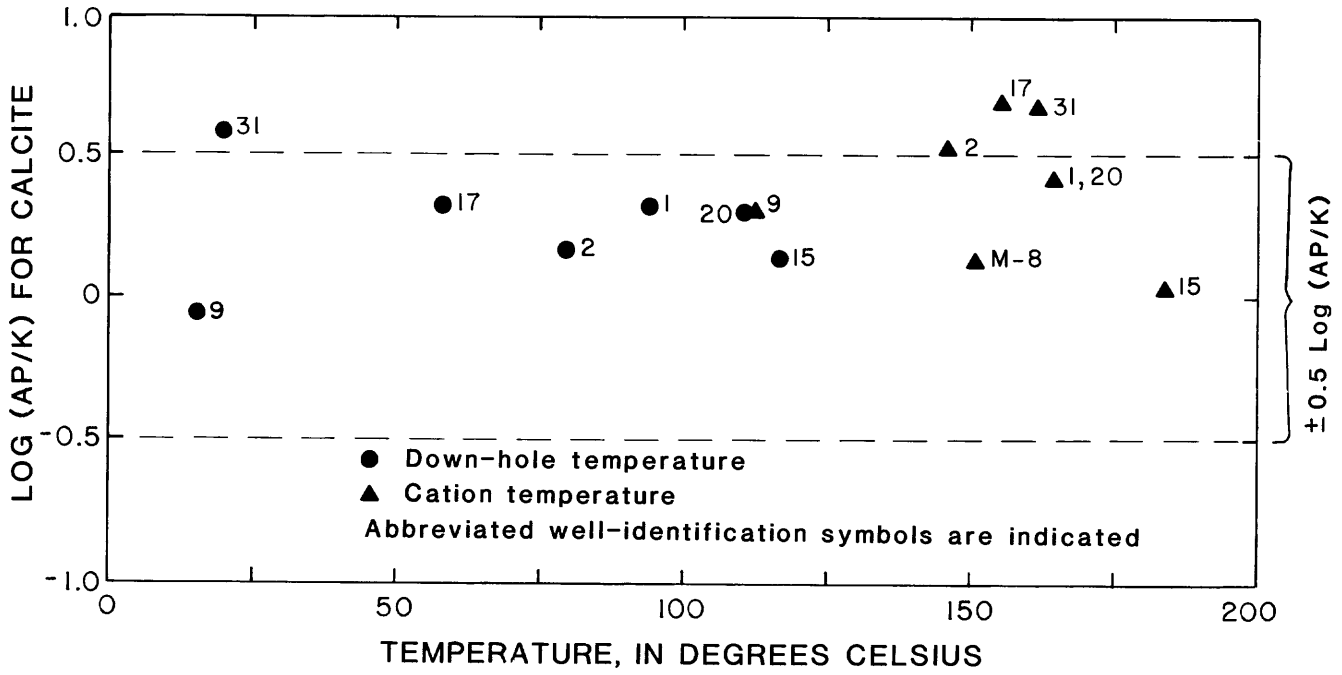

Figure 6. Values of log (AP/K) for calcite in well water at the down-hole temperature and at the magnesium-corrected Na-K-Ca geothermometer (cation) temperature (Fournier and Potter, 1979).

of the minerals barite, fluorite, cerussite, and rhodochrosite, respectively.

Barium concentrations at low temperatures may be controlled by barite ($BaSO_4$). Figure 7*A* indicates that all the samples collected from sources with temperatures less than 75 °C are near equilibrium with respect to barite. It is not known why water with source temperatures greater than 75 °C is undersaturated.

The fluoride concentrations appear to be controlled by the solubility of fluorite (CaF_2). Using the fluorite equilibrium relationship proposed by Nordstrom and Jenne (1977) and the program SOLMNEQ, we calculated a value for log (AP/K), which is plotted in figure 7*B* for each analysis included in this study. The log (AP/K) values calculated for fluorite at the measured, down-hole temperatures are all within the range from −0.5 to +0.5, indicating mineral-water equilibrium. This conclusion agrees with that of Mahon (1964) that fluorite is the controlling phase in thermal water. Using revised thermodynamic data, Nordstrom and Jenne (1977) concluded that fluorite is the controlling phase for fluoride in many thermal waters of the Western United States.

The three well waters that contain measurable lead concentrations (wells AH–1, AH–20, and DH–15) appear to be near saturation (saturation index range from −1.54 to 0.37) with respect to the carbonate mineral cerussite ($PbCO_3$). Only the divalent oxidation state (Pb^{2+}) was considered in the solubility calculations for lead. This approach is consistent with Hem's observation (1970, p. 205) that "over most of the water-stability region, the oxidation state of lead at equilibrium is $[Pb^{2+}]$ * * *."

Solubility of rhodochrosite ($MnCO_3$) may be the controlling factor for manganese concentrations in some parts of the study area (fig. 7*C*). Both of the most saline samples collected during this study (from wells AH–9 and DH–31) appear to be saturated with respect to rhodochrosite. Among the warmer well waters, those at the downgradient sites (wells AH–1, AH–2, and DH–17) appear to be controlled by rhodochrosite. In the solubility calculations, only the +2 valence state was considered for manganese. A dominance diagram presented by Hem (1970, p. 128) indicates that Mn^{2+} is the predominant aqueous species at redox potentials reasonable for the reducing to slightly oxidizing conditions probably present in the thermal waters being considered here.

The concentrations of bromide are strongly correlated with the chloride concentrations (fig. 8*B*) which, in turn, appear on the basis of the stable-isotope data to be largely controlled by evaporative concentration.

Boron, lithium, and strontium may be indicators of the presence of thermal water. Figure 8*A*, *C*, and *D* show that the lower temperature water from wells AH–4,

Table 2. Chemical and isotopic data for well waters in the Bradys Hot Springs and Desert Peak areas

[Results in milligrams per liter except as noted. All analyses by the U.S. Geological Survey Central Laboratory, Arvada, Colo., except as noted; --, no data measurement]

Name of well	Date of sample (yr–mo–day)	Temperature, water (°C)[1]	pH, field	Dissolved solids	Silica, dissolved (as SiO_2)	Calcium, dissolved (as Ca)	Magnesium, dissolved (as Mg)	Sodium, dissolved (as Na)	Potassium, dissolved (as K)	Bicarbonate, field (as HCO_3)	Carbonate, field (as CO_3)	Sulfate, dissolved (as SO_4)	Chloride, dissolved (as Cl)
Bradys Hot Springs area													
AH–1	1981–03–11	94.5	8.2	1,900	32	47	2.2	690	47	77	1	160	910
AH–2	1981–03–12	79.8	7.7	2,000	99	48	2.3	700	30	120	0	150	910
AH–4	1981–03–14	20.4	—	—	—	—	—	690	40	—	—	—	990
AH–5	1981–03–19	26.7	—	—	—	—	—	660	31	—	—	—	940
AH–8	1981–03–10	36.2	—	—	—	—	—	690	49	—	—	—	940
AH–9	1981–03–16	15.4	8.3	2,900	12	56	6.9	1,100	39	62	1	65	1,600
DH–15	1981–04–02	117	8.5	2,100	170	20	.2	720	53	66	1	170	930
DH–17	1981–02–20	58.0	8.0	2,300	110	56	2.6	780	42	170	1	67	1,100
AH–20	1981–03–17	111	7.9	2,100	120	46	1.4	670	39	86	0	150	980
M–8[3]	1979–07–06	>100	6.8	2,600	164	45	.3	850	36	111	0	320	1,100
Desert Peak area													
DH–31	1981–02–16	20.2	8.3	6,700	17	130	9.8	2,100	160	190	2	7.0	4,200
B21–2[4]	1978–03	160	—	6,800	350	100	<1	2,250	250	50	—	98	3,700
--------	1978–03	160	7.0	—	—	84	0.1	2,200	219	34	—	88	3,500

–5, and –9 generally plots below or to the right of the higher temperature water. This suggests that the higher boron, lithium, and strontium concentrations in the higher temperature samples may be a result of reactions occurring in the deep thermal aquifer. This conclusion is considered very tentative due to the very limited amount of data for nonthermal water.

Stable Isotopes[2]

With few exceptions, the stable-isotope composition of water from most geothermal systems has been found to reflect recharge of local meteoric water and modification by one or more physical or chemical processes (Truesdell, 1976, p. lx). The processes that can modify the initial isotopic composition are (1) exchange of oxygen with wall rocks, (2) mixing with cooler, local ground water, and (3) evaporation, either before recharge or in the upflow portion of a geothermal system.

The isotopic effect of exchange of oxygen with wall rocks, termed an "oxygen shift," is toward a heavier (less negative) value, as indicated in figure 9. Mixing of thermal water with cooler, local ground water will produce an isotopic composition intermediate between the two end members, with the exact composition being controlled by the mixing proportions. Evaporation results in a change in composition that is indicated in figure 9. The slope of the evaporation trend is controlled largely by the evaporation temperature.

The isotopic and chemical composition of thermal water in the Bradys Hot Springs system can be explained by the following sequence:

1. Meteoric water recharging a shallow ground-water system,
2. Evaporation affecting the shallow ground water,
3. Recharge to the thermal aquifer by ground water from the shallow system, and
4. Flow through the thermal aquifer, with discharge localized by faulting.

The isotopic composition of recharge to the local ground-water system (which would presumably be similar to that of the recharge to the thermal aquifer) could not be directly determined owing to a lack of wells and springs in local mountains or on the upper parts of alluvial fans (the assumed recharge areas). The estimated isotopic composition of recharge to the Bradys Hot Springs system, before it is affected by evaporation, is represented in figure 9 by field A, at the intersection of the arid-zone meteoric line and the local evaporation trend. The standard meteoric-water line in figure 9 generally

[2]The stable isotopes evaluated herein are oxygen-18, relative to oxygen-16, and deuterium (hydrogen-2), relative to hydrogen-1.

Table 2. Chemical and isotopic data for well waters in the Bradys Hot Springs and Desert Peak areas—Continued

Fluoride, dissolved (as F)	Bromide, dissolved (as Br)	Barium, dissolved (µg/L as Ba)	Boron, dissolved (µg/L as B)	Lead, dissolved (µg/L as Pb)	Manganese, dissolved (µg/L as Mn)	Strontium, dissolved (µg/L as Sr)	Zinc, dissolved (µg/L as Zn)	Lithium, dissolved (µg/L as Li)	Deuterium (D, in per mil)[2]	Oxygen-18 ($\delta^{18}O$, in per mil)[2]
					Bradys Hot Springs area					
6.6	1.4	160	3,400	93	150	1,700	800	1,600	−125.0	−14.65
5.0	1.5	110	4,100	<20	61	1,200	160	1,700	−126.0	−14.40
4.8	2.0	—	3,600	—	—	—	—	1,100	−127.0	−14.35
4.4	1.7	—	3,700	—	—	—	—	970	−123.0	−14.20
5.2	1.7	—	2,800	—	—	—	—	1,600	−123.0	−14.30
3.0	2.8	110	4,400	<30	830	940	1,500	1,100	−122.5	−14.00
6.2	1.6	60	4,400	56	18	1,300	100	1,800	−124.0	−14.20
2.9	1.6	240	4,300	<20	71	2,000	740	2,000	−125.5	−14.30
5.2	1.6	150	4,200	27	110	2,200	310	1,800	−125.5	−14.35
5.8	—	—	5,200	—	—	1,600	—	1,500	−121.2	−14.20
					Desert Peak area					
3.1	8.0	—	16,000	—	590	5,600	—	3,300	−113.5	−12.20
—	—	—	16,000	—	—	—	—	1,400	(5)	(5)
—	—	—	15,100	—	—	—	—	—	(5)	(5)

[1]For U.S. Geological Survey wells (all wells except M–8, and B21–2) measurements were made at midpoint of screen, winter 1975–76, by Franklin H. Olmsted, U.S. Geological Survey.

[2]Analyses were made under the supervision of Tyler B. Coplen, U.S. Geological Survey, Reston, Va. The δ values are defined as $\delta = [(R_x - 1)/R_{SMOW}] \times 1{,}000$, where R_x is the isotope ratio (deuterium/hydrogen-1 or oxygen-18/oxygen-16) of the sample and R_{SMOW} is the ratio for standard mean ocean water. A negative δ value indicates that the sample is isotopically lighter than the standard.

[3]Data from Robert H. Mariner (U.S. Geological Survey, written commun., 1981). Sample collected and processed in the same manner as described by Mariner and others (1974, 1975). An analysis of the gas phase indicates the following composition, in percent: $CH_4 = 2.63$, $CO_2 = 2.48$, $H_2 = 2.94$, $H_2S = <0.01$, $O_2 = <0.1$, Ar = 1.31, $N_2 = 90.14$, $C_2H_6 = 0.03$, He = 0.01, $SO_2 = <0.05$. This well was producing steam and water when sampled. Although no temperature was recorded during the sampling, it was doubtless well above 100 °C in the production zone. The pH was measured at 24 °C on a conductively cooled sample.

[4]From Benoit and others (1982, table 5; analyses by two laboratories, presumably on near-duplicate samples).

[5]Isotopic analyses (Benoit and others, 1982, table 7): March 16, 1977, $\delta D = -117.8$, $\delta^{18}O = -12.52$, and $\delta D = -115.1$, $\delta^{18}O = -12.8$ (two laboratories); March 17, 1977, $\delta D = -114.6$, $\delta^{18}O = -12.5$; Nov. 5, 1977, $\delta D = -116.0$, $\delta^{18}O = -12.9$; and Nov. 12, 1977, $\delta D = -115.6$.

represents a more humid climate; the arid-zone line provides a better estimate of recharge water in a climatic setting like that of the study area (Dansgaard, 1964).

The deuterium concentration in the water at the Bradys Hot Springs system appears to be a result of evaporation of shallow ground water as described by the Rayleigh distillation equation (Dansgaard, 1964). Further shallow evaporation of this same recharge could then form water that is the source of recharge to the Desert Peak system. Fractionation factors for deuterium calculated by using the method of Friedman and others (1976), which is based on the Rayleigh equation and the use of a conservative constituent, are very similar for the Bradys Hot Springs and Desert Peak systems. The values shown in table 3 were calculated on the basis of postulated recharge compositions and the assumption that chloride remains conservative during evaporation.

Although the fractionation factors (table 3) vary depending on the compositions used for the recharge, values calculated for the two systems are similar. Fractionation factors calculated for ground-water systems that have been affected by shallow evaporation in the Carson (Olmsted and others, 1984) and Black Rock Deserts (located about 100 miles north of Bradys Hot Springs, unpublished USGS data) are similar to those presented here, which indicates that values in the 1.002-to-1.005 range are not unreasonable for evaporation in ground water. This similarity of fractionation factors for the thermal and nonthermal water is taken as evidence that the same process (evaporation of shallow ground water) is primarily

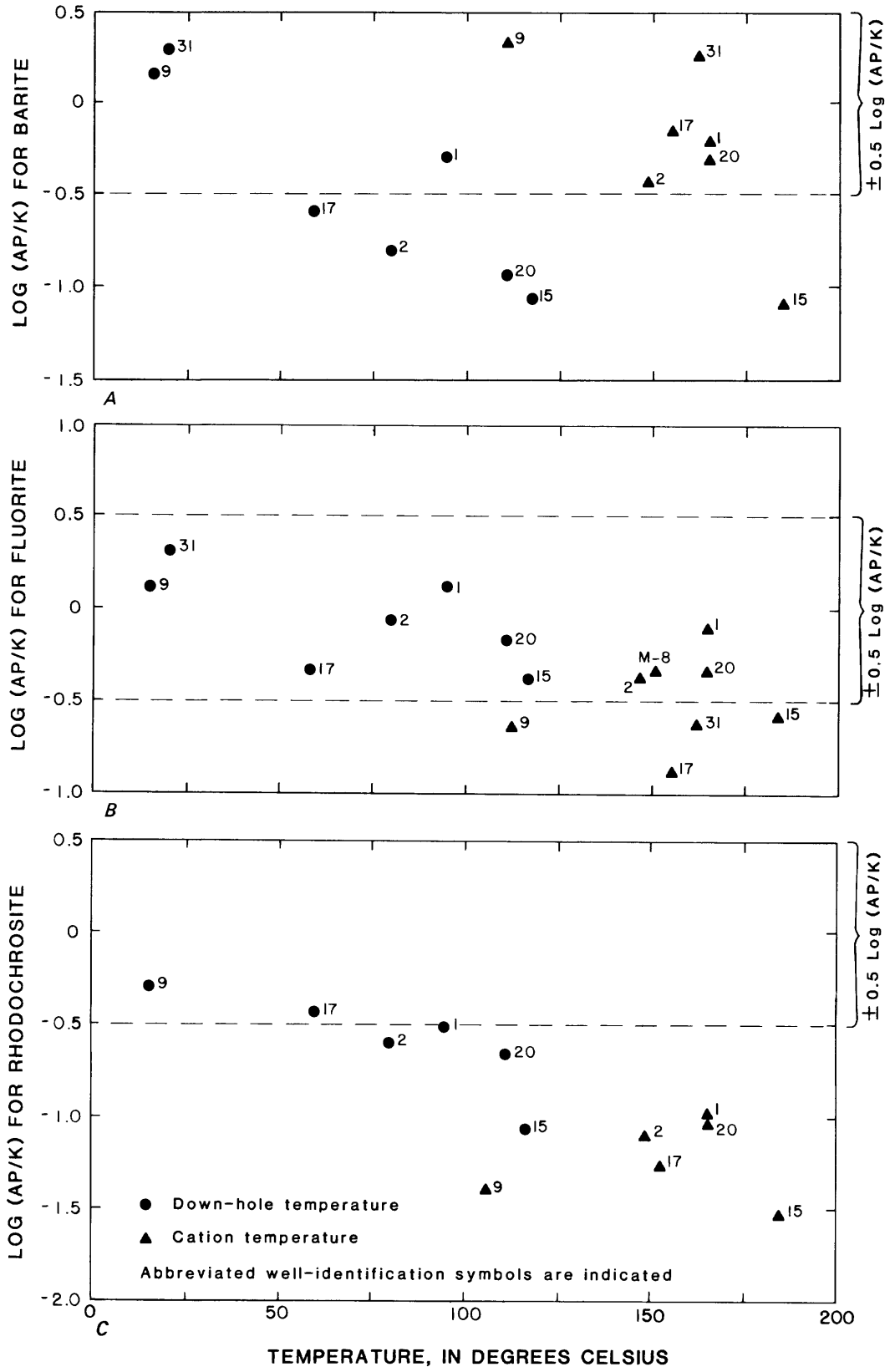

Figure 7. Values of log (AP/K) in well waters for (*A*) barite, (*B*) fluorite, and (C) rhodochrosite at the down-hole temperature and at the magnesium-corrected Na-K-Ca geothermometer (cation) temperature (Fournier and Potter, 1979).

Table 3. Apparent fractionation factors for deuterium based on estimated recharge chloride concentrations and isotope composition

Possible recharge compositions		
Recharge alternative	Chloride (mg/L)	Delta deuterium (per mil)
1	10	−128
2	50	−130
3	50	−135

Fractionation factors			
Well	Recharge alternative		
	1	2	3
Bradys Hot Springs well M–8	1.0016	1.0032	1.0051
Desert Peak well B21–2	1.0023	1.0038	1.0051

responsible for the increased deuterium and chloride concentrations. Although agreement between the calculated values and equilibrium laboratory determinations (Friedman and O'Neil, 1977) is poor, the similarity may indicate a single evolution path from recharge to Bradys Hot Springs to Desert Peak water. Thus, evaporation of a single meteoric water source may be the process responsible for the chloride concentrations and isotopic compositions of both the Bradys and Desert Peak systems.

The actual recharge area for the Bradys system is difficult to identify on the basis of the present information. One possible source of ground water that has been affected by evaporation is the western Carson Desert, east of the Hot Springs Mountains. This alternative is not supported by isotopic compositions indicated by recent sampling there by Olmsted and others (1984), however. As indicated in figure 9, ground water in the western Carson Desert is isotopically heavier than that seen in the present study area and, therefore, is not a good candidate for recharge.

Mixing of local meteoric water (with a composition as indicated by field A in fig. 9) with water from Desert Peak (field C) to form the observed composition at Bradys Hot Springs (field B) does not appear to be a viable possibility either. A mixture of about two parts Desert Peak water with one part meteoric water would form the approximate deuterium composition at well M–8, but the mixture would have a much higher chloride concentration (about 1,800 mg/L) than that observed (1,100 mg/L).

Accepting the arid-zone precipitation line as a good approximation of local rainfall, then if there is an oxygen shift at Bradys Hot Springs it is not more than 2 per mil. If evaporation is responsible for some of the departure from the initial isotopic composition (as discussed earlier), then the oxygen shift would be even less. A shift of 2 per mil is relatively small compared with that documented for some other thermal systems. The small shift may be due to a high ratio of water to wall-rock surface area, such as in a fractured-rock system. This is consistent with the obvious fault control present in the upflow part of the Bradys system. The small oxygen shift could also be related, at least in part, to a short fluid residence time, a modest deep-aquifer temperature, or both.

The water sampled at well DH–31 appears to have moved southwest from the Desert Peak system. Isotopes and chloride are consistent with an equilibrium fractionation factor for deuterium of about 1.04 (calculated by using average chloride and delta deuterium values for B21–2), which agrees with the experimentally determined value of 1.04 at about 75 °C (Friedman and O'Neil, 1977). [This fractionation factor also was calculated assuming that chloride is conservative in the aqueous phase, following the procedure presented by Friedman and others (1976).]

Geothermometry

Methods of estimating the temperature of a geothermal water have been developed that utilize both chemical and isotopic compositions. The most widely accepted methods, which are known as chemical geothermometers, are those based on silica concentrations and cation proportions. Estimates of aquifer temperature calculated by using several of these methods are listed in table 4.

Despite fairly good internal consistency among cation and silica geothermometer estimates for several well waters in the Bradys Hot Springs area, the estimates are all significantly lower than the highest reported temperature measurement. Garside and Schilling (1979, p. 147) indicate that a maximum down-hole temperature of 212 °C was measured in one well at Bradys. This is substantially higher than the Na-K-Ca (sodium-potassium-calcium) geothermometer estimate of 190 °C for well DH–15—the highest estimate listed in table 3 for the Bradys Hot Springs system. The difference may be a result of one or more of the following factors:

1. An inaccurately high reported temperature. The second highest down-hole temperature reported by Garside and Schilling (1979) is 188 °C, which is in much better agreement with the geothermometer estimates.
2. Mixing with nonthermal water.
3. Partial reequilibration of silica and cations, resulting in lower geothermometer estimates.
4. The possibility that 212 °C water was not sampled during this study. For water from well M–8 (probably the most reliable source of thermal water listed in table 4), the estimates range from 121 to 190 °C. The highest value, which is based on the gas geothermometer of D'Amore and Panichi (1980), is significantly higher than the other six estimates for well M–8.

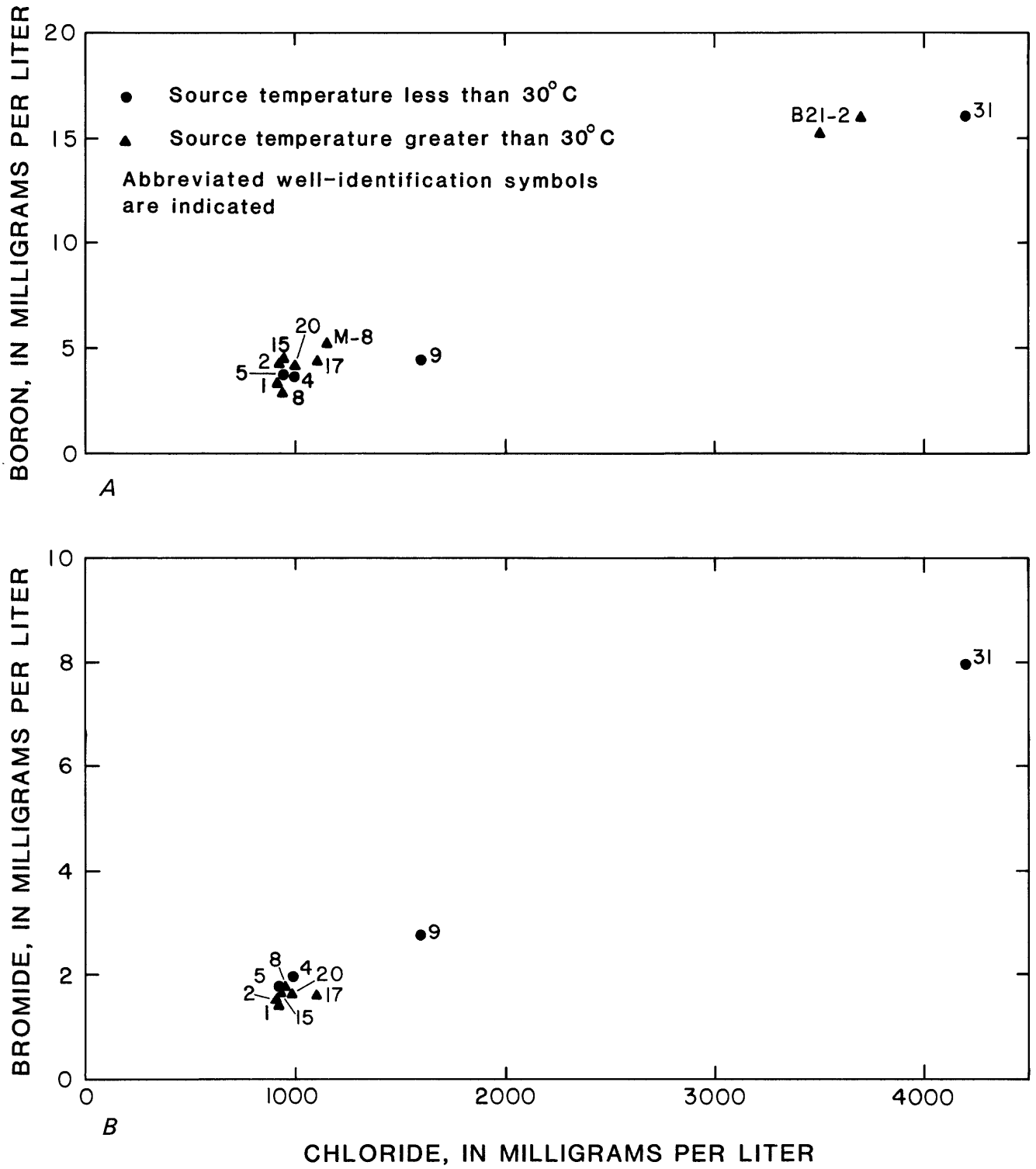

Figure 8. Relation between chloride and (*A*) boron, (*B*) bromide, (*C*) lithium, and (*D*) strontium in well waters.

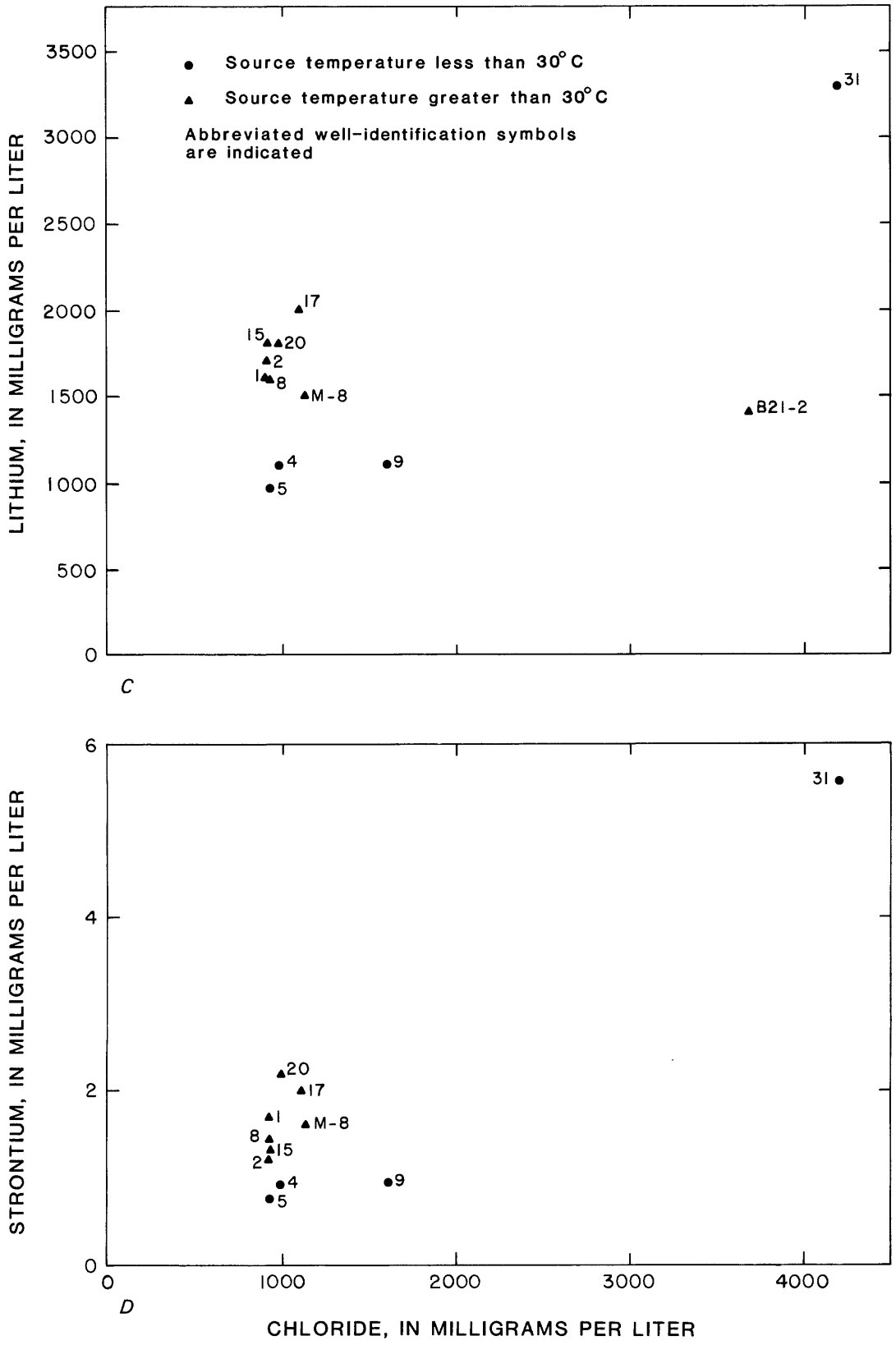

Figure 8. Continued.

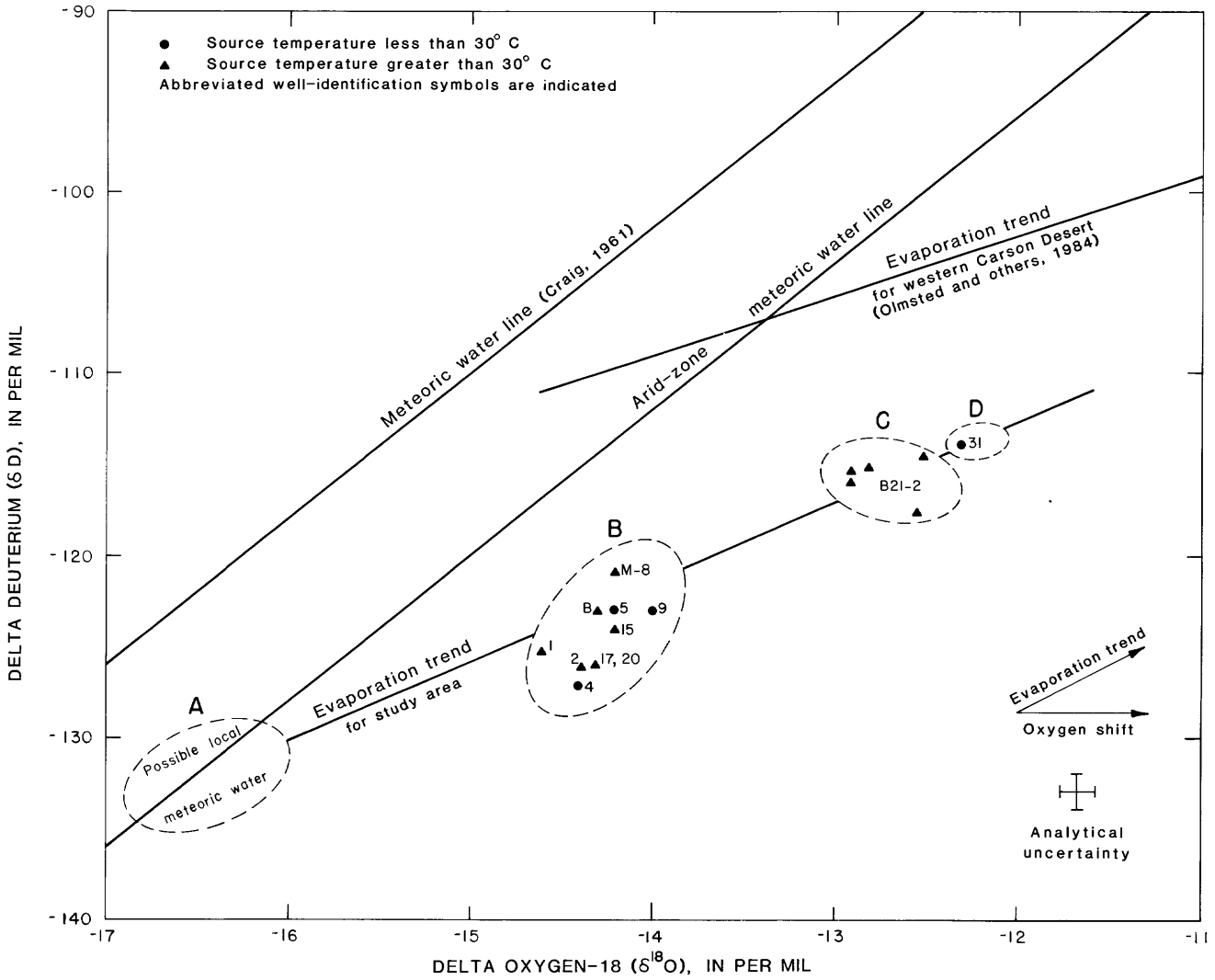

Figure 9. Stable-isotope composition of water in the study area. Dashed circles delineate ground-water fields having the following concentrations of chloride: A, assumed less than 50 mg/L; B, 910–1,600 mg/L; C, 3,500–3,700 mg/L; and D, 4,200 mg/L. Chloride concentrations and well locations given in table 2. Field B is Bradys Hot Springs area; fields C and D are Desert Peak area.

One technique for evaluating the internal consistency of temperature estimates, as discussed by Fournier and others (1979, p. 18–21), is to use a graphical comparison such as that shown in figure 10. The two geothermometer methods selected for comparison—conductive quartz and magnesium-corrected Na-K-Ca—are believed to be the best among the several silica and cation techniques. The conductive-quartz method was selected because the water at the sampling sites is believed to have been cooled conductively rather than adiabatically.

In general, agreement between the silica and cation values is fairly good for Bradys-area samples from wells with down-hole temperatures greater than 50 °C. The agreement is best for wells M–8, AH–2, DH–15, DH–17, and AH–20. On the basis of the internal consistency of the estimates for these five wells, a "best" estimate for the deep-aquifer temperature is a range from 137 to 184 °C. The poor agreement of this estimate with the reported down-hole measurement of 212 °C is difficult to reconcile but may be related to any of the four factors discussed earlier. Sampling of deeper wells and additional down-hole measurements would probably aid in finding the reason for this discrepancy.

The temperature estimates obtained for wells AH–1 and AH–9 probably represent either mixed or nonthermal water, although precipitation of silica (due in part to the unavoidable delay in sampling, discussed earlier) may be partly responsible for the poor agreement for the water at wells AH–1 and AH–9. The sampling problem is probably also, at least in part, responsible for the low temperatures estimated by using the silica geothermometer.

Table 4. Aquifer-temperature estimates for the Bradys Hot Springs and Desert Peak geothermal areas, based on chemical geothermometers

[Temperatures in degrees Celsius].

Well	Down-hole temperature[1]	Geothermometer method					Comments
		Silica[2]		Cation			
		Quartz, conductive	Quartz, adiabatic	Na-K[2]	Na-K-Ca[2]	Na-K-Ca, Mg-corrected[3]	
Bradys Hot Springs area							
AH–1	94.5	82	85	149	177	165	Thermal or possibly mixed water.
AH–2	79.8	137	132	122	154	147	Thermal water.
AH–9	15.4	45	53	112	151	112	Probable nonthermal or mixed water.
DH–15	117	169	159	154	190	184	Thermal water.
DH–17	58.0	143	137	135	166	155	Thermal water.
AH–20	111	148	142	140	169	165	Thermal water.
M–8[4]	>100	167	157	121	157	151	Hottest thermal water sampled.
Desert Peak area							
DH–31	20.2	57	64	157	195	162	Possibly related to the Desert Peak geothermal system.
B21–2	>100	222	202	196	222	215	Thermal water.

[1]See table 2.

[2]Fournier (1977) (Na, sodium; K, potassium; Ca, calcium).

[3]Fournier and Potter (1979) (Mg, magnesium).

[4]A sulfate-oxygen isotope geothermometer estimate of 165 °C is given by Nehring and others (1979, p. 7) for a conductively cooled sample. The gas geothermometer method of D'Amore and Panichi (1980) yields an estimate of 190 °C.

DISCUSSION OF RESULTS

The chemical and isotopic composition of water at the Bradys Hot Springs geothermal system can be explained by the following scenario: meteoric water is first concentrated by low-temperature evaporation then recharged to a deep, thermal aquifer. The low-temperature evaporation (as opposed to vapor loss due to boiling) is indicated by the relation between stable isotopes and chloride. In fact, the chloride concentration and isotopic compositions of water found in both the Bradys and Desert Peak systems could result from low-temperature evaporation of meteoric water with a low chloride concentration (less than 50 mg/L) and a deuterium isotopic composition in the general range from −128 to −135 per mil (as shown in fig. 9). In the northern Basin and Range province, evaporation commonly occurs in closed basins that generally contain alkaline, sodium-dominated water (Olmsted and others, 1984). Thus, the increased chloride concentration and modified isotopic composition may be expected in a geochemical environment that also would result in a sodium-dominated water. Locally, this general type of geochemical environment exists in the playas located in Hot Springs Flat and to the southeast of Bradys Hot Springs (fig. 4), which therefore represent possible sources of recharge to the geothermal systems. Unfortunately, data could not be collected to evaluate these areas as sources of recharge to the geothermal system, because properly located wells were not available. Recharge of a sodium-dominated, evaporation-affected water would require the following changes to produce a major-constituent and isotopic composition similar to that of water from well M–8: (1) an increase in silica concentration (to a limit controlled by equilibrium with quartz), (2) an increase in sulfate and a decrease in pH (perhaps due to the oxidation of sulfide minerals), (3) dissolution of a carbonate mineral (such as calcite) as a result of either the decrease in pH (causing the water to become undersaturated with respect to calcite) or a contribution of CO_2 from the deep crust or upper mantle, and (4) redistribution of the major cations within the aqueous phase.

The redistribution of cations is presumably caused by the same reactions that control the relation between sodium, potassium, and calcium in other geothermal systems—the reactions that provide the basis for a cation geothermometer. The water at Desert Peak well B21–2 could be formed in the same manner as described for the water at well M–8, with a meteoric water merely being affected to a greater extent by evaporation [resulting in a greater chloride concentration and a heavier (less negative) isotopic composition] prior to recharge.

The scenario described above requires no modification of the stable-isotope composition due to wall-rock interaction (oxygen shift) and only minor changes in the concentration of major constituents (with the exception of the silica increase). Flow within a fault system, where the ratio of wall-rock surface area to water volume is low, is

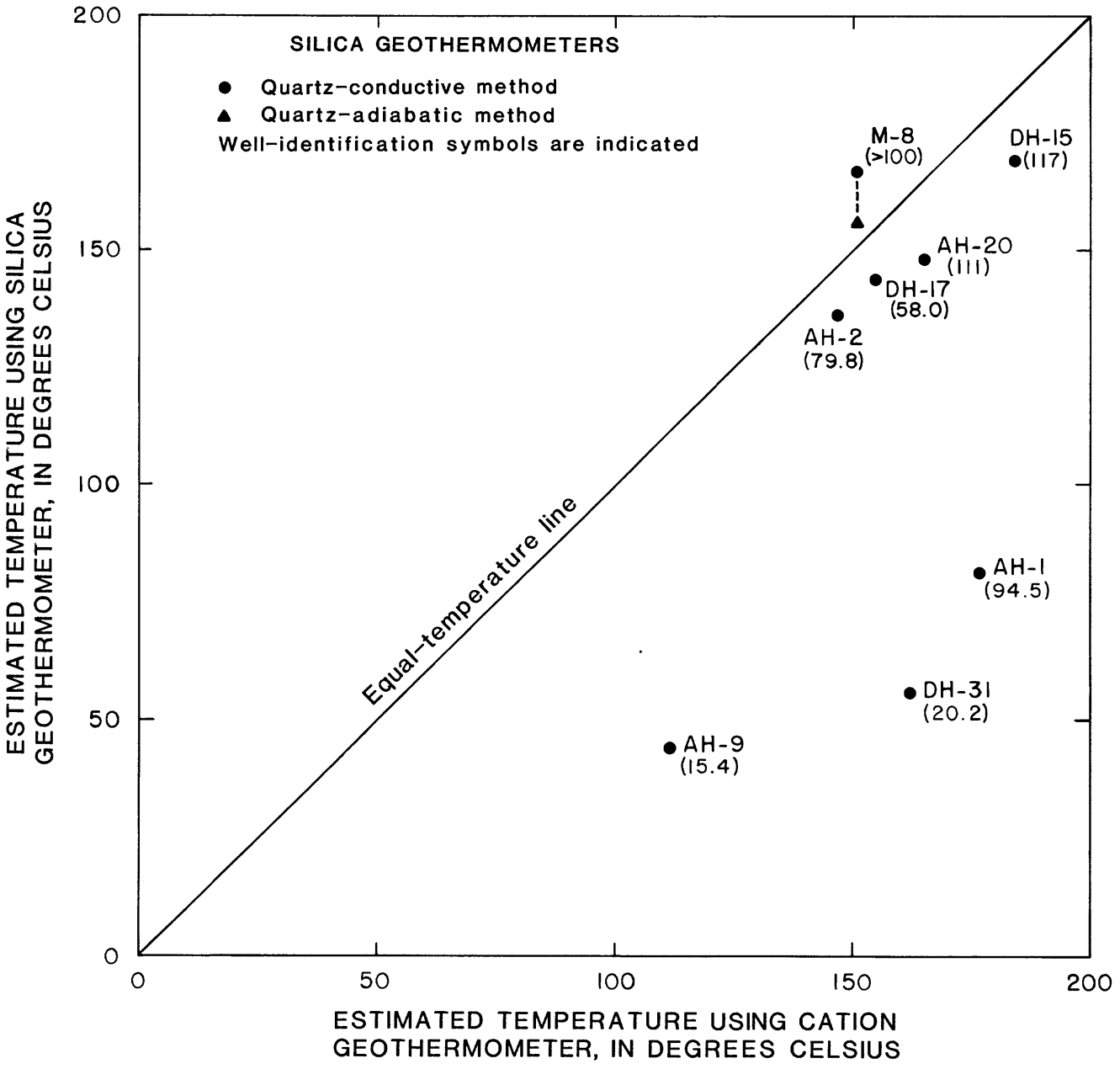

Figure 10. Comparison of aquifer temperatures estimated by using the silica and magnesium-corrected cation geothermometers for selected well waters. Numbers in parentheses are measured down-hole temperature, in degrees Celsius.

an environment where the water could equilibrate with the aquifer matrix with only limited change in water composition.

The oxygen shift also appears to be small at Leach Hot Springs—a geothermal system in the Basin and Range with an estimated temperature similar to that found at Bradys Hot Springs (Welch and others, 1981).

If the hydrogeochemical system outlined above is correct, then the concentrations of most minor constituents appear to increase only slightly as water flows through the thermal aquifer. The lack of dramatic increase in fluoride and barium (which might be expected due to evaporative concentration or dissolution reactions in the thermal aquifer) may be largely a result of a mineral-solubility control. The bromide concentrations are largely a result of evaporative concentration rather than augmentation with the thermal aquifer. The concentrations of lithium, strontium, and to a lesser extent boron

may be at least partly controlled by dissolution in the thermal aquifer; hence, these constituents may be useful "geothermal indicators" in the Bradys system.

The scenario discussed above must be considered tentative due to a paucity of geochemical data on local recharge and on the deep, high-temperature thermal water. Analysis of the chemical and isotopic composition of recharge water upgradient from the thermal system could assist significantly in evaluating the geochemistry of the area. Unfortunately, usable sampling points in the area have not as yet been identified.

REFERENCES CITED

Bailey, E.H., and Phoenix, D.A., 1944, Quicksilver deposits in Nevada: University of Nevada Bulletin, Geology and Mining Series no. 41, 206 p.

Barnes, Ivan, Irwin, W.P., and White, D.E., 1978, Global distribution of carbon dioxide discharges and major zones of seismicity: U.S. Geological Survey Water-Resources Investigations Report 78–39, 12 p.

Benoit, W.R., Hiner, J.E., and Forest, R.T., 1982, Discovery and geology of the Desert Peak geothermal field—a case history: Nevada Bureau of Mines and Geology Bulletin 97, 82 p.

Brook, C.A., Mariner, R.H., Mabey, D.R., Swanson, J.R., Guffanti, Marianne, and Muffler, L.J.P., 1979, Hydrothermal convection systems with reservoir temperatures ≥90 °C, *in* Muffler, L.J.P., ed., Assessment of geothermal resources in the United States—1978: U.S. Geological Survey Circular 790, p. 18–85.

Clarke, F.W., and Chatard, T.M., 1884, A report of work done in the Washington laboratory during the fiscal year 1883–84: U.S. Geological Survey Bulletin 9, 40 p.

Craig, Harmon, 1961, Isotopic variations in meteoric waters: Science, v. 133, no. 3465, p. 1702–1703.

D'Amore, Franco, and Panichi, Costanzo, 1980, Evaluation of deep temperatures of hydrothermal systems by a new gas geothermometer: Geochimica et Cosmochimica Acta, v. 44, no. 3, p. 549–556.

Dansgaard, W., 1964, Stable isotopes in precipitation: Tellus, v. 16, p. 436–467.

Fournier, R.O., 1977, Chemical geothermometers and mixing models for geothermal systems: Geothermics, v. 5, p. 41–50.

Fournier, R.O., and Potter, R.W., II, 1979, Magnesium correction to the Na-K-Ca chemical geothermometer: Geochimica et Cosmochimica Acta, v. 43, no. 9, p. 1543–1550.

Fournier, R.O., Sorey, M.L., Mariner, R.H., and Truesdell, A.H., 1979, Chemical and isotopic prediction of aquifer temperatures in the geothermal system at Long Valley, California: Journal of Volcanology and Geothermal Research, v. 5, p. 17–34.

Friedman, Irving, and O'Neil, J.R., 1977, Compilation of stable isotope fractionation factors of geochemical interest, *in* Fleischer, Michael, ed., Data of geochemistry (6th ed.): U.S. Geological Survey Professional Paper 440-K, 12 p.

Friedman, Irving, Smith, G.I., and Hardcastle, K.G., 1976, Studies of Quaternary saline lakes—II. Isotopic and compositional changes during desiccation of the brines in Owens Lake, California, 1967–1971: Geochimica et Cosmochimica Acta, v. 40, no. 5, p. 501–511.

Garside, L.J., 1979, Moana Hot Springs, Steamboat Springs and Brady's Hot Springs; Guidebook for field trip No. 4, Geothermal Resources Council 1979 annual meeting: Reno, Nev., 32 p.

Garside, L.J., and Schilling, J.H., 1979, Thermal waters of Nevada: Nevada Bureau of Mines and Geology Bulletin 91, 163 p.

Harrill, J.R., 1970, Water-resources appraisal of the Granite Springs Valley area, Pershing, Churchill, and Lyon Counties, Nevada: Nevada Division of Water Resources, Reconnaissance Report 55, 36 p.

Hem, J.D., 1970, Study and interpretation of the chemical characteristics of natural water [2nd ed.]: U.S. Geological Survey Water-Supply Paper 1473, 363 p.

Hiner, J.E., 1979, Geology of the Desert Peak geothermal anomaly, Churchill County, Nevada: Reno, University of Nevada, unpub. M.S. thesis, 63 p.

Kharaka, Y.K., and Barnes, Ivan, 1973, SOLMNEQ—solution mineral equilibrium computations: Menlo Park, Calif., U.S. Geological Survey Computer Contribution, 81 p. Available only from National Technical Information Service, U.S. Department of Commerce, Springfield, VA 22161, accession no. PB–215 899.

Kharaka, Y.K., and Mariner, R.H., 1977, Solution-mineral equilibrium in natural water-rock systems, *in* Paquet, H., and Tardy, Y., eds., Proceedings of the Second International Symposium on Water-Rock Interaction, Strasbourg, France, August 17–25, 1977: Section IV, p. IV66–IV75.

Mahon, W.A.J., 1964, Fluorine in the natural thermal waters of New Zealand: New Zealand Journal of Science, v. 7, p. 3–28.

Mariner, R.H., Presser, T.S., Rapp, J.B., and Willey, L.M., 1975, The minor and trace elements, gas, and isotope compositions of the principal hot springs of Nevada and Oregon: U.S. Geological Survey Open-File Report, 27 p.

Mariner, R.H., Rapp, J.B., Willey, L.M., and Presser, T.S., 1974, The chemical composition and estimated minimum thermal reservoir temperatures of the principal hot springs of northern and central Nevada: U.S. Geological Survey Open-File Report, 32 p.

Nehring, N.L., and Mariner, R.H., 1979, Sulfate-water isotopic equilibrium temperatures for thermal springs and wells of the Great Basin, *in* Expanding the geothermal frontier: Geothermal Resources Council Transactions, Davis, California, v. 3, p. 485–488.

Nehring, N.L., Mariner, R.H., White, L.D., Huebner, M.A., Roberts, E.D., Harmon, Karen, Bowen, P.A., and Tanner, Lane, 1979, Sulfate geothermometry of thermal waters in the Western United States: U.S. Geological Survey Open-File Report 79–1135, 11 p.

Nordstrom, D.K., and Jenne, E.A., 1977, Fluorite solubility equilibria in selected geothermal waters: Geochimica et Cosmochimica Acta, v. 41, no. 2, p. 175–188.

Olmsted, F.H., Glancy, P.A., Harrill, J.R., Rush, F.E., and Van Denburgh, A.S., 1973, Sources of data for evaluation

of selected geothermal areas in northern and central Nevada: U.S. Geological Survey Water-Resources Investigations 44–74, 78 p.

———1975, Preliminary hydrogeologic appraisals of selected hydrothermal systems in northern and central Nevada: U.S. Geological Survey Open-File Report 75–56, 267 p.

Olmsted, F.H., Welch, A.H., Van Denburgh, A.S., and Ingebritzen, S.E., 1984, Geohydrology, aqueous geochemistry, and thermal regime of the Soda Lakes and Upsal Hogback geothermal systems, Churchill County, Nevada: U.S. Geological Survey Water-Resources Investigations 84–4054, 166 p.

Paces, Thomas, 1972, Chemical characteristics of equilibrium in natural water-felsic rock CO_2 system: Geochimica et Cosmochimica Acta, v. 36, no. 2, p. 217–240.

Rudisill, J.M., 1978, Recent reservoir developments at Brady Hot Springs, Nevada, *in* Kruger, Paul, and Ramey, H.J., Jr., eds., Proceedings of the Fourth Workshop on Geothermal Reservoir Engineering, December 13–15, 1978: Stanford, Calif., Stanford University, Report SGP–TR–30, p. 218–227.

Truesdell, A.H., 1976, Summary of section III, geochemical techniques in exploration, *in* Proceedings, Second United Nations Symposium on the Development and Use of Geothermal Resources, San Francisco, Calif., 20–29 May, 1975: Berkeley, Calif., Lawrence Berkeley Laboratory, v. 1, p. liii–lxxix.

Voegtly, N.E., 1981, Geologic reconnaissance of the Hot Springs Mountains and adjacent areas, Churchill County, Nevada: U.S. Geological Survey Open-File Report 81–134, 10 p.

Welch, A.H., Sorey, M.L., and Olmsted, F.H., 1981, The hydrothermal system in southern Grass Valley, Pershing County, Nevada: U.S. Geological Survey Open-File Report 81–915, 193 p.

Wood, W.W., 1976, Guidelines for collection and field analysis of ground-water samples for selected unstable constituents: U.S. Geological Survey Techniques of Water-Resources Investigations Book 1, Chapter D2, 24 p.

Investigation of the Possible Formation of Diethylnitrosamine Resulting from the Use of Rhodamine WT Dye as a Tracer in River Waters

By Thomas R. Steinheimer *and* Sharon M. Johnson

Abstract

Surface water contamination by nitrosamines formed from rhodamine WT and nitrite ion has been studied. A method for residue analysis of N,N-diethyl-N-nitrosamine (NDEA) has been developed and evaluated using river samples spiked with rhodamine WT and nitrite ion. It permits rapid and reliable determination of NDEA at a minimum concentration of 0.03 microgram per liter. The method used solid-phase extraction and capillary gas chromatography with N-P detectors. Analysis time is less than two hours.

River conditions under which rhodamine WT is introduced into a stream for time-of-travel or dispersion studies were simulated in laboratory experiments. Results show that nitrosamine formation did not occur in the spiked river samples at concentrations typically encountered during dye injection studies. At atypical, or very high, nitrite concentrations (>0.10 milligram per liter), small amounts of nitrosamine may form, but atypical conditions were not studied here. NDEA persistence in river water was determined by monitoring its rate of disappearance from a spiked sample. At a concentration of approximately 2 micrograms per liter, the half-life of the nitrosamine at 20 degrees Celsius is less than three hours at pH 8.

Samples collected from four different rivers during actual rhodamine dye injections were analyzed for residual NDEA. Results indicate that, under customary dye-study practices, NDEA resulting from the use of rhodamine WT does not constitute an environmental hazard.

INTRODUCTION

The U.S. Geological Survey, as well as many other Federal and State agencies and private consulting engineering firms, uses dyes extensively in a variety of hydrologic studies. Rhodamine WT is used by surface water hydrologists for time-of-travel and dispersion studies to determine streamflow characteristics. The properties of this dye that led to its widespread use include high water solubility, presumed inertness with respect to other chemicals in the stream, and intense red fluorescence in very dilute solutions, which facilitates rapid and accurate field measurements. This material has largely replaced rhodamine B as the dye of choice in water-tracer studies because of its increased water solubility and attendant ease of handling in the field.

The chemical structure of rhodamine WT (fig. 1) includes two diethylamino- functional group sites. Because the sites are chemically equivalent, this dye can undergo hydrolysis of either or both of these moieties, producing diethylamine, the necessary intermediate to react with nitrite ion or other nitrosating agents to form a highly toxic derivative. Therefore, when the dye is introduced into a stream in the presence of nitrite ion, the possibility exists for the formation of N-nitrosodiethylamine (NDEA). This nitrosamine is soluble in water and most organic solvents, and it is moderately volatile at room temperature.

Concentrations of nitrosamines of less than 50 μg/kg for solid samples, μg/L for liquids, or μg/m^3 for gaseous samples to less than 1 ng/kg, ng/L, or ng/m^3 have been recorded in air, water, soil, plants, pesticides, food, drugs, and cosmetics (Fine and Rounbehler, 1976, p. 260, 1977, p. 579–580; Rhoades and others, 1980, p. 382; Khan, 1981, p. 275–286; Dean-Raymond and Alexander, 1976, p. 394; Sander and others, 1975, p. 208; Castegnaro and Walker, 1980, p. 451; Oliver, 1981, p. 349–351; Fine and others, 1977, p. 300–304; Hotchkiss and others, 1980, p. 366; Fazio and others, 1980, p. 422–428; Sen and others, 1980, p. 457–460; Taylor and others, 1980, p. 581–585; Fellion and others, 1980, p. 442); a U.S. Environmental Protection Agency survey (1977) reported concentrations ranging from less than 0.1 μg/L in industrial effluents to less than 10 μg/L in ambient waters. Anthropogenic sources probably contribute negligibly to the overall environmental levels, since N-nitrosamines are widely distributed throughout nature. The extent of exposure of the general population to nitrosamines is unknown, but the most significant exposure resulting from anthropogenic sources may be

restricted to industrial and agricultural areas (Fine and Rounbehler, 1981, p. 207; Fine and others, 1977, p. 304).

The biohazardous nature of N-nitroso compounds is well established: they are among the most potent of all known carcinogens, as well as being mutagenic, teratogenic, hepatotoxic, transplacentally carcinogenic, and lethally embryotoxic (Montesano and Bartsch, 1976, p. 217; Lijinsky and Taylor, 1977, p. 1582; Napalkov, 1973, p. 3–7; Magee and others, 1976, p. 501; Magee, 1973, p. 143–147; and Druckrey, 1973, p. 49, 56). About 80 percent of all N-nitrosamines studied have been found to be carcinogenic in a large variety of laboratory test animals with a wide range of susceptible organs and many different routes of exposure, and tumor production can occur after a single dose or after long-term exposure to small doses (Montesano and Bartsch, 1976, p. 183, 216; Lijinsky and Taylor, 1977, p. 1579–1580).

The widespread occurrence of nitrosamines and their precursors (Sander, 1973, p. 159) and concern about their diversely biohazardous nature has led to legislative and regulatory action and a continuing search for increasingly sensitive and specific methods for their detection. We have developed a rapid and relatively simple method for the specific determination of NDEA in water and have studied the potential for NDEA formation by simulating stream conditions during a rhodamine WT dye injection. We have also examined the persistence (lifetime) of this compound by determining its rate of disappearance in a spiked river-water sample under simulated stream conditions. Finally, we have analyzed samples collected during actual dye injections conducted on four different rivers. Our results are presented and discussed in this report.

EXPERIMENTAL

Literature Survey of the Determination of Low Molecular Weight Aliphatic Nitrosamines

Determination of nitrosamines in environmental matrices is one of the most difficult challenges facing an analytical chemist. Methods for determining nitrosamines are complicated by the fact that these compounds tend to occur in the environment at very low concentrations, often below 1 μg/L. This means either that very large test samples must be taken or that very extensive concentration must be done, or both. Another problem in analysis of nitrosamines is their natural occurrence in many commercial products, so that the analyst must be very certain that the detected concentration in the sample does not include nitrosamine detected in reagents or glassware. Another important precaution is making sure that the method does not synthesize or destroy the nitrosamine. Reliable methods have been devised, and the most successful approaches are presented in recent publications (Egan and

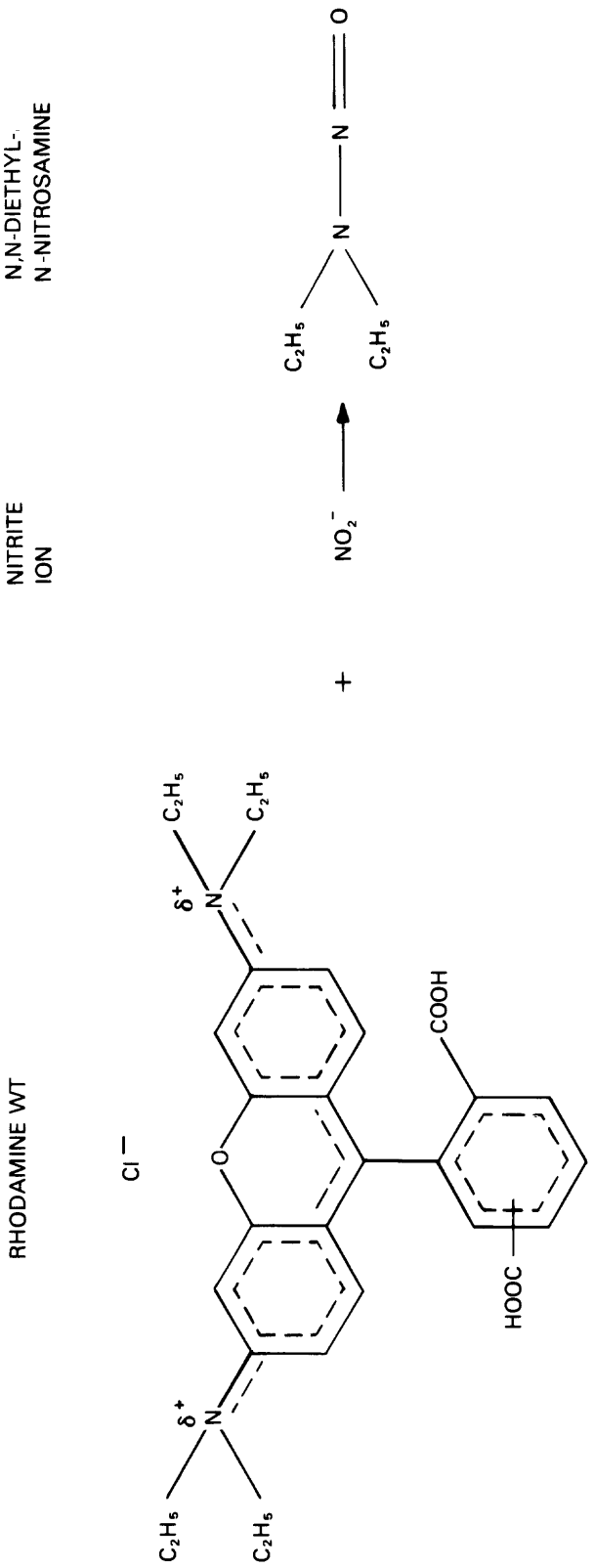

Figure 1. Proposed decomposition reaction of rhodamine WT in the presence of nitrite ion leading to the formation of N,N-diethyl-N-nitrosamine (NDEA).

others, 1978; Walker and others, 1980; Scanlan and Tannenbaum, 1981). Most of these procedures use extraction, optional cleanup of the extract, concentration, and gas chromatography with element-specific or functional group-selective detectors. The use of a detector system that discriminates on the basis of nitrogen or nitroso content simplifies sample treatment before instrumental analysis.

Three nitrosamines are on the U.S. Environmental Protection Agency list of Consent Decree Priority Pollutant chemicals. Although NDEA is similar in structure to these three, it is not included. It is reasonable to assume, however, that NDEA can be determined at environmental residue concentrations by Method 607 as specified in the Federal Register (U.S. Environmental Protection Agency, 1979). This procedure is recommended for determination of N-nitrosodimethylamine (NDMA) and N-nitrosodi-*n*-propylamine (NDPA) in municipal and industrial discharges. Method 607 states a detection limit of 0.15 μg/L for NDMA and 0.46 μg/L for NDPA, and recovers only 40–70 percent of the total amount present in wastewater samples. In addition, this technique is labor-intensive and requires large volumes of solvent and large quantities of glassware. In order to meet the need for a rapid and sensitive determination of NDEA formed from rhodamine WT usage, we have developed an analysis procedure that requires a very small sample and that can be completed in a few hours. The chemistry of the procedure furnishes concentrated extracts, which are suitable for direct instrumental analysis.

Procedure for Determination of NDEA

A 75-mL test sample was saturated with a 1-*M* (molar) sulfite/bisulfite salt mixture. The solid-phase extraction apparatus (fig. 2) was assembled with a phenyl cartridge. The sorbent bed of the cartridge was prewashed under aspirator vacuum with 5 mL of methanol followed by two 5-mL portions of HPLC (high-performance liquid chromatography) grade water. The sample was transferred to the reservoir and drawn through the cartridge under vacuum at a flow rate of 5–10 mL/min. The cartridge was placed inside a conical centrifuge tube and centrifuged at 1,000 r/min (revolutions per minute) for 3 min to remove occluded water. The cartridge, which contained any NDEA present in the water sample, was placed in a clean centrifuge tube; 1.00 mL of HPLC ethyl acetate was added from a microdispenser; and elution was carried out by centrifugation at 1,000 r/min for 3 min. Ethyl acetate was added to the centrifuge tube to bring the total volume of ethyl acetate to 1.0 mL, and the sample was mixed on a vortex mixer. The layers were separated and the organic phase was drawn into a capillary pipet and transferred to an assembled membrane filtration apparatus. The sample was filtered through a 0.2-μm porosity nylon membrane directly into an auto-sampler vial, which was capped with a septum seal for instrumental analysis.

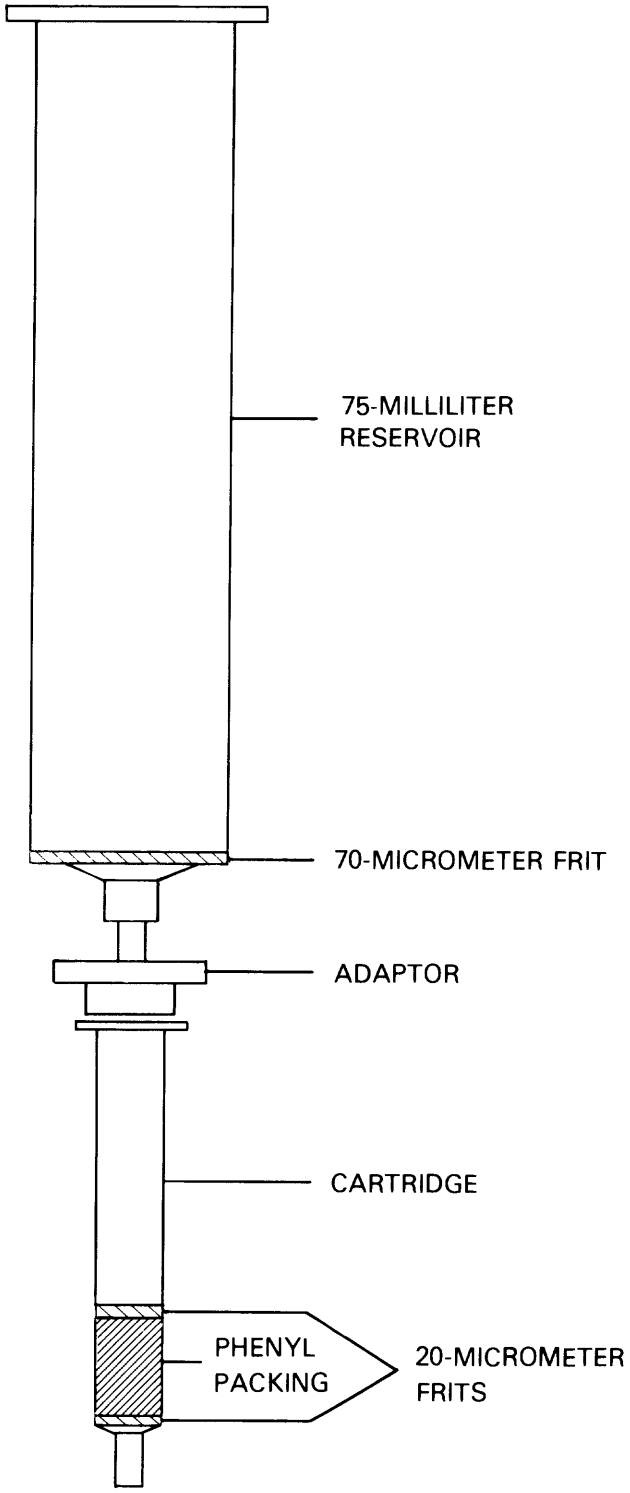

Figure 2. Solid-phase extraction apparatus used to isolate N,N-diethyl-N-nitrosamine (NDEA).

The gas chromatographic system consisted of a Hewlett-Packard Model 5840A gas chromatograph (GC) equipped with a nitrogen-phosphorus (N-P) detector, a Model 5840A GC Terminal, a Model 7672A Auto-Sampler, and a Model 18835B Capillary Inlet System. All analyses were carried out on an OV–351 fused silica wall-coated open tubular (WCOT) column, 60 m by 0.25 mm inside diameter (ID) with a film thickness of 0.25 μm. Linear velocity of the helium carrier gas (butane at 50 °C) was 25.4 cm/s. Following a splitless mode injection, the oven was held at 50 °C for 1 min, then ramped at 20 °C/min to 110 °C, then ramped at 1 °C/min to 129 °C for the NDEA analysis. Following elution of all materials of interest, the column was ramped at 30 °C/min to a maximum of 230 °C, where it was held for 30 min. Total analysis time was 56.3 min.

Laboratory Determination of Formation Potential of NDEA in River Water

Water samples taken from the South Platte River near Denver were used to study NDEA formation potential. Samples were taken on July 25, 1983, from a point within the Denver city limits but about 8 mi south (upstream) of the main metropolitan area. This sampling point was about one mile above a secondary treatment facility influent. Streamflow was moderately high, about 1,340 ft^3/s as a result of both snowmelt runoff and unusually heavy precipitation. Some water-quality characteristics of this matrix are given in table 1.

Table 1. Water-quality characteristics of the South Platte River at the time of sampling for NDEA analysis
[Concentrations in milligrams per liter except as indicated: μS/cm at 25 °C, microsiemens per centimeter at 25 °C]

	Value
pH	7.9
Specific conductance	242 μS/cm at 25 °C
Alkalinity, as $CaCO_3$ (calcium carbonate)	115
Dissolved oxygen	6.4
Dissolved organic carbon	5.4
NO_2 (nitrite)	0.033
$NO_3 + NO_2$ (nitrate plus nitrite)	0.67
PO_4 (phosphate)	0.01
Cl (chloride)	21
Na (sodium)	14
K (potassium)	2.2
Ca (calcium)	25
Mg (magnesium)	5.2
Fe (iron)	0.023
Mn (manganese)	0.005
Zn (zinc)	0.014
Sr (strontium)	0.187
Si (silicon)	12

Each sample was spiked with rhodamine WT and nitrite ion, then placed in a large beaker in an illuminating chamber (fig. 3) constructed to simulate river conditions during a time-of-travel study. Exposure to sunlight, extent of aeration and mixing, and temperature were taken into account. Concentrations of dye and nitrite were chosen to simulate levels found in a stream during a dye injection study. Dye concentration was set at 20 μg/L. On the basis of a single reactive site in the rhodamine WT molecule, a five-fold molar excess of nitrite ion was added. Taking into account the amount of nitrite reported in the stream as well, this corresponded to a total nitrite concentration of about 43 μg/L. The light unit consisted of eight lamps in one bank, mounted on the underside of a frame positioned above a Plexiglas tank containing water recirculating at 20 °C. The unit contained four each of alternately placed Westinghouse FS20 fluorescent sunlamps and General Electric F20T12BL fluorescent black lamps. The heat generated by these lamps was compensated for by immersing the beakers in a constant-temperature water bath. This apparatus is similar to those described previously by Hirt and others (1960, p. 709, 712) and by Abidi (1982, p. 200). The beakers containing the samples were placed directly beneath the light source. The distance between the light bank and the surface of the sample averaged 23 cm during the 24-hour time period when aliquots were removed periodically for analysis by the method described previously. Samples were exposed to artificial sunlight while being mixed by aeration, and temperature was held constant at 20 °C. Portions were analyzed for NDEA levels at time 0, 0.5, 1, 2, 6, 12, 18, and 24 hours.

Laboratory Determination of Persistence of NDEA in River Water

South Platte River samples collected on August 30, 1983, were spiked at the same levels described before: rhodamine WT at 20 μg/L and nitrite ion at a five-fold molar excess based on reaction of a single functional group on the dye. Assuming 50 percent conversion at this stoichiometric ratio, NDEA was added at the calculated concentration of 2 μg/L. These samples were then positioned under the light box under the same conditions as those for the formation study. The rate of disappearance of nitrosamine was determined by taking aliquots for analysis at time intervals of 0, 0.5, 1, 1.5, 2, 3, 4, and 5 hours. Initial pH values of 5 and 8 were used for these experiments.

Field Studies Carried Out During Actual Dye Injections

Water tracing with rhodamine WT has proven to be a practical approach for determining time-of-travel and

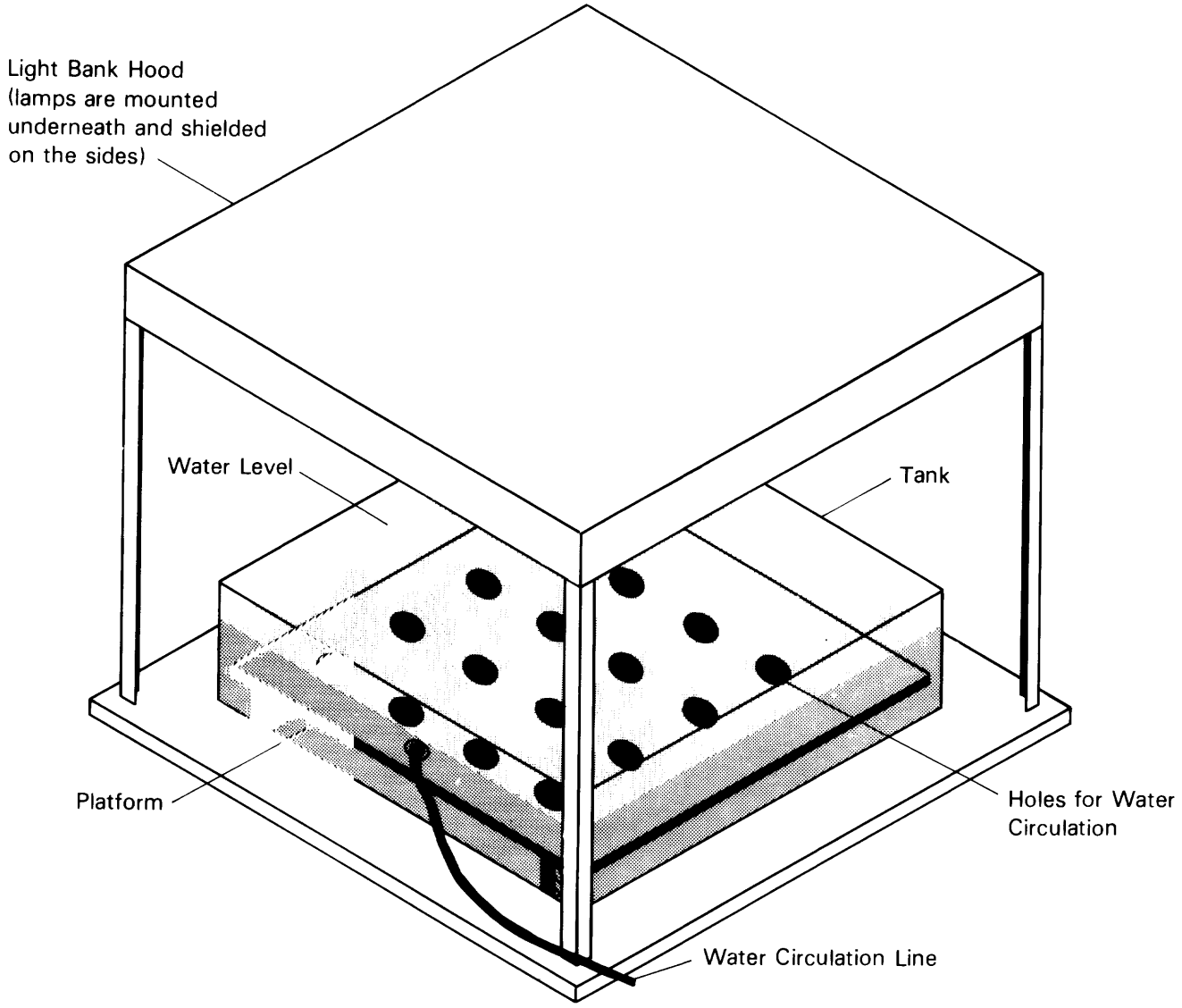

Figure 3. Apparatus for simulation of stream conditions.

dispersion in streams. A recently revised Techniques of Water-Resources Investigations (TWRI) report (Hubbard and others, 1982) discussed theory, application, data computation and analysis, and potential problems. In August and September 1983, USGS District offices in New England, Wisconsin, Missouri, and Colorado conducted dye injection studies on selected streams. In conjunction with these efforts, because each study involved the use of rhodamine WT, these offices provided samples for both NDEA and nitrite ion analyses as part of their reaeration or time-of-travel studies. The streams chosen included the Assabet River (Maynard, Mass., 20 mi west of Boston), the Bark River (a tributary of the Rock River, 40 mi east of Madison, Wis.), the Meramec River (20 mi southwest of St. Louis, Mo.), and the South Platte River (8 mi south of downtown Denver, Colo.). Samples were collected from several sites along each stream, beginning at the injection point before injection of the dye. This first sample served as a matrix-background reference for the laboratory analysis. Subsequent samples were taken at each downstream monitoring point prior to and at the time of passage of the dye peak as determined by fluorometric measurements. Temperature, specific conductance, dissolved oxygen, and pH measurements were also recorded at the time of sampling. The sample for NDEA analysis was collected in the standard glass bottle used for pesticide analyses, and the nitrite sample was collected in the standard brown plastic bottle and preserved with mercuric chloride. All samples were held in ice, shipped to the laboratory overnight, and analyzed for both

parameters upon receipt (usually within 24 hours of sampling). Characteristics of streams used in the field study are summarized in table 2.

RESULTS AND DISCUSSION

Analytical and Statistical Considerations

To establish the presence of NDEA formed from the use of rhodamine WT in streams, it became necessary to develop a rapid and sensitive method of analysis. Classical methods, including those for structurally similar EPA Consent Decree Priority Pollutant nitrosamines, are generally laborious and inefficient (poor recovery) and thus were judged to be unsuitable for this application. Solid-phase extraction (SPE) offers an alternative to liquid-liquid partition for removal of organic contaminant residues from water. When this method uses an extraction cartridge containing silica packing derivatized with phenyl groups, the technique is applicable to nitrosamine analysis. Our results show that, in a water matrix containing a 1-*M* sulfite/bisulfite salt mixture at pH 7, this extraction system is selective for aliphatic nitrosamines. Solutes of higher molecular weight such as rhodamine dyes are strongly retained on the column and are not recovered by elution with ethyl acetate. This solvent provided cleaner chromatograms on water blanks than either acetone or methanol, both of which also showed some variation in NDEA retention time. In addition, rhodamine is not soluble in ethyl acetate under the conditions of elution, so instrumental analysis is not encumbered by the presence of the dye. SPE provides a means of isolating and concentrating the NDEA present in a natural water sample containing rhodamine dye in a single laboratory operation. Other types of pre-packed cartridges were evaluated and found to be less suitable than the phenyl. The n-octadecyl, n-octyl, cyano, and vic-diol packings were found to give zero percent recovery of NDEA in spiked samples. The primary/secondary amino and the cyclohexyl packings resulted in chromatograms too complex for reliable interpretation.

Capillary gas chromatographic separations achieved on a microbore column for NDEA in a reference standard and in a spiked river-water extract are shown in figure 4. These chromatograms are representative of those obtained throughout the study. This extract was generated from the procedure described previously. The NDEA spiking solution also contained an equivalent amount of NDPA to be used as a reference compound. Instrument parameters were optimized so that both nitrosamine peaks were clearly isolated from other constituents that might interfere. In the South Platte River matrix blank, no interfering peaks are found within the retention window where NDEA would occur. (One unidentified peak does elute approximately 1.4 min after NDEA, but it does not interfere with either of the nitrosamines.) This is the matrix on which the formation potential and persistence studies were carried out.

Table 2. Selected characteristics of the four rivers examined for NDEA information at the time and point of dye injection

River	Number of downstream sampling points	pH	Temperature (°C)	Dissolved oxygen (mg/L)	Specific conductance (µS/cm at 25 °C)	Nitrite ion (µg/L)
Assabet	2	6.9	22	5.7	302	46
Bark	2	7.8	22	8.5	536	2
Meramec	2	7.9	22	7.6	343	4
South Platte	4	7.8	15	8.5	460	10

Low-level nitrosamine analysis requires very careful handling and treatment to avoid degradation of analyte, which is particularly significant when dealing with low molecular weight, volatile, aliphatic compounds. A comparison of electron impact mass spectra of isolated and reference NDEA is shown in figure 5. Ion abundances are nearly identical for the major fragments above mass-to-charge ratio (m/z) 40. Similarities in the two spectra clearly show that NDEA is not significantly degraded by our method and that NDEA was verified as the compound being determined.

Confidence interval estimation for NDEA determination is shown in figures 6*A* and 6*B*. It was assumed that if nitrosamine formed in the stream it would do so at environmental-residue concentrations (less than 1 mg/L). Thus, precision and accuracy data focused on samples spiked over one order of magnitude only, and within that range. The points plotted represent two sets of four replicate determinations each, at seven concentrations covering the range 0.07 to 1.4 µg/L. One spiked recovery sample was lost. Six additional points at 2.1 µg/L were added from the initial determinations for the persistence study. In addition, nine more data points were obtained from NDEA recovery of spiked samples to which rhodamine WT had also been added. Altogether, a total of 70 passes through the method were required, during which no procedural problems were observed.

The graphs in figures 6*A* and 6*B* are designed to provide a better estimate of actual concentrations of NDEA in samples analyzed by our method. The plot in figure 6*A* permits estimation of the range associated with a single NDEA determination in river water. The dotted line passing through the origin represents 100 percent recovery. The solid line represents the linear regression of Y on X for all 70 data points, where Y is the dependent variable, the amount of NDEA recovered, and X is the independent or controlled variable, the amount of NDEA spiked into the sample. The two dashed lines represent the 90-percent confidence interval for a single response.

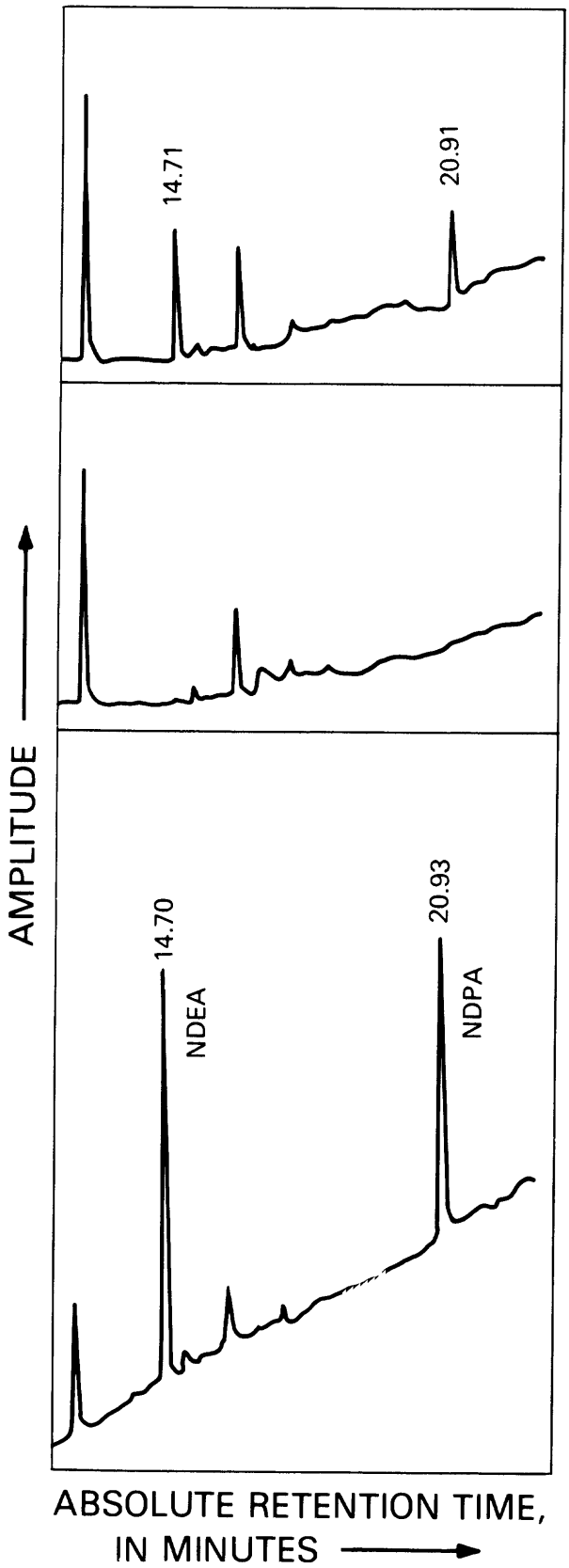

South Platte River Water:

Spiked at 0.07 micrograms NDEA per liter

South Platte River Water:

Blank

Standard:

Equivalent to
0.27 micrograms NDEA per liter,
0.32 micrograms NDPA per liter

Gas Chromatograph Conditions:

OV-351 Fused silica capillary column, 60 meters by 0.25 millimeter ID

Helium carrier gas linear velocity 25.4 centimeters per second (Butane at 50°C)

Oven temperature 50°C for one minute, ramped at 20°C per minute to 110°C, ramped at 1°C per minute to 129°C

N-P Detector

Figure 4. Identification of N,N-diethyl-N-nitrosamine (NDEA) in river-water extract by capillary gas chromatography using N,N-di-*n*-propyl-N-nitrosamine (NDPA) as a reference compound.

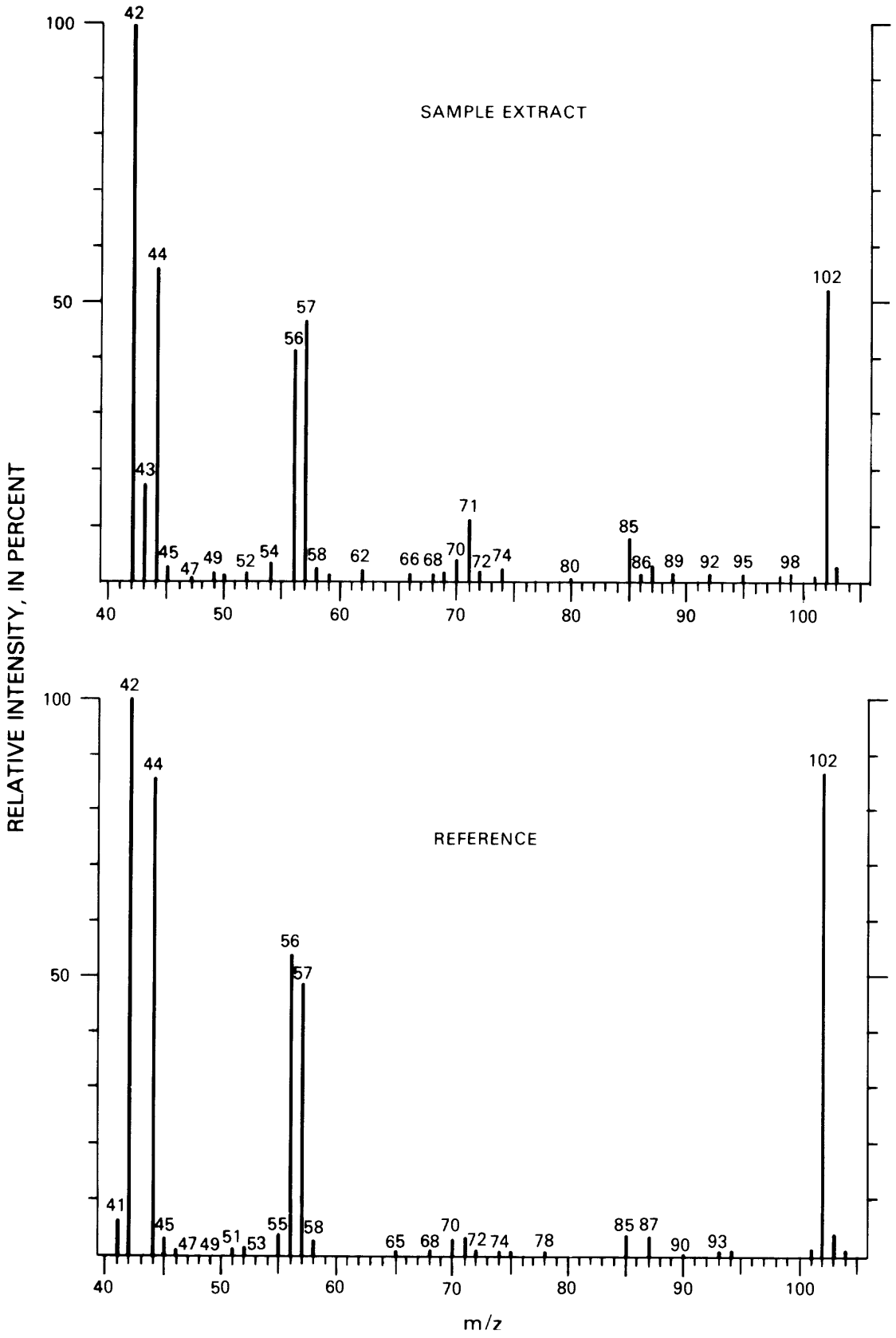

Figure 5. Electron impact mass spectra of compound recovered from spiked river water in a sample extract and reference compound N,N-diethyl-N-nitrosamine (NDEA).

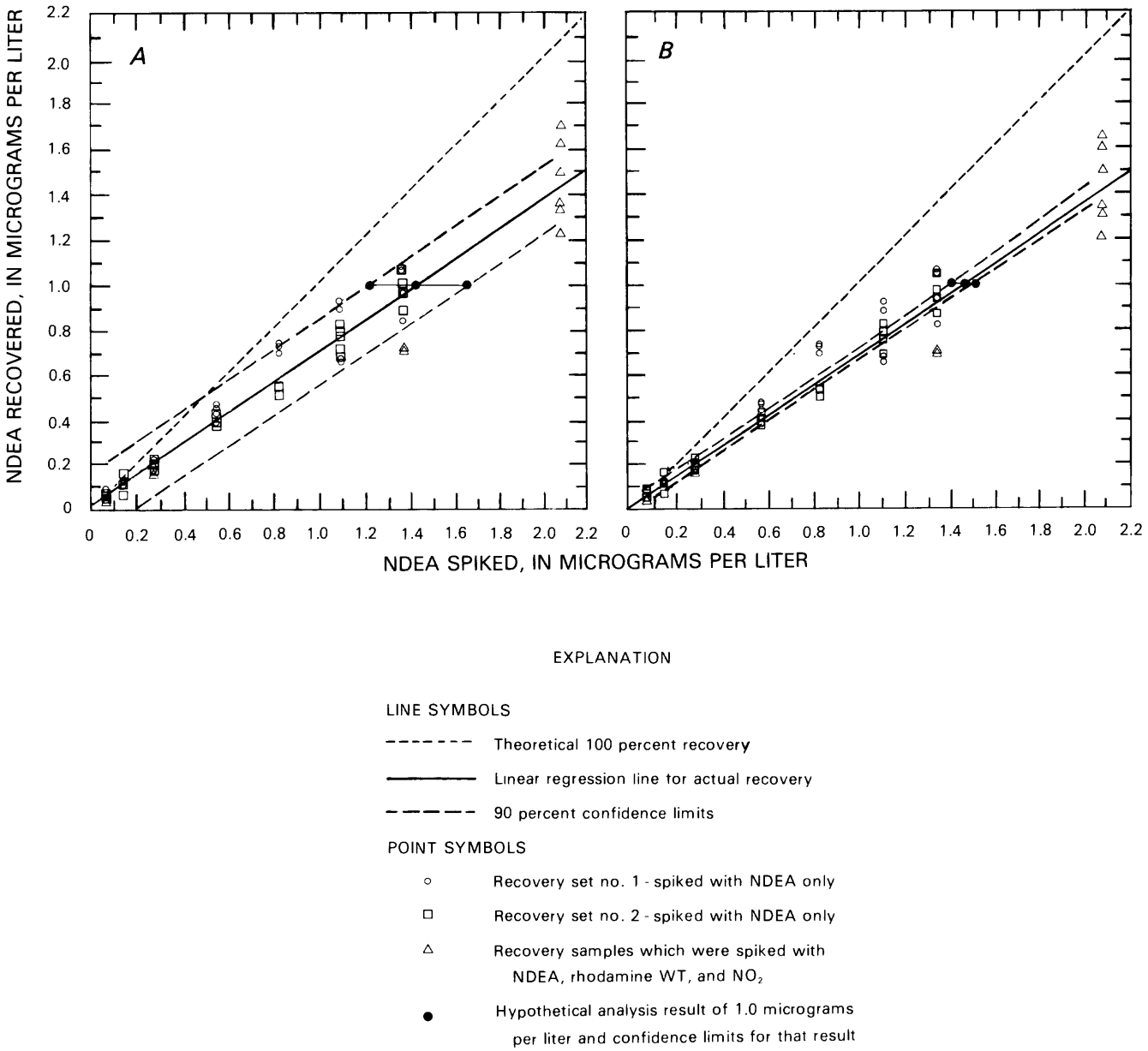

Figure 6. Recovery of N,N-diethyl-N-nitrosamine (NDEA) from spiked river-water samples and determination of measurement bias; (*A*) Confidence interval estimate based on a single analysis, and (*B*) Confidence interval estimate based on multiple analyses.

Reading directly from the linear calibration graph, a single NDEA determination using our method [which gives a result of 1 μg/L] will recover about 70 percent of the total material present (1.46 μg/L). Furthermore, there is a 90-percent confidence that the actual amount in the sample will fall between 1.24 and 1.68 μg/L. The interval estimate for an NDEA determination on an unknown sample can be reduced significantly (fig. 6*B*) by performing a series of repetitive analyses on the same sample. In a sample giving a mean result of 1 μg/L NDEA, the same 70-percent recovery level lies in a 90-percent confidence interval between 1.41 and 1.52 μg/L. At an actual concentration of 0.1 μg/L, about 85 percent of the NDEA present can be recovered by our method, while at a concentration of 1.0 μg/L, about 70 percent can be recovered.

The plots show that bias of determination and scatter of replicate points within a given spiking level increase at higher concentrations, which suggests that the analytical efficiency of our method breaks down somewhat at higher concentrations. The salt mixture imparts a modest buffer capacity (at pH 7) to a 75-mL test sample, but even though this is a poorly buffered system, calculations show that its capacity is not exceeded in our samples. The same spiking solution was used for the entire concentration range of recovery samples, involving a 20-fold volume increase of ethyl acetate (ethyl acetate ranged from 0.006 to 0.125 percent of the total 75-mL sample volume). It is possible that the sorptive capacity of the packing material is exceeded under these conditions at higher NDEA concentrations. The most plausible explanation seems to be that the combination of increasing ethyl acetate content and increasing NDEA concentration results in a progressively diminished effect from the 1-*M* sulfite/bisulfite salt mixture. Thus, the analyte is not as efficiently removed from the aqueous solution by "salting out," and less material is recovered.

Formation and Persistence Studies in the Laboratory and in the Field

The potential for NDEA formation to occur as a result of the use of rhodamine WT has been examined in river water obtained from the South Platte River. The samples were not buffered, and experiments were carried out at pH 8 and at pH 5. Each sample was spiked with rhodamine WT and nitrite ion, placed in the illuminating chamber in a recirculation bath at 20 °C, and purged with air from a bubbler to simulate river mixing and to approximate dissolved oxygen concentrations. Determinations of nitrosamine concentrations were made in triplicate over a 24-hour period. At pH 8 and at pH 5, with an added-nitrite/dye ratio of 5, no nitrosamine was formed in any of the samples tested. Reagent and apparatus blanks were repeatedly analyzed for the presence of traces of NDEA at the same time as the samples were analyzed. No traces were found in the blanks. It has recently been reported (Bencala and others, 1983, p. 943) that streambed sand and gravel interaction with rhodamine WT dye may account for instream dye concentrations as low as 45 percent of that expected in a short-term study in a mountain stream environment. In order to investigate the possibility that particulates in the water were a major reason why no NDEA was found in the formation studies, another formation experiment was run on river water that was first filtered through 0.2-μm nylon membrane filters. No traces of NDEA were found in this particulate-free experiment. These results indicate that, if the NDEA was formed under these conditions, the maximum concentrations to be expected would be somewhere below 0.03 μg/L, the nominal limit of detection for this analytical method. This concentration of NDEA is nearly two orders of magnitude below the maximum concentration of residual dye permitted for water withdrawal at an intake point. Thus, it would appear that an adequate margin of safety does exist with respect to the use of rhodamine WT in water-tracing studies.

Our results contradict the findings of similar experiments conducted by another investigator (Abidi, 1982, p. 202–204). In those studies, river-water samples containing rhodamine WT at 1–20 μg/L concentrations were spiked with nitrite ion at the 10–100 μg/L level and stirred at 20 °C for up to 24 hours. Concentrations of naturally occurring nitrite were between 10 and 27 μg/L, and pH was in the range of 7.3 to 8.3. Under these conditions, NDEA formation was maximized at pH 8, dye concentrations of 20 μg/L, and nitrite ion concentrations of 114 μg/L. When the added-nitrite concentration was reduced tenfold, the yield of NDEA was diminished significantly. In other laboratory nitrosation experiments in an aqueous pH-buffered solution where the dye was reacted with sodium nitrite at constant temperature for a fixed length of time, Abidi suggested an optimum situation at a nitrite/dye mole ratio of 11 and a pH of 5 at 80 °C for 12 hours. Conditions listed for this study were nitrite/dye mole ratios of 2, 5, and 11; pH values of 2, 5, and 7; and temperatures of 20, 50, and 80 °C.

The major differences in experimental conditions between our findings and those reported by Abidi are in two key areas. In each of our experiments dealing with formation potential, the samples were spiked with a five-fold molar excess of nitrite ion in addition to the amount originally present in the river water. Abidi added a fifty-fold molar excess in the only studies that included illumination with artificial sunlight. Although her studies incorporating varying nitrite levels were apparently not done in the presence of artificial sunlight, the results indicate that the large excess of added nitrite increased the formation of NDEA. However, the addition of a fifty-fold molar excess of nitrite creates an unstable situation, which would represent a condition that would not occur commonly in nature. This high nitrite level would probably be converted rapidly to nitrate in the river; thus, it would not be available for the formation of NDEA. Another key difference in experimental conditions involves the purging of samples with air during the formation studies. Dissolved oxygen in each of the streams sampled in our experiments ranged between 6 and 9 mg/L, which corresponds to 80 to 100 percent saturation at 20 °C. As a result of variable consumption rates, the dissolved oxygen content of a river is a highly transient property with a measurement significant only at the time and place of sampling. In our field studies, dissolved oxygen measurements were made at each site, whenever NDEA and nitrite samples were collected. These values were consistently above 80 percent saturation. To simulate this condition in the labora-

tory, all samples were purged at 20 °C with a stream of air.

To be accurate in laboratory simulation of field conditions under which the nitrosamine formation chemistry must occur, it is essential to (1) recognize the effects of radiant energy; (2) avoid creating artificial nitrite levels; and (3) consider the effects of dissolved oxygen on the entire system. Photochemical alteration of man-made organic chemicals is a widely recognized and well-documented phenomenon (Crosby, 1977, 1978; Crosby and Li, 1969). It is possible that the rate of photochemical decomposition of NDEA in the presence of dissolved air and nitrite at environmental levels is approximately the same as its rate of formation from the dye, so that NDEA essentially becomes a transient species with a very short half-life in river water.

To determine the persistence of NDEA in river water, its rate of disappearance from a spiked sample was determined. Experimental conditions described previously emphasize that every attempt was made to duplicate hydrologic conditions under which rhodamine WT is introduced into a stream. Residual nitrosamine concentrations were carefully monitored over a period of 5 hours. These results are plotted in figures 7*A* and 7*B*. The curves show that, under these conditions, the rate of disappearance or decomposition is relatively rapid. In figure 7*A*, the half-life for NDEA (the time required for the disappearance of 50 percent of the original material) at a concentration of 2.1 µg/L is less than 3 hours. Similarly, after 6 hours of reaction, less than 25 percent of the original material remains. The rate of disappearance is more rapid at pH 8 than at pH 5. If the principal decomposition pathway involves the loss of gaseous nitric oxide (NO), it is reasonable to presume that this reaction may be retarded somewhat at the lower pH, where NDEA may be partly ionized by protonation of the amino nitrogen. This mechanism would explain a somewhat longer half-life at lower pH.

In figure 7*B*, the disappearance curves are extrapolated through a 24-hour interval at which time the NDEA remaining is negligible. Other investigators studying NDEA persistence in water have reported results very similar to ours (Sanders and others, 1975, p. 207). In one study, 1,000 µg of NDEA was dissolved in 1 L of water and exposed to daylight conditions. Following 2 hours of exposure to bright sunlight, only 147 µg of nitrosamine was recovered. After 16 hours of exposure, an average of only 43 µg of NDEA remained. The authors concluded that decomposition occurs rapidly, probably leading to no detectable residue after 24 hours. In contrast, Abidi concluded, from photolytic-nitrosation studies on river water containing dye at 20 µg/L and nitrite at 100 µg/L, that NDEA exhibits some degree of persistence in the aquatic environment in spite of its tendency toward slow photodecomposition.

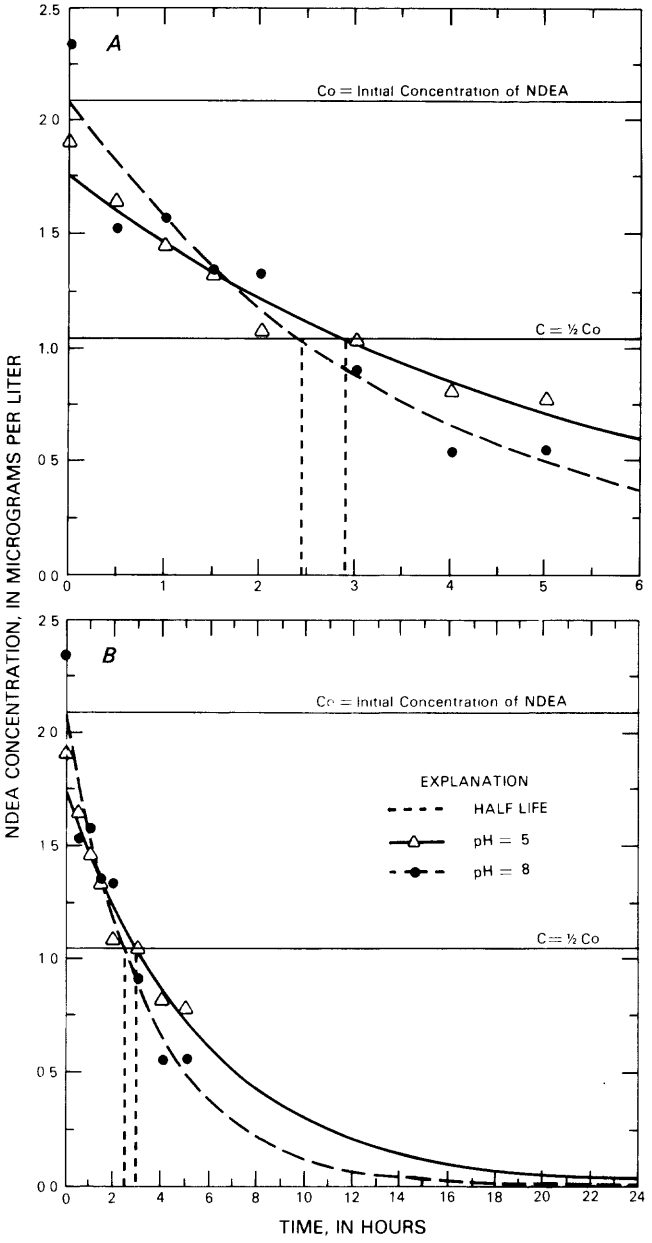

Figure 7. Rate of disappearance of N,N-diethyl-N-nitrosamine (NDEA) from spiked river water containing 20 µg/L rhodamine WT and 43 µg/L total nitrite ion; (*A*) Data for the time span of the experiment (5 hours), and (*B*) extrapolation of data to 24 hours.

In the field studies, diethylnitrosamine was not detected in any of the samples taken from rivers in which dye had been injected. Nitrite ion concentrations ranged between 2 and 46 µg/L. None of the samples collected at downstream sampling points at the time of passage of the dye peak contained NDEA. These studies were conducted under climatic conditions in which irradiation from bright

sunlight or diffuse daylight were factors in the formation of NDEA. In each of the streams characterized in table 2, field procedures recommended by the Water Resources Division were carefully followed. Our findings indicate that, under these conditions of recommended usage, rhodamine WT as an agent for surface-water-tracing studies does not constitute an environmental hazard associated with manmade nitrosamines in the environment.

REFERENCES CITED

Abidi, S.L., 1982, Detection of diethylnitrosamine in nitrite-rich water following treatment with rhodamine flow tracers: Water Research, v. 16, p. 199–204.

Bencala, K.E., Rathbun, R.E., Jackman, A.P., Kennedy, V.C., Zellweger, G.W., and Avanzino, R.J., 1983, Rhodamine WT dye losses in a mountain stream environment: Water Resources Bulletin, v. 19, no. 6, p. 943–950.

Castegnaro, M., and Walker, E.A., 1980, Report on collaborative studies of the determination of volatile nitrosamines in cheese and pesticides, *in* Walker, E.A., Griciute, L., Castegnaro, M., and Borzsonyi, M., eds., N-nitroso compounds: analysis, formation and occurrence—Proceedings, 6th International Symposium on N-nitroso Compounds, Budapest, October 1979; IARC Scientific Publications No. 31: Lyon, France, International Agency for Research on Cancer, p. 445–453.

Crosby, D.G., 1977, The environmental chemistry of herbicides, *in* Plimmer, J.R., ed., Division of Pesticide Chemistry Symposium, 171st Meeting, American Chemical Society, New York, April, 1976; ACS Symposium Series 37: Washington, D.C., American Chemical Society, p. 93–108.

———1978, Conquering the monster—the photochemical destruction of chlorodioxins, *in* Kennedy, M.V., ed., Disposal and decontamination of pesticides, Division of Pesticide Chemistry Symposium, 174th Meeting, American Chemical Society, Chicago, August 29–September 2, 1977; ACS Symposium Series 73: Washington, D.C., American Chemical Society, p. 1–12.

Crosby, D.G., and Li, Ming-Yu, 1969, Herbicide photodecomposition, *in* Kearney, P.C., and Kaufman, D.D., eds., Degradation of herbicides: New York, Marcel Dekker, Inc., p. 321–361.

Dean-Raymond, Deborah, and Alexander, M., 1976, Plant uptake and leaching of dimethylnitrosamine: Nature, v. 262, p. 394–396.

Druckrey, H., 1973, Chemical structure and action in transplacental carcinogenesis and teratogenesis, *in* Tomatis, L., and Mohr, U., eds., Transplacental carcinogenesis, Meeting at Midizinische Hochschule, Hannover, Federal Republic of Germany, October 6–7, 1971, Proceedings; IARC Scientific Publications No. 4: Lyon, France, International Agency for Research on Cancer, p. 45–58.

Egan, H., Preussmann, R., Walker, E.A., Castegnaro, M., and Wassermann, A.E., eds., 1978, Environmental carcinogens—selected methods of analysis, Volume I—Analysis of volatile nitrosamines in food; IARC Scientific Publications No. 18: Lyon, France, International Agency for Research on Cancer, 212 p.

Fazio, T., Havery, D.C., and Howard, J.W., 1980, Determination of volatile N-nitrosamines in foodstuffs: I. A new clean-up technique for confirmation by GLC–MS; II. A continued survey of foods and beverages, *in* Walker, E.A., Griciute, L., Castegnaro, M., and Borzsonyi, M., eds., N-nitroso compounds: analysis, formation, and occurrence—Proceedings, 6th International Symposium on N-nitroso Compounds, Budapest, October 1979; IARC Scientific Publications No. 31: Lyon, France, International Agency for Research on Cancer, p. 419–431.

Fellion, Y., De Smedt, J., and Brudney, N., 1980, An HPLC–UV method for the direct evaluation of N-nitrosodiethanolamine in some cosmetic products and raw materials, *in* Walker, E.A., Griciute, L., Castegnaro, M., and Borzsonyi, M., eds., N-nitroso compounds: analysis, formation and occurrence—Proceedings, 6th International Symposium on N-nitroso Compounds, Budapest, October 1979; IARC Scientific Publications No. 31: Lyon, France, International Agency for Research on Cancer, p. 435–443.

Fine, D.H., and Rounbehler, D.P., 1976, N-nitroso compounds in water, *in* Keith, L.H., ed., Identification and analysis of organic pollutants in water: Ann Arbor, Michigan, Ann Arbor Science Publishers Inc., p. 255–263.

———1977, Determination of dimethylnitrosamine in air and water by thermal energy analysis: validation of analytical procedures: Environmental Science and Technology, v. 11, no. 6, p. 577–580.

———1981, Occurrence of N-nitrosamines in the workplace; some recent developments, *in* Scanlan, R.A., and Tannenbaum, S.R., eds., N-nitroso compounds, Divisions of Agricultural and Food Chemistry and Pesticide Chemistry Symposium, 181st Meeting, American Chemical Society, Atlanta, March 31–April 1, 1981; ACS Symposium Series 174: Washington, D.C., American Chemical Society, p. 207–216.

Fine, D.H., Rounbehler, D.P., Fan, T., and Ross, R., 1977, Human exposure to N-nitroso compounds in the environment, *in* Hiatt, H.H., Watson, J.D., and Winsten, J.A., eds., Origins of human cancer, Book A, Incidence of cancer in humans; Cold Spring Harbor Conferences on Cell Proliferation, Volume 4: Cold Spring Harbor, New York, Cold Spring Harbor Laboratory, p. 293–307.

Hirt, R.C., Schmitt, R.G., Searle, N.D., and Sullivan, A.P., 1960, Ultraviolet spectral energy distributions of natural sunlight and accelerated test light sources: Journal of the Optical Society of America, v. 50, no. 7, p. 706–713.

Hotchkiss, J.H., Libbey, L.M., Barbour, J.F., and Scanlan, R.A., 1980, Combination of a GC–TEA and a GC–MS–Data system for the μg/kg estimation and confirmation of volatile N-nitrosamines in foods, *in* Walker, E.A., Griciute, L., Castegnaro, M., and Borzsonyi, M., eds., N-nitroso compounds: analysis, formation and occurrence—Proceedings, 6th International Symposium on N-nitroso Compounds, Budapest, October 1979; IARC Scientific Publications No. 31: Lyon, France, International Agency for Research on Cancer, p. 361–373.

Hubbard, E.F., Kilpatrick, F.A., Martens, L.A., and Wilson, J.F., Jr., 1982, Measurement of time of travel and dispersion in streams by dye tracing, chap. A9 *of* bk. 3, Applications of hydraulics: U.S. Geological Survey Techniques of Water-Resources Investigations, 44 p.

Khan, S.U., 1981, N-nitrosamine formation in soil from the herbicide glyphosate and its uptake by plants, *in* Scanlan, R.A., and Tannenbaum, S.R., eds., N-nitroso compounds, Divisions of Agricultural and Food Chemistry and Pesticide Chemistry Symposium, 181st Meeting, American Chemical Society, Atlanta, March 31–April 1, 1981; ACS Symposium Series 174: Washington, D.C., American Chemical Society, p. 275–287.

Lijinsky, W., and Taylor, H.W., 1977, Nitrosamines and their precursors in food, *in* Hiatt, H.H., Watson, J.D., and Winsten, J.A., eds., Origins of human cancer, Book C, Human risk assessment; Cold Spring Harbor Conferences on Cell Proliferation, Volume 4: Cold Spring Harbor, New York, Cold Spring Harbor Laboratory, p. 1579–1590.

Magee, P.N., 1973, Mechanisms of transplacental carcinogenesis by nitroso compounds, *in* Tomatis, L., and Mohr, U., eds., Transplacental carcinogenesis, Meeting at Midizinische Hochschule, Hannover, Federal Republic of Germany, October 6–7, 1971, Proceedings; IARC Scientific Publications No. 4: Lyon, France, International Agency for Research on Cancer, p. 143–148.

Magee, P.N., Montesano, R., and Preussmann, R., 1976, N-nitroso compounds and related carcinogens, *in* Searle, C.E., ed., Chemical carcinogens: American Chemical Society Monograph 173, p. 491–625.

Montesano, Ruggero, and Bartsch, Helmut, 1976, Mutagenic and carcinogenic N-nitroso compounds: possible environmental hazards: Mutation Research, v. 32, p. 179–228.

Napalkov, N.P., 1973, Some general considerations on the problem of transplacental carcinogenesis, *in* Tomatis, L., and Mohr, U., eds., Transplacental carcinogenesis, Meeting at Midizinische Hochschule, Hannover, Federal Republic of Germany, October 6–7, 1971, Proceedings; IARC Scientific Publications No. 4: Lyon, France, International Agency for Research on Cancer, p. 1–13.

Oliver, J.E., 1981, Pesticide-derived nitrosamines, occurrence and environmental fate, *in* Scanlan, R.A., and Tannenbaum, S.R., eds., N-nitroso compounds, Divisions of Agricultural and Food Chemistry and Pesticide Chemistry Symposium, 181st Meeting, American Chemical Society, Atlanta, March 31–April 1, 1981; ACS Symposium Series 174: Washington, D.C., American Chemical Society, p. 349–362.

Rhoades, J.W., Hosenfeld, J.M., Taylor, J.M., and Johnson, D.E., 1980, Comparison of analyses of wastewaters for N-nitrosamines using various detectors, *in* Walker, E.A., Griciute, L., Castegnaro, M., and Borzsonyi, M., eds., N-nitroso compounds: analysis, formation and occurrence—Proceedings, 6th International Symposium on N-nitroso Compounds, Budapest, October 1979; IARC Scientific Publications No. 31: Lyon, France, International Agency for Research on Cancer, p. 377–385.

Sander, Johannes, 1973, The formation of N-nitroso compounds in the stomach of animals and man and in the diet, *in* Tomatis, L., and Mohr, U., eds., Transplacental carcinogenesis, Meeting at Midizinische Hochschule, Hannover, Federal Republic of Germany, October 6–7, 1971, Proceedings; IARC Scientific Publications No. 4: Lyon, France, International Agency for Research on Cancer, p. 159–163.

Sander, J., Ladenstein, M., LaBar, J., and Schweinsberg, F., 1975, Experiments on the degradation of nitrosamines by plants, *in* Bogovski, P., and Walker, E.A., eds., N-nitroso compounds in the environment—International Agency for Research on Cancer, Working conference, Lyon, France, October 17–20, 1973, Proceedings; IARC Scientific Publications No. 19: Lyon, France, International Agency for Research on Cancer, p. 205–210.

Scanlan, R.A., and Tannenbaum, S.R., eds., 1981, N-nitroso compounds, Divisions of Agricultural and Food Chemistry and Pesticide Chemistry Symposium, 181st Meeting, American Chemical Society, Atlanta, March 31–April 1, 1981; ACS Symposium Series 174: Washington, D.C., American Chemical Society, 400 p.

Sen, N.P., Seaman, S., and McPherson, M., 1980, Further studies on the occurrence of volatile and non-volatile nitrosamines in foods, *in* Walker, E.A., Griciute, L., Castegnaro, M., and Borzsonyi, M., eds., N-nitroso compounds: analysis, formation and occurrence—Proceedings, 6th International Symposium on N-nitroso Compounds, Budapest, October 1979; IARC Scientific Publications No. 31: Lyon, France, International Agency for Research on Cancer, p. 457–463.

Taylor, P., Braddock, P., and Carter, D., 1980, The analysis of N-nitrosodimethylamine in antihistamines and cough/cold preparations, *in* Walker, E.A., Griciute, L., Castegnaro, M., and Borzsonyi, M., eds., N-nitroso compounds: analysis, formation and occurrence—Proceedings, 6th International Symposium on N-nitroso Compounds, Budapest, October 1979, IARC Scientific Publications No. 31: Lyon, France, International Agency for Research on Cancer, p. 581–585.

U.S. Environmental Protection Agency, 1977, Scientific and technical assessment report on nitrosamines: EPA 600/6–77–001, Washington, D.C., Office of Research and Development, U.S. Environmental Protection Agency, 105 p. (NTIS PB–273–055)

———1979, Guidelines establishing test procedures for the analysis of pollutants; proposed regulations: Federal Register, v. 44, no. 233, p. 69496–69500.

Walker, E.A., Griciute, L., Castegnaro, M., and Borzsonyi, M., eds., N-nitroso compounds: analysis, formation and occurrence—Proceedings, 6th International Symposium on N-nitroso Compounds, Budapest, October 1979, IARC Scientific Publications No. 31: Lyon, France, International Agency for Research on Cancer, p. 349–463.

Estimating Stream-Aquifer Interactions in Coal Areas of Eastern Kansas by Using Streamflow Records

By Hugh E. Bevans

Abstract

Stream-aquifer interactions for drainage basins in coal areas of eastern Kansas were estimated from streamflow records and are presented as an alternative or supplement to digital modeling. Streams draining coal-mined parts of this area usually are contaminated during low flow by ground water containing large concentrations of sulfate discharged from the mines. The capacity of a stream to assimilate the coal-mine drainage is governed by the availability of base flow for dilution. Although digital models for simulating interactions between streams and aquifers are available, representative values of aquifer properties necessary to calibrate the models commonly are unavailable and are expensive to obtain.

Values of the stream-aquifer property T/a^2S (where T is the transmissivity of the aquifer, a is the average distance from the stream to the ground-water divide, and S is the storage coefficient of the aquifer) ranging from 0.012 to 0.049 per day were determined from the slopes of base-flow regression curves recorded at 18 selected streamflow-gaging stations. Correlation and regression analysis was used to develop an equation for predicting T/a^2S for ungaged streams in the study area:

$$T/a^2S = 0.050 - 0.0133 \log DA,$$

where DA is the drainage area, in square miles. The correlation coefficient for this relationship is -0.99, and the standard error of estimate is 0.001 per day. Examples of procedures for estimating ground-water storage, recharge, discharge, and evapotranspiration by means of streamflow records and T/a^2S values are presented.

INTRODUCTION

Information concerning stream-aquifer interactions is needed to manage the hydrologic impacts of coal mining. Streams draining coal-mined areas of eastern Kansas usually are contaminated by ground-water discharge from abandoned and reclaimed coal mines. Large concentrations of sulfate, derived from the oxidation of iron sulfide minerals, and other dissolved constituents in the coal-mine drainage can seriously degrade the quality of a receiving stream during low flow. The capacity of a stream to assimilate coal-mine drainage is primarily a function of the availability (magnitude and duration) of base flow for dilution. The availability of base flow is governed by the extent and geohydrologic properties of aquifers that provide it.

Although digital ground-water flow models for simulating stream-aquifer interactions are available, representative values of aquifer properties necessary to calibrate the models commonly are unavailable and are expensive to obtain. Also, because aquifer properties vary considerably with rock type, the cyclic stratigraphic succession of Pennsylvanian rocks found in eastern Kansas and throughout the Western Interior Coal Province precludes the determination of representative values by aquifer tests.

An alternative approach to determining the stream-aquifer interaction for a particular drainage basin is based on the analysis of the recession curve of base flow. The slope of the base-flow recession curve has been shown by Rorabaugh (1964) to be related to the stream-aquifer property, T/a^2S, where T is the transmissivity of the aquifer; a is the average distance from the stream to the ground-water divide, which, for stream-aquifer systems, usually corresponds to the drainage-basin divide; and S is the storage coefficient of the aquifer.

Purpose and Objectives

The purpose of this report is to describe the use of streamflow records to estimate stream-aquifer interactions. The principal objectives are as follows:

1. Present the theoretical development and assumptions underlying the relationship between the slope of the base-flow recession curve and the stream-aquifer property, T/a^2S;
2. Describe a procedure for determining T/a^2S from base-flow recession curves;
3. Compute T/a^2S for streams in the study area that have adequate streamflow records;
4. Develop a relationship between T/a^2S and drainage area so that T/a^2S can be estimated for ungaged basins in the study area; and
5. Provide examples of estimating ground-water recharge, storage, discharge, and evapotranspiration by using streamflow records.

Study Area

The study area (fig. 1) is that part of eastern Kansas where rocks of Pennsylvanian age crop out. Most of the coal mines and remaining coal reserves in Kansas are in this approximately 13,000-mi^2 area, which includes all or parts of 26 counties. The eastern boundary is the Kansas-Missouri State line, except for the extreme southeast corner of the State where rocks of Mississippian age crop out; the southern boundary is the Kansas-Oklahoma State line; the western boundary approximates the outcrop of the geologic contact between Permian and Pennsylvanian rocks; and the northern boundary is the Kansas River. Although Pennsylvanian rocks occur north of the Kansas River, overlying deposits of glacial drift and loess make this area hydrologically different from the study area.

The Pennsylvanian bedrock consists of cyclic deposits of marine shale and limestone and nonmarine coal, underclay, and some sandstone (Merriam, 1963). The strata dip gently towards the northwest at about 20 ft/mi exposing progressively older rocks of the Virgilian, Missourian, and Desmoinesian Series from the northwest to the southeast. The thickness of Pennsylvanian rocks ranges from almost zero at the outcrop of the geologic contact between Pennsylvanian and Mississippian rocks in the southeast corner of the study area to about 2,000 ft at the outcrop of the geologic contact between Permian and Pennsylvanian rocks along the western edge of the study area. In addition to the cyclic nature and the relatively gentle slope of the Pennsylvanian strata, other characteristics include (1) the lateral persistence of very thin strata, (2) the large ratio of stratum width to the thickness, and (3) the extreme abruptness of the boundaries between strata.

The study area is included in the Osage Plains unit of the Central Lowlands physiographic province (Schoewe, 1949). The land surface slopes gently towards the southeast and comprises broad, level flood plains and gently rolling to hilly uplands. Differential erosion of the alternating layers of shale and limestone has formed northeast-trending cuestas with gentle northwest-dipping slopes and steep southeast-facing escarpments (Merriam, 1963). Local relief is generally less than 250 ft.

The climate is humid continental with cold, dry polar air masses dominating during the winter and warm, moist air masses from the Gulf of Mexico dominating during the summer. Mean annual precipitation increases from about 36 inches in the northwest to about 40 inches in the southeast (according to an unpublished map distributed by the Kansas Agricultural Experiment Station that was based on National Weather Service data for 1941–70). Most of the precipitation occurs during the growing season, April–October, as rain from intense local thunderstorms or longer duration storms of great areal

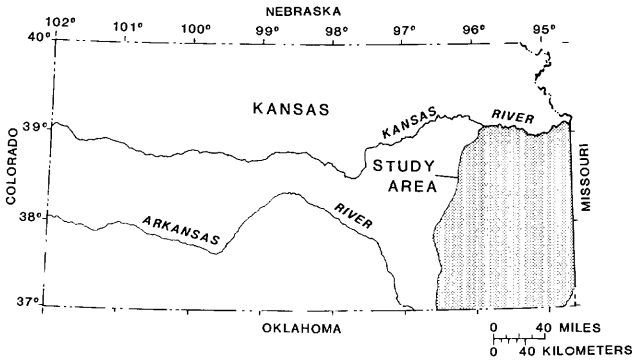

Figure 1. Location of study area in Kansas.

extent. Droughts can occur at any time of the year but are particularly severe during July and August when evapotranspiration rates are the greatest.

Streamflow in the study area is mainly a result of overland runoff from storms. Base flow is not well sustained because of the predominance of fine-grained marine shale bedrock.

THE STREAM-AQUIFER PROPERTY, T/a^2S

Theoretical Development

Rorabaugh developed an equation for determining the hydraulic diffusivity of an aquifer or the ratio of transmissivity (T) to the storage coefficient (S), from the slope of the water-level recession in an observation well (Rorabaugh, 1960, p. 317, eq. 5).

$$\frac{T}{S} = \frac{4a^2\ 2.303\ \log(h_1/h_2)}{\pi^2\ (t_2 - t_1)} = \frac{0.933\ a^2\ \log(h_1/h_2)}{(t_2 - t_1)}, \quad (1)$$

where T = transmissivity of the aquifer, in feet squared per day,
S = storage coefficient of the aquifer, dimensionless,
a = half-width of the aquifer, in feet,
h_1 = initial water level, in feet, at time t_1, in days,
h_2 = water level, in feet, at time t_2, in days, and
π = 3.14.

The assumptions underlying the application of equation 1 are:

1. The aquifer is thick relative to the change in water level;
2. The aquifer is wide relative to its thickness;
3. The aquifer is uniform in shape, isotropic, and homogeneous;
4. The aquifer is underlain by relatively impermeable material, and its side boundaries are vertical and fully penetrating;

5. The initial water level is everywhere horizontal prior to recharge;
6. The recharge that raises the water level is instantaneous and evenly distributed;
7. Sufficient time has passed so that the water level is declining exponentially with time; and
8. Extraneous natural factors (such as precipitation and evapotranspiration) and human-induced factors (such as irrigation) are not affecting the water level.

Because base flow is ground-water discharge, a base-flow recession curve also should decline exponentially with time after recharge ceases. Rorabaugh used this hypothesis to develop an equation for computing the ground-water discharge to one side of a stream per unit of stream length (Rorabaugh, 1964, p. 433, eq. 1):

$$q = 2T(h_o/a)(e^{-\pi^2 Tt/4a^2S} + e^{-9\pi^2 Tt/4a^2S} + e^{-25\pi^2 Tt/4a^2S} + \ldots) \quad (2)$$

where T, S, a, and π are the same as in equation 1,

q = ground-water discharge, in cubic feet per second, along one side of a stream per foot of stream length, at any time (t), in days, after recharge ceases,

h_o = an instantaneous rise in water level, in feet, and

e = exponential.

Rorabaugh evaluated equation 2 and determined that when Tt/a^2S is greater than 0.2, the plot of the logarithm of streamflow versus time becomes a straight line and only the first exponential term in equation 2 is significant. Therefore, equation 2 reduces to (Rorabaugh, 1964, p. 433, eq. 3):

$$q = 2T\,(h_o/a)\,e^{-\pi^2\,Tt/4a^2S}. \quad (3)$$

Because the logarithm of streamflow decreases exponentially with time after $Tt/a^2S = 0.2$, the critical time (t_c) in days, after recharge ceases when this occurs is computed by (Rorabaugh, 1964, p. 434):

$$t_c = \frac{0.2a^2S}{T}. \quad (4)$$

As the equations were used by Rorabaugh, a reasonably accurate value of the aquifer half-width (a) was required. However, because the base flow in any stream is a function of both T/S and a, there is no need to determine a because it can be used as part of a lumped parameter with T and S, and equation 1 can be written as:

$$\frac{T}{a^2S} = \frac{0.933 \log (h_1/h_2)}{(t_2 - t_1)}, \quad (5)$$

where T/a^2S, in d^{-1}, is a constant that represents base-flow recession in the basin for which it is computed.

Further, if the base-flow recession curve is evaluated after t_c to determine the time required for streamflow to decline through one log cycle (Δt/log cycle), equation 5 reduces to (Rorabaugh and Simons, 1966, p. 12):

$$\frac{T}{a^2S} = \frac{0.933}{\Delta t/\text{log cycle}}, \quad (6)$$

which can be rewritten as

$$\frac{a^2S}{T} = \frac{\Delta t/\text{log cycle}}{0.933}, \quad (7)$$

and combined with equation 4 to compute the critical time

$$t_c = \frac{0.2\ (\Delta t/\text{log cycle})}{0.933}. \quad (8)$$

The applications of equations 5, 6, 7, and 8 to compute the stream-aquifer properties, T/a^2S and t_c, do not require the determination of a. Therefore, the assumptions necessary to apply these equations are simplified considerably from those required for equation 1. In fact, if the slope of the base-flow recession curve is a straight line that declines exponentially with time after the critical time has been reached and that is not being affected by factors other than the hydrologic properties of the contributing aquifers, then the required assumptions virtually have been met.

Determining T/a^2S from Streamflow Records

Selecting Streamflow Records

The most critical factors to consider in selecting streamflow records for determining T/a^2S are those that could alter the slope of the base-flow recession curve from what would be expected if aquifer characteristics alone were determining the slope. These extraneous factors include: (1) streamflow regulation by reservoirs, (2) withdrawals for water supplies and return flow, (3) evapotranspiration, and (4) streamflow provided by surface runoff from precipitation or snowmelt.

Proper selection of streamflow records can eliminate the effects of extraneous factors. Avoiding streamflow records that are affected by large reservoirs, extensive watershed projects (such as erosion-control structures), or water withdrawals for irrigation, industrial, and municipal supplies and subsequent return flows will

eliminate human-induced extraneous factors. Small, scattered stock ponds probably have minimal regulating effects and do not need to be considered. Effects of evapotranspiration can be eliminated by selecting periods of record during the nongrowing season. It usually is difficult to eliminate the effects of streamflow provided by overland runoff from precipitation or snowmelt. It is especially difficult to determine periods of record when there has been sufficient time between periods of precipitation for the slope of the base-flow recession curve to stabilize. However, if the streamflow records are long term and climatological data (rainfall, snowfall, and air temperature) are available, adequate periods of record usually can be selected. If long-term, base-flow recession data are not available, a recession curve can be developed by combining segments of base-flow recession curves that are straight or that are approaching a straight line on a semilogarithmic plot (Trainer and Watkins, 1974, p. 126).

In drainage basins that have two or more geologically distinct and hydrologically different aquifers, the base-flow recession curve may be compound. Compound curves are base-flow recession curves that have breaks in slope. The breaks in slope occur at rates of base streamflow where base-flow recession begins to be controlled by a hydrologically different aquifer or group of aquifers. The slope and length of each straight-line segment of the compound curve depend on the hydraulic properties and the extent of the aquifer or group of aquifers it represents. Compound curves may represent basins with significant unconsolidated aquifers of alluvium, terrace deposits, or glacial drift, in addition to the bedrock aquifer. Following recharge, initial base-flow recession and the resulting slope of the base-flow recession curve would be controlled by the unconsolidated deposits. After the unconsolidated deposits are drained, the bedrock aquifer would control base-flow recession, and the slope of the base-flow recession curve would change. Drainage basins with geologically different types of bedrock, shale and sandstone for example, also may have compound curves.

Compound curves were not a factor in this investigation because the study area was selected to represent only Pennsylvanian bedrock. Although there are alternating thin layers of shale and limestone, the stratigraphy is relatively constant throughout the study area, and alluvial, terrace, and glacial deposits are relatively insignificant.

Computing T/a^2S

If periods of streamflow record are selected according to the constraints discussed in the preceding section and the base-flow recession curve declines exponentially with time after the critical time has been reached, then the assumptions required to determine T/a^2S from the streamflow record virtually have been met. Values of T/a^2S are determined by the following procedure:

1. The time that recharge occurred (t_o) is assumed to be the point at which the streamflow hydrograph reaches its peak (Wilder and Simmons, 1978, p. 11).
2. The slope of the base-flow recession curve, in days per log cycle (d/log cycle), is determined from the recession curve after it becomes a straight line, either by the observed decrease through one log cycle or by extrapolating the straight-line part of the base-flow recession curve through one log cycle if additional recharge occurs before streamflow declines through one log cycle.
3. The slope of the base-flow recession curve is inserted into equation 8 as Δt/log cycle, and the critical time (t_c), in days (d), is computed.
4. The computed critical time is checked against the streamflow hydrograph. The computed critical time needs to be equivalent to the period from the hydrograph peak to the point on the recession curve where the curve becomes a straight line. If computed and observed critical times are the same, then the slope of the base-flow recession curve can be used in equation 6 to compute T/a^2S in d^{-1}. If the computed and observed critical times differ significantly, then extraneous factors probably are affecting the slope of the base-flow recession curve and that particular streamflow record is not appropriate for determining T/a^2S.
5. T/a^2S values are determined from several base-flow recession curves, representing different ranges of base-flow rate, and compared to see if T/a^2S is constant. If the values are constant or are within a narrow range, then T/a^2S can be considered a stream-aquifer constant. If T/a^2S varies with the rate of base flow, it may be necessary to construct a compound curve, reflecting base-flow contributions from geologically and hydrologically dissimilar aquifers. The straight-line segments that represent ranges of base-flow rate contributed by different aquifers can be developed individually as simple curves and joined together to form the compound curve, or the entire compound curve can be developed from base-flow recessions that drain all of the contributing aquifers.

As an example, this procedure was used to determine T/a^2S for Big Hill Creek near Cherryvale, Kans. (station 16 in fig. 3). Although streamflow at this station has been regulated by Big Hill Lake since 1981, data from before regulation are available (data from unpublished records on file with the U.S. Geological Survey, Lawrence, Kans.). Base-flow recession curves for five periods, selected to satisfy the required assumptions, are plotted in figure 2. The extrapolated slope of the base-flow recession curves, represented by the dashed line, was determined to be 32 d/log cycle. By inserting 32 d into equation 8, the critical time (t_c), or the time required for the slope of the recession curve to become a straight line, can be computed:

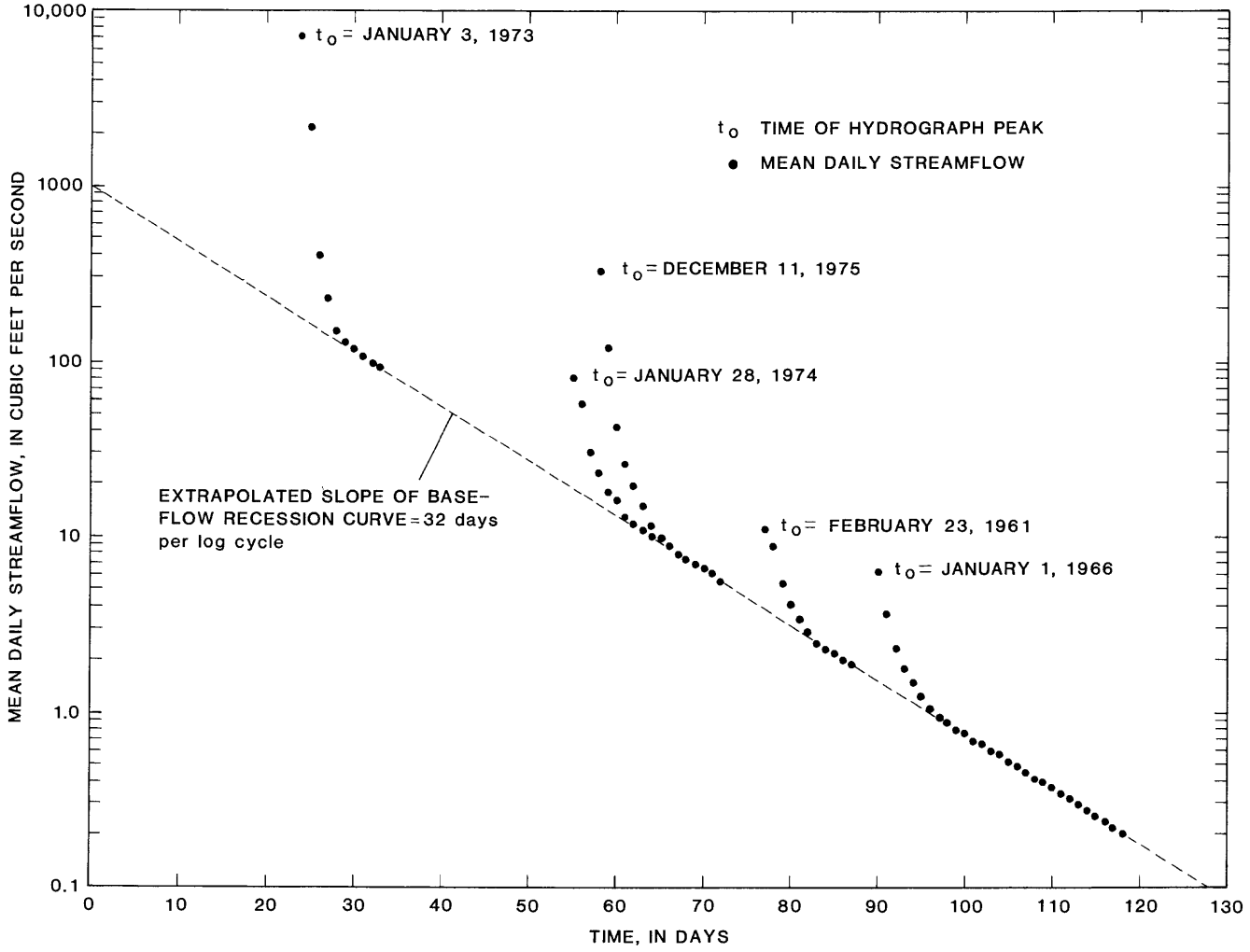

Figure 2. Determination of the slope of the base-flow recession curve for Big Hill Creek near Cherryvale.

$$t_c = \frac{0.2\ (32\ \text{d})}{0.933} = 6.86\ \text{d}\ .$$

Comparison of the computed value of t_c, 6.86 d, with the base-flow recession curves in figure 2 indicates that the computed value agrees very well with the graphical representation of the time required for the recession curves to become straight lines. Therefore, the base-flow recession slope of 32 d/log cycle is a reasonable estimate and 32 d can be inserted into equation 6 to compute T/a^2S:

$$\frac{T}{a^2S} = \frac{0.933}{32\ \text{d}} = 0.029\ \text{d}^{-1}\ .$$

Also, because the slope of the base-flow recession curve does not vary with the rate of base flow after t_c, the recession curve is simple as opposed to compound.

Values of T/a^2S, in d^{-1}, were computed from selected periods of streamflow records for streamflow-gaging stations in the study area (fig. 3) and are presented in table 1. The slopes of the base-flow recession curves for all the stations did not vary with base-flow rate after the critical time (t_c), allowing the recessions to be represented by simple curves.

Estimating T/a^2S for Ungaged Streams

Many streams, particularly those draining small basins, have not been gaged, and streamflow records for determining T/a^2S are unavailable. To estimate T/a^2S in ungaged basins, a regional relationship between T/a^2S and drainage area was developed through correlation and regression analysis.

The Pennsylvanian bedrock that controls the slope of the base-flow recession curve is predominantly shale with some limestone, coal, underclay, and sandstone. The cyclic nature, lateral persistence, and uniform thinness of Pennsylvanian rock strata result in the occurrence of relatively constant proportions of rock types in drainage

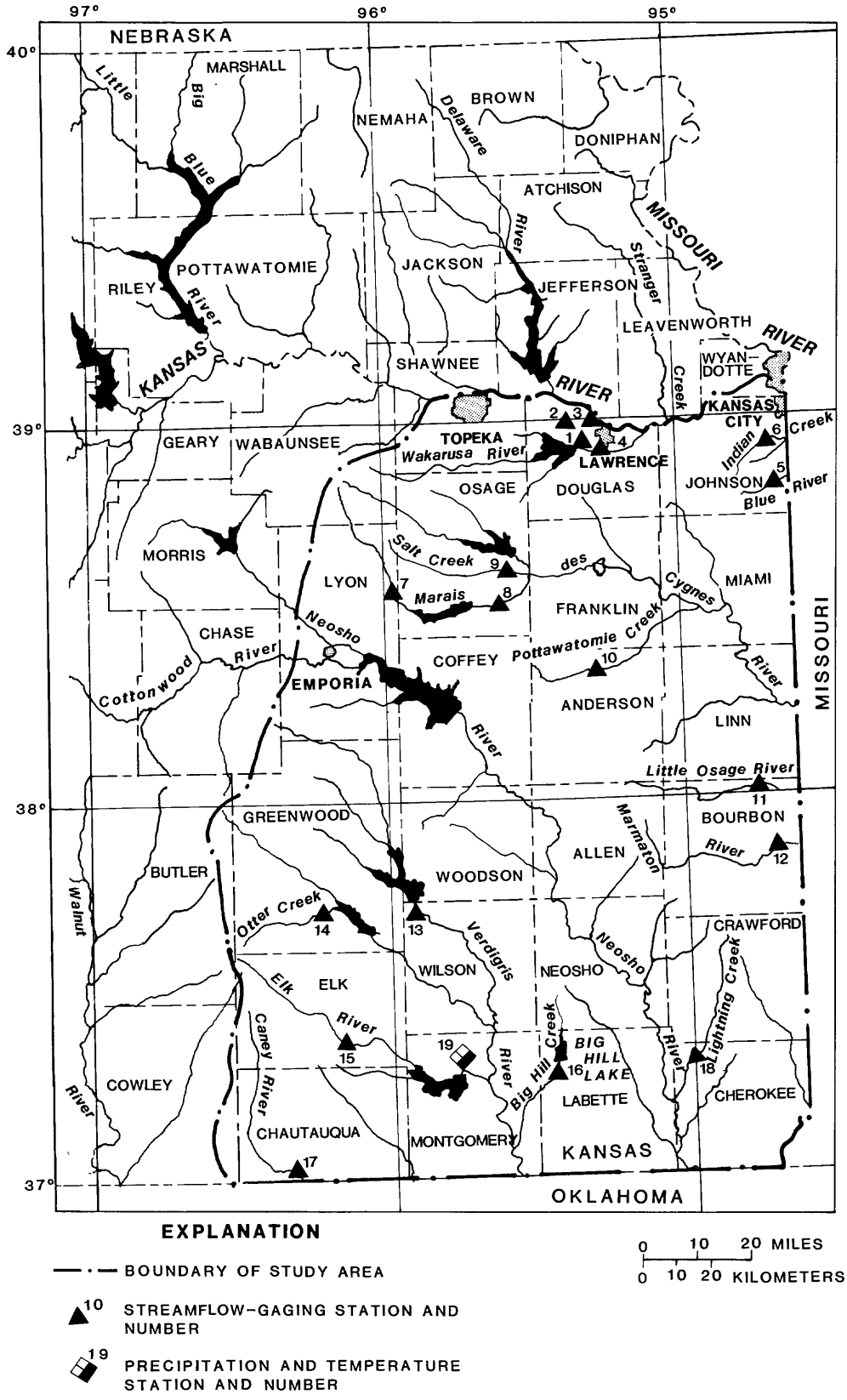

Figure 3. Location of streamflow-gaging and weather stations.

Table 1. Drainage area, slope of base-flow recession curve, critical time (t_c), and T/a^2S determined for selected streams

Station number (see fig. 3)	Station name	Drainage area (mi^2)	Slope of base-flow recession curve (d/log cycle)	Critical time (t_c) (d)	T/a^2S (d^{-1})
1	Yankee Tank Creek near Lawrence	3.90	22	4.72	0.042
2	East Branch Yankee Tank Creek near Lawrence	1.35	19	4.07	.049
3	West Branch Yankee Tank Creek near Lawrence	1.85	20	4.29	.047
4	Wakarusa River near Lawrence	425	59	12.6	.016
5	Blue River near Stanley	46.0	34	7.29	.027
6	Indian Creek near Overland Park	26.6	27	5.79	.034
7	Marais des Cygnes River near Reading	177	45	9.65	.021
8	Marais des Cygnes River at Melvern	351	52	11.1	.018
9	Salt Creek near Lyndon	111	38	8.14	.024
10	Pottawatomie Creek near Garnett	334	51	10.9	.018
11	Little Osage River at Fulton	295	56	12.0	.017
12	Marmaton River near Fort Scott	408	58	12.4	.016
13	Verdigris River near Coyville	747	80	17.1	.012
14	Otter Creek at Climax	129	45	9.65	.021
15	Elk River at Elk Falls	220	53	11.4	.018
16	Big Hill Creek near Cherryvale	37.0	32	6.86	.029
17	Caney River near Elgin	445	62	13.3	.015
18	Lightning Creek near McCune	197	46	9.86	.020

basins throughout the study area. Therefore, it is reasonable to assume that average basin values of hydraulic diffusivity (T/S) are relatively constant and that variation in average distance from the stream to the ground-water divide (a) is the major factor causing variation in T/a^2S. In an area of relatively constant geology, climate, and physiography, drainage basins usually develop similarly in shape, and probably will be related directly to drainage-area size. Therefore, assuming that T/a^2S primarily is a function of a, there probably is a direct relationship between drainage area and T/a^2S.

A relationship between drainage area and T/a^2S determined for 18 selected streamflow-gaging stations in the study area (table 1) was developed by correlation and regression analysis. Drainage area, in square miles, was designated the independent variable and T/a^2S, in d^{-1}, the dependent variable. The resulting correlation coefficient of -0.99 between these two variables indicates a significant inverse relationship. Squaring the correlation coefficient indicates that 98 percent of the variation in T/a^2S results from variation in drainage area. The scatter diagram, regression line, and 95-percent prediction interval for this relationship are shown in figure 4. The regression equation is semilogarithmic in form with T/a^2S, in d^{-1}, expressed in arithmetic units and drainage area in square miles (DA), expressed in log units:

$$T/a^2S = 0.050 - 0.0133 \log DA. \quad (9)$$

The standard error of estimate for this equation is 0.001 d^{-1}. This regression equation is adequate for predicting T/a^2S for ungaged streams in the study area.

ESTIMATING STREAM-AQUIFER INTERACTIONS BY USING STREAMFLOW RECORDS

Methods are available that use the stream-aquifer property (T/a^2S) to estimate volumes of ground-water storage, recharge, and discharge from one or a series of recharge occurrences and to estimate rates of evapotranspiration.

Estimating Ground-Water Storage, Recharge, and Discharge

Rorabaugh (1964) developed equation 3 for computing the ground-water discharge to one side of a stream per unit of stream length. This equation is valid after the critical time ($t_c = 0.2a^2S/T$) required for the base-flow recession curve to become a straight line. Glover (1964) showed that at the critical time approximately one-half of the ground water from a period of recharge has been discharged into the stream as base flow if the required assumptions for computing T/a^2S have been met. Therefore, if the volume of ground water remaining in storage from the recharge can be determined at t_c, the volume

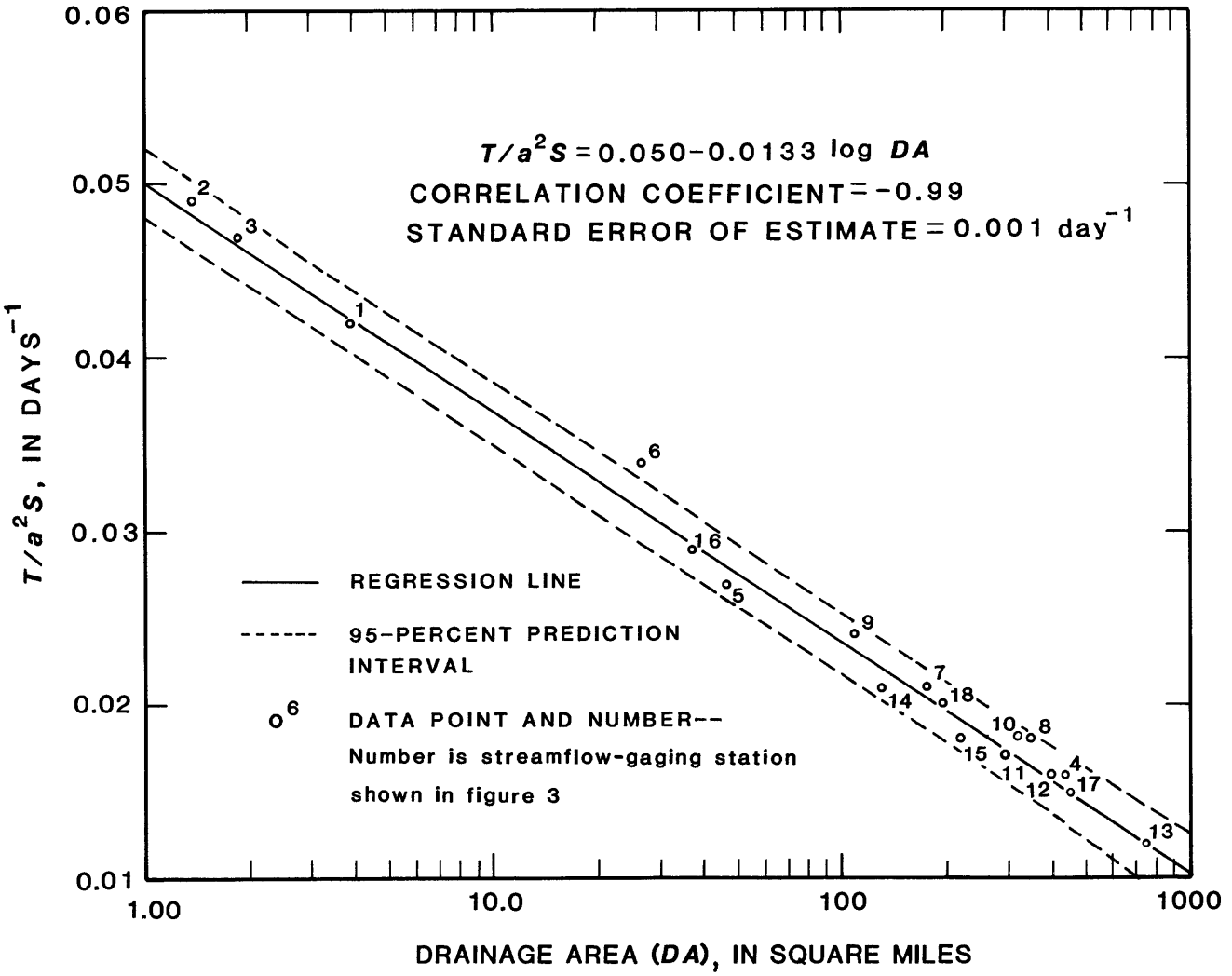

Figure 4. Relationship between drainage area and T/a^2S for selected streams.

discharged by that time is equal to the volume of the ground water remaining in storage, and the recharge is equal to the sum of the volume of ground water remaining in storage and the volume already discharged.

Rorabaugh integrated equation 3 with respect to time to compute the volume (v), in cubic feet, of ground water remaining in storage on one side of a stream per foot of stream length, at any time after t_c (Rorabaugh, 1964, p. 490, eq. 11):

$$v = q\left(\frac{4a^2S}{\pi^2 T}\right), \tag{10}$$

where q is ground-water discharge, in cubic feet per second, along one side of a stream per foot of stream length.

Equation 10 can be modified to compute the total volume of ground water remaining in storage at t_c. At t_c we know from equation 7 that $a^2S/T = \Delta t/0.933$, where Δt is the time required for the base flow to recede through one log cycle. By rearranging equation 7, we also know that $\Delta t = 0.933\ a^2S/T$. Substituting for a^2S/T and then for Δt, in equation 10, we get:

$$v = \frac{qt_c\ (0.933a^2S/T)}{2.3}, \tag{11}$$

where qt_c is the ground water discharged along one side of the stream per foot of stream length at t_c. To compute the ground water remaining in storage at t_c on both sides of the stream and along its entire reach (V, in cubic feet), replace qt_c with the rate of base flow at t_c (Qt_c, in cubic feet per second):

$$V = \frac{Qt_c\ (0.933a^2S/T)}{2.3} \tag{12}$$

Because one half of the ground water in storage from the recharge period has been discharged to the stream by t_c, the ground-water discharge (D) is equal to V and the recharge (R) is equal to D plus V or $2V$.

If equation 12 is applied to a single recession slope, it can be used only to compute the volume of ground water remaining in storage from all previous periods of recharge. To compute storage, recharge, and discharge for a single recharge occurrence, the ground water remaining in storage from previous recharge needs to be removed. The procedures are illustrated using a section of a streamflow hydrograph for Big Hill Creek near Cherryvale (fig. 5). If interest lies only in knowing the volume of ground water remaining in storage at t_{c3}, then Qt_{c3} (which is the summation of base flow from recharge period 3 and all previous periods) needs to be determined. The value of Qt_{c3} is estimated in the following manner:

1. The slope of the recession curve has been determined previously to be 32 d/log cycle, so
2. $0.933\ a^2S/T = 32$ d, and
3. $t_c = 0.2\ (a^2S/T) = 6.86$ d; then
4. Extrapolate the declining limb of the hydrograph for recharge period 3 to time = t_{c3}, or 6.86 d after the peak, where the base-flow recession curve becomes a straight line with a slope of 32 d/log cycle; and
5. Determine the base flow at time = t_{c3} ($Qt_{c3} = 17$ ft^3/s) from figure 5; and
6. Insert the determined values into equation 12 to compute the volume of ground water remaining in storage at time = t_{c3} from recharge period 3 and all previous periods of recharge:

$$V = (17\ \text{ft}^3/\text{s})(32\ \text{d})/2.3 \times 86{,}400\ \text{s/d}$$
$$= 20{,}000{,}000\ \text{ft}^3$$
$$= 460\ \text{acre-ft}.$$

To compute storage, recharge, and discharge at time = t_{c3} that have resulted only from recharging period 3, the base flow from previous periods of recharge needs to be removed. This is accomplished by the following procedure:

1. Extrapolate the declining limb of the hydrograph for recharge period 2 to time = t_{c2} or 6.86 d after the peak;
2. After t_{c2} the slope of the base-flow recession curve, 32 d/log cycle, is extended to point B directly below t_{c3};
3. At time = t_{c3} the ground water remaining in storage from recharge period 3 ($V3$) is:

$$V3 = (Qt_{c3} - QB)\ (0.933\ a^2S/T)/2.3 \times 86{,}400$$
$$= (17\ \text{ft}^3/\text{s} - 16\ \text{ft}^3/\text{s})(32\ \text{d})/2.3 \times 86{,}400\ \text{s/d}$$
$$= 1{,}200{,}000\ \text{ft}^3$$
$$= 27.5\ \text{acre-ft};$$

4. Recharge from period 3 ($R3$) is:

$$R3 = 2V3$$
$$= 2{,}400{,}000\ \text{ft}^3$$
$$= 55\ \text{acre-ft}; \text{ and}$$

5. Discharge from period 3 ($D3$) is:

$$D3 = V3$$
$$= 1{,}200{,}000\ \text{ft}^3$$
$$= 27.5\ \text{acre-ft}.$$

This procedure is used also to compute ground-water storage, recharge, and discharge from period 2 at time = t_{c2} (fig. 5).

Estimating Evapotranspiration

Daniel (1976) extended a previously developed but unpublished method by M. I. Rorabaugh for computing ground-water discharge from an aquifer underlain by a leaky boundary, to determine evapotranspiration rates. The equation developed by Rorabaugh is (Daniel, 1976, p. 361, eq. 7):

$$q = (h_oT/a)\ (Ca^2S/h_oT)$$
$$\cdot \left[1 + 2 \sum_{m=1,3,5}^{\infty} \left(\frac{h_oT}{Ca^2S} - \frac{4}{\pi^2m^2}\right) e^{-m^2\pi^2Tt/4a^2S}\right] \quad (13)$$

where C is a constant rate of head change dh/dt, and all other terms are as previously defined. In the case of constant leakage or evapotranspiration, dh/dt is negative. Constant rates of water-level decline ($C = -dh/dt$) from either leakage or evapotranspiration cause the base-flow recession curve to bend downward.

A dimensionless family of type curves representing equation 13 when C is negative and qa/h_oT is equal to or greater than 0.01 is shown in figure 6. This family of curves can be compared to base-flow recessions that are affected by evapotranspiration to determine the rate of evapotranspiration.

The assumptions, in addition to those discussed for computing T/a^2S, that need to be met before this procedure can be used to estimate the average rate of evapotranspiration affecting base-flow recession are: (1) There is no leakage, (2) the evapotranspiration rate is constant throughout the period for which it is computed, and (3) evapotranspiration occurs at an equal rate throughout the basin. If the base-flow recession is a straight line after t_c during periods when evapotranspiration is insignificant

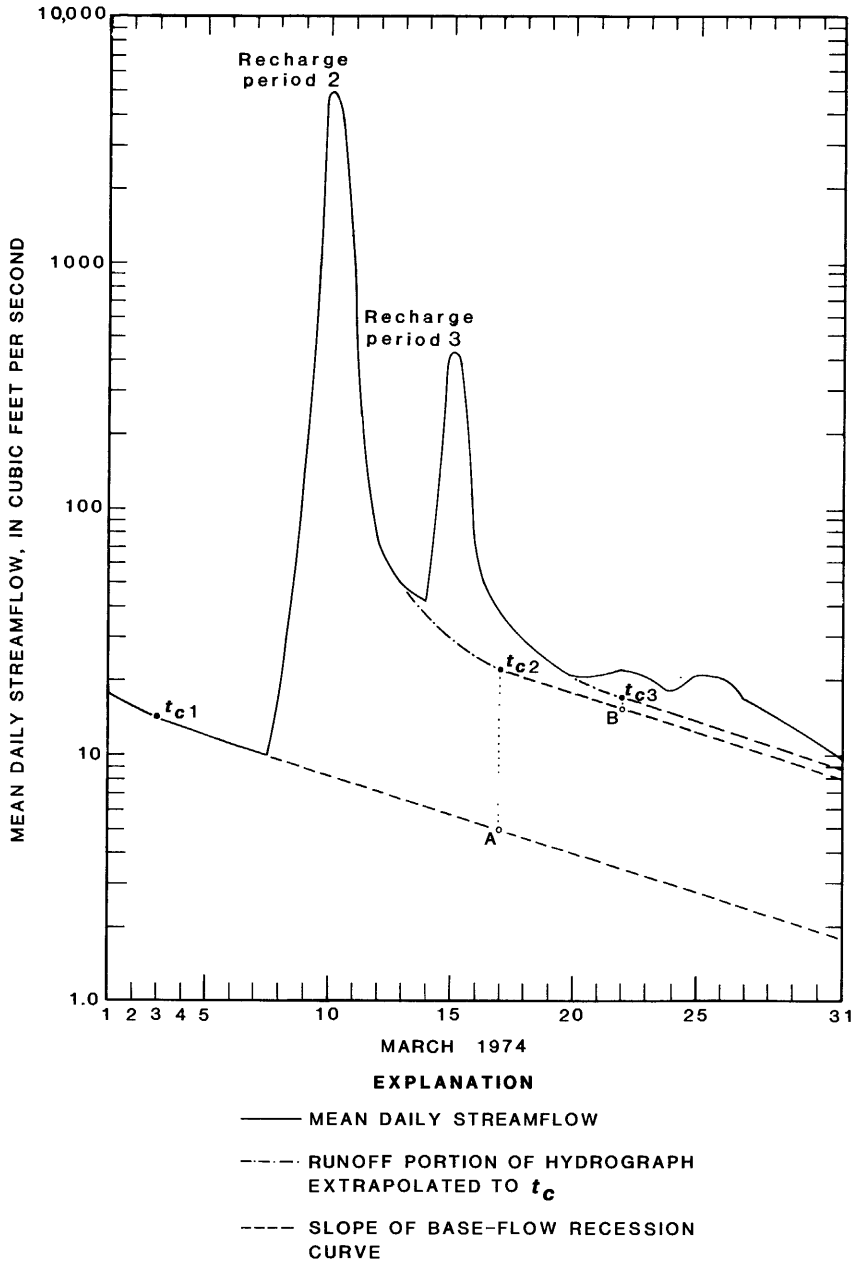

COMPUTING GROUND-WATER STORAGE (V_2), RECHARGE (R_2), AND DISCHARGE (D_2) FROM RECHARGE PERIOD 2 AT TIME = t_{c2}

Given:

Slope of base-flow recession curve = 32 d/log cycle;

therefore,

$a^2 S/T = 34.3$ d, and

$t_c = 6.86$ d

$V_2 = (Qt_{c2} - Q_A)\ (0.933\ a^2 S/T)/2.3 \times 86{,}400$

$= (23\ ft^3/s - 5\ ft^3/s)(32d)/2.3 \times 86{,}400\ s/d$

$= 22{,}000{,}000\ ft^3$

$= 500$ acre-ft

$R_2 = 2V_2$

$= 1000$ acre-ft

$D_2 = V_2$

$= 500$ acre-ft

Figure 5. Streamflow hydrograph for Big Hill Creek near Cherryvale used to estimate ground-water storage, recharge, and discharge.

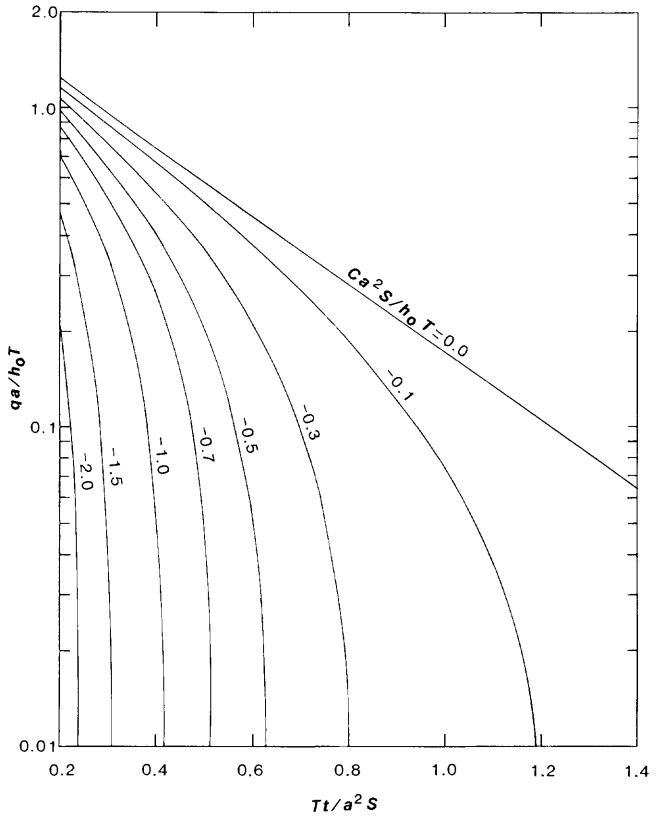

Figure 6. Family of dimensionless type curves representing the effects of constant rates of evapotranspiration on base-flow recession (modified from Daniel, 1976).

(during winter months), then there is no leakage and the first assumption is met. If the effect of evapotranspiration on base-flow recession is constant through the observed period, assumptions 2 and 3 will be met. However, the result applies to the effect of evapotranspiration on base flow and does not provide an areal evapotranspiration rate.

This procedure was used to determine the rate of evapotranspiration from a streamflow hydrograph for Big Hill Creek near Cherryvale (fig. 7). The first step is to replot the recession curve with the time scale converted to Tt/a^2S. To convert time to Tt/a^2S, set the time when recharge stopped (should be at the critical time) to $t = 0$, and then divide the time, in days following recharge, by a^2S/T (32 d/0.933 = 34.3 d). The critical factor in this step is to realize that recharge continues during overland runoff, and the base-flow recession curve, affected by evapotranspiration and with the time scale converted to Tt/a^2S, will not be defined by equation 13 until overland runoff ceases. Also, the assumption of recharge occurring instantaneously at the streamflow peak may be in error, and a slight mechanical shifting along the time scale usually is necessary to match the replotted base-flow recession curve with one of the type curves.

The replotted recession curve for Big Hill Creek near Cherryvale is shown in figure 8. For this example, June 12 was used as $t = 0$. The recession curve matches the type curve in figure 6 where $Ca^2S/h_oT = -0.3$. If the match point is chosen where $qa/h_oT = 1.0$, to simplify the solution, then the evapotranspiration rate (E) is equal to $-0.3\ Q$ (where Q is the base flow, in cubic feet per second, when $qa/h_oT = 1.0$ in fig. 8). At the point where $qa/h_oT = 1.0$, $Q = 4.3$ ft^3/s, and the evapotranspiration rate is

$$E = -0.3\ Q$$

$$= -1.29\ \text{ft}^3/\text{s}.$$

This rate applies to the period (June 12–July 9, 1974) for which it was determined. The temperature and precipitation data for a nearby weather station (Elk City Dam, station 19 in fig. 3) show that no major climatic change occurred after June 9 (fig. 7). Climatic consistency and the close match of the observed recession with the type curve indicate that the required assumption of a constant rate of evapotranspiration during the period has been met and that the estimated evapotranspiration rate for this period is reasonably valid.

SUMMARY

Information concerning stream-aquifer interactions in coal areas is necessary to manage stream contamination that commonly results from coal mining. Although digital models for determining stream-aquifer interactions are available, representative aquifer properties necessary to calibrate the models usually are unavailable and are expensive to obtain. An alternative approach to determine stream-aquifer interactions involves the analysis of base-flow recession curves.

The theoretical development and assumptions underlying the relationship between the base-flow recession curve and the stream-aquifer property, T/a^2S, are presented. The procedure developed for computing T/a^2S within a framework of assumptions is used to compute T/a^2S values (ranging from 0.012 to 0.049 d^{-1}) for 18 selected streams in the coal area of eastern Kansas. A relationship for predicting T/a^2S for ungaged streams in the study area was developed:

$$T/a^2S = 0.050 - 0.0133 \log DA,$$

where DA is the drainage area, in square miles. Procedures and accompanying examples of estimating groundwater storage, recharge, and discharge and the rate of evapotranspiration with T/a^2S values and streamflow records are presented. Values determined by using these procedures are adequate for estimating stream-aquifer interactions.

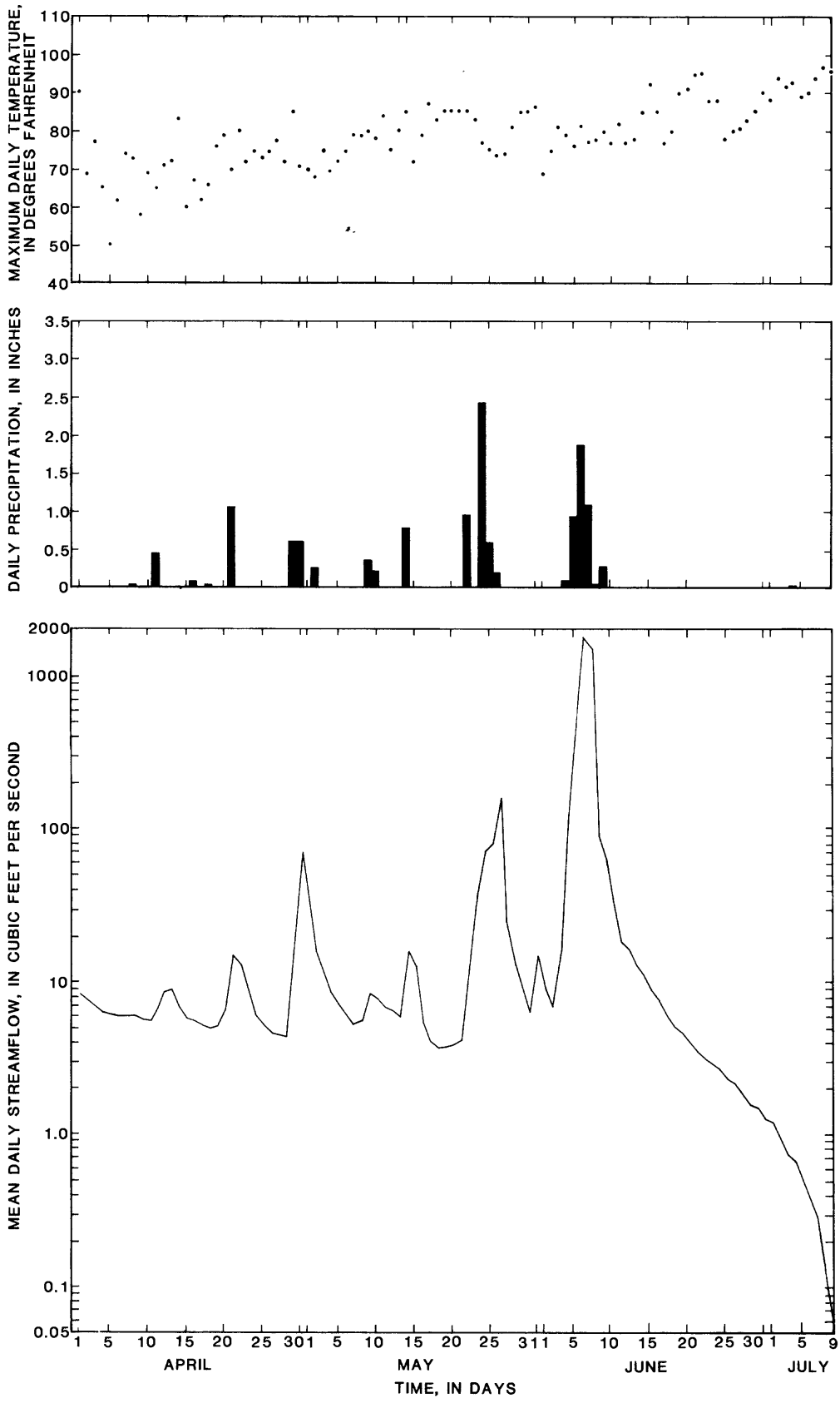

Figure 7. Daily maximum temperature and daily precipitation at Elk City Dam and mean daily streamflow at Big Hill Creek near Cherryvale, for April 1–July 9, 1974.

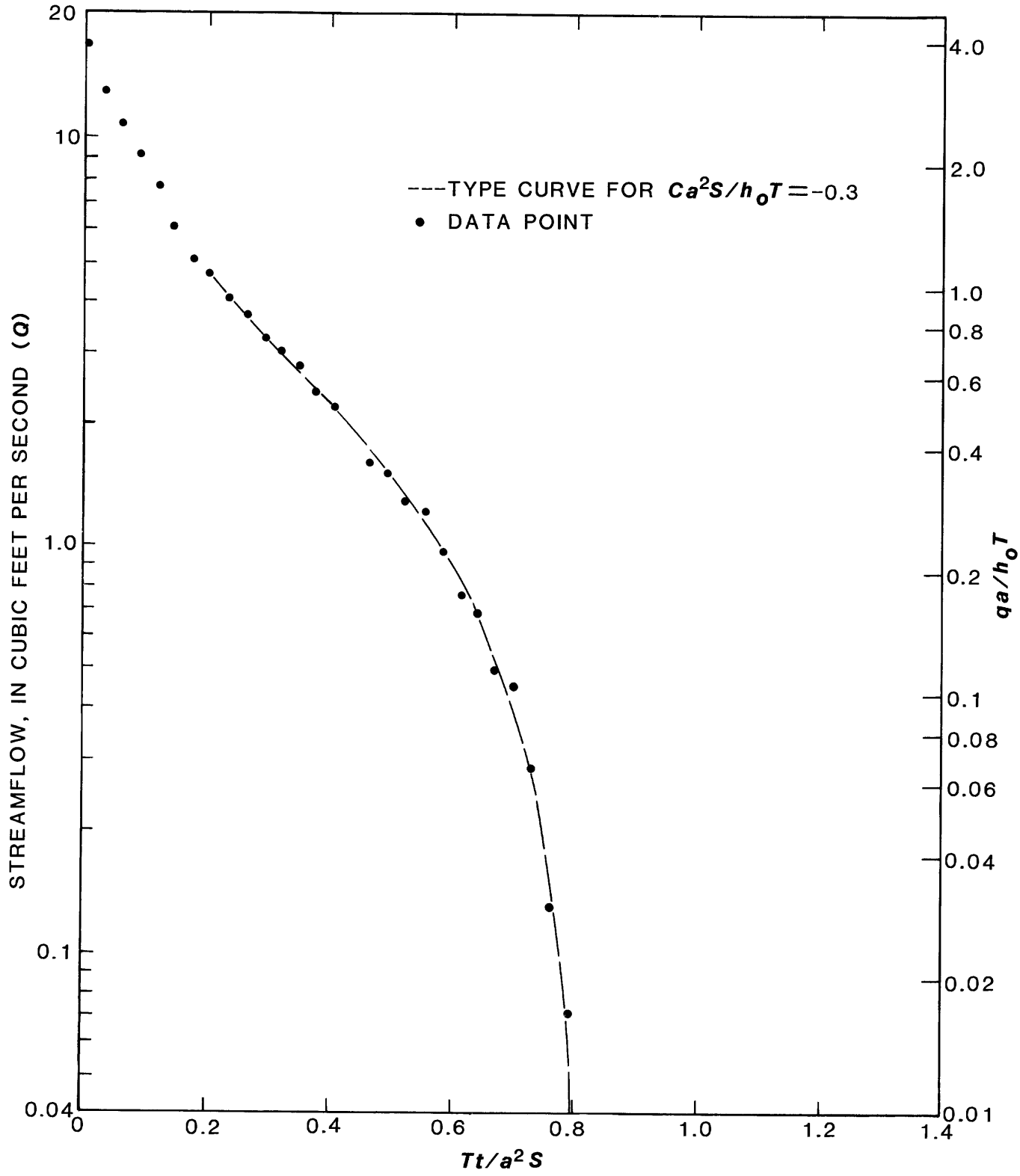

Figure 8. Match between dimensionless curve for $Ca^2S/h_oT = -0.3$ and base-flow recession curve for Big Hill Creek near Cherryvale (June 12–July 9, 1974) used to estimate evapotranspiration rate.

REFERENCES CITED

Daniel, J.F., 1976, Estimating ground-water evapotranspiration from streamflow records: Water Resources Research, v. 12, no. 3, p. 360–364.

Glover, R.E., 1964, Ground-water movement: U.S. Bureau of Reclamation Engineering Monograph 31, p. 31–34.

Merriam, D.F., 1963, The geologic history of Kansas: Kansas Geological Survey Bulletin 162, p. 103–135.

Rorabaugh, M.I., 1960, Use of water levels in estimating aquifer constants in a finite aquifer: International Association of Scientific Hydrology Commission of Subterranean Waters, Publication No. 52, p. 314–323.

———1964, Estimating changes in bank storage and ground-water contribution to streamflow: International Association of Scientific Hydrology Symposium Surface Waters, Publication No. 63, p. 432–441.

Rorabaugh, M.I., and Simons, W.D., 1966, Exploration of methods relating ground water to surface water, Columbia River basin—Second phase: U.S. Geological Survey Open-File Report, 62 p.

Schoewe, W.H., 1949, The geography of Kansas, part 2, Physical geography: Transactions of Kansas Academy of Science, v. 52, no. 3, p. 261–333.

Trainer, F.W., and Watkins, F.A., Jr., 1974, Use of base-runoff recession curves to determine areal transmissivities in the Upper Potomac River basin: U.S. Geological Survey Journal of Research, v. 2, no. 1, p. 125–131.

Wilder, H.B., and Simmons, C.B., 1978, Program for evaluating stream quality in North Carolina: U.S. Geological Survey Circular 764, p. 8–12.

Investigations of Organic Contaminants Derived From Wood-Treatment Processes in a Sand and Gravel Aquifer Near Pensacola, Florida

By Wilfred E. Pereira *and* Colleen E. Rostad

Abstract

Discharge of effluent wastes containing creosote and pentachlorophenol into surface impoundments at a wood-treatment facility has resulted in contamination of a sand and gravel aquifer near Pensacola, Florida. Six sites, consisting of three to five clustered wells per site, were sampled to study changes in ground-water chemistry downgradient of the impoundments and to define background concentrations of organic contaminants. Vertical and horizontal distributions of concentrations of dissolved organic carbon indicated the presence of a contaminant plume that had moved a considerable distance from the source of contamination.

Analysis of ground water by gas chromatography-mass spectrometry near the source of contamination revealed the presence of approximately 84 organic contaminants. Classes of compounds identified included phenols, polycyclic aromatic hydrocarbons, and heterocycles, containing oxygen, nitrogen, and sulfur. A selected number of compounds from each chemical class was quantified in ground-water samples. Vertical and horizontal distributions of phenols, polycyclic aromatic hydrocarbons, and heterocycles indicated the presence of an "oil zone," a main contaminant plume, and a secondary contaminant plume. Two explanations for the presence of the secondary contaminant plume are postulated. The plume may have its origin in an interruption to discharge or may result from "up-coning" of the contaminant plume in the vicinity of a perennial stream. Results of this study indicated that, in aquifer materials of low organic-carbon content (<0.1 percent), processes such as sorption are relatively insignificant, resulting in the migration of different classes of organic compounds en masse through the porous medium.

INTRODUCTION

Advances in technology in the last few decades have resulted in the generation of millions of tons of chemical wastes that have the potential for being hazardous to human health and the environment. In the past, many of these chemicals were improperly disposed of on land and in the Nation's waterways, resulting in degradation of ground- and surface-water quality (Freeze and Cherry, 1979).

Organic compounds that are applied to land surfaces are subject to various mechanisms that tend to prevent or retard their migration through the unsaturated zone. These attenuating mechanisms include chemical precipitation, chemical degradation, volatilization, biotransformations, and adsorption (Freeze and Cherry, 1979). When soil is heavily contaminated by chemical wastes, to the point of exceeding its adsorptive-retention capacity, then many diverse organic compounds can seep through the unsaturated zone and reach the water table (Page, 1981). Once a contaminant reaches the water table and enters the saturated zone, it still may be influenced by various physical, chemical, and biological processes. These processes include dilution, buffering of pH, precipitation by reaction of water with indigenous waters or solids, precipitation due to hydrolysis, removal due to oxidation or reduction, mechanical filtration, biological assimilation or degradation, radioactive decay, membrane filtration, and sorption (Page, 1981).

The wood-preservation industry generates significant quantities of chemical wastes in its effluents. The U.S. Environmental Protection Agency (1981) estimated that there are more than 415 wood-preserving plants in the United States. This industry applies chemical preservatives to wood products such as utility poles, fence posts, and railroad ties in order to impart fungicidal, insecticidal, and fire-retardant properties. Some of these chemicals include creosote, pentachlorophenol, and water-soluble formulations of salts of copper, chromium, and arsenic. In addition to these chemicals, effluents from wood-treatment plants often contain natural organic compounds derived from wood, such as lignin, tannic acid, and resin acids.

Effluent wastewaters from these plants are often discharged into surface impoundments or ponds that may be lined or unlined. In areas where unlined impoundments are constructed in highly permeable soils, fluid wastes can infiltrate through the sides and bottoms of these ponds into the ground water. Solid wastes may be leached by precipitation and similarly enter the ground-water regime. Once these wastes reach the water table,

they have the potential for moving downgradient in an aquifer and being discharged at some point into a nearby lake or stream. The resultant effect of discharging chemical wastes into unlined surface impoundments is the degradation of both ground- and surface-water quality.

In 1982, the Office of Hazardous Waste Hydrology of the U.S. Geological Survey instituted an interdisciplinary research study to investigate the behavior, movement, and fate of hazardous chemical wastes in ground water. To better understand processes controlling the fate and movement of organic compounds derived from creosote and pentachlorophenol wastes in the subsurface environment, a study was initiated at an abandoned wood-treatment facility near Pensacola, Fla. Because of the presence of similar classes of chemical compounds in wastes derived from coal and oil shale conversion processes, research findings at this site may have significant transfer value to ground-water contamination problems associated with alternate fuel technologies. This report describes results of our preliminary investigations.

Acknowledgments

The authors are grateful to David Troutman, Bernard Franks, and Robert Kirkland of the Florida District, U.S. Geological Survey, for providing ground-water and porous-media core samples used in this study.

SITE DESCRIPTION

A creosote works, located within the city limits of Pensacola, Fla., operated from 1902 until 1981 and has since discontinued all operations. The plant was situated approximately 550 m north of Pensacola Bay near the entrance to Bayou Chico (fig. 1) and occupied an area of approximately 72,846 m^2. Prior to 1950, creosote was used exclusively as a wood preservative in the treatment of southern-pine utility poles. Since 1950, a mixture of creosote and pentachlorophenol, with diesel fuel as a solubilizing agent, was used in the treatment process. It is

Figure 1. Areal map showing location of the creosote works site, Pensacola, Fla.

estimated that approximately 94.63 m^3 per month of each preservative was used at this facility, before its closure in 1981.

During the course of operation, wastewaters containing entrained oils generated from the treatment process were discharged into two unlined surface impoundments. These impoundments were constructed with clay embankments at the surface and are in direct contact with an unconsolidated sand and gravel aquifer. The main impoundment or recirculation pond occupied 7,689.3 m^2 and held approximately 9,370.8 m^3 of wastewater. The second impoundment was used as an overflow pond and occupied 3,237.6 m^2. It held approximately 3,945.6 m^3 of wastewater. Periodically, when water levels in the ponds became high, some of the wastewater was discharged and allowed to evaporate in evaporation areas north of the recirculation pond and in an adjacent area east of the overflow pond.

A shallow perennial stream located south of the impoundments intersects the water table in the vicinity of Pensacola Yacht Club, causing ground water adjacent to the stream channel to discharge into the stream. This stream discharges into Pensacola Bay.

The wastes contain polycyclic aromatic compounds (PAC's), many of which are suspected carcinogens and mutagens. Seepage of these chemical wastes from surface impoundments has also resulted in vertical migration of an oil phase through the unsaturated zone to the groundwater table. This oil phase evidently has migrated within the capillary fringe in a horizontal direction parallel to the ground-water table, in the direction of the ground-water gradient, towards the perennial stream and Pensacola Bay. The stream and bay are being contaminated by pools of black oily material that is denser than water. It is possible that many organic contaminants in the capillary fringe partition between the oil and water phases, resulting in ground-water contamination. The oil phase is thereby enriched in PAC and higher molecular weight polymers during its passage through the capillary fringe towards the stream and Pensacola Bay.

The sand and gravel aquifer is the principal source of ground water in northwest Florida (Leach, 1982). The aquifer is at land surface near the eastern extremity and near the creosote works (southeast Escambia County); the aquifer is 91.4–121.9 m thick and extends to 213.4 m or more in depth in southwest Escambia County. The aquifer is unconfined and consists of unconsolidated sand and gravel, interbedded with discontinuous layers of clay, which significantly affects the flow of ground water in the contaminated area. The aquifer is recharged by rainfall. Where clay lenses do not impede the movement of water, the aquifer is porous, and permeabilities tend to be high (Musgrove and others, 1965). Details of the site and the hydrogeology of the area were reported by Troutman and others (1984).

LOCATION OF WELLS

Six well sites were selected for multidepth sampling (fig. 2). Well J1 is located upgradient of the surface impoundments and serves as a control site. Five additional well locations, J3 through J7, are situated downgradient of the surface impoundments. Well J2 was constructed at a later date and hence was not sampled. These locations and sampling depths were selected to study vertical and horizontal subsurface migration of organic contaminants, obtain information concerning changes in ground-water chemistry downgradient of the impoundments, and define background concentrations. Ground-water samples were not collected at specific depths in certain wells due to problems encountered during drilling. For example, in well J4 at a depth of 6.1 m and in well J6 at a depth of 12.2 m the presence of clay lenses precluded the collection of water samples.

METHODS OF ANALYSIS

Sample Collection

In general, each well was developed by using a centrifugal pump until the pH, specific conductance, and temperature of the ground water stabilized. Some 2.54-cm diameter wells (sites 3 and 4, in particular) were developed only with a peristaltic pump for a "reasonable" time period, equivalent to, typically, 10 or more casing volumes. Stability of standard field parameters was not achieved in all cases in order to (1) avoid significant plume movement, (2) limit the water samples to the (small, 0.6-m) screened interval for investigation of vertical variations, and (3) minimize the disposal problem. Samples were collected in clean amber 1-L glass bottles, using a peristaltic pump. Samples were chilled in ice and transported immediately to the laboratory for analysis.

Sample Preparation

Organic compounds were isolated from ground water by a solid-phase extraction technique (Rostad and others, 1984) on a cartridge of surface-modified silica (Bondelut™—cyclohexyl-bonded phase; Analytichem International, Inc.). The cartridge was sequentially washed with 10-mL volumes of methylene chloride, methanol, and distilled water on a vacuum manifold (Baker–10). The ground-water sample was filtered through a glass-fiber filter (Gelman A–E; Gelman Sciences, Inc.) to remove particulate matter and oil droplets, and 50–100 mL of the filtrate was passed through the cartridge under aspirator vacuum at a flow rate of 10–20 mL/min. The cartridge was centrifuged at 1,000 r/min (revolutions per

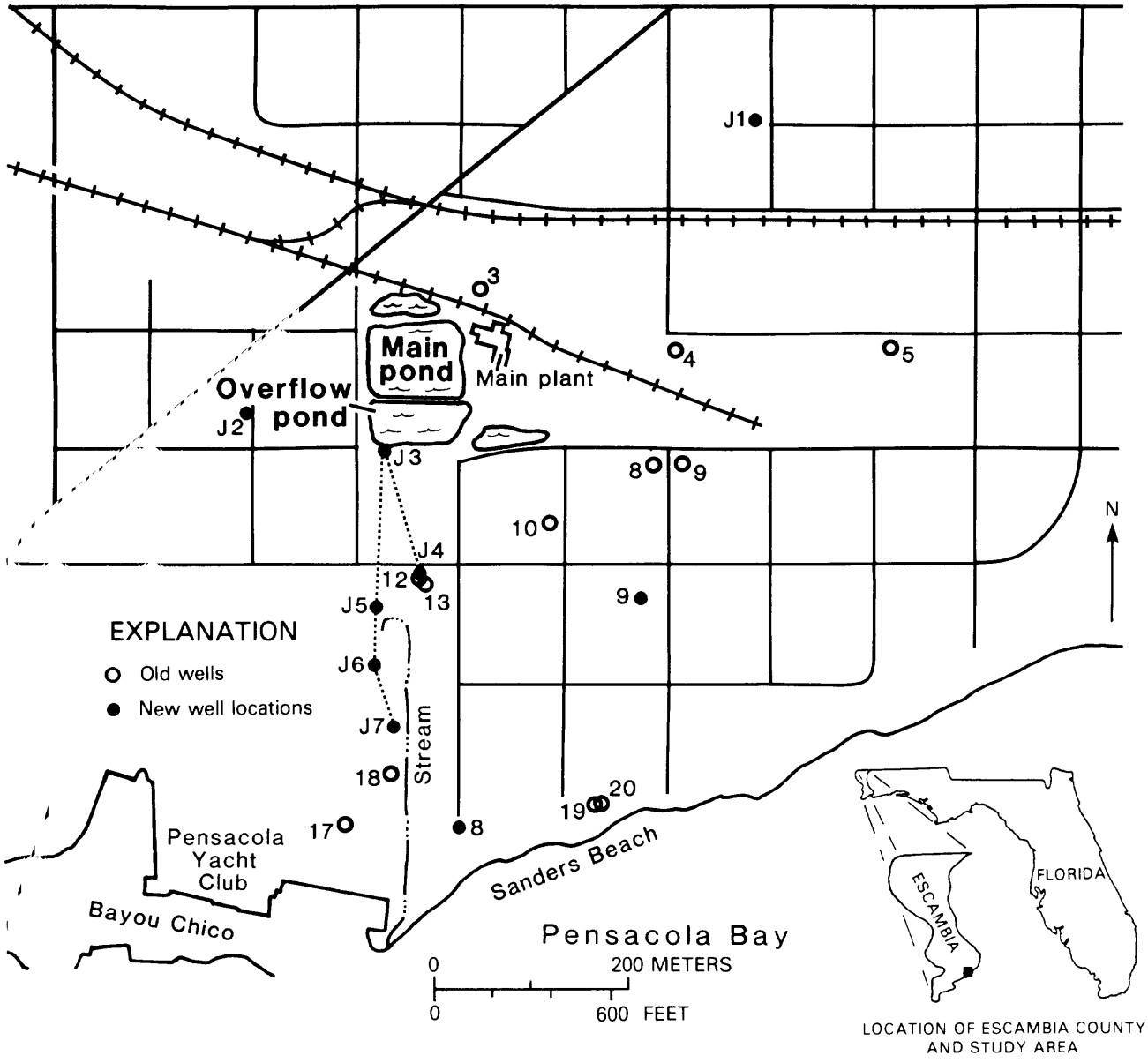

Figure 2. Map showing locations of wells at the creosote works study site.

minute) for 1 min to remove most of the entrapped water. The cartridge was placed in a 15-mL graduated centrifuge tube, 1 mL of acetonitrile was added to the cartridge, and it was eluted by centrifugation at 1,000 r/min for 1 min. The cartridge was centrifuged with 3 mL of methylene chloride to elute the remaining organic compounds. The combined acetonitrile-methylene chloride eluate was then passed through a microcolumn containing anhydrous sodium sulfate into a 10-mL graduated receiver. The combined organic extract was evaporated to a volume of 100 μL under a stream of dry nitrogen and analyzed by gas chromatography–mass spectrometry (Rostad and others, 1984).

Instrumental Analyses

Instrumental analyses were performed on a Finnigan OWA 20 capillary-gas chromatography, mass-spectrometry system. The gas chromatographer (GS) was equipped with a wall-coated open tubular (WCOT) fused-silica capillary column 30 m long by 0.26 mm ID (internal diameter) coated with DB–5 (J. & W. Scientific). The linear velocity of helium through the column was 29 cm/s; injections were made by means of the splitless-injection technique. The GC oven was held at 50 °C for 4 min and programmed at 6 °C/min to a maximum of 300 °C. One μL of each sample extract was injected at

50 °C. The vent valve was automatically opened at 45 s, and the filament and multiplier was automatically turned on at 240 s. Data acquisition began simultaneously with injection of the sample. The mass spectrometer (MS) was operated in the electron-impact mode using an ionizing voltage of 70 eV and an ionization current of 250 μA. The instrument was scanned repetitively from 40 to 450 atomic mass units (AMU) in 0.9 s.

Determination of Organic Contaminants in Ground Water

A standard solution for GC–MS analysis was prepared containing 100 ng/μL of each compound to be quantified. A library of mass spectra of these standard compounds was established with d_{10}-phenanthrene (the standard for quantitation) as the first entry in the library. For each library entry, a response factor, a specific ion used for quantitation, and the amount of the compound was entered. Solutions of the standard mixture at three different concentrations were analyzed by GC–MS to determine response factors for each compound, relative to d_{10}-phenanthrene. A computer quantitation routine searched for each compound within an elution-time window. If the library spectrum matched a peak in this time window, the area of the specific preselected ion was quantified. This area was converted to a specific amount, by means of the response factors determined previously. Recovery studies were also conducted by spiking native ground water at various concentration levels and determining the recovery of individual compounds. Details of this procedure are reported in Rostad and others (1984).

Compound identification and confirmation.—Individual organic compounds in ground water were confirmed by comparison of their mass spectra and retention indices (Kovats, 1958) with those of standard reference compounds. Compounds for which standard reference materials were not available were tentatively identified by comparing their mass spectra with spectra contained in the National Bureau of Standards Library. All compounds quantified were confirmed by comparison of their mass spectra and retention indices with authentic standards analyzed under identical conditions.

Physical appearance and pH.—Ground-water samples obtained at different sampling depths from wells J1 and J3 through J7 were physically inspected for oil droplets, and the pH of each sample was determined after transport to the laboratory. These data are shown in table 1. In addition to fine-grained quartz sand, some samples contained small dispersed oil droplets, or a surface film of oil; samples obtained from a depth of 12.2 m in wells J3 and J5 contained an oil phase that was denser than water. Native ground water from well J1 had an average pH of approximately 7.18, whereas samples near the zone of contamination had a pH of approximately 5.1–7.3. The generally lower pH of these samples was attributed to the presence of acidic compounds, which are known to occur in creosote.

Table 1. Physical appearance and pH of ground-water samples from wells J1 and J3 through J7

[---, sample not collected; two-phase, a small amount of oil was present as a separate phase]

Sampling depth (m)	Physical appearance and pH of ground-water samples from wells					
	J1	J3	J4	J5	J6	J7
3	---	---	7.20 Oil film	---	---	---
6.1	7.52	5.40 Oil film	---	7.31 Oil film	6.22 Oil droplets	7.58
12.2	---	5.51 Two-phase	6.00 Oil droplets	5.06 Two-phase	---	---
18.3	7.69	6.36 Oil film	5.70 Oil droplets	7.45	7.68	6.89
24.4	---	6.20	6.97	7.36	6.40	7.81
30.5	6.32	7.29	7.36	7.54	7.00	7.33

Dissolved organic carbon (DOC).—Ground-water samples obtained from wells J1 and J3 through J7 were analyzed for DOC by the U.S. Geological Survey, Denver Central Laboratory. Samples were filtered through a 0.45-μm silver membrane filter (Selas Corporation) before analysis.

RESULTS AND DISCUSSION

DOC concentrations in ground-water samples collected from wells J1 and J3 through J7 as a function of sampling depth are shown in table 2. DOC concentrations in native ground water (well J1) ranged from 10 to 13 mg/L. DOC concentrations in natural ground-water samples collected from various parts of the United States range from less than 0.1 to 15 mg/L with a median value of 0.7 mg/L (Leenheer and others, 1974). At each depth, in general, the horizontal distribution of DOC concentrations indicated a decrease in DOC values with increasing distance from the contamination source. However, in well

Table 2. Dissolved organic carbon (DOC) concentrations (in milligrams per liter) in ground-water samples from wells J1 and J3 through J7

[---, sample not collected]

Sampling depth (m)	DOC concentrations of ground-water samples from wells					
	J1	J3	J4	J5	J6	J7
3	---	---	50	---	---	---
6.1	13	200	---	40	10	18
12.2	---	40	40	30	---	---
18.3	10	50	20	13	21	12
24.4	---	6	6	4.8	15	9.6
30.5	12	3	5.1	3.2	4.3	5.8

J6, DOC concentrations were elevated at depths of 18.3 and 24.4 m. These high DOC values indicated the presence of a contaminant plume that moved through the aquifer a considerable distance from the source of contamination. As expected, the vertical distribution of DOC concentrations within each well indicated a general decrease in DOC values with increasing depth. Although nonspecific, gross-pollution parameters (such as DOC) are generally considered to be of little value for samples that may contain trace amounts of toxic or hazardous contaminants (Jungclaus and others, 1976), DOC measurements are useful in assessing trends in concentrations of organic compounds in ground water (Leenheer and others, 1974) and in delineating the extent of degradation of ground-water quality (Hughes and others, 1974).

Characterization of Organic Contaminants in Ground Water

To evaluate vertical and horizontal distributions of organic contaminants in the porous medium of the saturated zone, it was necessary to isolate and characterize organic compounds in ground water near the source of contamination, prior to their migration in the aquifer. A sample from well J3 at a depth of 12.2 m was analyzed by GC–MS for organic compounds, to determine compound classes and specific organic compounds in ground water before they are further influenced by physical, chemical, and biological processes. Identified organic compounds with their molecular weights, molecular formulas, and Kovats' retention indexes (Kovats, 1958) are listed in table 3.

Data in table 3 indicate that the major classes of compounds present include phenols, polycyclic aromatic hydrocarbons (PAH's), and heterocycles containing nitrogen, oxygen, and sulfur. By far the majority of compounds listed in table 3 are derived either from creosote or from commercial pentachlorophenol, used in the wood-treatment process. A few minor compounds, such as α-terpineol and the alkylated benzaldehydes, probably are of natural origin, occurring in the tissues of southern-pine logs and poles. Polycyclic aromatic compounds (PAC's) with as many as four rings were identified in ground water. Higher molecular weight PAC's, which are known to occur in creosote and coal-tar (Pereira and others, 1983), were not detected in ground water. These larger annulated PAC's probably are associated with the oil phase and sediments in the surface impoundments. Because of the compositional complexity of the organic contaminants in ground water, the study was limited to a few selected compounds from each chemical class (tables 4–9). These compounds were selected to study (1) vertical and horizontal distributions of organic contaminants in ground water downgradient of the impoundments and

Table 3. Organic compounds in ground water from well J3 at a depth of 12.2 m

[Retention indexes from Kovats (1958); ---, reference standard not available; *, major component]

Peak no.	Compound	Molecular weight	Molecular formula	Retention index	
				Sample	Standard
1.	Phenol*	94	C_6H_6O	972.7	977.9
2.	Benzonitrile	103	C_7H_5N	977.6	---
3.	Benzofuran	118	C_8H_6O	991.3	995.8
4.	Indane	118	C_9H_{10}	1040.1	1036.1
5.	1H-indene	116	C_9H_8	1041.9	1045.3
6.	Phenol, 2-methyl-*	108	C_7H_8O	1050.3	1055.2
7.	Ethanone, 1-phenyl-	120	C_8H_8O	1064.7	---
8.	Phenol, 3-methyl-*	108	C_7H_8O	1073.1	1077.3
9.	Phenol, 2,6-dimethyl-*	122	$C_8H_{10}O$	1105.0	1107.6
10.	C_2-phenol	122	$C_8H_{10}O$	1111.2	---
11.	C_2-phenol	122	$C_8H_{10}O$	1118.6	---
12.	C_2-phenol	122	$C_8H_{10}O$	1126.7	---
13.	C_2-phenol	122	$C_8H_{10}O$	1131.1	---
14.	C_2-phenol	122	$C_8H_{10}O$	1143.5	---
15.	Phenol, 2,4-dimethyl-*	122	$C_8H_{10}O$	1149.1	1150.0
16.	Phenol, 3,5-dimethyl-*	122	$C_8H_{10}O$	1170.2	1171.1
17.	Phenol, 2,3-dimethyl-	122	$C_8H_{10}O$	1178.3	1180.8
18.	Naphthalene*	128	$C_{10}H_8$	1188.8	1186.0
19.	Phenol, 3,5-dimethyl-	122	$C_8H_{10}O$	1192.6	1193.6
20.	α-terpineol	154	$C_{10}H_8O$	1194.4	---
21.	Benzo[b]thiophene	134	C_8H_6S	1195.7	1193.9
22.	Phenol, 2,4,6-trimethyl-	136	$C_9H_{12}O$	1204.6	1203.9
23.	Phenol, 3-(1-methylethyl)-	136	$C_9H_{12}O$	1228.1	---
24.	C_3-phenol	136	$C_9H_{12}O$	1234.0	---
25.	C_3-phenol	136	$C_9H_{12}O$	1238.6	---
26.	Quinoline*	129	C_9H_7N	1242.5	1238.1
27.	C_3-phenol*	136	$C_9H_{12}O$	1260.1	---
28.	Isoquinoline	129	C_9H_7N	1265.4	1261.4
29.	C_3-phenol	136	$C_9H_{12}O$	1268.0	---
30.	Phenol, 2,3,5-trimethyl-	136	$C_9H_{12}O$	1272.6	1275.3
31.	1H-inden-1-one, 2,3-dihydro-	132	C_9H_8O	1285.0	---
32.	Naphthalene, 2-methyl-*	142	$C_{11}H_{10}$	1298.7	1298.4
33.	C_3-phenol	136	$C_9H_{12}O$	---	---
34.	Quinoline, 2-methyl-	143	$C_{10}H_9N$	1313.3	1311.1
35.	Benzo [b]thiophene, 3-methyl-	148	C_9H_8S	1314.7	1316.0
36.	Naphthalene, 1-methyl-*	142	$C_{11}H_{10}$	1316.8	1316.0
37.	Benzaldehyde, 2,5-dimethyl	134	$C_9H_{10}O$	1319.6	---
38.	C_1-quinoline	143	$C_{10}H_9N$	1322.4	---
39.	Benzaldehyde, 3,4-dimethyl-*	134	$C_9H_{10}O$	1342.0	---
40.	C_1-quinoline	143	$C_{10}H_9N$	1358.0	---
41.	1,1'-biphenyl*	154	$C_{12}H_{10}$	1383.9	1384.4
42.	Naphthalene, 2,6-dimethyl-	156	$C_{12}H_{12}$	1410.5	1411.1
43.	Naphthalene, 1,6-dimethyl-	156	$C_{12}H_{12}$	1425.4	1425.9
44.	C_2-naphthalene	156	$C_{12}H_{12}$	1429.1	---
45.	Naphthalene, 2,3-dimethyl-	156	$C_{12}H_{12}$	1446.3	1446.7
46.	1H-indole-2-carbonitrile, 3-methyl	156	$C_{10}H_8N_2$	1463.4	---
47.	1H-indole, 2,3-dihydro, 4-methyl-	133	$C_9H_{11}N$	1479.1	---
48.	Acenaphthene*	154	$C_{12}H_{10}$	1494.0	1494.1

Table 3. Organic compounds in ground water from well J3 at a depth of 12.2 m—Continued

Peak no.	Compound	Molecular weight	Molecular formula	Retention index	
				Sample	Standard
49.	1-naphthalenecarbonitrile*	153	$C_{11}H_7N$	1503.2	1500.4
50.	1-naphthol	144	$C_{10}H_8O$	1514.3	1516.3
51.	[1,1'-biphenyl]-2-ol	170	$C_{12}H_{10}$	1521.4	---
52.	2-naphthol	144	$C_{10}H_8O$	1522.2	1525.4
53.	Dibenzofuran*	168	$C_{12}H_8O$	1525.4	1523.6
54.	2-naphthalenecarbonitrile	153	$C_{11}H_7N$	1529.4	---
55.	Phenol, 2,3,4,6-tetrachloro-	230	$C_6H_2OCl_4$	1562.7	---
56.	1-indolinecarboxaldehyde	147	C_9H_9ON	1584.9	---
57.	9H-fluorene*	166	$C_{13}H_{10}$	1594.4	1593.1
58.	C_1-napthalenecarbonitrile	167	$C_{12}H_9N$	1600.0	--
59.	C_1-acenaphthene	168	$C_{13}H_{12}$	1606.7	--
60.	C_1-acenaphthene	168	$C_{13}H_{12}$	1612.5	--
61.	C_1-acenaphthene	168	$C_{13}H_{12}$	1620.0	--
62.	C_1-dibenzofuran	182	$C_{13}H_{10}O$	1631.7	--
63.	C_1-dibenzofuran	182	$C_{13}H_{10}O$	1645.0	--
64.	C_1-naphthalenecarbonitrile	167	$C_{12}H_9N$	1653.3	--
65.	[1,1'-biphenyl]-3-ol	170	$C_{12}H_{10}O$	1708.8	--
66.	3-quinolinol	171	C_9H_7ON	1718.4	--
67.	2(1H)-quinolinone*	145	C_9H_7ON	1736.0	--
68.	9H-fluorene-9-one	180	$C_{13}H_8O$	1751.8	1752.5
69.	Dibenzothiophene*	184	$C_{12}H_8S$	1767.5	1766.1
70.	Pentachlorophenol	264	C_6HOCl_5	1771.9	1771.7
71.	D_{10}-phenanthrene (internal standard)	188	$C_{14}D_{10}$	1793.0	--
72.	Phenanthrene*	178	$C_{14}H_{10}$	1797.4	1793.6
73.	Acridine*	179	$C_{13}H_9N$	1805.6	1818.8
74.	C_1-2(1H)quinolinone	159	$C_{10}H_9ON$	1826.9	--
75.	Phenanthridine	179	$C_{13}H_9N$	1840.7	1839.8
76.	9H-carbazole*	167	$C_{12}H_9N$	1851.9	1849.1
77.	Dibenzo[b.e.][1,4]-dioxin	184	$C_{12}H_8O_2$	1878.7	--
78.	Phenanthrene, 3-methyl-	192	$C_{15}H_{12}$	1910.8	--
79.	C_1-9H-carbazole	181	$C_{13}H_{11}N$	1928.4	--
80.	4H-cyclopenta [d.e.f.]phenanthrene*	190	$C_{15}H_{10}$	1936.3	--
81.	9,10-phenanthrenedione	208	$C_{14}H_8O_2$	1989.2	--
82.	Fluoranthene*	202	$C_{16}H_{10}$	2084.7	2083.7
83.	Pyrene*	202	$C_{16}H_{10}$	2139.4	2140.2
84.	9(10H)acridinone	195	$C_{13}H_9ON$	2362.1	--

(2) possible mechanisms that might influence the distribution of organic compounds in ground water, such as partitioning between oil-water phases and sorption-desorption on aquifer material, resulting in a "chromatographic effect." Results of chemical analyses for selected organic contaminants in ground water in wells J1 and J3 through J7 are shown in tables 4–9. (Concentrations of individual compounds in tables 4–9 are not corrected on the basis of recovery data reported in the methodology (Rostad and others, 1984)).

Vertical Distribution of Organic Contaminants in Ground Water

Data in tables 4–9 indicate that none of the organic contaminants derived from wood-treatment processes were detected in well J1. The only sample from well J1 that showed any evidence of contamination was the one collected at a depth of 6.1 m. This sample showed the presence of trace amounts of benzo[a]pyrene, which was probably introduced as an artifact during the isolation and analytical scheme. Having established background concentrations in native ground water, we studied vertical distributions of these contaminants in wells J3 through J7. These results are illustrated in figure 3, which shows the concentrations of total phenols, PAH's, and heterocycles as a function of well depth. Each total is the sum of the concentrations of individual compounds in each class. Depth profiles in well J3 and J5 showed two zones of contamination: one highly concentrated zone (oil zone) extending down to depth of 12.2 m, and a less concentrated zone extending to a depth of 24.4 m (main plume). Concentration of contaminants in this latter zone was greatest at a depth of 18.3 m. The oil zone contained droplets of oil and possibly microemulsions that were not removed by filtration, which explains the high concentrations of contaminants in this zone. The main plume contained lower concentrations of contaminants, which were leached from the oil zone by native ground water. In addition to the oil zone and main plume, two other zones are evident in well J3 and J5 centered at depths of 12.2 m and 24.4 m, above and below the main contaminant plume.

Vertical distributions of contaminants in wells J3 and J5 indicated all three classes of contaminants migrated down the column of aquifer material at the same rate, resulting in no apparent "chromatographic effect." In other words, the porous media were not capable of resolving classes of compounds of different polarities, such as phenols, heterocycles, and PAH's. These observations led to the conclusion that sorption to the porous media and interactions between minerals and organic matter are not important processes governing the vertical migration of organic contaminants in this system.

Well J4 showed a different pattern of vertical migration of contaminants from that in wells J3 and J5 (fig. 3). This anomalous behavior was explained as follows: (1) Well J4 is not in the vertical cross section between wells J3 and J5. (2) A clay lens in well J4 at a depth of 6.1 m impedes the flow of ground water and vertical migration of organic contaminants.

This lens is also present (and thicker) at J5, J6, and J7. Except for the presence of small amounts of 2,4-dimethylphenol and napthalene in well J6 at a depth of 6.1 m, wells J6 and J7 did not show any evidence of contamination down to a depth of approximately 18.3 m.

Table 4. Chemical analyses for selected organic contaminants in ground water in wells J1 and J3 through J7 at a depth of 3 m
[Results in micrograms per liter; n.d., not detected; ---, sample not collected; totals have been rounded]

Compound	Well numbers					
	J1	J3	J4	J5	J6	J7
Phenols						
Phenol	---	---	n.d.	---	---	---
2-methylphenol	---	---	n.d.	---	---	---
2,4-dimethylphenol	---	---	644	---	---	---
3,5-dimethylphenol	---	---	836	---	---	---
2,3,5-trimethylphenol	---	---	53.3	---	---	---
1-naphthol	---	---	2.9	---	---	---
2-naphthol	---	---	1.2	---	---	---
Pentachlorophenol	---	---	n.d.	---	---	---
Total phenols	---	---	1,537.0	---	---	---
Polycyclic aromatic hydrocarbons						
Indane	---	---	n.d.	---	---	---
Naphthalene	---	---	36.4	---	---	---
2-methylnaphthalene	---	---	6.6	---	---	---
1-methylnaphthalene	---	---	5.7	---	---	---
Biphenyl	---	---	n.d.	---	---	---
Acenaphthene	---	---	12.1	---	---	---
Fluorene	---	---	9.4	---	---	---
Phenanthrene	---	---	10.7	---	---	---
Anthracene	---	---	1.4	---	---	---
Fluoranthene	---	---	2.7	---	---	---
Pyrene	---	---	1.7	---	---	---
Benzo[a]pyrene	---	---	13.7	---	---	---
Total PAH's	---	---	100.0	---	---	---
Nitrogen heterocycles						
2,4-dimethylpyridine	---	---	7.7	---	---	---
Quinoline	---	---	n.d.	---	---	---
2-methylquinoline	---	---	18.0	---	---	---
2-quinolinone	---	---	236	---	---	---
Acridine	---	---	0.8	---	---	---
Carbazole	---	---	35.1	---	---	---
Acridinone	---	---	118.7	---	---	---
Total nitrogen heterocycles	---	---	416.0	---	---	---
Sulfur heterocycles						
Benzo[b]thiophene	---	---	8.6	---	---	---
Dibenzothiophene	---	---	1.2	---	---	---
Total sulfur heterocycles	---	---	10.0	---	---	---
Oxygen heterocycles						
Dibenzofuran	---	---	4.9	---	---	---
Total oxygen heterocycles	---	---	5.0	---	---	---

Lack of contamination above 18 m at wells J6 and J7 is related to the presence of this clay lens (affecting the flow system) plus the possible stream interactions with the upper 3–6.1 m of the aquifer. The main plume in wells J6 and J7 is located at a depth of approximately 18.3–30.5 m.

Horizontal Distribution of Organic Contaminants in Ground Water

Horizontal distributions of organic contaminants in wells J3 through J7 at different depths are illustrated in figure 4. In general, at each depth, concentrations of or-

Table 5. Chemical analyses for selected organic contaminants in ground water in wells J1 and J3 through J7 at a depth of 6.1 m
[Results in micrograms per liter; n.d., not detected; ---, sample not collected; totals have been rounded]

Compound	Well numbers					
	J1	J3	J4	J5	J6	J7
Phenols						
Phenol	n.d.	5,493	---	n.d.	n.d.	n.d.
2-methylphenol	n.d.	5,182	---	n.d.	n.d.	n.d.
2,4-dimethylphenol	n.d.	7,219	---	951	10.6	n.d.
3,5-dimethylphenol	n.d.	8,223	---	975	n.d.	n.d.
2,3,5-trimethylphenol	n.d.	483	---	109	n.d.	n.d.
1-naphthol	n.d.	315	---	121	n.d.	n.d.
2-naphthol	n.d.	691	---	4.1	n.d.	n.d.
Pentachlorophenol	n.d.	n.d.	---	n.d.	n.d.	n.d.
Total phenols	n.d.	27,606	---	2,160.0	11.0	n.d.
Polycyclic aromatic hydrocarbons						
Indane	n.d.	40	---	33.8	n.d.	n.d.
Naphthalene	n.d.	6,600	---	768	9.3	n.d.
2-methylnaphthalene	n.d.	413	---	46.8	n.d.	n.d.
1-methylnaphthalene	n.d.	225	---	29.0	n.d.	n.d.
Biphenyl	n.d.	60.8	---	6.3	n.d.	n.d.
Acenaphthene	n.d.	353	---	42.4	n.d.	n.d.
Fluorene	n.d.	154	---	19.5	n.d.	n.d.
Phenanthrene	n.d.	162	---	9.8	n.d.	n.d.
Anthracene	n.d.	---	---	0.9	n.d.	n.d.
Fluoranthene	n.d.	6.1	---	0.3	n.d.	n.d.
Pyrene	n.d.	n.d.	---	n.d.	n.d.	n.d.
Benzo[a]pyrene	0.4	n.d.	---	n.d.	n.d.	n.d.
Total PAH's	0.4	8,014.0	---	957.0	9.0	n.d.
Nitrogen heterocycles						
2,4-dimethylpyridine	n.d.	n.d.	---	n.d.	n.d.	n.d.
Quinoline	n.d.	288	---	n.d.	n.d.	n.d.
2-methylquinoline	n.d.	297	---	11.8	n.d.	n.d.
2-quinolinone	n.d.	9,987	---	414	n.d.	n.d.
Acridine	n.d.	n.d.	---	n.d.	n.d.	n.d.
Carbazole	n.d.	265	---	64.6	n.d.	n.d.
Acridinone	n.d.	n.d.	---	14.3	n.d.	n.d.
Total nitrogen heterocycles	n.d.	10,837	---	505.0	n.d.	n.d.
Sulfur heterocycles						
Benzo[b]thiophene	n.d.	409	---	669	n.d.	n.d.
Dibenzothiophene	n.d.	n.d.	---	1.3	n.d.	n.d.
Total sulfur heterocycles	n.d.	409	---	670.0	n.d.	n.d.
Oxygen heterocycles						
Dibenzofuran	n.d.	204	---	15.9	n.d.	n.d.
Total oxygen heterocycles	n.d.	204	---	16.0	n.d.	n.d.

ganic contaminants decreased with increasing distance from the contamination source, well J3 having the highest concentrations of organic compounds and well J7 the lowest. At a depth of 6.1 m, all three classes of compounds migrated 215.5 m to well J6. At depths of 18.3 to 30.5 m, all three classes of compounds have migrated 273.4 m to well J7. The presence of two contaminant plumes at depths of 18.3 to 30.5 m is evident in figure 4. The main or primary contaminant plume extended from the discharge point to well J5, a distance of 161.5 m. A secondary contaminant plume, which is most concentrated at well J6, extended between wells J5 and J7 and possibly

Table 6. Chemical analyses for selected organic contaminants in ground water in wells J1 and J3 through J7 at a depth of 12.2 m
[Results in micrograms per liter; n.d., not detected; ---, sample not collected; totals have been rounded]

Compound	Well numbers					
	J1	J3	J4	J5	J6	J7
Phenols						
Phenol	---	42.0	n.d.	n.d.	---	---
2-methylphenol	---	94.8	n.d.	n.d.	---	---
2,4-dimethylphenol	---	372	807	31.6	---	---
3,5-dimethylphenol	---	332	960	22	---	---
2,3,5-trimethylphenol	---	13.1	39.9	n.d.	---	---
1-naphthol	---	2.7	n.d.	n.d.	---	---
2-naphthol	---	3.3	n.d.	n.d.	---	---
Pentachlorophenol	---	141	n.d.	n.d.	---	---
Total phenols	---	1,001.0	1,807.0	54.0	---	---
Polycyclic aromatic hydrocarbons						
Indane	---	1.1	18.6	n.d.	---	---
Napthalene	---	328	749	n.d.	---	---
2-methylnaphthalene	---	41.6	22.9	n.d.	---	---
1-methylnaphthalene	---	23.8	14.9	n.d.	---	---
Biphenyl	---	10.6	n.d.	n.d.	---	---
Acenaphthene	---	103.2	17.5	n.d.	---	---
Fluorene	---	72.6	3.6	n.d.	---	---
Phenanthrene	---	125.4	n.d.	n.d.	---	---
Anthracene	---	11.0	n.d.	n.d.	---	---
Fluoranthene	---	20.4	n.d.	n.d.	---	---
Pyrene	---	10.8	n.d.	n.d.	---	---
Benzo[a]pyrene	---	n.d.	n.d.	n.d.	---	---
Total PAH's	---	749.0	827.0	n.d.	---	---
Nitrogen heterocycles						
2,4-dimethylpyridine	---	n.d.	n.d.	n.d.	---	---
Quinoline	---	44.5	n.d.	n.d.	---	---
2-methylquinoline	---	5.9	n.d.	n.d.	---	---
2-quinolinone	---	394	2,354	n.d.	---	---
Acridine	---	1.4	n.d.	n.d.	---	---
Carbazole	---	134.9	21.6	n.d.	---	---
Acridinone	---	20.9	n.d.	3.7	---	---
Total nitrogen heterocycles	---	602.0	2,376.0	4.0	---	---
Sulfur heterocycles						
Benzo[b]thiophene	---	25.4	43.7	n.d.	---	---
Dibenzothiophene	---	7.4	n.d.	n.d.	---	---
Total sulfur heterocycles	---	33.0	44.0	n.d.	---	---
Oxygen heterocycles						
Dibenzofuran	---	59.2	4.0	n.d.	---	---
Total oxygen heterocycles	---	59.0	4.0	n.d.	---	---

into Pensacola Bay. All three classes of contaminants migrated at the same rate in the aquifer, without any apparent "chromatographic effect." Lack of resolution of individual classes of organic compounds in the porous media indicates that processes such as sorption to aquifer material or organic matter–mineral interactions did not play a significant role in their transport. Lack of differential attenuation of organic contaminants down the hydraulic gradient is not in itself proof that sorption has not occurred. Reversible sorption is a process that retards the first arrivals of individual constituents. With an essentially constant source concentration (such as that provided by the dissolving organic fluids creating the plume), all constituents will eventually break through. This being the

Table 7. Chemical analyses for selected organic contaminants in ground water in wells J1 and J3 through J7 at a depth of 18.3 m
[Results in micrograms per liter; n.d., not detected; ---, sample not collected; totals have been rounded]

Compound	Well numbers					
	J1	J3	J4	J5	J6	J7
Phenols						
Phenol	n.d.	13.3	n.d.	n.d.	n.d.	n.d.
2-methylphenol	n.d.	456	7.8	15.9	44.7	2.3
2,4-dimethylphenol	n.d.	1,835	623	83	178	405
3,5-dimethylphenol	n.d.	1,666	548	13.5	999	6.6
2,3,5-trimethylphenol	n.d.	317	36.5	35.9	218.8	60.9
1-naphthol	n.d.	360	n.d.	111	316	138
2-naphthol	n.d.	317	n.d.	2.4	13.3	81.1
Pentachlorophenol	n.d.	11.6	n.d.	n.d.	n.d.	n.d.
Total phenols	n.d.	4,976.0	1,215.0	262.0	1,770.0	694.0
Polycyclic aromatic hydrocarbons						
Indane	n.d.	19.0	n.d.	54.7	435	186
Napthalene	n.d.	1,976	27.3	1,038	271	1,072
2-methylnaphthalene	n.d.	159	1.1	87.3	437	156
1-methylnaphthalene	n.d.	91.1	0.5	44.7	260	81.3
Biphenyl	n.d.	22.0	---	7.8	53.2	15.4
Acenaphthene	n.d.	157	1.2	44.9	246	75.9
Fluorene	n.d.	82.1	1.2	17.3	103.4	34.5
Phenanthrene	n.d.	57.2	1.6	2.9	49.4	12.5
Anthracene	n.d.	3.2	n.d.	n.d.	n.d.	n.d.
Fluoranthene	n.d.	2.8	0.2	n.d.	n.d.	n.d.
Pyrene	n.d.	1.6	0.2	n.d.	n.d.	n.d.
Benzo[a]pyrene	n.d.	n.d.	n.d.	n.d.	n.d.	n.d.
Total PAH's	n.d.	2,571.0	33.0	1,298.0	1,858.0	1,634.0
Nitrogen heterocycles						
2,4-dimethylpyridine	n.d.	n.d.	n.d.	n.d.	n.d.	n.d.
Quinoline	n.d.	3.5	n.d.	n.d.	n.d.	n.d.
2-methylquinoline	n.d.	n.d.	n.d.	n.d.	2.7	n.d.
2-quinolinone	n.d.	1,217	125	214	517	94
Acridine	n.d.	1.0	n.d.	n.d.	n.d.	n.d.
Carbazole	n.d.	339	13.5	52.5	299	104
Acridinone	n.d.	12.4	n.d.	2.2	11.4	2.4
Total nitrogen heterocycles	n.d.	1,573.0	139.0	269.0	830.0	200.0
Sulfur heterocycles						
Benzo[b]thiophene	n.d.	268	6.0	82.7	442	157
Dibenzothiophene	n.d.	3.6	0.5	4.9	4.4	1.1
Total sulfur heterocycles	n.d.	272.0	7.0	88.0	446.0	158.0
Oxygen heterocycles						
Dibenzofuran	n.d.	89.3	0.5	15.1	101.1	31.1
Total oxygen heterocycles	n.d.	89.0	1.0	15.0	101.0	31.0

case, the original leading edge of the plume probably passed the most distant well at least 50 years ago. It is therefore reasonable to assume that at this late stage in plume development, one should not expect to find major "chromatographic effects."

It has been stated that transfer of nonionic organic compounds from water to the soil organic phase is essentially a process of partitioning rather than physical adsorption (Chiou and others, 1979, 1983). The distribution coefficient (K_d) for a given solute is proportional to the organic-carbon content of soil; the larger the organic-carbon content of a soil or sediment, the greater the value of K_d (Karickhoff and others, 1979). In addition, adsorption by the soil mineral fraction is relatively unimportant

Table 8. Chemical analyses for selected organic contaminants in ground water in wells J1 and J3 through J7 at a depth of 24.4 m
[Results in micrograms per liter; n.d., not detected; ---, sample not collected; totals have been rounded]

Compound	Well numbers					
	J1	J3	J4	J5	J6	J7
Phenols						
Phenol	---	16.5	n.d.	n.d.	n.d.	n.d.
2-methylphenol	---	19.2	n.d.	n.d.	n.d.	n.d.
2,4-dimethylphenol	---	17.0	n.d.	5.0	521	176
3,5-dimethylphenol	---	21.3	n.d.	3.9	527	208
2,3,5-trimethylphenol	---	n.d.	n.d.	n.d.	50.6	19.6
1-naphthol	---	3.5	n.d.	n.d.	197	66.0
2-naphthol	---	2.6	n.d.	n.d.	1.9	0.8
Pentachlorophenol	---	74.3	n.d.	n.d.	n.d.	n.d.
Total phenols	---	154.0	n.d.	9.0	1,298.0	470.0
Polycyclic aromatic hydrocarbons						
Indane	---	3.8	91.0	8.9	239	60.8
Napthalene	---	392	9.9	155	1,436	639
2-methylnaphthalene	---	85.2	0.7	6.7	159.4	46.4
1-methylnaphthalene	---	37.2	19.2	3.1	87.9	27.3
Biphenyl	---	17.2	n.d.	n.d.	14.9	4.6
Acenaphthene	---	108	17.4	3.1	77.2	25.6
Fluorene	---	67.7	6.8	0.9	13.4	11.3
Phenanthrene	---	148	4.8	n.d.	9.5	4.1
Anthracene	---	11.4	n.d.	n.d.	n.d.	n.d.
Fluoranthene	---	56.2	n.d.	n.d.	n.d.	n.d.
Pyrene	---	34.0	n.d.	n.d.	n.d.	n.d.
Benzo[a]pyrene	---	n.d.	n.d.	n.d.	n.d.	n.d.
Total PAH's	---	961.0	150.0	178.0	2,037.0	819.0
Nitrogen heterocycles						
2,4-dimethylpyridine	---	n.d.	n.d.	n.d.	n.d.	n.d.
Quinoline	---	0.5	n.d.	n.d.	n.d.	n.d.
2-methylquinoline	---	n.d.	n.d.	n.d.	n.d.	n.d.
2-quinolinone	---	178	n.d.	n.d.	284	23.5
Acridine	---	n.d.	n.d.	n.d.	n.d.	n.d.
Carbazole	---	23.8	40.0	n.d.	146	46.8
Acridinone	---	20.7	n.d.	n.d.	n.d.	3.1
Total nitrogen heterocycles	---	223.0	40.0	n.d.	430.0	73.0
Sulfur heterocycles						
Benzo[b]thiophene	---	16.6	49.8	10.6	198.7	57.9
Dibenzothiophene	---	9.4	0.2	n.d.	5.1	1.5
Total sulfur heterocycles	---	26.0	50.0	11.0	204.0	59.0
Oxygen heterocycles						
Dibenzofuran	---	59.8	11.5	1.1	28.0	9.9
Total oxygen heterocycles	---	60.0	12.0	1.1	28.0	10.0

in wet soils, presumably because of strong dipole interactions between soil minerals and water; the poor adsorption excludes neutral organic compounds from this part of the soil (Chiou and others, 1983). Analysis of the porous media in the vicinity of the secondary contaminant plume showed no detectable amounts of organic contaminants, such as PAH's, associated with the sediments. A recent independent study (Goerlitz and others, 1984) using column elution experiments has shown that sorption of phenols or PAH's by the aquifer sediments is insignificant. The organic-carbon content of the porous media in the Pensacola sand and gravel aquifer is less than 0.07 percent. Furthermore, the sediments are saturated with water that deactivates mineral surfaces. The low organic-carbon content of the sediments, coupled with the water-saturated deactivated mineral surfaces, minimizes processes such as sorption, resulting in movement of the contaminants at an average velocity equal to the average

Table 9. Chemical analyses for selected organic contaminants in ground water in wells J1 and J3 through J7 at a depth of 30.5 m
[Results in micrograms per liter; n.d., not detected; totals have been rounded]

Compound	Well numbers					
	J1	J3	J4	J5	J6	J7
Phenols						
Phenol	n.d.	n.d.	n.d.	n.d.	6.7	n.d.
2-methylphenol	n.d.	n.d.	n.d.	n.d.	n.d.	n.d.
2,4-dimethylphenol	n.d.	n.d.	29.1	n.d.	n.d.	n.d.
3,5-dimethylphenol	n.d.	n.d.	26.2	n.d.	4.5	n.d.
2,3,5-trimethylphenol	n.d.	n.d.	n.d.	n.d.	n.d.	n.d.
1-naphthol	n.d.	n.d.	6.0	n.d.	n.d.	n.d.
2-naphthol	n.d.	n.d.	0.9	n.d.	n.d.	n.d.
Pentachlorophenol	n.d.	n.d.	n.d.	n.d.	n.d.	n.d.
Total phenols	n.d.	n.d.	62.0	n.d.	11.0	n.d.
Polycyclic aromatic hydrocarbons						
Indane	n.d.	n.d.	21.6	n.d.	3.1	n.d.
Napthalene	n.d.	81.4	217	24.1	33.8	n.d.
2-methylnaphthalene	n.d.	27.1	8.2	0.7	0.6	n.d.
1-methylnaphthalene	n.d.	11.3	14.1	n.d.	0.2	n.d.
Biphenyl	n.d.	5.6	n.d.	n.d.	n.d.	n.d.
Acenaphthene	n.d.	31.6	24.0	n.d.	n.d.	n.d.
Fluorene	n.d.	23.2	6.9	n.d.	n.d.	n.d
Phenanthrene	n.d.	53.4	1.9	n.d.	n.d.	n.d
Anthracene	n.d.	3.1	n.d.	n.d.	n.d.	n.d
Fluoranthene	n.d.	8.5	n.d.	n.d.	n.d.	n.d
Pyrene	n.d	4.3	n.d.	n.d.	n.d.	n.d.
Benzo[a]pyrene	n.d	n.d.	n.d.	n.d.	n.d.	n.d.
Total PAH's	n.d	250.0	294.0	25.0	38.0	n.d.
Nitrogen heterocycles						
2,4-dimethylpyridine	n.d.	n.d.	n.d.	n.d.	n.d.	n.d.
Quinoline	n.d.	n.d.	n.d.	n.d.	n.d.	n.d.
2-methylquinoline	n.d.	n.d.	n.d.	n.d.	n.d.	n.d.
2-quinolinone	n.d.	n.d.	n.d.	n.d.	n.d.	n.d.
Acridine	n.d	n.d.	n.d.	n.d.	n.d.	n.d.
Carbazole	n.d	7.1	19.8	n.d.	n.d.	n.d.
Acridinone	n.d.	n.d.	n.d.	n.d.	n.d.	n.d.
Total nitrogen heterocycles	n.d.	7.0	20.0	n.d.	n.d.	n.d.
Sulfur heterocycles						
Benzo[b]thiophene	n.d.	n.d.	46.3	n.d.	n.d.	n.d.
Dibenzothiophene	n.d.	2.9	0.2	n.d.	n.d.	n.d.
Total sulfur heterocycles	n.d.	3.0	47.0	n.d.	n.d.	n.d.
Oxygen heterocycles						
Dibenzofuran	n.d.	22.3	7.7	n.d.	0.2	n.d.
Total oxygen heterocycles	n.d.	22.0	8.0	n.d.	0.2	n.d.

linear velocity of ground water, a process termed advection. Two possible explanations for the presence of the secondary contaminant plume, maximizing in concentration at well J6, are postulated.

1. Interruption of discharge. The evidence presented indicates that interactions of the secondary contaminant plume with the aquifer material are negligible and that this plume moves by advection. If discharge of effluent wastes into the ponds was interrupted for any length of time, then the maximum-contaminant concentration at the discharge point, as measured along the vertical cross-section of the plume, would be expected to decrease. As a function of time (ground-water flow), the maximum peak would be expected to move toward the bay. This peak maximum was measured at well J6. The difference in concentration between the discharge point and well J6 represents plume-widening (dilution). In the ground-water flow system, there is also a significant, vertical distance

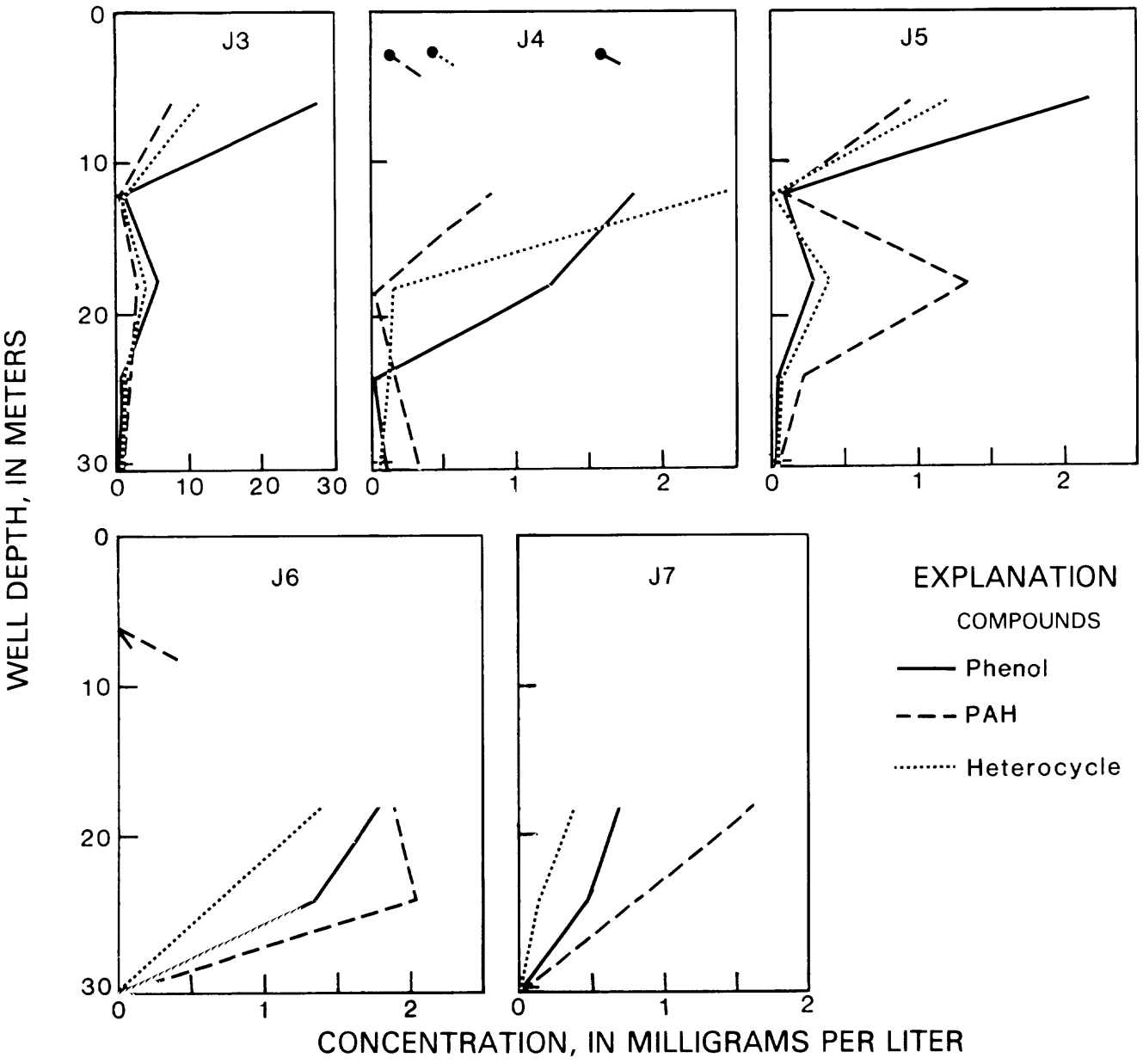

Figure 3. Vertical distributions of total phenols, PAH's (polycyclic aromatic hydrocarbons), and heterocycles in ground-water samples collected from wells J3 through J7.

component, as well as an impermeable clayey-silt facies affecting flow distance (times) and rates. Preliminary flow data (B.J. Franks, written commun., 1984) indicate the potential for significant upward ground-water flow south of the contamination site, as well as distinct differences in horizontal ground-water velocities at different depths (presumably influenced by permeability differences in nearby horizontal stratigraphic horizons). The suggested plant interruption would have to have lasted for several months (considering the ponds would continue seeping into the aquifer) to permit plume discrimination. Examining the records of the creosote works would indicate if the discharge of plant-effluent wastes was interrupted during the plant's operational history.

2. "Up-coning" of contaminant plume. A shallow perennial stream located south of the impoundments intersects the water table near Pensacola Yacht Club, between wells J5 and J6, causing ground water adjacent to the

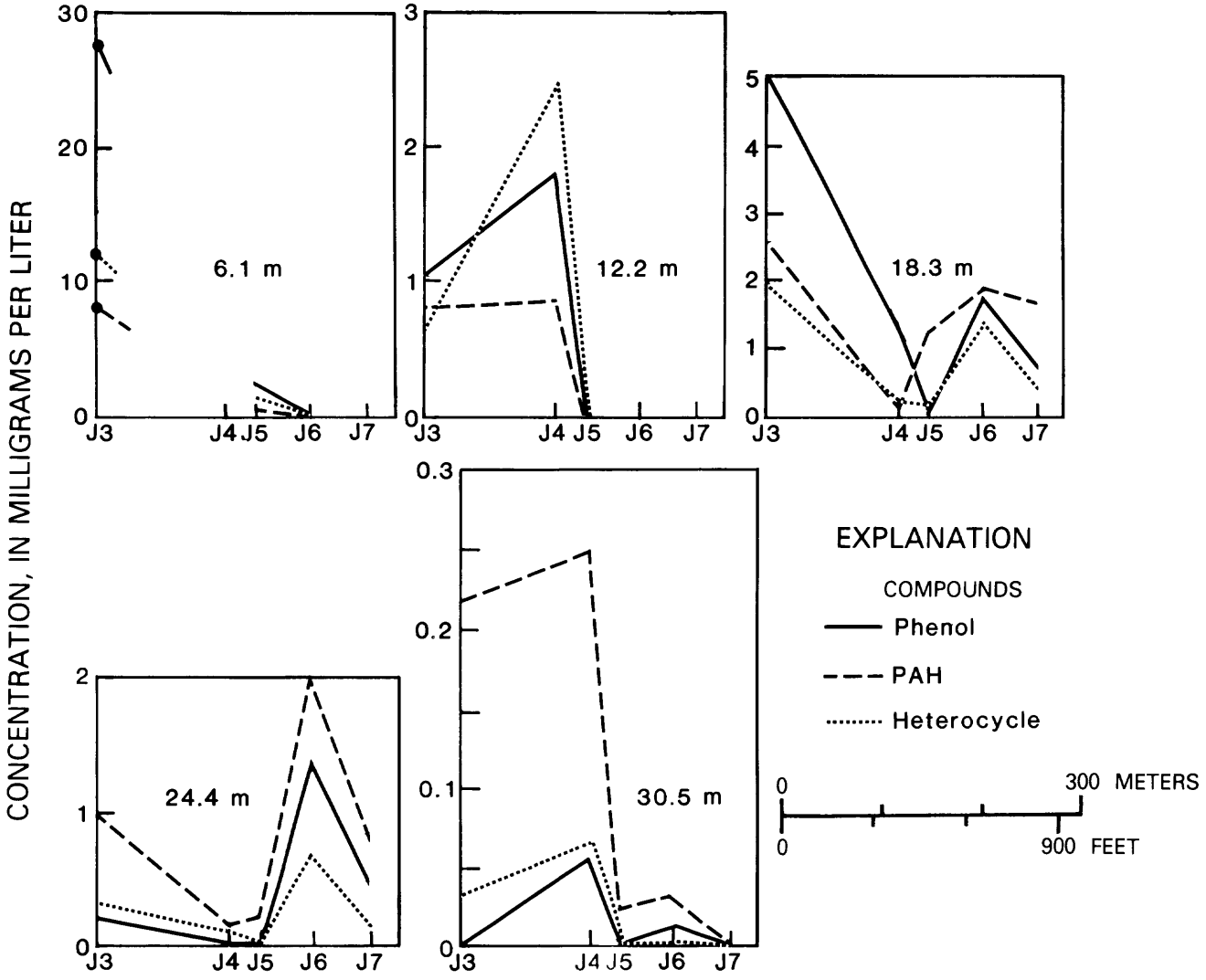

Figure 4. Horizontal distributions of total phenols, PAH's (polycyclic aromatic hydrocarbons), and heterocycles in groundwater samples collected from wells J3 through J7.

stream to discharge into the stream. Ground-water recharge of the stream may cause "up-coning" of the contaminant plume in the vicinity of well J6. A diagrammatic representation of the contaminant plume in the vicinity of wells J5 and J6 is shown in figure 5; if no stream existed, the contaminant plume would be as shown as in figure 5*A*. Sample points x and y would contain approximately 50 percent each of main plume and dispersion zone. Because of the contribution by the dispersion zone, the overall concentrations of contaminants at points x and y would be reduced. However, groundwater recharge of the perennial stream may cause "up-coning" of the contaminant plume (fig. 5*B*). Since point y is in the main body of the plume in figure 5*B*, the concentration of contaminants would be greater at point y than at point x. Thus "up-coning" of the contaminant plume, in the vicinity of well J6, may explain the peak-concentration maximum at well J6.

CONCLUSIONS

Results presented in this report suggest that discharge of chemical wastes containing creosote and pentachlorophenol resulted in contamination of a sand and gravel aquifer in Pensacola, Fla. Studies of vertical and horizontal distributions of phenols, PAH's, and heterocycles indicate that all three classes of compounds migrated at the same rate in the porous medium, with little or no retardation, and that processes such as sorption are relatively insignificant in the transport of organic compounds through aquifer material of low organic-carbon content.

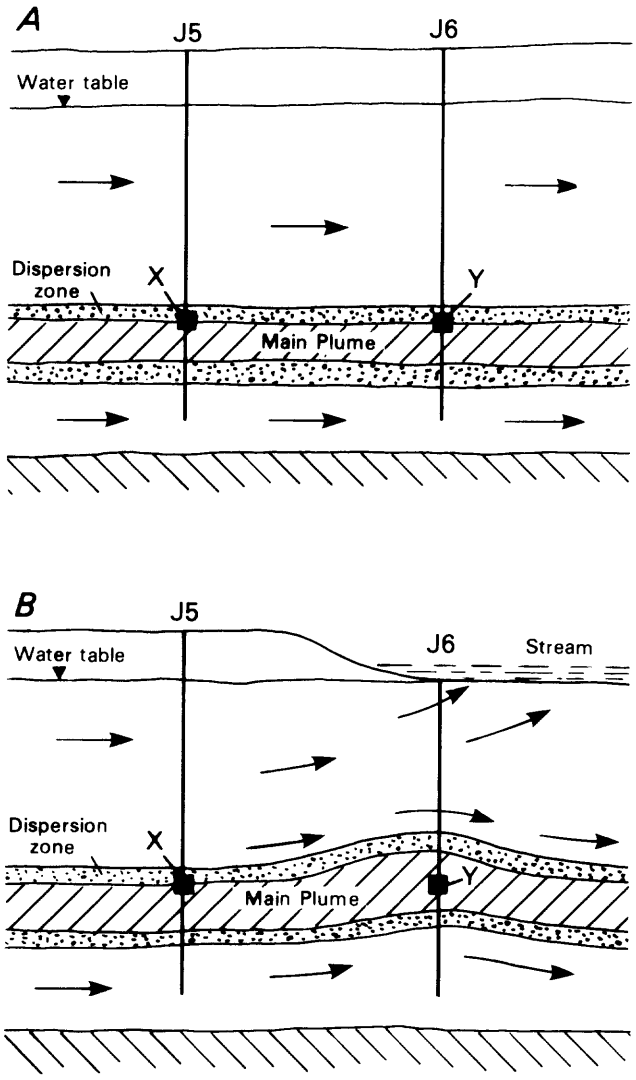

Figure 5. Diagrammatic representation of the contaminant plume in the vicinity of wells J5 and J6: *A*, without perennial stream; *B*, with perennial stream.

REFERENCES CITED

Chiou, C.T., Peters, L.J., and Freed, V.H., 1979, A physical concept of soil-water equilibria for nonionic organic compounds: Science, v. 206, no. 16, p. 831–832.

Chiou, C.T., Porter, P.E., and Schmedding, D.W., 1983, Partition equilibria of nonionic compounds between soil organic matter and water: Environmental Science and Technology, v. 17, no. 4, p. 227–231.

Freeze, R.A., and Cherry, J.A., 1979, Ground water: Englewood Cliffs, N.J., Prentice-Hall, Inc., 603 p.

Goerlitz, D.F., Godsy, E.M., Troutman, D.E., and Franks, B.J., 1984, Chemistry of ground water at a creosote works, Pensacola, Florida, *in* Movement and fate of creosote waste in ground water, Pensacola, Florida: U.S. Geological Survey Open-File Report 84–466, 93 p.

Hughes, J.L., Eccles, L.A., and Malcolm, R.L., 1974, Dissolved organic carbon (DOC), an index of organic contamination in ground water near Barstow, California: Ground Water, v. 12, no. 5, p. 283–290.

Jungclaus, G.A., Games, L.M., and Hites, R.A., 1976, Identification of trace organic compounds in tire manufacturing plant wastewaters: Analytical Chemistry, v. 48, no. 13, p. 1894–1896.

Karickhoff, S.W., Brown, D.S., and Scott, T.A., 1979, Sorption of hydrophobic pollutants on natural sediments: Water Research, v. 13, p. 241–248.

Kovats, E., 1958, Gas-chromatographische Charakterisierung organischer Verbindungen. Teil I: Retentionsindices aliphatischer Halogenide, Alkohole, Aldehyde und Ketone: Helvetica Chimica Acta, v. 41, pt. 2, no. 206, p. 1915–1932.

Leach, S.D., 1982, Source, use, and disposition of water in Florida: U.S. Geological Survey Water-Resources Investigations Report 82–4090, 337 p.

Leenheer, J.A., Malcolm, R.L., McKinley, P.W., and Eccles, L.A., 1974, Occurrence of dissolved organic carbon in selected ground-water samples in the United States: U.S. Geological Survey Journal of Research, v. 2, no. 3, p. 361–369.

Musgrove, R.H., Barraclough, J.T., and Grantham, R.G., 1965, Water resources of Escambia and Santa Rosa counties, Florida: Florida Geological Survey Report of Investigations 40, 102 p.

Page, W.G., 1981, Comparison of ground water and surface water for patterns and levels of contamination by toxic substances: Environmental Science and Technology, v. 15, no. 12, p. 1475–1481.

Pereira, W.E., Rostad, C.E., Garbarino, J., and Hult, M.F., 1983, Ground-water contamination by organic bases derived from coal-tar wastes: Environmental Toxicology and Chemistry, v. 2, no. 3, p. 283–294.

Rostad, C.E., Pereira, W.E., and Ratcliff, S.M., 1984, Bonded-phase extraction column isolation of organic compounds in ground water at a hazardous waste site: Analytical Chemistry, v. 56, no. 14, p. 2856–2860.

Troutman, D.E., Godsy, E.M., Goerlitz, D.F., and Ehrlich, G.G., 1984, Phenolic contamination in the sand-and-gravel aquifer from a surface impoundment of wood treatment wastes, Pensacola, Florida: U.S. Geological Survey Water-Resources Investigations Report 84–4230, 36 p.

U.S. Environmental Protection Agency, January 1981, Development document for effluent limitations guidelines and standards for the timber products point source category: EPA–440/1–81/023, 498 p.

Evaluating Strategies for Ground-Water Contaminant Plume Stabilization and Removal

By Steven M. Gorelick *and* Brian J. Wagner

Abstract

Optimal remedial alternatives for contaminated aquifers can be selected by combining simulation and management models. Such models identify wells and pumping or recharge rates that will best stabilize contaminant plumes. Plumes may be contained by using pumping and recharge wells to control the hydraulic gradient at the perimeter of a plume. The technique is applied to a hypothetical system in which contaminated ground water must be isolated and removed. Experimenting with a variety of designs enables the user to identify acceptable solutions to site-specific problems of aquifer restoration.

INTRODUCTION

The management of contaminated aquifers has become a critical national problem. One tool in the management and cleanup of contaminated aquifers is the use of optimization techniques combined with aquifer simulation for hydraulic management. Management modeling methods have a powerful capability to predict through simulation and, simultaneously, to determine optimal design strategy. The management model can indicate the best selection of wells and the best pumping/recharge rates to stabilize contaminant plumes.

Ground-water hydrologists typically are versed in modern methods of aquifer simulation. Unfortunately, predictive simulation is rarely sufficient to design aquifer restoration schemes. Although simulation alone can be used to predict the effects of trial schemes that employ selected well configurations, prediction is only half the story. The other half is determination of management options: selecting wells and determining pumping and recharge rates to guarantee successful control of hydraulic gradients. Even though the methods presented in the literature may appear to be complicated, they are in fact simple, tremendously versatile, and easy to use.

In this brief report we show how an aquifer management model can be used to inspect alternatives for restoring aquifers by controlling the hydraulic gradient. We display the methodology for a fairly general hypothetical case. The simulation-management model determines the best set of wells and their pumping or recharge rates to prevent plume migration during aquifer restoration. Sensitivity analysis shows the impact on the hydraulic design of differing contaminant withdrawal rates and of differing potential well configurations. Further analysis shows the impact upon restoration system design of working in a closed system (pumping equals recharge) or an open system (pumping does not equal recharge).

Acknowledgments

We gratefully acknowledge Jeff Lefkoff for his linear programming matrix generating program. We are also grateful to Jean Bahr and Eric Reichard for their fine review comments.

OUTLINE OF PROCEDURE

The main idea of using hydraulic gradient control for aquifer restoration is to select wells and pumping or recharge rates so that the contaminant plume does not migrate during cleanup (see Remson and Gorelick, 1980; Atwood and Gorelick, 1985). We call this plume stabilization. As long as the plume is stationary, contaminated water can be removed, treated, and disposed of or recharged. In the absence of hydraulic controls, the plume will migrate and disperse with the existing and future ground-water flow fields. Therefore, control wells placed around the perimeter of the plume are essential to counter the regional antecedent hydraulic gradient. The placing of these wells is known as hydraulic screening. The problems are where to place the wells, which wells to pump and which to recharge, and what rates to use for pumping and recharge. Finally, the well configuration should guarantee plume stabilization and should minimize costs or some surrogate for costs such as total pumping rates.

Figure 1 is a complex hypothetical system used to demonstrate the methodology for design and evaluation of a hydraulic screening system. The system consists of a heterogeneous aquifer with nonuniform steady flow, which is generally from top to bottom of the figure. It is treated as two-dimensional and steady, but three-dimensional and transient systems present no conceptual

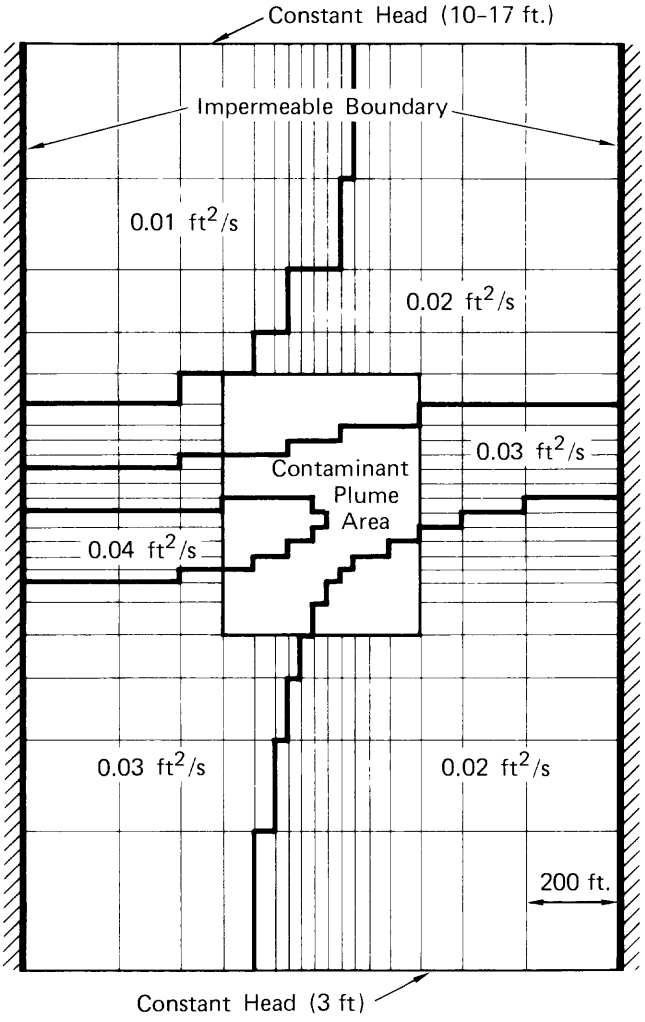

Figure 1. Aquifer system and finite difference grid with boundary conditions and zones of transmissivity.

difficulties in applying the method (Walbridge, 1985). Near the center is a contaminant plume area, shown in detail in figure 2. Within this area a plume has been delineated and plume stabilization by means of hydraulic screening is desired. Potential well sites for hydraulic gradient control have been selected around the perimeter of the plume. In addition, a single pumping well (shown as a hexagon) in the center of the plume is planned in order to remove and subsequently treat the contaminated ground water.

This is a typical situation for which aquifer restoration alternatives must be targeted and compared. One cannot model a system until there is an understanding of what controls that system. One should not attempt to manage a system until this understanding is in hand and a model that describes the basic functioning of the system has been developed. The general procedure used to develop a ground-water hydraulic management model is as follows:

1. Collect data, make field measurements and tests, do laboratory work as required, and complete preliminary analysis for site characterization.
2. Define contaminant plume and determine whether or not a plume stabilization and contaminant removal scheme is appropriate. One must consider such factors as composition of the minerals that make up the aquifer, physical and surface characteristics of the media, chemical properties of the contaminant(s), and practicality and economics of surface treatment and disposal.
3. Develop and calibrate a ground-water flow simulation model and become familiar with the system's sensitivity to parameter uncertainty.
4. Develop a menu of management constraints and potential objectives. The items on such a menu will be site specific and might include the time frame for cleanup, restrictions regarding the number and locations of wells, treatment plant and process constraints, and the efficacy (logistics, costs, legal constraints, and so forth) of a pumping system, recharge system, or pumping-recharge system.
5. Formulate the hydraulic screening problem as an optimization problem (usually a linear, quadratic, or nonlinear programming problem). This formulation requires specifying an objective and a series of constraints. The constraints must include some type of

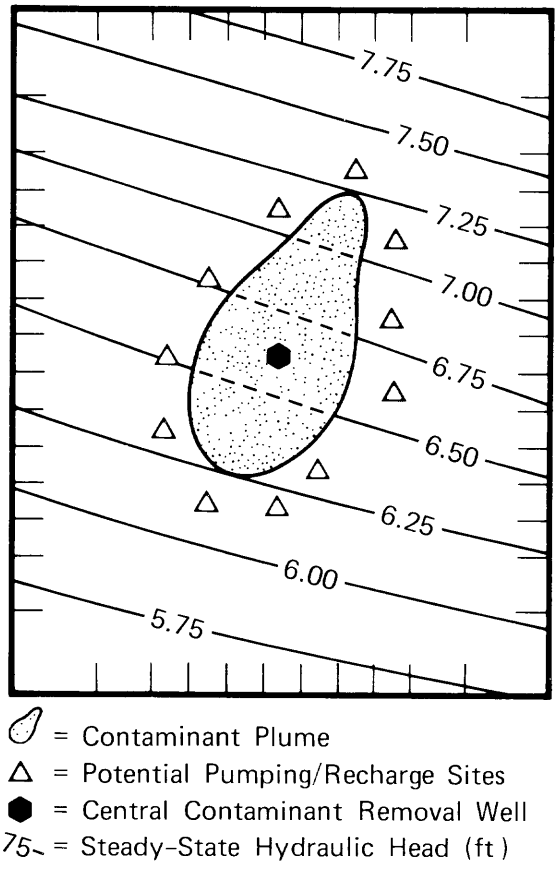

Figure 2. Contaminant plume area.

aquifer simulation model so that the physical behavior of the system is considered in the management solution.

6. Assuming that the problem can be formulated as a linear or quadratic programming problem, a hydraulic response matrix is developed. Run the simulation model to determine the hydraulic responses that characterize the behavior of the system. Each hydraulic response run (one for each potentially managed well in the system) shows how the local drawdowns or gradients change with respect to a "unit impulse" at each potential well site.
7. Fill in the matrix coefficients for execution of the optimization problem.
8. Solve the simulation-optimization problem with an existing optimization code.
9. See if the results appear to be reasonable and verify the solution by using the aquifer simulation model.
10. Conduct sensitivity studies to assess the influences of parameter uncertainty and stress variation on the optimal solution.
11. Experiment with various constraints and objectives from the objective/constraint menu that was developed previously (step 4).
12. Analyze results by comparing the design alternatives.

MATHEMATICAL FORMULATION

In the example system, steady state ground-water flow is described by the governing equation,

$$\frac{\partial}{\partial x}\left(T\frac{\partial h}{\partial x}\right) + \frac{\partial}{\partial y}\left(T\frac{\partial h}{\partial y}\right) = q \quad , \qquad (1)$$

where h is the hydraulic head, in feet;
T is the transmissivity, in square feet per second;
q is the volumetric source/sink rate per unit area, in feet per second; and
x,y are cartesian coordinates, in feet.

The above equation is also applicable to unconfined aquifers as long as the drawdown is small compared to the saturated thickness. Equation 1 is linear, and the principle of linear superposition applies. One can therefore simulate the system's behavior by summing the influences of all pumping and recharge wells plus the influence of boundary conditions. If one can calculate the influence of each well upon the local drawdowns and the influence of the boundary conditions, the total system response is defined. For transient systems one must also calculate the influence of initial conditions and keep track of changes in drawdown over time.

Because the system is described by a linear governing equation, linear programming can be used in conjunction with simulation for optimal design if the objective is also a linear function. Linear programming is a method from operations research aimed at optimally allocating scarce resources. Given a linear objective function, or goal, and a set of linear restrictions, or constraints, one can determine the best set of activities. In hydraulic management, we view water and the costs to restore its quality as scarce resources. Pumping, treatment, and reinjection each have associated costs. The linear constraints ensure that plume migration does not occur and can include other restrictions such as a mass balance or local limits on drawdowns and pumping rates.

Let us assume that steps 1 through 4 from the general procedure above have been completed. We have a good understanding of the system and a properly working flow model, and we want to evaluate pumping and recharge systems for plume stabilization.

The simulation-management problem can be formulated as a linear program. This formulation consists of the objective function of the design strategy. Treatment, pumping, and disposal costs commonly are related to the rate at which water is pumped and reinjected after treatment. The goal might be to minimize the total of pumping plus recharge, or

$$Minimize \sum_{j=1}^{m} (q(j)_{pumping} - q(j)_{recharge}) \quad , \qquad (2)$$

where $q(j)_{pumping}$ is the pumping rate at well j, $q(j)_{recharge}$ is the recharge rate (negative pumping rate) at well j, and m is the number of wells.

This particular formalization of the objective function is simple, and because it is a linear function it can be easily dealt with in the context of a linear management problem. Although minimizing total pumping plus recharge probably reflects the essential goal of the design problem, it should be recognized that this objective function is a surrogate for the more complicated one of minimizing total costs. Consideration of costs associated with pumping and treatment processes usually generates a nonlinear objective function, which can be handled but is beyond the scope of our demonstration here.

Next we must identify the constraints placed on the design of the plume stabilization system. We want the hydraulic heads outside the plume boundary to be greater than those within the plume boundary to guarantee that the plume does not migrate. This can be done by first defining drawdowns as a linear function of pumping and recharge,

$$\sum_{j=1}^{m} R(ij)\cdot q(j)_{pumping} + \sum_{j=1}^{m} R(ij)\cdot q(j)_{recharge} = s(i) \qquad i=1,n \quad , \qquad (3)$$

where $R(ij)$ is a coefficient of the hydraulic response matrix, $[R]$, which will be described presently, $s(i)$ is the drawdown at gradient control check location i, and n is the number of gradient control check locations. Other terms are defined above.

Next, the hydraulic heads at the gradient control check locations must be defined. The final hydraulic heads are equal to the heads at steady state minus the drawdowns, or

$$h(i) = h(i)_{steady} - s(i) \qquad i=1,n \ , \tag{4}$$

where $h(i)$ is the unknown hydraulic head at location i, and $h(i)_{steady}$ is the steady state head (before hydraulic screening) at location i.

The hydraulic heads at each location outside the plume boundary must be greater than or equal to those inside the plume boundary, or

$$h(i)_{out} \geq h(i)_{in} \qquad i=1,k \tag{5}$$

for all gradient control check pairs, where k is the number of gradient control check pairs. Each gradient control check pair consists of one well just outside the plume boundary and one well just inside the plume boundary. In the example problem, there were 15 gradient control check pairs involving 30 finite difference nodes.

The pumping rates are non-negative and the recharge rates are non-positive, or

$$q(j)_{pumping} \geq 0 \qquad j=1,m \tag{6}$$

$$q(j)_{recharge} \leq 0 \qquad j=1,m \ . \tag{7}$$

We will consider two optional constraints. First, one may wish to fix the pumping rate at the central treatment plant well, and this fixed rate may be varied systematically, or

$$q_{center} = q_{treatment\ capacity} \ . \tag{8}$$

Second, one may wish to force all recharge to equal all pumping. This is called a mass balance constraint, or

$$\sum_{j=1}^{m} q(j)_{pumping} = -\sum_{j=1}^{m} q(j)_{recharge} \ . \tag{9}$$

The above objective function and constraints constitute a linear programming formulation, which can be solved by using an available code. The solutions presented for this demonstration used MINOS (Murtagh and Saunders, 1980), which is a nonlinear programming solution code that can handle linear programming problems as a subset.

Of key interest in this formulation is the inclusion of a hydraulic response matrix, $[R]$, which transforms pumping (or recharge) rates into drawdowns at locations of interest. The coefficients of $[R]$, $R(ij)$, represent the drawdown at location i due to a unit stress at location j. Multiplication of $[R]$ by the vector of pumping and recharge rates, $\{q_{pumping}, q_{recharge}\}$, produces a vector of drawdowns at locations of interest. Therefore, the hydraulic response matrix is a compact aquifer simulator (see Wattenbarger, 1970; Maddock, 1972; Rosenwald and Green, 1974; Morel-Seytoux, 1975; Schwarz, 1976). It works because the ground-water flow equation 1 is linear and therefore the change in drawdown is a linear function of the pumping and recharge rates. The coefficients in this matrix are developed by using finite difference, finite element, or analytic solutions to equation 1 for the system of interest.

The idea underlying the hydraulic response matrix is quite simple. For purposes of exposition consider an aquifer system at steady state. Suppose you observe a drawdown of 4 ft at some location and it is due to pumping 0.1 ft^3/s at a nearby well. Now suppose the nearby well were to double its rate to 0.2 ft^3/s. This would cause an additional 4 ft of drawdown. That is, there is a simple linear relationship between the drawdown and the stresses (or boundary excitations) on the system. The influences of each well plus the influences of initial and boundary conditions can be superposed to simulate the impact of any combination of wells pumping at any combination of rates. If we can determine the constants that transform the pumping rate at each well into local drawdowns, we can build a hydraulic response matrix, $[R]$.

In practice all that needs to be done to determine $[R]$ is to run one aquifer simulation once for each managed well in the system. Each run shows the influence on drawdowns of an arbitrary but known pumping impulse (0.1 ft^3/s in the above example), in the absence of any other system change. In our plume stabilization example, each simulation run was accomplished using the code of Trescott and others (1976). Each run was used to fill in one column of the response matrix. Eleven simulations were required to obtain the response information for the external wells, one was required to determine the influence of the central well, and one was needed to specify the influence of boundary conditions.

RESULTS

The simulation-management design problem was solved. Several different strategies were considered with regard to fixing or not fixing the central well pumping rate, insisting upon mass balance wherein pumping equals recharge, allowing recharge only or pumping only at the perimeter wells, and considering the number of wells that

may be active in the design solution. Although the examples in this paper are for a system at steady state, transient problems have also been solved.

The results for the unrestricted case in which all well rates are determined by the optimization procedure are shown in figure 3. Two solutions are presented. Figure 3*A* shows the best combination of wells when total pumping was forced to equal total recharge. That is, the mass balance constraint (equation 9) above was included in the problem formulation. In the best solution, pumping occurs only at the central treatment plant well. Two recharge wells are selected along the downgradient portion of the plume boundary. The solution presented in figure 3*B* does not include the mass balance constraint. In that case pumping at the central well accounted for approximately 85 percent of the total rate and accomplished most of the hydraulic gradient control. Two recharge wells accounted for the remaining 15 percent. The hydraulic head surfaces that guarantee plume stabilization are also shown in figure 3.

Next we considered the case in which the central treatment plant well pumps at a specified rate of 0.03 ft^3/s. We solved the management problem to determine the best selection of recharge wells and rates only (fig. 4*A*), assuming that much of the recharge water could be imported. The results showed that 0.07 ft^3/s must be recharged at the downgradient portion of the plume to achieve stabilization. We also solved the problem to determine the best selection of pumping wells and rates only (fig. 4*B*) for successful hydraulic gradient control with no recharge wells. In that case 0.06 ft^3/s must be pumped to stabilize the plume. Both design solutions indicated that four wells should be selected in addition to the central well.

It is also possible to consider strategies involving fewer potential hydraulic screening wells. For example, figure 5 shows a 3-well configuration with a mass balance constraint (fig. 5*A*) and without mass balance constraint (fig. 5*B*). In both cases the central well pumping rate was fixed at 0.04 ft^3/s. Surprisingly in both cases only two of the three possible wells were selected. When a mass balance was required, a 0.01 ft^3/s pumping rate that is in addition to the central well pumping rate was needed for plume stabilization. Also, a 0.05 ft^3/s recharge rate was required for the dual purpose of stabilizing the plume and meeting the mass balance requirement. When

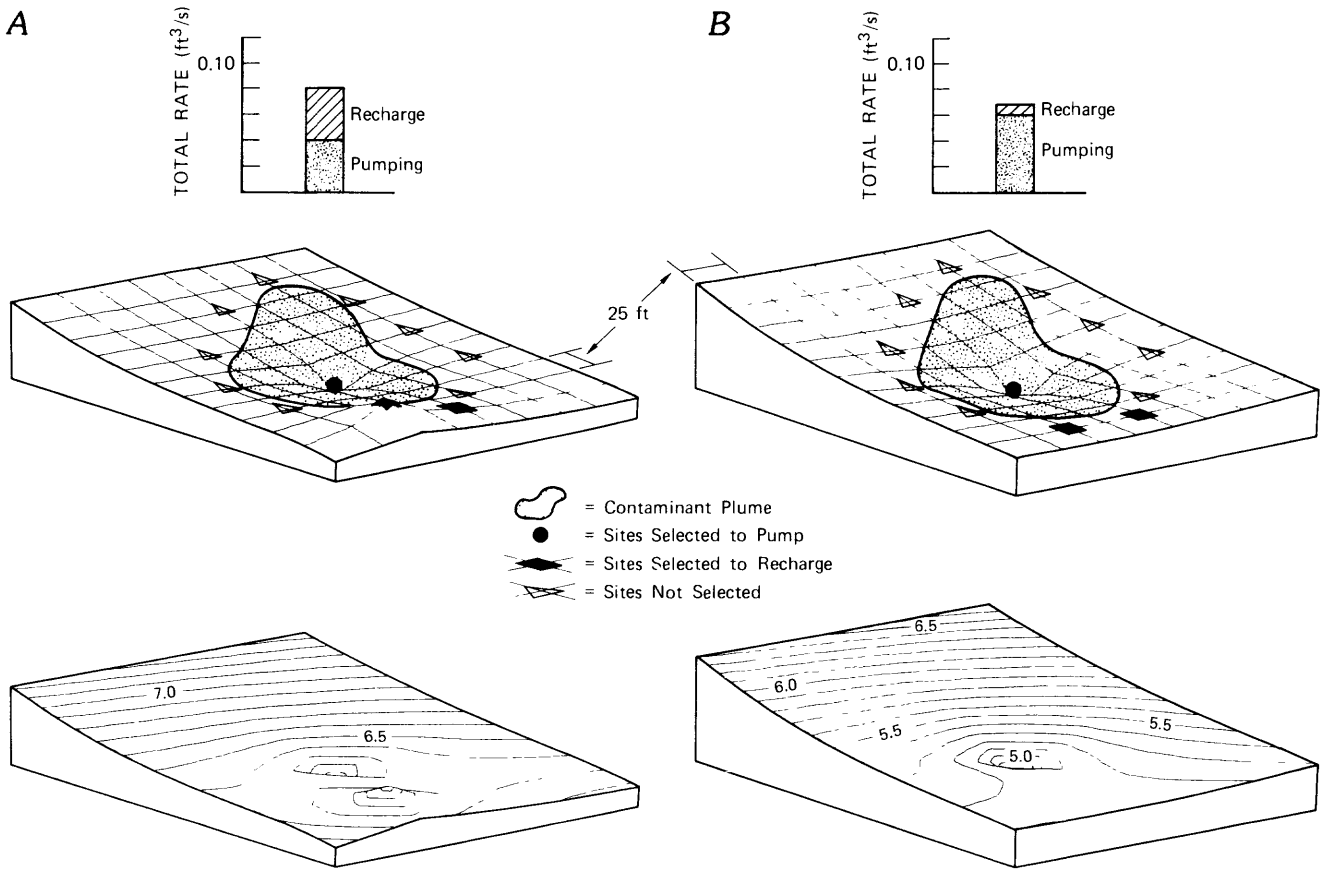

Figure 3. Results of unrestricted optimization (*A*) with mass balance; (*B*) without mass balance. Contours on lower figures show hydraulic head.

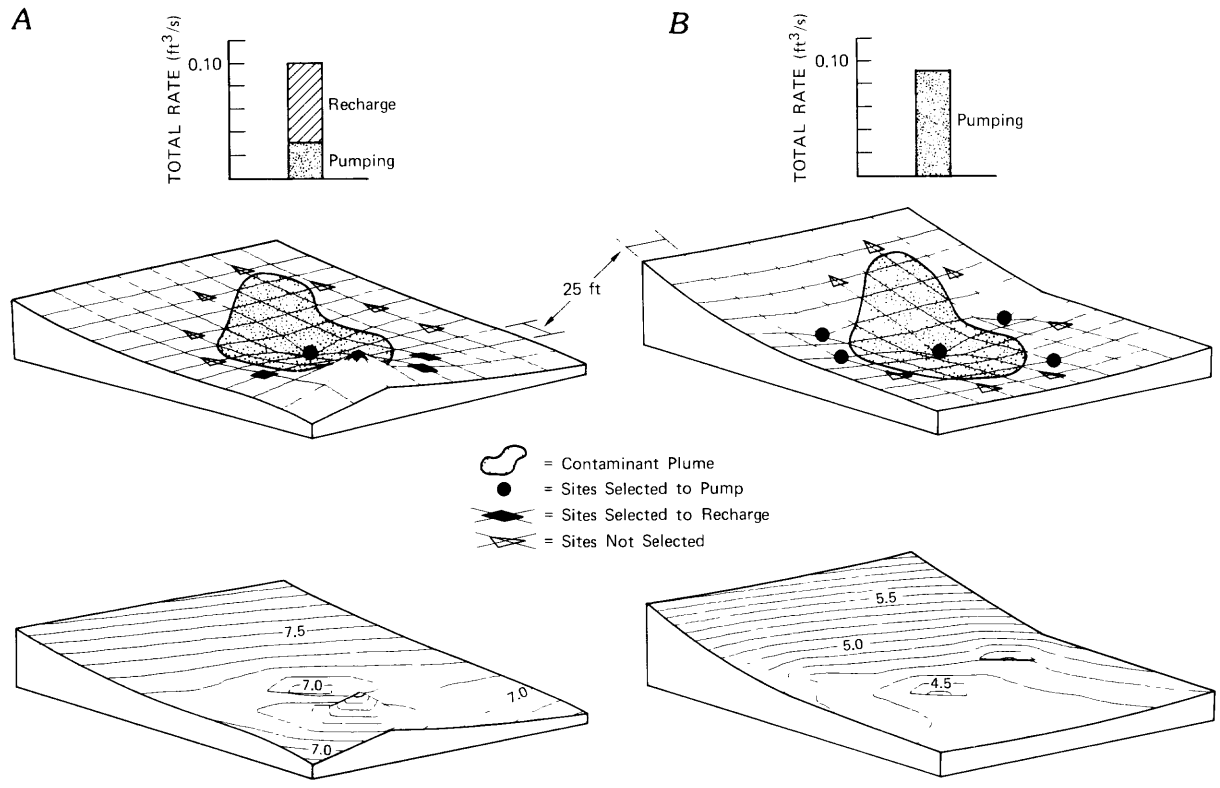

Figure 4. Results with fixed pumping rate of 0.03 ft^3/s at the central well and perimeter wells restricted to (*A*) recharge; (*B*) pumping. Contours on lower figures show hydraulic head.

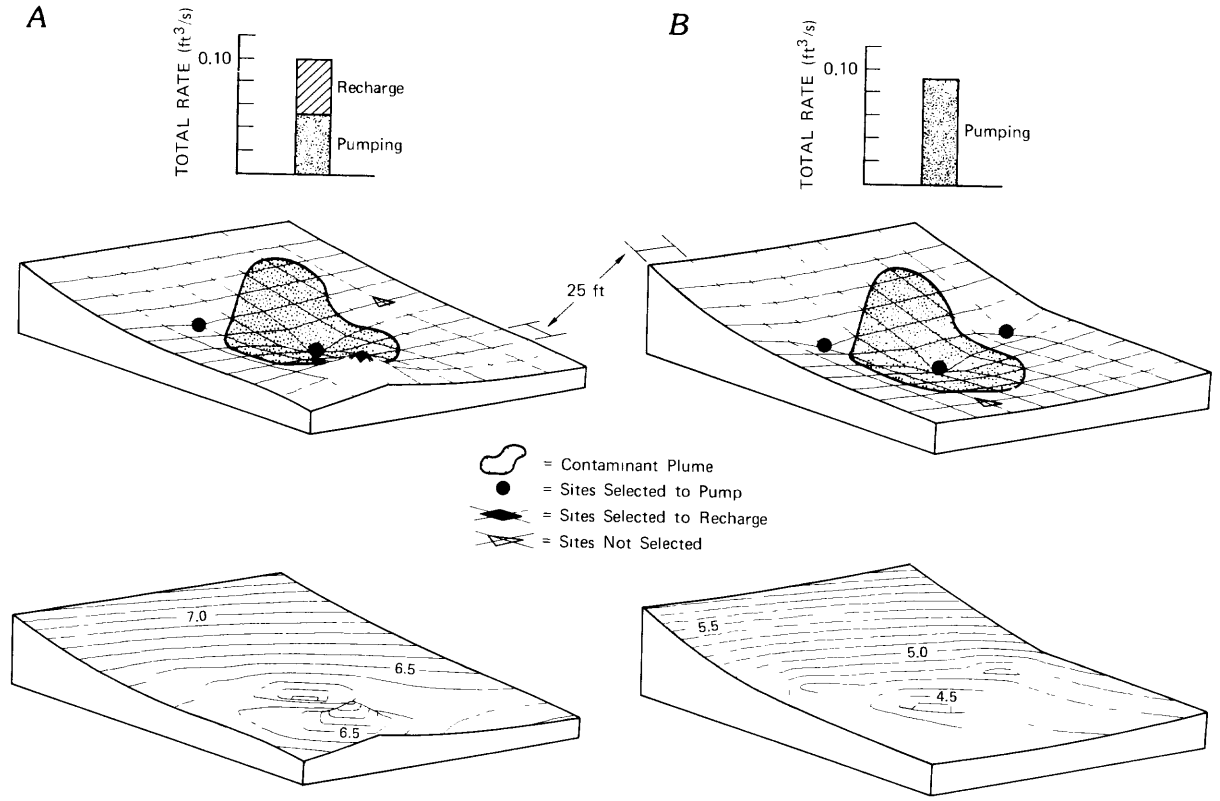

Figure 5. Results for 3-well strategy with fixed pumping rate of 0.04 ft^3/s at central well (*A*) with mass balance; (*B*) without mass balance. Contours on lower figures show hydraulic head.

mass balance was not required, a total pumping rate of 0.05 ft^3/s was needed at the perimeter wells.

A final evaluation involved the impact of the central well pumping rate upon the well-field design. The central well is used to pump contaminated ground water, which must be treated and then disposed of or recharged. Therefore, it is of key interest to determine the tradeoff between the treatment capacity (as represented by the central well pumping rate) and the number of and total rate for all wells, including the hydraulic gradient control wells. To make this determination, we solved 22 different simulation-management problems. For 11 of the design-model runs, the central well pumping rate was systematically varied from 0.0 to 0.1 ft^3/s by increments of 0.01 ft^3/s. These solutions included the mass balance constraints. In the second group of 11 design-model runs, the central well pumping rate was varied in an identical manner, but here the mass balance constraint was omitted.

The sensitivity of the well-field design to variation in the central well pumping rate is shown in figures 6 and 7. Figure 6 shows the well selection with mass balance (a) and without mass balance (b) constraints and gives the

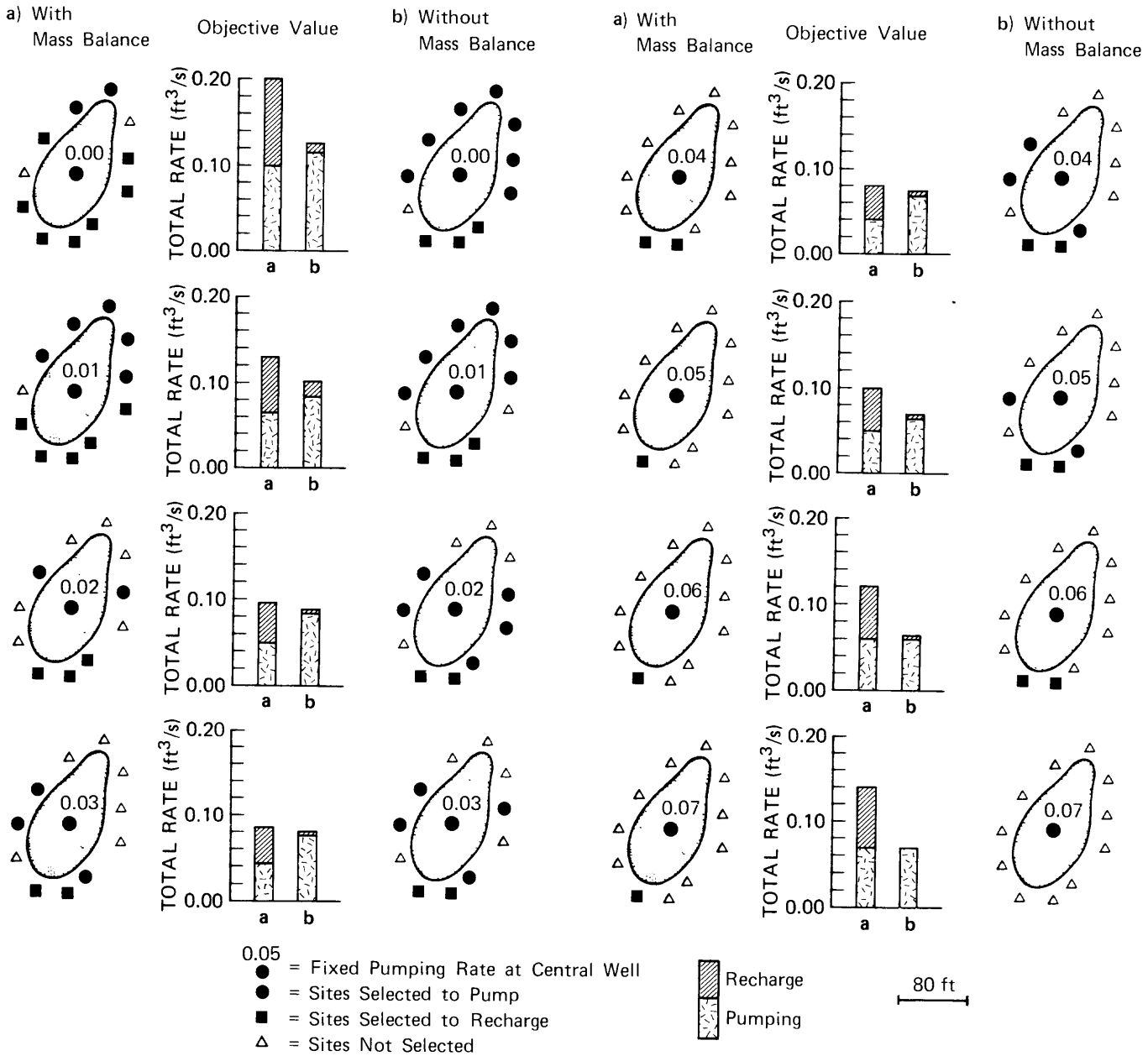

Figure 6. Results when central well pumping rate is varied with mass balance (a) and without mass balance (b).

objective values or total well rates (includes pumping rate at the central well) for 16 of the 22 cases. Results for central well pumping rates of 0.08, 0.09, and 0.1 ft^3/s are not shown. For these 6 cases (3 mass balance, 3 no mass balance), well selection was identical to that found for a central well rate of 0.07 ft^3/s. Also, the objective values were equal to the central well pumping rate for the 3 no mass balance cases and twice the central well rate for the 3 mass balance cases. In general, the number of wells required for best hydraulic screening decreases as the central well pumping rate increases. This trend is seen for both the mass balance and no mass balance cases. Generally, fewer wells were used in the mass balance cases than in the no mass balance cases. It is noteworthy that in no case were all of the potential wells selected. The simulation-management modeling method is therefore a potentially valuable tool for well site selection. This is particularly important in view of the fact that plume stabilization can often be achieved with just a few wells.

Figure 7 is a plot of the total pumping and recharge versus the central well pumping rate. Curves for the mass balance and no mass balance cases are shown in the figure, and the objective values are displayed as circles and squares. For the unrestricted cases presented earlier (cases in which all rates are determined by the optimization procedure), objective values are represented by a solid circle and square. When the mass balance constraint was included, the tradeoff curve reached a minimum with the central well pumping at about 0.04 ft^3/s. To the left of this point the curve increases rapidly, which indicates that the central well is a considerable aid to stabilizing the plume. For example, by increasing the central well pumping rate from 0.0 ft^3/s to 0.01 ft^3/s we achieve a 35 percent reduction in the objective value. To the right of this point the tradeoff curve increases, and total pumping rate is twice the rate at the central well. This results from the mass balance requirement that all water pumped must be reinjected. The steep curve indicates that the plume has already been stabilized and increased pumping is of no benefit. Water pumped from the central well must be disposed of (again owing to the mass balance restriction), which forces a departure from optimum functioning. It is clear that if there is an intention to reinject water after treatment, the central well rate should not exceed 0.04 ft^3/s. In the case of no mass balance, the minimum total rate is lower than it is when mass balance is required; this minimum rate is achieved at a central well rate of about 0.06 ft^3/s. The tradeoff curve for the no mass balance case is also much gentler than that for the mass balance case. This gentler slope indicates that when operating under an open system, the total of pumping and recharge rates is less sensitive to the choice of a central well rate.

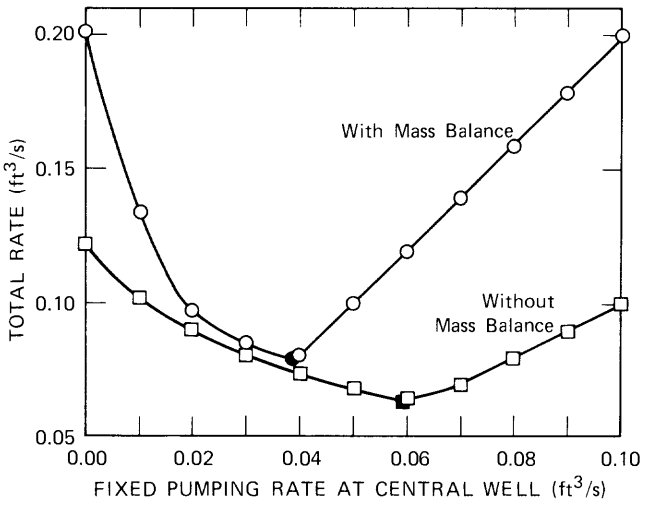

Figure 7. Plot of total pumping and recharge versus fixed pumping rate at central well. Circles and squares represent management model runs for cases with mass balance and without mass balance, respectively. Solid circle and square represent unrestricted model runs.

SUMMARY AND DISCUSSION

This report presented a method for hydraulic management of contaminated aquifers. The procedure combines aquifer simulation with simple linear optimization to identify alternative aquifer restoration schemes using hydraulic gradient control. If the ground-water flow simulation model accurately represents the system, the management model can select well locations from among potential well sites and can determine associated pumping and recharge rates to best stabilize the plume. Four steady-state examples demonstrated how selection of constraints and goals can provide the hydrologist with various schemes for stabilizing a contaminant plume.

Hydrogeologic analysis should not stop once a simulation model has been developed and run a few times, because aquifer-simulation models alone are inadequate to explore ground-water management alternatives. What is needed is the combination of aquifer simulation with optimization. The use of the simulation-management modeling method can help the knowledgeable hydrologist understand an aquifer's sensitivity to various design possibilities that might arise when evaluating restoration strategies. The simulation-management modeling methodology does not take away any creative or analytic thinking process during evaluation of restoration alternatives by somehow automating the design. On the contrary, it is another tool that the hydrologist can employ to understand better the resource and suggest management options that are both safe and efficient.

SELECTED REFERENCES

Atwood, D.F., and Gorelick, S.M., 1985, Hydraulic gradient control for groundwater contaminant removal: Journal of Hydrology, v. 76, p. 85–106.

Gorelick, S.M., 1983, A review of distributed parameter groundwater management modeling methods: Water Resources Research, v. 19, no. 2, p. 305–319.

Maddock, Thomas, III, 1972, Algebraic technologic function from a simulation model: Water Resources Research, v. 8, no. 1, p. 129–134.

Morel-Seytoux, H.J., 1975, A simple case of conjunctive surface-groundwater management: Ground Water, v. 13, no. 6, p. 505–515.

Murtagh, B.A., and Saunders, M.A., 1980, MINOS/AUGMENTED user's manual: Systems Optimization Laboratory Technical Report 80–14, Department of Operation Research, Stanford Univ., Stanford, Calif., 51 p.

Remson, Irwin, and Gorelick, S.M., 1980, Management models incorporating groundwater variables, *in* Yaron, Dan, and Tapiero, C.S., eds., Operations research in agriculture and water resources: Amsterdam, North-Holland, p. 333–356.

Rosenwald, G.W., and Green, D.W., 1974, A method for determining the optimum location of wells in a reservoir using mixed-integer programming: Society of Petroleum Engineers Journal, v. 14, p. 44–54.

Schwarz, J., 1976, Linear models for groundwater management: Journal of Hydrology, v. 28, p. 377–392.

Trescott, P.C., Pinder, G.F., and Larson, S.P., 1976, Finite-difference model for aquifer simulation in two dimensions with results of numerical experiments: U.S. Geological Survey Techniques of Water-Resources Investigations, Book 7, Chapter C1, p. 116.

Walbridge, S., 1985, Development of optimization techniques and application to purge well network design for the Gloucester landfill, Canada: Stanford University, Department of Applied Earth Sciences, Stanford, Calif., M.S. thesis, 87 p.

Wattenbarger, R.A., 1970, Maximizing seasonal withdrawals from gas storage reservoirs: Journal of Petroleum Technology, v. 22, no. 8, p. 994–998.

Recent Growth of Gulkana Glacier, Alaska Range, and its Relation to Glacier-Fed River Runoff

By Lawrence R. Mayo *and* Dennis C. Trabant

Abstract

A hydrologically important shift in climate within the past decade is indicated for the Alaska Range, a glacierized region of relatively high river runoff rates. From 1910 to 1976 Gulkana Glacier thinned and receded. Water released from glacier storage during this period augmented river runoff. Since 1976 the glacier has thickened in the accumulation zone, has thinned slightly in the ablation zone, and is approaching a state of glacier mass and ice-flow equilibrium. The long recession is apparently ended. Recent moraines indicate that all other glaciers in the Alaska Range behaved similarly, which suggests that climatic variations affecting Gulkana are widespread.

River flow from the Alaska Range increased during the recent period of glacier growth, suggesting that this growth was caused by increased precipitation. The hypothesis that glacier growth in the Alaska Range could signal a period of diminished streamflow is not supported.

INTRODUCTION

Glaciers of the Alaska Range, without a known exception, have receded during the past century, leaving conspicuous ice-cored moraines. Sellmann (1962, p. 31) illustrated the magnitude of the large retreat at Gulkana Glacier using comparative photographs taken in 1910 and 1952 (fig. 1).

Anderson (1970, sheet 3) estimated that approximately 5 percent, 50 m^3/s, of the Tanana River flow since 1910 was derived from glacier ice storage loss. Harrison and others (1983, p. 101–102) measured similar ice losses from 1949 to 1980 at an unnamed glacier 70 km west of Gulkana. They concluded that ice loss contributed 13 percent of the Susitna River discharge during the measurement period from 1949 to present.

Two scenarios of possible responses of glacier-fed river runoff to glacier growth in the Alaska Range were suggested by Bowling (1983). If glacier growth occurs by increased airflow from arctic regions, diminished glacier melting and precipitation would produce less streamflow. Conversely, if glacier growth occurs by increased airflow from the Pacific Ocean, glaciers would grow as a result of increased snow precipitation. At the same time runoff would increase due to increased melting and precipitation. This scenario is already known to occur at Wolverine Glacier in south-central Alaska (Mayo and Trabant, 1984).

Therefore, measurements of whether glaciers in the Alaska Range are continuing to recede or growing, continuous monitoring of glacier-fed rivers, and interpretation of the causes of fluctuations are critical to understanding long-term trends in water supply and potential hydropower.

GULKANA GLACIER ALTITUDE DATA

Glaciers in the Alaska Range have been observed for a relatively short period. The longest and most complete set of observations available is for Gulkana Glacier (lat 63.3°N., long 145.5°W.). Péwé and Reger (1983, p. 110) determined the dates of recent advances of Gulkana from lichenometric and geological evidence. They concluded that the last advance, during what is often referred to as the "Little Ice Age", culminated between 1875 and 1900.

F.H. Moffit obtained the first known photographs of Gulkana Glacier in the summer of 1910 (fig. 1). These photographs show the ice margins to be close to the position of the latest advance dated by Péwé and Reger. The 1910 altitude profile of the lower part of the glacier (fig. 2) was interpreted by comparing the photographs with detailed topographic maps.

The first altitude measurements of the glacier were made by the U.S. Geological Survey as part of the national mapping program. The Gulkana Glacier part of the Mt. Hayes, Alaska, topographic maps was produced by photogrammetric techniques from stereo aerial photographs taken in 1949.

In 1960, Rutter (1961, plate 1) prepared a topographic map of Gulkana Glacier from plane-table surveys. A resurvey by us of a monument (Station "M") left by Rutter and Sellmann (Sellmann, 1962, pl. 3) indicates that the altitudes reported by Rutter are 11.78 m too high. Therefore, we have subtracted 12 m from the altitudes reported by Rutter.

In 1973, we remeasured the longitudinal profile by theodolite surveys, and in 1975 we initiated a program of

1910

1952

Figure 1. Photograph of Gulkana Glacier in 1910 by F.H. Moffit. U.S. Geological Survey photographs 423–424, July 15, 1910. Photograph from the same location in 1952 by T.L. Péwé (photographs 666–668, July 12, 1952).

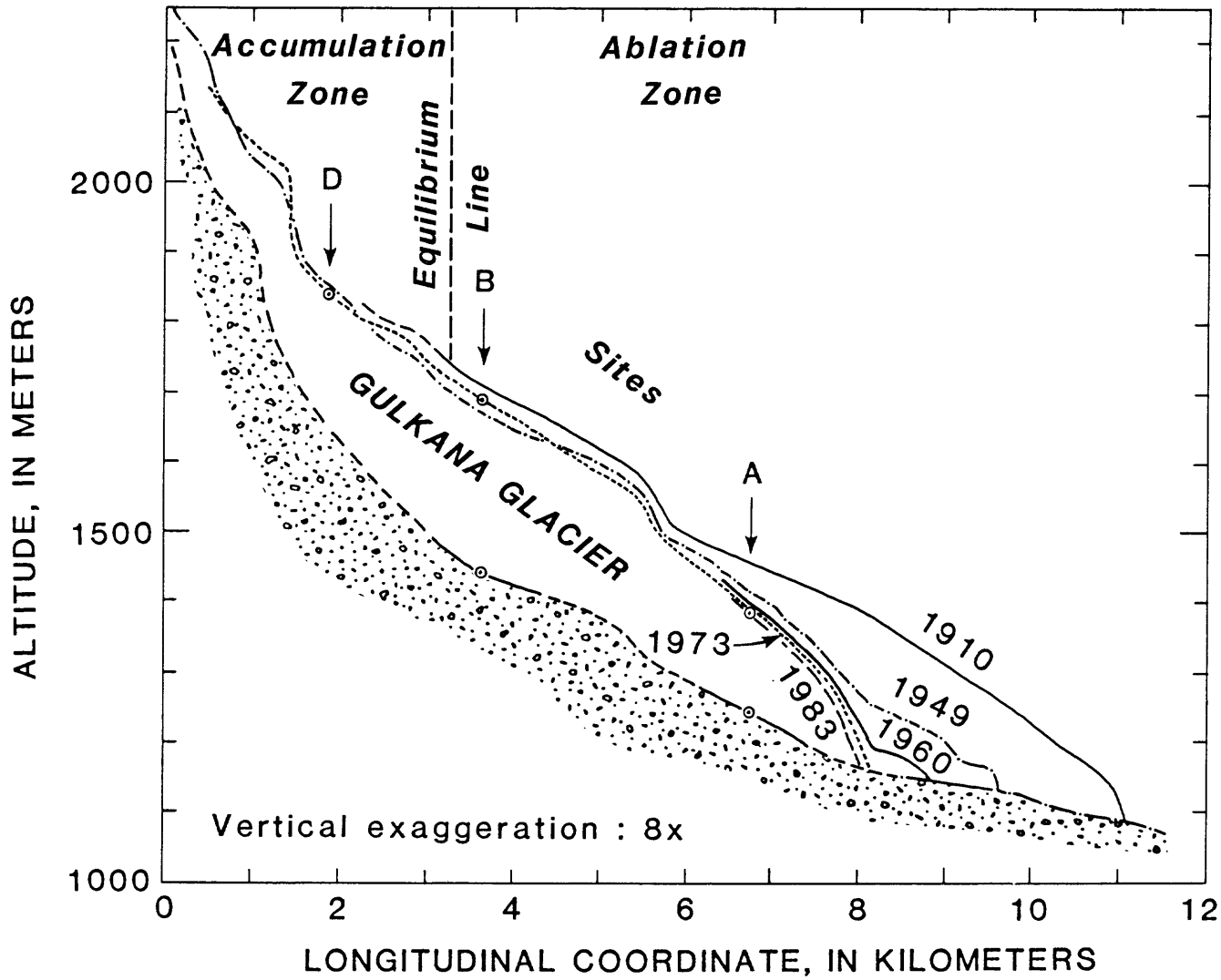

Figure 2. Longitudinal profiles of Gulkana Glacier from 1910 to 1983. Positions of seasonal altitude measurement sites A, B, and D are indicated by arrows. The glacier bed altitude was measured at two sites along the center line by low-frequency radar techniques.

precise altitude measurements several times a year at three fixed locations along the glacier centerline (table 1, fig. 3). The altitude of the glacier bed (fig. 2) was measured in 1976 by low-frequency mono-pulse radar techniques.

The accuracy of altitude information has increased steadily with time. The 1910 photographs cannot be interpreted with more confidence than ±30 m. The 1949 aerial photogrammetry is generally considered accurate within about ±15 m altitude, except in the snow-covered areas where the errors are usually larger. The 1960 map probably has an accuracy of ±5 m after the −12 m correction is applied. The 1973 centerline survey has an accuracy of about ±1.0 m. Finally, the seasonal altitude measurements made repeatedly since 1975 at fixed coordinates have an accuracy of ±0.1 m.

Interpretation of the Altitude Profiles

Glaciers that end on land advance or recede due to fluctuations in climate and flow instabilities. Post (1969, p. 232) classified Gulkana as a surging glacier on the basis of its moraine patterns, suggesting that Gulkana can advance due to both causes.

The 1910 photographs of Gulkana show the glacier to be fairly smooth, not crevassed by surging. Other smaller glaciers shown in the 1910 photographs (fig. 1) were also much thicker than in 1952. Therefore, the advance is interpreted to have been controlled primarily by climate. A minor flow instability, or glacier pulse, may have modified the extent of this advance.

There is no evidence, such as push moraines or deformed medial moraines on the glacier surface, to indicate that Gulkana Glacier has surged since 1910. The

Table 1. Sea level-scale local coordinates (in meters) for reference monuments and measurement sites at Gulkana Glacier

Name of site	X	Y	Z
Moore	6882.55	7663.62	2089.45
Slim	5523.92	7085.96	1909.56
Pass	5508.45	8560.38	1908.51
No	4435.04	7674.12	1761.42
Yes	4451.60	7657.95	1756.93
Rotor	2858.27	7405.42	2090.21
IGY	1490.10	5981.82	2000.76
"M"	4618.34	3854.13	1449.25
"M" (Sellmann, 1962)			1461.03
Downdraft	2806.95	4795.99	1599.13
Army	4713.65	3042.53	1677.40
Péwé	1933.74	1619.33	1151.75
Site A	3944.10	4293.80	
Site B	4847.60	7237.70	
Site D	6118.00	7200.10	

surge- and pulse-induced medial moraine patterns on the glacier surface near the terminus at the present time are judged to be remnant from flow instabilities that occurred during the 19th century. Thus, surging probably has not modified the longitudinal profile or the terminus position of Gulkana during this century.

From 1910 to 1949, Gulkana thinned an average of 100 m in the lower part of the ablation zone of the glacier (see fig. 2). The terminus retreated 1.6 km. The upper part of the glacier thinned much less. Moraines at the equilibrium line are only 20–30 m above the present ice surface.

By 1949, the lowest 1.5-km section of the glacier had become nearly stagnant. The convex profile above the 8.2-km longitudinal coordinate (see fig. 2) suggests that glacier flow in 1949 was replenishing part of the ice loss due to ablation; that is, it appeared then that the climate could support a glacier length of approximately 8.0 km.

The 1960 map of Gulkana Glacier (Rutter, 1961, pl. 1) shows that the glacier had thinned and retreated a small amount from 1949, but without any other major changes.

By 1973 the glacier had retreated to a length of 8.2 km, had lost almost all of the stagnant ice tongue, and had regained a convex longitudinal profile near the terminus. Small differences in the profiles in the accumulation zone of the glacier from 1949 to 1973 are probably due to inaccuracies in mapping snow surfaces from the 1949 aerial photography. No net gain or loss is indicated in the accumulation zone during this period. The fact that only insignificant quantities of stagnant ice remained near the terminus in 1973 and that the glacier had regained a convex profile near the terminus indicated that the glacier would not recede much farther. Thus, the glacier was, even then, approaching a size, flow regime, and profile of equilibrium with climate and mass balance conditions.

Detailed Study from 1975 to Present

In 1975 we began a series of seasonal measurements of snow and ice balance, glacier motion, and glacier surface altitude at three sites, one in the accumulation zone (site D, fig. 3), one near the equilibrium line (site B), and one in the ablation zone (site A). Precise altitude measurements of the glacier surface and base of the seasonal snow pack (fig. 4) are measured at horizontally fixed locations at each of these three measurement sites. Surveys are made by techniques developed to ensure that errors due to meteorological variations in atmospheric refraction are adequately corrected (Mayo and others, 1979; Mayo and Trabant, 1982).

In the accumulation zone (site D), the glacier surface altitude decreased from 1975 to 1976 then alternately increased and decreased from 1976 to 1979 but showed an overall gain. From 1979 to 1983, the rate of new firn accumulation continuously exceeded the submergence flow of the glacier. As a result, the glacier thickened 2.4 m. Thus, 1976 was the date of the end of glacier thinning in the accumulation zone as indicated at this site.

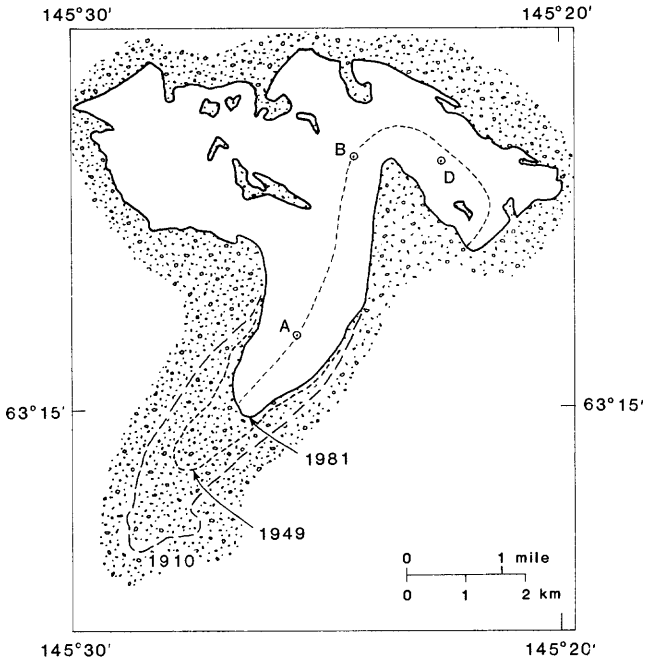

Figure 3. Map showing locations of the terminus, centerline profile, and altitude measurement sites (A, B, and D) on Gulkana Glacier. The glacier position in 1910 was mapped by Rutter (1961). The 1949 position was mapped by the U.S. Geological Survey, Mt. Hayes (A–3 and B–3), Alaska, topographic maps.

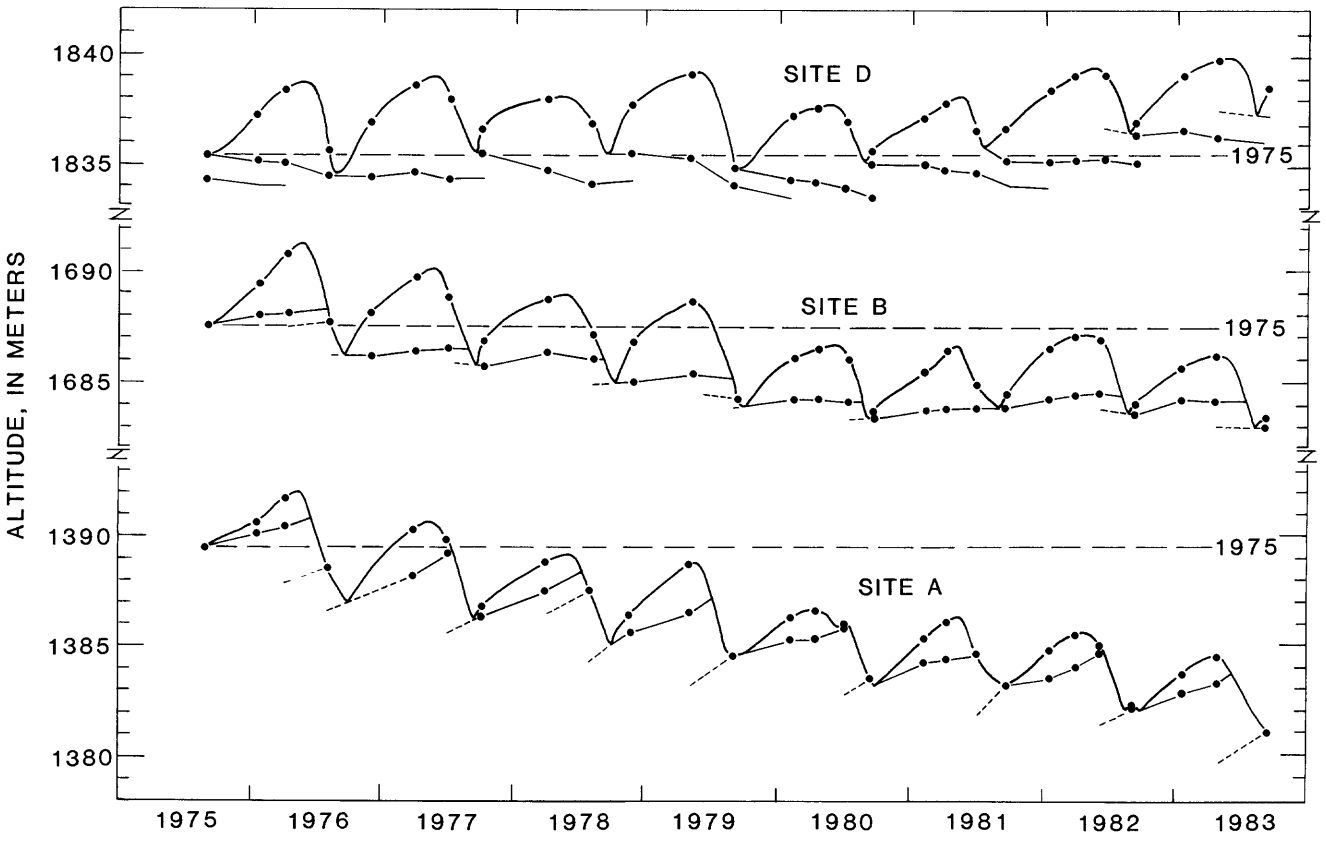

Figure 4. Graph showing changes in altitude from 1975 to 1983 at three measurement sites on Gulkana Glacier. The locations of the sites are shown on figure 3. The altitude of the summer surface, the base of the seasonal snow pack, is also shown. The rate of change of altitude of the base at the summer surface and the dashed lines indicate the rate of emergence of ice relative to the glacier surface.

At site B, 1.0 km below the equilibrium line, 4.2 m of thinning occurred from 1975 to 1980. But since 1980 continuous thinning has ceased, and alternate thickening and thinning has produced only 0.5 m of further thinning.

Lower in the ablation zone, at site A, thinning has been continuous from 1975 to the present time, at an average rate of 1.0 m/yr. The greatest thinning rate, 2.5 m/yr, occurred in 1976.

Closely spaced altitude measurements along cross and longitudinal profiles in 1973 were remeasured in 1985 to determine whether or not single points on a glacier are representative of larger areas. Site A thinned 12.8 m, and the cross profile thinned an average of 13.3 m. Site B thinned 8.1 m, and the cross profile there also thinned 8.1 m. We conclude that single points on Gulkana are representative of large areas.

The three altitude measurement sites represent unequal parts of the glacier. Site A represents 3.8 km^2; B, 4.1 km^2; and D, 11.6 km^2. The area-weighted seasonal altitude changes of the glacier surface (fig. 5) indicate that the glacier mass reached a minimum in 1980 and has grown since that time. Thus, there was a 4-yr lag from the time when thickening was detected locally at site D and when the glacier began growing.

SUMMARY OF GLACIER REGIME

The climatic regime in the Alaska Range from about 1875 to 1976 caused continual ice loss from Gulkana and other glaciers of the central Alaska Range. In 1949, when Gulkana Glacier was first mapped, a considerable amount of ice had been lost since the 1910 photograph was taken, and only a remnant of the previously extended ice tongue remained.

Since 1976 the glacier has thickened in the accumulation zone, beginning slowly but increasing to an average of 0.6 m/yr from 1979 to 1983. The effects on glacier flow from this thickening have propagated downglacier, reducing the rate of thinning in the upper part of the ablation zone from 0.8 to 0.1 m/yr. The lower part of the glacier is still thinning at an average rate of 1.0 m/yr. The glacier speed at site A has increased from 20 m/yr in

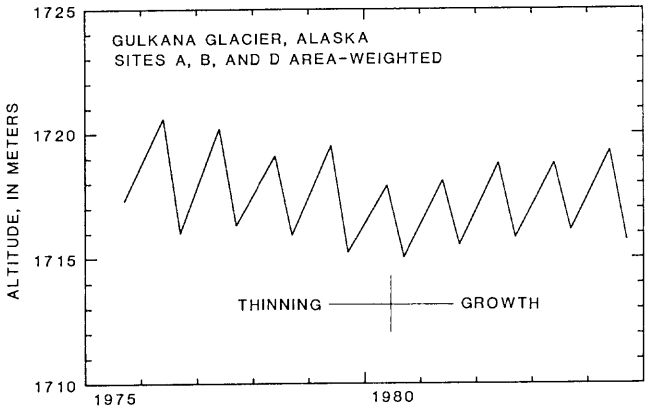

Figure 5. Graph showing glacier-averaged maximum and minimum altitude of the surface of Gulkana Glacier based on measurements at three sites from August 1975 to August 1984.

1961 (Sellmann, 1961, pl. 3) to 27 m/yr in 1983. We expect in the near future that the effects of thickening in the accumulation zone will increase the ice flow sufficiently to stabilize the lower part of the glacier.

Thus, the period in which glacier runoff exceeded precipitation ended by 1980, and the century-long recession of the Gulkana Glacier terminus is about to end. The glacier mass is, at this time, approximately but not exactly stable with climate. The glacier is still slightly overextended in length, and the glacier flow has not yet adjusted fully. We anticipate that Gulkana Glacier will recede less than 100 m more. If the ice volume in the accumulation zone continues to increase, the glacier will eventually readvance as a consequence of the present climatic regime.

An important question remains. Did Gulkana Glacier recede until it became adjusted to the prevailing climate of this century, or did the climate change about 1976? The fact that the glacier is now becoming thicker in the accumulation zone, at the same time the glacier gradient and speed are increasing, rather than simply stabilizing at a fixed height indicates that a glaciologically significant shift in climate did occur, at least for a decade.

Whether or not Gulkana is "representative" of other glaciers in the Alaska Range is critical to the problem of understanding the hydrology of the Alaska Range in general. Recent, unvegetated, ice-cored moraines high above Gulkana and other valley glaciers in the area indicate that the response of these other glaciers to variations in climate during the past century has been similar to that of Gulkana and that the knowledge gained at Gulkana does have transfer value over the entire central and eastern Alaska Range region.

RUNOFF FROM GLACIERS

The long-term regime of glacier-fed rivers may change in ways that are linked indirectly to climate because glaciers control a large part of the river flow. For example, Harrison and others (1983, p. 102) proposed that the part of river flow derived from ice storage loss is a resource that cannot be relied on for the future. For the Susitna Basin (fig. 6), the site of two proposed large hydropower projects (Watana and Devils Canyon), their studies indicate that more than 13 percent of the total measured flow for the period of record came from glacier ice losses in the basin and, therefore, is of economic significance and possibly may not be available in the future.

There are three processes by which the glacier runoff could decrease in the future. First, if glaciers diminish in size through time, runoff could gradually decrease. Second, if glaciers grow due to a climatic cooling without increases in precipitation, then less melt runoff is available. And third, if precipitation decreases, then the rainfall component of runoff could decrease.

A related ambiguity exists regarding glacier changes. Glaciers can cease declining and begin growing due either to decreases in temperature, which would cause corresponding decreases in river flow, or to increases in precipitation, which would cause increases in streamflow. If glacier regime and glacier-fed runoff are measured simultaneously for a period in which climatic shifting occurs, the ambiguity can be resolved and the controlling climatic variable identified.

Gulkana Glacier runoff flows into the Tanana River, which has been gaged since 1962 (see map, fig. 6). Other adjacent basins with glaciers have also been gaged.

The variability of annual runoff measurements can be smoothed to show the time trend of runoff (fig. 7). The method we use involves weighting the measurement for each previous year in the past by a number in the half-life decay series. A problem with this solution is that the variability of the smoothed values is greater early in the series because fewer terms are considered. To solve this, a series of average values (the average of the first five years) is entered arbitrarily for the unmeasured five years prior to the beginning of measured values. The half-life weighted time series smoothing is calculated by:

$$\overline{X}_t = \frac{\Sigma_{i=1}^{t} 0.5^{(t-i)/p} D_i}{\Sigma_{t=1}^{t} 0.5^{(t-i)/p}} , \qquad (1)$$

where $\overline{X}_t$ is the tth weighted mean value of the series,
i is the index of summation,
t is the sequence number in the time series,
p is the half-life period, 5 years in this case, and
D is the measured or estimated value.

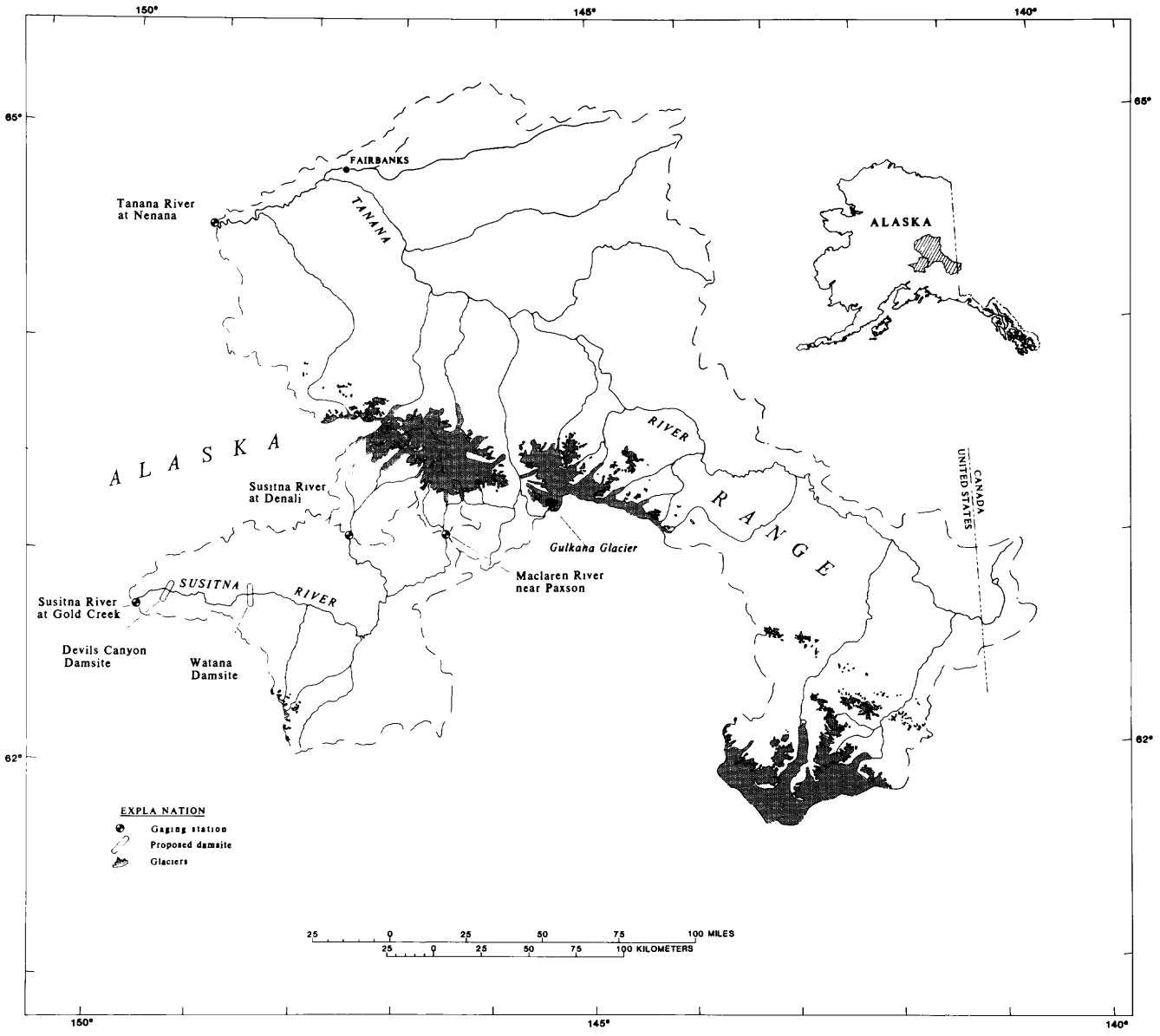

Figure 6. Map of gaged, glacierized basins in central Alaska with measurements of sufficient duration to calculate trends in runoff.

Estimates are useful, as stated above, for decreasing the variability for the first part of the sequence and also for years with missing data.

In general, runoff from glacierized basins in the Alaska Range has gradually increased during the past 10 to 15 years.

RELATION OF CLIMATE, GLACIER REGIME, AND RIVER RUNOFF

The recent period of increasing runoff is the same period during which Gulkana Glacier is known to have changed from recession to growth. Thus, the mass balance trend of Gulkana, and likely of other glaciers in the Alaska Range, is shown to be in phase with measured runoff trends in the region. This is the key information required to unravel the previously stated ambiguity. Had the glacier grown due to cooler temperatures from arctic air masses, the contribution to streamflow from ice storage loss would have decreased, and total runoff would have decreased. Even though the glacier and non-glacier components of runoff have not been analyzed separately, the data indicate that the dominant climatic factor controlling glacier mass balance and runoff variations over periods of years in the Alaska Range is precipitation from

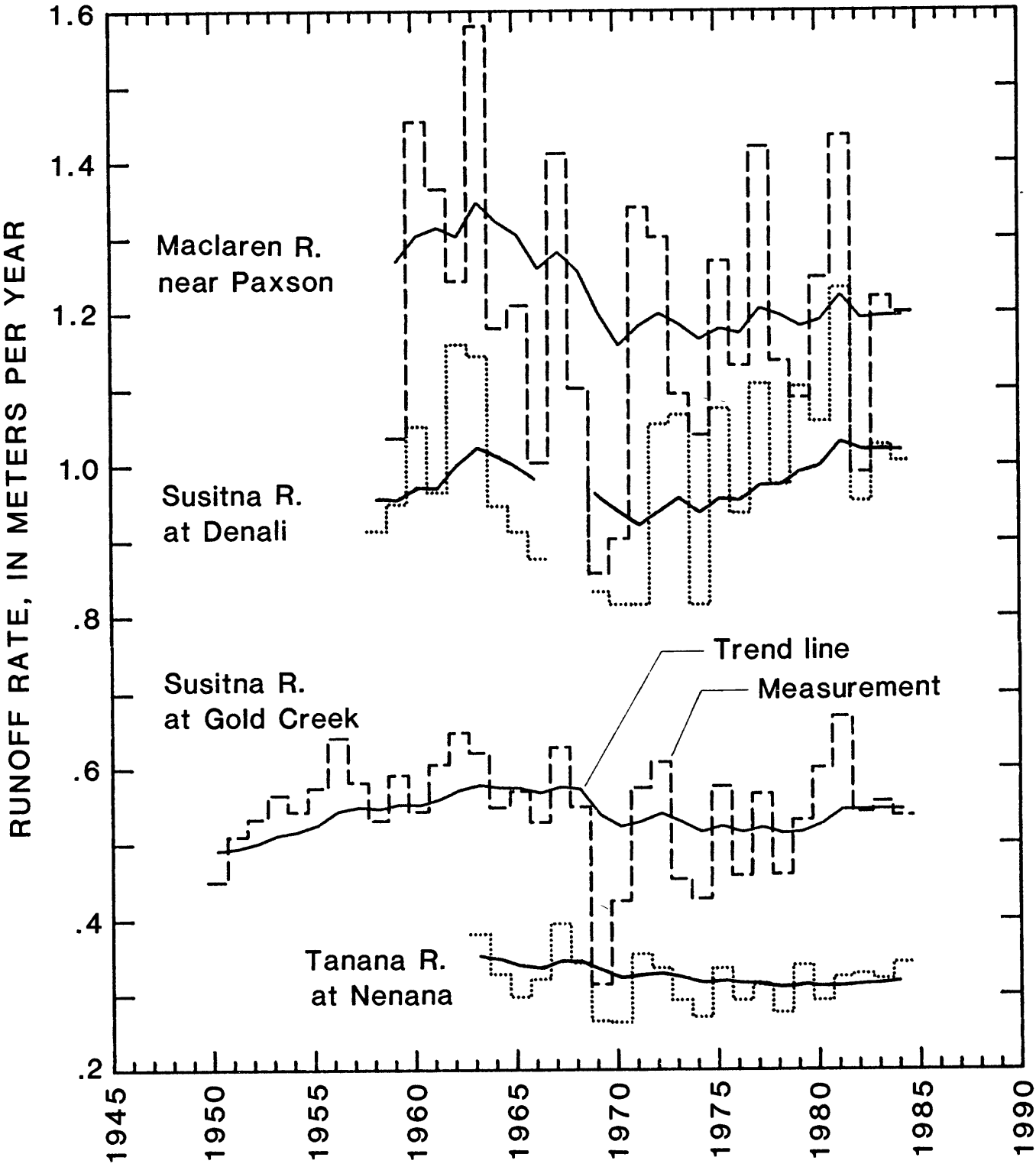

Figure 7. Graph showing measured runoff and runoff trends at four glacier-fed rivers flowing from the Alaska Range. See text for method of calculation of the trend line.

the Gulf of Alaska, probably coupled with smaller variations in temperature. This long-term response is opposite to the seasonal response, in which glacier runoff is related primarily to temperature.

REFERENCES CITED

Anderson, G.S., 1970, Hydrologic reconnaissance of the Tanana Basin, central Alaska: U.S. Geological Survey Atlas, HA–319. 4 sheets.

Bowling, S.A., 1983, Climatic fluctuations and water yield from basins in Alaska [abs.]: EOS, v. 64, no. 9, p. 88.

Harrison, W.D., Drage, B.T., Bredthauer, Stephen, Johnson, Douglas, Schoch, Carl, and Follett, A.B., 1983, Reconnaissance of the glaciers of the Susitna River Basin in connection with proposed hydroelectric development: Annals of Glaciology, v. 4, p. 99–104.

Mayo, L.R., and Trabant, D.C., 1982, Geodetic trisection, altitude, and ice-radar surveying techniques used at Knik Glacier, Alaska, and summary of 1979, 1980, and 1981 data: U.S. Geological Survey Open-File Report 82–685, 26 p.

———1984, Observed and predicted effects of climate change on Wolverine Glacier, southern Alaska, *in* McBeath, J.H., Juday, G.P., Weller, Gunter, and Murray, Mayo, eds., The potential effects of carbon dioxide-induced climate change in Alaska: Fairbanks, University of Alaska Miscellaneous Publication 83–1, p. 114–123.

Mayo, L.R., Trabant, D.C., March, Rod, and Haeberli, Wilfried, 1979, Columbia Glacier stake location, mass balance, glacier surface altitude, and ice radar data, 1978 measurement year: U.S. Geological Survey Open-File Report 79–1168, 71 p.

Péwé, T.L., and Reger, R.D., eds., 1983, Guidebook to permafrost and Quaternary geology along the Richardson and Glenn Highways between Fairbanks and Anchorage, Alaska; Fourth International Conference on Permafrost, Fairbanks, Guidebook 1: Fairbanks, Alaska Geological Survey, 263 p.

Post, Austin, 1969, Distribution of surging glaciers in western North America: Journal of Glaciology, v. 8, no. 53, p. 229–240.

Rutter, N.W., 1961, Foliation and other structures of Gulkana Glacier, central Alaska Range, Alaska: Fairbanks, University of Alaska, M.S. thesis, 51 p.

Sellmann, P.V., 1962, Flow and ablation of Gulkana Glacier, central Alaska Range, Alaska: Fairbanks, University of Alaska, M.S. thesis, 36 p.

Extension of the Unsteady One-Dimensional Open-Channel Flow Equations For Flow Simulation in Meandering Channels With Flood Plains

By Lewis L. DeLong

Abstract

Simulation of unsteady flow in natural rivers is complicated by significant variation in hydraulic properties as a meandering river inundates a flood plain. In this paper, the unsteady one-dimensional open-channel flow equations are generalized to include variation in channel length with depth of flow. Hydraulic properties of complex channel cross sections are represented through variation of momentum coefficients and conveyance with depth of flow.

Flood peaks were numerically routed through hypothetical rivers with and without meanders, and downstream hydrographs were compared at equivalent main-channel distance. Flood-plain inundation during high flow reduced effective channel length of the meandering river and resulted in nearly a one-third reduction in flood-peak travel time.

The governing equations were solved by using an orthogonal-collocation, finite-element method, formulated in terms of cross-sectional area and discharge. Although the main channel and flood plain are treated as a continuous cross-sectional area, top width does not appear directly in the governing equations or numerical computations. Consequently, the sudden expansion in top width as flow spills onto the flood plain does not cause numerical failure in this method as it commonly does in other methods formulated in terms of depth of flow or stage, top width, and discharge.

INTRODUCTION

Simulation of unsteady flow in natural rivers is often complicated by significant variation in hydraulic properties of the wetted channel with depth of flow. As a meandering river inundates a flood plain, the effective channel length may decrease significantly while the channel top width increases tenfold or more. Meandering rivers and associated complications in flow simulation are not limited to older river systems with extensive flood plains and flat-sloped channels. Small streams such as those found on the plains of Wyoming (Lowham and others, 1981) often exhibit sinuosities (ratios of stream length to main valley length) greater than two at low flow with valley slopes as large as one percent. The development of the flow equations for complex channels and the numerical solution thereof were initiated in a study of transport and quality of runoff in small, plains streams conducted cooperatively with the U.S. Bureau of Land Management in Wyoming.

The purpose of this paper is to present a form of the unsteady one-dimensional open-channel flow equations that allows for complex channel geometry and variation in channel length with the depth of flow. The extended form of the equations is solved numerically to simulate an over-bank flood in a hypothetical river that meanders through a wide flood plain. Results are compared with those obtained earlier by Fread (1976). In this paper, the numerical technique applied is secondary in importance to the form of the equations and is only briefly described.

GOVERNING EQUATIONS

Equations describing one-dimensional, unsteady flow in rigid open channels may be written (Cunge and others, 1980; Strelkoff, 1969) as

$$\frac{\partial A}{\partial t} + \frac{\partial Q}{\partial s} - q(s) = 0, \text{ and}$$

$$\frac{\partial Q}{\partial t} + \frac{\partial}{\partial s}\left(\frac{\beta Q^2}{A}\right) + gA\left(\frac{\partial y}{\partial s} + S_f(s)\right) = 0 \ , \tag{1}$$

where s = channel distance, t = time, A = cross-sectional area, Q = volumetric discharge, q = lateral inflow per unit of channel length, g = acceleration due to gravity, and y = distance of water surface above a given datum. S_f is the friction slope, which may be represented as

$$S_f = \frac{Q|Q|}{K^2} \ , \tag{2}$$

where K = conveyance. β is the momentum coefficient resulting from nonuniform velocity distribution and is defined as

$$\beta = \frac{\int v^2 dA}{V^2/A} , \quad (3)$$

where v = velocity and V = mean velocity in the cross section.

In the use of equations 1 it is assumed that: Flow is one dimensional to the extent that the momentum coefficient can sufficiently account for nonuniform velocity distribution, streamline curvature and vertical accelerations are negligible, effects of turbulence and friction are adequately described by the resistance laws used for steady flow, and the channel slope is sufficiently mild so that the cosine of its angle with the horizontal is close to unity. To the extent that steady-flow resistance laws and the momentum coefficient can approximate hydraulic properties during unsteady flow conditions, hydraulic properties of complex cross sections can be represented by allowing momentum coefficients and conveyance to vary appropriately with depth of flow (Chow, 1959).

Effective channel length may decrease significantly as flow inundates the flood plain. A "channel-flood plain" model presented by Fread (1976) allowed for separate specification of hydraulic properties and channel lengths for a main and flood-plain channel. The ratio of discharges in the main and over-bank channels was assumed equal to the corresponding ratio of normal discharges. In the approach used herein, hydraulic properties of the composite channel may be approximated by various methods, independent of model formulation, and changes in channel length are introduced through a change in the independent variables.

Equations 1 may be integrated over a surface in the s-t coordinate system (fig. 1) resulting in the integral equations

$$\iint \left(\frac{\partial A}{\partial t} + \frac{\partial Q}{\partial s} - q(s)\right) ds\, dt = 0 , \text{ and}$$

$$\iint \left(\frac{\partial Q}{\partial t} + \frac{\partial}{\partial s}\left(\frac{\beta Q^2}{A}\right) + gA\left(\frac{\partial y}{\partial s} + S_f(s)\right)\right) ds\, dt = 0 , \quad (4)$$

which by the use of Green's theorem (Wylie, 1960) are equivalent to

$$-\oint A ds + \oint Q dt - \iint q(s)\, ds\, dt = 0 , \text{ and}$$

$$-\oint Q ds + \oint \frac{\beta Q^2}{A} dt + \iint gA\left(\frac{\partial y}{\partial s} + S_f(s)\right) ds\, dt = 0 . \quad (5)$$

It is convenient to transform equations 5 from s-t coordinates (fig. 1), where an increment of stream length (Δs) may change with time, to x-t coordinates, where an increment of reference length (Δx) is unchanging in time. This transformation is accomplished through the introduction of a metric coefficient (M) that is a function of space and time such that

$$ds = M dx . \quad (6)$$

Substituting equation 6 into equations 5 results in

$$-\oint AM\, dx + \oint Q\, dt - \iint q(x)\, dx\, dt = 0 , \text{ and}$$

$$-\oint QM\, dx + \oint \frac{\beta Q^2}{A} dt + \iint gA\left(\frac{\partial y}{\partial x} + S_f(x)\right) dx\, dt = 0 , \quad (7)$$

where $\frac{1}{M} q(x) = q(s)$,

$\frac{1}{M}\frac{\partial y}{\partial x} = \frac{\partial y}{\partial s}$, and

$\frac{1}{M} S_f(x) = S_f(s)$.

Integral equations in x-t coordinates may be obtained from equations 7 through the use of Green's theorem reverse in order to its use in obtaining equations 5 and, when differentiated with respect to x and t, result in the differential equations

$$\frac{\partial (AM)}{\partial t} + \frac{\partial Q}{\partial x} - q(x) = 0 , \text{ and}$$

$$\frac{\partial (QM)}{\partial t} + \frac{\partial}{\partial x}\left(\frac{\beta Q^2}{A}\right) + gA\left(\frac{\partial y}{\partial x} + S_f(x)\right) = 0 . \quad (8)$$

When the x coordinate is aligned with the main valley length and s is aligned with the thalweg, M may be thought of as sinuosity. In practice M may vary with stage and can be approximated for a given cross section and stage as

$$M = \frac{1}{A}\sum_{i=1}^{n} m_i a_i , \quad (9)$$

where n = number of subsections, m = subsection sinuosity, and a = subsection area.

When cross-sectional area (A) and discharge (Q) are selected as dependent variables, sinuosity (M) is the only nonlinear term in the conservation-of-mass equation. In the momentum equation (equation 8) the water-surface slope ($\partial y/\partial x$) can be replaced by

$$\frac{\partial y}{\partial x} = \left.\frac{\partial y}{\partial x}\right|_A + \left.\frac{\partial y}{\partial A}\right|_x \frac{\partial A}{\partial x} , \quad (10)$$

and friction slope (S_f) by equation 2 resulting in

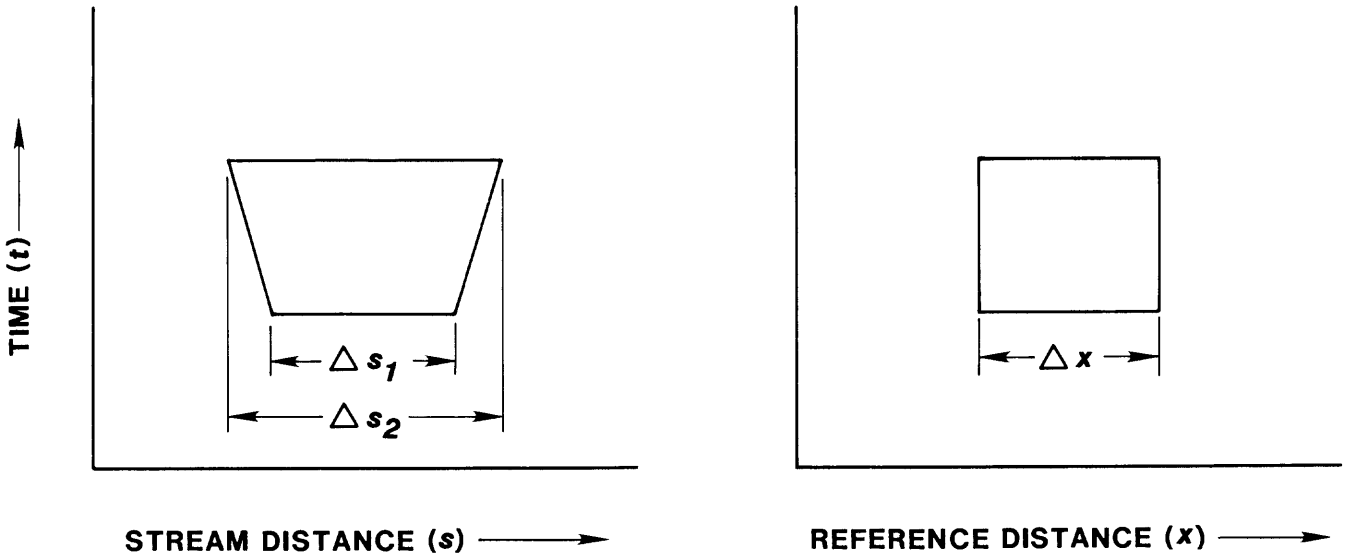

Figure 1. Transformation from s-t to x-t coordinates.

$$\frac{\partial(AM)}{\partial t} + \frac{\partial Q}{\partial x} - q(x) = 0\,, \text{ and}$$

$$\frac{\partial(QM)}{\partial t} + \frac{\partial}{\partial x}\left(\frac{\beta Q^2}{A}\right) + gA\left(\frac{\partial y}{\partial x}\bigg|_A + \frac{\partial y}{\partial A}\bigg|_x \frac{\partial A}{\partial x} + \frac{Q|Q|}{K^2}\right) = 0\,. \quad (11)$$

NUMERICAL SOLUTION

Equations 11, in general, are not amenable to analytical solution. An orthogonal-collocation, finite-element method is used to solve the governing equations. Description of the basic scheme may be found in texts such as Lapidus and Pinder (1982), and Pinder and Shapiro (1979) have applied it to one-dimensional transport (similar in some aspects to the problem addressed here). The method involves (1) approximation of the dependent variables A and Q over discrete reaches (elements) of the channel by Hermite polynomials, (2) substitution of the approximating functions into the governing equations, (3) formulation of the differential equations at Gaussian quadrature points within each element leading to a set of equations in time and the dependent variables, and (4) numerical integration of the set of equations over time.

RESULTS

Simulation of flood flow through an idealized meandering river, as presented by Fread (1976), demonstrates the utility of the governing equations. Identical input hydrographs are routed through river systems that differ in meander ratio (ratio of main-channel to flood-plain lengths). For all examples, main-channel slope (fig. 2) is 1 ft/mi, and Manning's n = 0.030 and 0.060 for main channel and flood plain, respectively. Two-mile distance and one-hour time increments were used in the numerical solution of equations 11.

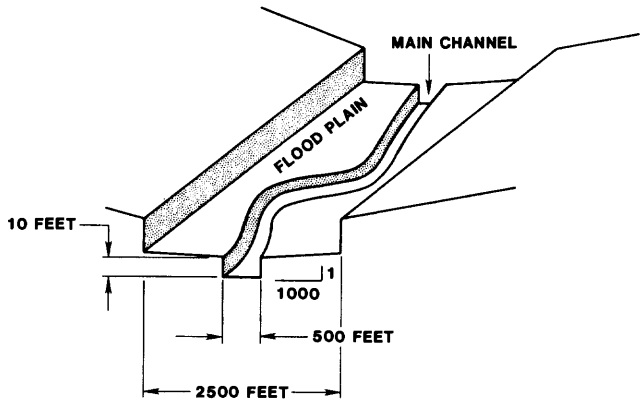

Figure 2. Hypothetical meandering channel and flood plain (not to scale).

The hydrographs computed by equations 11 at a main-channel distance of 100 mi generally compare well with results of Fread's "channel-flood plain" model when there is no meander (fig. 3). The rate of increase in discharge decreases as flow begins to inundate the flood plain. Lack of agreement in this part of the hydrograph, and later on the recession as flow returns to the main channel, may be due to differences in numerical dissipation and (or) discretization of hydraulic properties between computational cross sections. Total volumes under the three hydrographs agree within 2 percent. The timing and magnitude of the main-channel and maximum discharge peaks at 100 mi are nearly identical.

Computational problems reported by Fread (1976) in the unsuccessful application of a "composite-section" model were not experienced in the present study. Although the governing equations 11 treat the channel and flood plains as a continuous cross-sectional area, as did Fread's "composite-section" model, top width does not appear directly in the equations or subsequent numerical computations. Consequently, the sudden change in top width as flow spills onto the flood plain, which often causes solutions formulated in terms of depth of flow, top width, and discharge to fail, does not directly affect the present solution.

Travel time of the discharge peak is reduced when the meander ratio is increased from 1.0 to 1.5. For comparison, hydrographs simulated in river systems with meander ratios of 1.0 (previously shown in fig. 3) and 1.5 are plotted in figure 4. Following Fread's example (1976), main-channel slope and length are the same in both systems. Consequently, the flood plain is one-third shorter and steeper in the system with a 1.5 meander ratio, resulting in about a one-third reduction in travel time of the discharge peak. As expected, the part of the hydrographs representing main-channel flow before flood-plain inundation is not affected by the meander ratio.

Significantly different results are reported by Fread (1976). As shown in figure 5, there is good agreement before flood-plain inundation and on overall volumes, but, in contrast to this model's one-third reduction in travel time, travel time of the maximum-discharge peak simulated by Fread's "channel-flood plain" model is only slightly reduced from the no-meander example. A slight reduction in travel time would occur if the flood-plain slope were reduced without a corresponding reduction in length. To demonstrate the effect of slope reduction without a reduction in length, the solutions of equations 11 at a main-channel distance of 150 mi are compared to Fread's results at 100 mi (fig. 6), both with 1.5 meander ratios. The flood-plain length at a main-channel distance of 150 mi with meander would be equivalent to a flood-plain length at a main-channel distance of 100 mi without meander. There is good agreement in both timing and magnitude of the discharge peak. It appears that Fread's "channel-flood plain" model does not adequately account for reduction in flood-plain length with increased meander ratio.

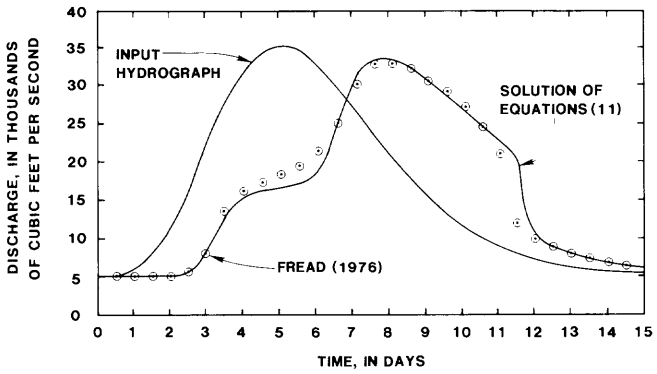

Figure 3. Comparison of hydrographs at 100 main-channel miles with no meander.

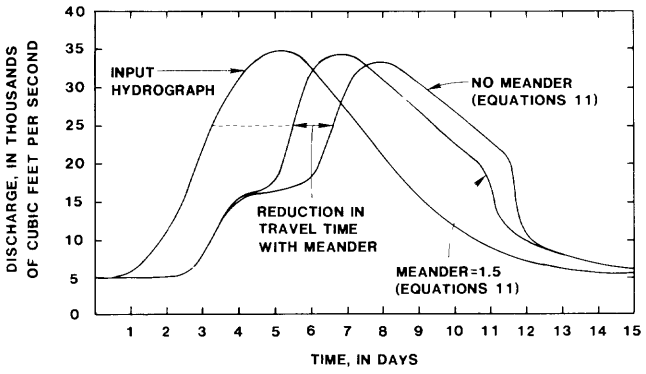

Figure 4. Effect of meander on travel time of maximum-discharge peak at 100 main-channel miles.

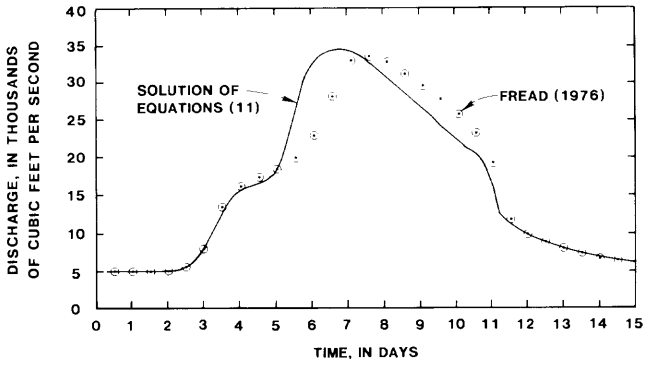

Figure 5. Comparison of hydrographs at 100 main-channel miles with meander ratio of 1.5.

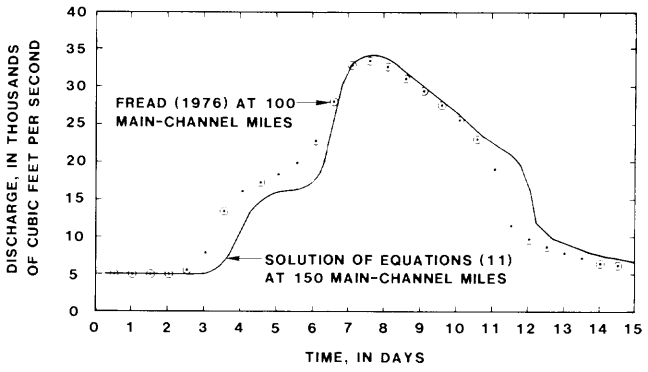

Figure 6. Comparison of solution of equations 11 at 150 main-channel miles with Fread's (1976) solution at 100 main-channel miles. (Meander ratio is 1.5.)

POTENTIAL FIELD APPLICATION

As shown in the preceding examples, channel and flood-plain geometry may have a significant effect on the shape and timing of hydrographs and timing of discharge peak. Multidimensional effects in natural channels such as result from main-channel and flood-plain interaction, secondary flow, and turbulence are not explicitly treated in the formulation of equations 11 but in practice may enter through empirical determination of conveyance and the momentum coefficient. Ideally, the sinuosity term (M) could be computed directly from sub-channel lengths measured along streamlines and corresponding cross-sectional areas. In practice, uncertainty in determining streamline location and length and appropriate cross-sectional areas might justify adjustments during model calibration. As formulated, the sinuosity term (M) should mainly affect unsteady flow results, allowing separate validation and (or) calibration of sinuosity with unsteady flow data and of conveyance and momentum coefficients with steady flow data.

CONCLUSIONS

Shape of flood hydrographs and timing of flood peaks may be significantly affected by the meander ratio. The one-dimensional flow equations have been extended to include the slope and volumetric effects of channel sinuosity that varies with stage. It appears that the "channel-flood plain" model presented by Fread (1976) does not adequately account for reduction in flood-plain length. Solving the generalized flow equations in terms of cross-sectional area and discharge seems to provide a more stable solution when flood-plain flow occurs.

REFERENCES CITED

Chow, V.T., 1959, Open-channel hydraulics: New York, McGraw-Hill, 680 p.

Cunge, J.A., Holly, F.M., Jr., and Verwey, A., 1980, Practical aspects of computational river hydraulics: London, Pitman Publishing Ltd., 420 p.

Fread, D.L., 1976, Flood routing in meandering rivers with flood plains, *in* Rivers 76, v. 1: 3d Annual Symposium on Inland Waterways for Navigation, Flood Control and Water Diversions, Colorado State University, August 1976, 906p.

Lapidus, Leon, and Pinder, G.F., 1982, Numerical solution of partial differential equations in science and engineering: New York, John Wiley and Sons, Inc., 677 p.

Lowham, H.W., DeLong, L.L., Collier, K.R., and Zimmerman, E.A., 1981, Hydrology of Salt Wells Creek—a plains stream in Southwestern Wyoming: U.S. Geological Survey Water-Resources Investigations 81–62, 52 p.

Pinder, G.F., and Shapiro, Allen, 1979, A new collocation method for the solution of the convection-dominated transport equation: Water Resources Research, v. 15, no. 2, p. 1177–1182.

Strelkoff, Theodor, 1969, One-dimensional equations of open-channel flow: American Society of Civil Engineers Proceedings, Journal of Hydraulics Division, May 1969, 16 p.

Wylie, C.R., Jr., 1960, Advanced engineering mathematics (2d ed.): New York, McGraw-Hill, 696 p.

Comparison of Two Stream-Discharge Record Reconstruction Techniques for Eight Gaging Stations in Maine

By Richard A. Fontaine

Abstract

An analysis of two commonly used stream-discharge record-reconstruction methods shows that the standard error of estimate for a missing record can be improved by using independent observations of stage. The accuracy of a missing record reconstructed by using both techniques is evaluated at eight stream gages in Maine where independent observations of stage and correlative stream gage data from other sites are available. The average standard error for a missing record reconstructed with flow data from other stream gages is 52.9 percent. The average standard error for a missing record reconstructed with independent observations of stage at the same site is 15.0 percent. The average standard error of published streamflow data in Maine is currently 17.7 percent. This average standard error could be reduced to approximately 13.0 percent if independent observations of stage are available to estimate the missing record.

INTRODUCTION

The U.S. Geological Survey began a 5-year nationwide analysis of its stream-gaging program in 1983. A significant part of the analysis is a determination of the accuracy of stream-discharge data published by the Survey. A study of stream gages in Maine (Fontaine and others, 1984) documented that periods of missing record currently average 5.6 percent and that missing records have a significant adverse effect on the accuracy of stream-discharge data.

The purpose of this report is to evaluate the accuracy of discharge records at eight stream gages (fig. 1) calculated by using two commonly used techniques for reconstructing missing records. The evaluation documents the errors associated with missing records reconstructed by using data from other gaged locations and the errors associated with missing records reconstructed by using independent observations of stage at the same site. Independent observations of stage can be readings from an observer, readings from a backup recorder, or readings from remote sensing devices such as a telemark. The accuracy of data reconstructed by using the two methods is compared, and the effect of the reconstructed data on the overall record accuracy at the sites is examined.

COMPARISON OF METHODS OF RECONSTRUCTING RECORDS

Methods for Determining the Error of Estimated Records

The error associated with estimated records for which no other correlative data are available provides a base from which improvements can be measured. When stream-discharge data are missing at a station and no concurrent data exist that can be used to reconstruct the missing record, then there are at least two methods for estimating the discharge: A recession curve can be applied from the time of recorder failure until the recorder functions again, or an average value of discharge for the period of missing data can be used as an estimate. Fontaine and others (1984) used the average-value method, and it was used for calculations in this report.

In the average-value method, the estimate of missing record on a given day is the average value of discharges observed on that day in previous years. The average value for the i^{th} day in a year (μ_i) is an average of the daily streamflow data previously collected at the site for the i^{th} day in each year that the gage has been operated. The average error of the estimated discharge on the i^{th} day in a year can be expressed as a percentage by the coefficient of variation (Cv_i) which is defined as follows:

$$Cv_i = 100\left(\frac{\sigma_i}{\mu_i}\right) , \qquad (1)$$

where σ_i is the standard deviation of daily discharges for the i^{th} day of the year.

Cv varies seasonally, but because the time when record is missing cannot be anticipated, the seasonally averaged coefficient of variation ($\overline{Cv}$) is used:

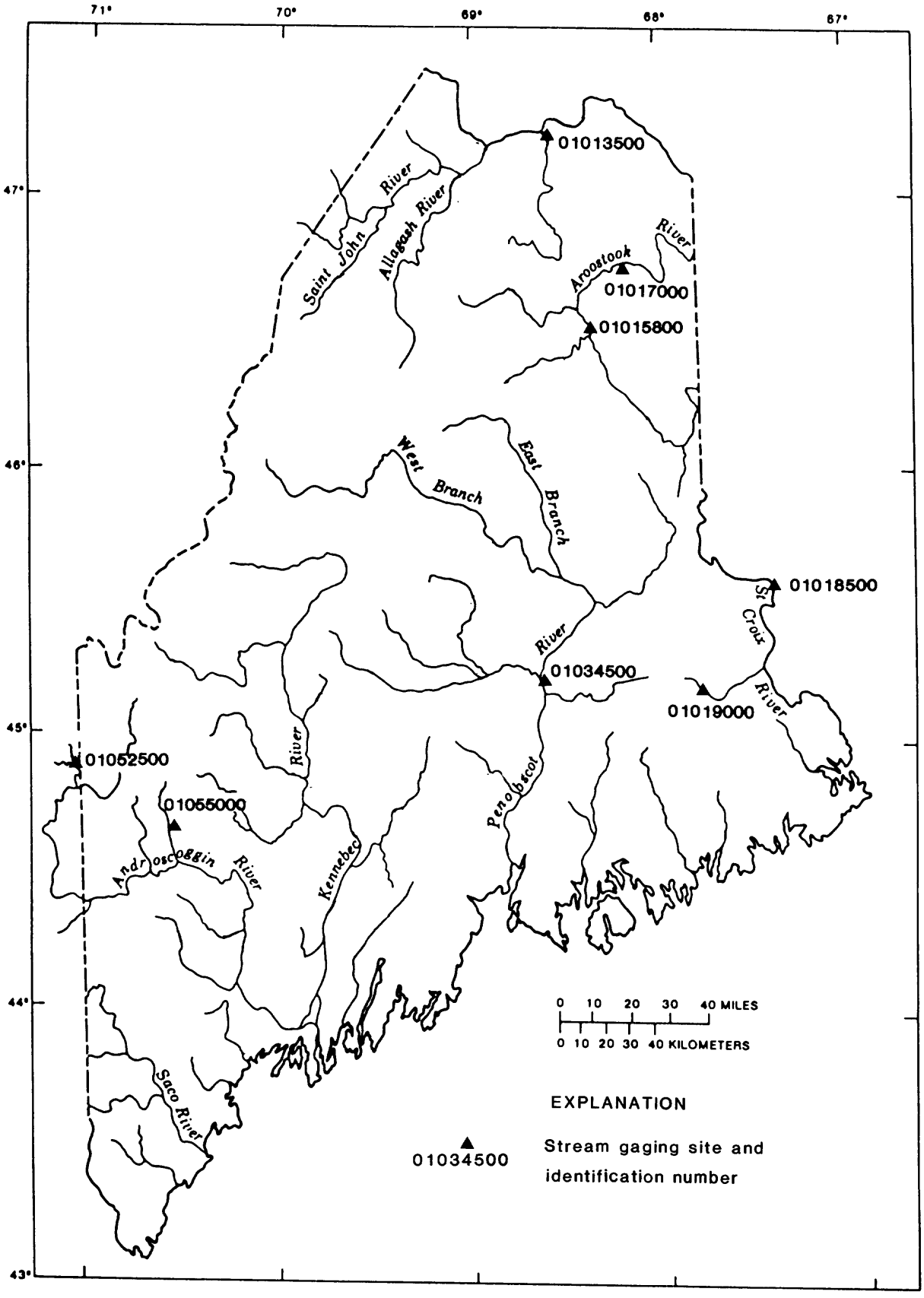

Figure 1. Locations of stream gages.

$$\overline{Cv} = 100 \left(\frac{1}{365} \sum_{i=1}^{365} \frac{\sigma_i^2}{\mu_i} \right)^{0.5} . \quad (2)$$

Typically, when record is missing at a station, concurrent data in some form are available to aid in the estimation of the missing record. Commonly, data from other, nearby stations are used to estimate missing record, in which case the mean square error in percent, (Vr), is estimated on the basis of the correlation between records at the site of interest and records from nearby gaged sites. If ρc is the correlation coefficient between the detrended streamflows (streamflows with seasonal trends removed) at the site of interest and detrended streamflows at another site, the fraction of mean square error at the primary site explained by data from the other site is ρc^2. The fraction of unexplained mean square error at the primary site is given by $1 - \rho c^2$. For any given day of the year the average mean square error of streamflow record estimated on the basis of record at another gage (Vr) is given by:

$$Vr = (1 - \rho c^2)\, \overline{Cv}^2 . \quad (3)$$

The standard error in percent (σ) is the square root of Vr.

The same basic technique described above to estimate error can be extended to cases when independent observations of stage are available at a gage to estimate missing record.

To determine the accuracy or mean square error associated with record reconstructed by using independent observations of stage, a second correlation coefficient, ρc*, is required. This correlation coefficient is determined for the relationship between mean daily discharge at a station and discharges obtained from observations of stage that have been converted by using the stage-discharge relationship at the site. The second correlation coefficient ρc* can then be used in place of ρc in equation 3 to determine the mean square error of missing streamflow record estimated on the basis of independent observations of stage (Vr).

Results

Eight representative stream gaging stations selected from the set used by Fontaine and others (1984) were used for the comparison of the two estimation methods. These eight gages, listed in table 1, have independent observations of stage once or twice daily from either observers or remote interrogation equipment. For these stations, the $\overline{Cv}$ ranged from 64.6 percent to 142 percent.

For the method in which missing record is estimated by using flow from another gaging station, the maximum of the correlations with other stations was used as ρc. They range from 0.408 to 0.963 and are summarized in table 2.

For the method in which missing record is estimated by independent stage observations, both a single daily reading at 0700 and twice-daily readings at 0700 and 1900 were evaluated. The value used for the correlation coefficient ρc* was the maximum of the multiple correlation coefficients from several linear regressions using current-day, previous-day, and succeeding-day stages converted to discharges.

For stations where only once-daily stage readings are available, the value ρc* was chosen as the maximum multiple correlation coefficient from the linear regressions between the dependent variable, mean daily discharge (*MDAY*), and the following independent variables: the morning stage reading converted to discharge (*AM*), the similar discharge from the previous morning (*PAM*), and that from the following morning (*FAM*). For the case of twice-daily stage observations, the value ρc* was chosen as the maximum of the multiple correlation coefficients in the linear regressions between the dependent variable, *MDAY*, and the following independent variables: *AM*, *FAM*, evening stage reading converted to discharge (*PM*), and readings from the previous evening (*PPM*).

Data used in the analysis were from consecutive days. Days on which readings of stage were affected by backwater from ice were not included in the analysis. The maximum multiple correlation coefficients, the length of record analyzed, and the best fit linear-regression models are summarized in table 3.

Table 1. Gaging stations in Maine with independent observations of stage

Station no.	Station name	Drainage area (mi^2)	Period of record
01013500	Fish River near Fort Kent	873	July 1903–December 1908; May 1911; November 1911–present.
01015800	Aroostook River near Masardis	892	September 1957–present.
01017000	Aroostook River at Washburn	1,654	August 1930–present.
01019000	St. Croix River at Vanceboro	413	October 1928–present.
01019000	Grand Lake Stream at Grand Lake Stream	227	October 1928–present.
01034500	Penobscot River at West Enfield	6,671	November 1901–present.
01052500	Diamond River near Wentworth Location, N.H.	152	July 1941–present.
01055000	Swift River near Roxbury	96.9	June 1929–present.

Table 2. Statistics of record reconstruction by using data from other stream gages

Station no.	Coefficient of variation $\overline{Cv}$ (percent)	Correlation coefficient ρc	Sample size (years)	Station number of sites used to reconstruct missing record	
01013500	82.6	0.853	30	01014000	
01015800	101	.936	25	01017000	
01017000	106	.936	25	01015800	
01018500	72.5	.571	30	01020000	
01019000	68.7	.408	30	01020000	
01034500	64.6	.954	30	01030500	01030000
01052500	114	.700	18	01054200	
01055000	142	.884	30	01057000	01052500

Values of $\overline{Cv}$ and ρc, for reconstruction of missing record with data from other stream gages, and of ρc*, for reconstruction of missing record with independent observations of stage, were used to determine the standard error of estimated discharges in percent at each of the eight stations studied. These data are summarized in table 4.

Standard errors for missing records reconstructed with data from other stream gages ranged from 19.4 to 81.4 percent. Standard errors for missing records reconstructed with independent observations of stage ranged from 2.9 to 37.2 percent. To summarize the standard error data and to allow a comparison between the two methods of missing record reconstruction, an average standard error ($\overline{\sigma}$), in percent, was calculated as follows:

$$\overline{\sigma} = \left(\frac{\sum_{i=1}^{n} Vr}{n} \right)^{0.5} . \qquad (4)$$

This measure shows that the method in which independent observations of stage provide the correlative data yields an average standard error of 15.0 percent, whereas the method in which other gaging station records provide the correlative data yields an average standard error of 52.9 percent.

The average effect that this difference has on the accuracy of data published for a station in Maine can be evaluated by application of the following equation:

with $$V = EfVf + ErVr + EeVe \ , \qquad (5)$$

where $$Ef + Er + Ee = 1 \ , \text{ and}$$

where V is the average relative variance of the errors of streamflow estimates,

Ef is the fraction of time that the primary recorders are functioning,

Vf is the relative variance of the errors of flow estimates from primary recorders,

Table 3. Statistics of record reconstruction with independent readings of stage from the stream gage

Station no.	Source of reconstructed records	Sample size (days)	Correlation coefficient ρc*	Best fit linear regression model for *MDAY*
01013500	Telemetry; read daily	275	0.999	$MDAY = 2.857 + 0.864\ (AM) + 0.135\ (FAM)$
01015800	Telemetry; read twice daily	238	.999	$MDAY = 2.387 + 0.543\ (AM) + 0.458\ (PM)$
01017000	Telemetry; read twice daily	275	.999	$MDAY = 7.846 + 0.599\ (AM) + 0.400\ (PM)$
01018500	Observer; reads daily	256	.992	$MDAY = 11.063 + 0.535\ (AM) + 0.411\ (FAM)$
01019000	Observer; reads daily	275	.998	$MDAY = 3.196 + 0.439\ (AM) + 0.575\ (FAM)$
01034500	Observer; reads twice daily	275	.999	$MDAY = 19.931 + 0.439\ (AM) + 0.443\ (PM)$
01052500	Telemetry; read daily	275	.990	$MDAY = 2.246 + 0.797\ (AM) + 0.198\ (FAM)$
01055000	Telemetry; read daily	728	.965	$MDAY = 4.969 + 0.694\ (AM) + 0.336\ (FAM)$

Table 4. Error, in percent, associated with reconstruction of missing record in Maine

(1) Station no.	(2) Standard error of missing records reconstructed with data from other stream gages (σ)	(3) Standard error of missing records reconstructed with independent observations of stage (σ)	(4) Change in standard error Col 2 − Col 3
01013500	43.1	3.7	39.4
01015800	28.3	4.5	23.8
01017000	28.6	4.7	23.9
01018500	59.5	9.2	50.3
01019000	62.7	4.3	58.4
01034500	19.4	2.9	16.5
01052500	81.4	16.1	65.3
01055000	66.4	37.2	29.2
Average standard error $\bar{\sigma}$	52.9	15.0	37.9

Er is the fraction of time that secondary data are available to reconstruct streamflow records given that the primary data are missing,

Vr is the relative error variance of flow estimates reconstructed from secondary data,

Ee is the fraction of time that primary and secondary data are not available to compute streamflow records, and

Ve is the relative error variance of the third situation.

The average standard error of streamflow estimates for any number of stations ($\bar{S}$) can be calculated as follows:

$$\bar{S} = \left(\frac{\sum_{i=1}^{n} (S_i)^2}{n} \right)^{0.5} \qquad (6)$$

where S_i is the standard error of streamflow estimates at station i, in percent. The standard error S_i is the square root of V.

Analysis of stations in the Maine surface-water program by Fontaine and others (1984) determined $\bar{S}$ to be 17.7 percent and *Er* to be 5.6 percent for current operational conditions. If the assumption is made that the first and third products in equation 5, *EfVf* and *EeVe*, remain constant with different policies of record reconstruction, then a change in V and therefore in $\bar{S}$ can be evaluated by computing change in the term *ErVr*. When missing records are reconstructed with data from other stream gages, *Er* is 0.056 and *Vr* is $(52.9)^2$ and *ErVr* is 157 percent squared. When missing records are reconstructed with data from independent observations of stage, *Er* remains 0.056 and *Vr* changes to $(15.0)^2$ and *ErVr* becomes 13 percent squared. Again, assuming all other current conditions remain constant, a potential reduction in average value of V of 144 percent squared (157 − 13) is possible when using independent observations of stage instead of data from other stream gages to reconstruct missing record. This reduction in the average value of V can be converted to a corresponding lower value of $\bar{S}$ as follows:

$$\bar{S} = (V_{\text{original}} - V_{\text{reduction}})^{0.5} , \qquad (7)$$

therefore

$$\bar{S} = \left[(17.7)^2 - 144\right]^{0.5}$$

$$= 13.0 \text{ percent.}$$

The average standard error for estimates of streamflow at gaging stations in Maine could potentially be reduced from 17.7 percent to 13.0 percent by using independent observations of stage to reconstruct missing record.

SUMMARY AND CONCLUSION

Missing records at a stream gage are commonly reconstructed with correlative information from other stream gages or with independent observations of stage that have been converted to discharge. At eight stream gages in Maine where both independent observations of stage and other stream gage data were available, the accuracy of missing record reconstructed by using both techniques was evaluated.

At each of the eight stations considered, standard errors of missing record estimates can be improved by using independent observations of stage. The average standard error for the missing record reconstructed with data from other stream gages was 52.9 percent. The average standard error for missing record reconstructed with data from independent observations of stage was 15.0 percent. Fontaine and others (1984) noted that the average standard error of estimates of streamflow data in Maine was 17.7 percent. Results from the study indicate that this error could be reduced to approximately 13.0 percent if independent observations of stage were available to estimate missing records.

Independent observations of stage at stream gages in Maine provide valuable information that can be used to improve the accuracy of streamflow records.

REFERENCE CITED

Fontaine, R.A., Moss, M.E., Smath, J.A., and Thomas, W.O., Jr., 1984, Cost-effectiveness of the streamgaging program in Maine—a prototype for nationwide implementation: U.S. Geological Survey Water-Supply Paper 2244, 39 p.

Channel Widening Characteristics and Bank Slope Development Along a Reach of Cane Creek, West Tennessee

By Andrew Simon *and* Cliff R. Hupp

Abstract

Channelization and its related effects have led to 17 feet of degradation and 150 feet of widening of Cane Creek at Hunter Road from 1970 to 1983. The causes of widening are (1) overheightening of the loess channel banks beyond the critical bank height (H_c) by incision and (2) deflection of flow towards the right bank, caused by entrapped trees from upstream bank failures, that resulted in severely scalloped banks on the outside bends of the high-flow thalweg.

Tree-ring evidence and channel-geometry data indicate a minimum bank-widening rate of about 4 feet per year. Widening occurs predominantly by initial detachment from the bank by slab failure followed by deep-seated rotational failures on the upper banks. Piping and tension-crack development play important roles in these processes.

Estimates of further channel widening over the short term (10 to 20 years) range from 23 feet to approximately 60 feet. The slough-line angle, used as a measurement of temporary stability in the development of the reach's banks, is diagnostic in determining amounts of widening. The slough-line angle has probably flattened from the angle of internal friction (approximately 26° for the loess banks) to the present inclination (about 20°), and it should continue to flatten as Cane Creek develops a new flood plain at an elevation lower than its present one.

INTRODUCTION

The streams of west Tennessee are cut into unconsolidated and highly erosive formations, predominantly of Quaternary age. Erosion and silting of dredged channels of the region are major problems affecting river-crossing structures and lands adjacent to these channels. Channel instability since 1970, following channelization along Cane Creek, has resulted in the loss of arable farmland and is believed to have contributed to bridge failure.

The purposes of this investigation were (1) assessment of bank-slope stability and morphologic changes in response to channel modification; (2) identification of specific process and response mechanisms (such as downcutting—bank failures; aggradation—lower bank stability and vegetation establishment; piping—bank destabilization) related to bank slope development; and (3) use of an interdisciplinary approach including aspects of soil mechanics, channel geometry, and geobotany to estimate rates and durations of channel widening and the renewal of stable bank conditions along an unstable reach of Cane Creek (fig. 1). Dendrogeomorphic techniques are particularly applicable in determining morphologic change through time and have had wide use in other interdisciplinary geomorphic studies (Sigafoos, 1964; Hupp, 1983).

The Cane Creek basin is representative of many areas of west Tennessee with highly dispersive loess soils. It is located in the Mississippi embayment, Gulf Coastal Plain physiographic region, and is tributary to the Hatchie River. The drainage basin is blanketed by a layer of brown silty loess ranging in thickness from 20 ft in the eastern part to 60 ft in the western part, as determined by soils investigations conducted in the late 1960's by the Soil Conservation Service (SCS). This material is well drained, uniform, and of low to medium plasticity with an average plasticity index (PI) of approximately 6.

The broad alluvial valley of Cane Creek has been largely cleared of native forests for cultivation. Sheet and gully erosion are prevalent in the upland areas. Remaining streambank (riparian) vegetation commonly consists of species such as black willow, cottonwood, silver maple, and river birch. Cottonwood, hackberry, green ash, and black willow appear to be important species reestablishing on disturbed bank surfaces. Where bank slopes are particularly unstable, only small saplings and herbaceous vegetation survive.

Cane Creek has a basin area of approximately 60 mi^2 above Hunter Road. A U.S. Geological Survey stream gage 4.5 mi upstream of Hunter Road at State Route 19, Ripley, Tenn., was operated between 1958 and 1962.

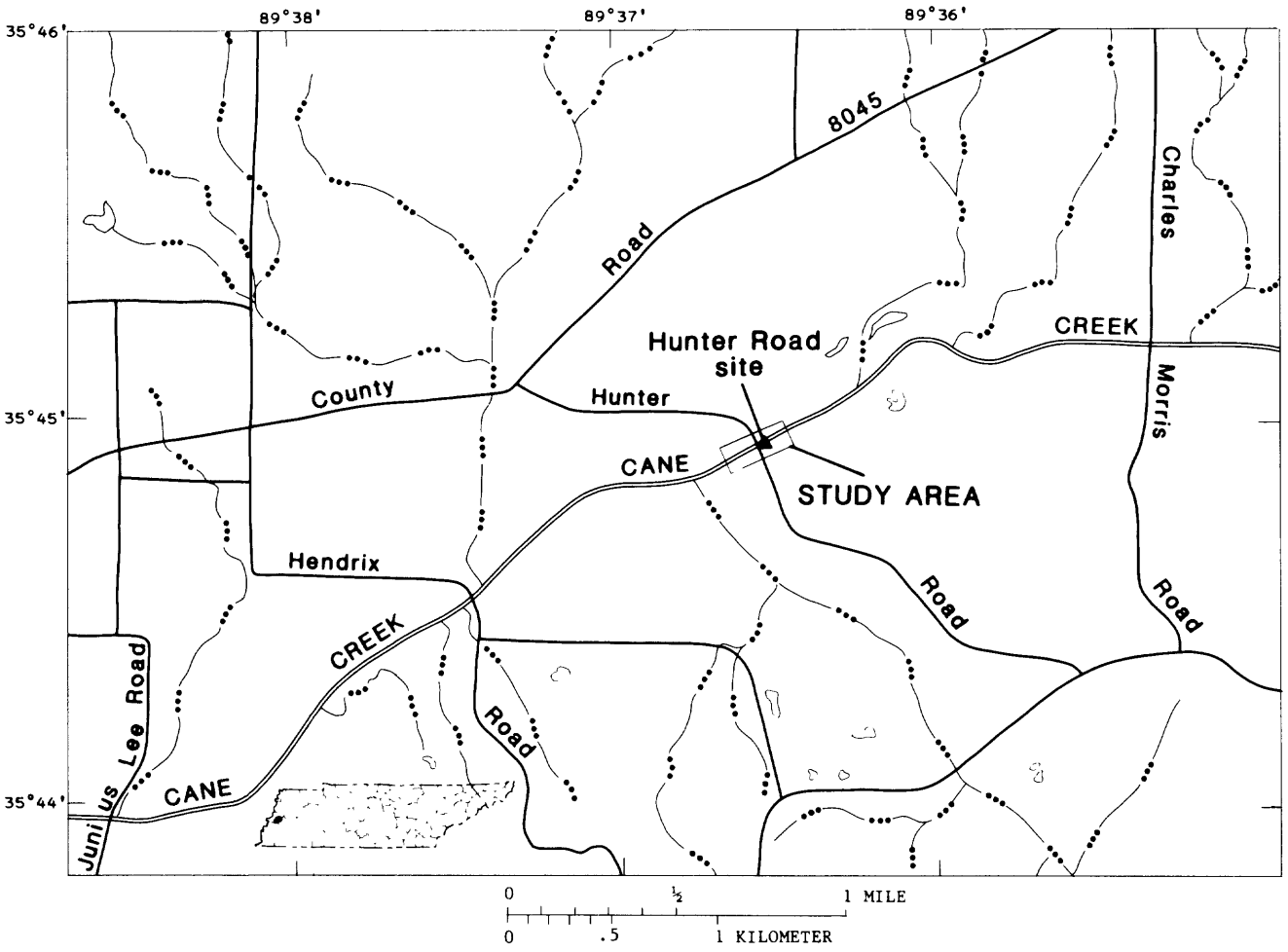

Figure 1. Location of study area in Cane Creek basin, west Tennessee.

BACKGROUND AND SITE DESCRIPTION

Before the 1970 channel modifications, Cane Creek showed no evidence of degradation. " ***Both the banks and bottom of the existing channel appeared to be very stable. Trees were numerous on the existing banks from the base flow line up" (Soil Conservation Service, Nashville, written commun., 1967, p. 1). Channel geometry in 1968, as described by the width-depth ratio (W/D) and measured from the flood-plain level, ranged from 6.45 to 41.6 within a 6-mi stretch of the creek that encloses the study reach. The U-shapes of channel cross sections surveyed in 1968 by the SCS indicate that aggradation was occurring along Cane Creek. Because stream banks were stable, the aggradation suggests that sediment production from the uplands and tributaries was greater than the transport capabilities of the stream.

The continued loss of channel capacity led to the development of a watershed workplan designed to reduce flood elevations and the frequency of overbank flows. Cane Creek, like most channels in west Tennessee, was channelized to improve flood-plain drainage. In 1970, 22.7 mi of sinuous channel were modified into a series of straight reaches 16.5 mi in length, an overall shortening of approximately 27 percent. This work increased the average channel gradient by approximately 40 percent, from approximately 3.7 to 5.2 ft/mi. Gradient in the study reach was constructed to approximately 5.1 ft/mi.

The increase in gradient combined with the reduced frictional losses inherent in straightened channels suggests that stream power and the energy available for sediment transport in the channel increased significantly. These changes, in turn, initiated an adjustment by degradation that affected modified reaches as well as adjacent reaches and unmodified tributaries. Bed-level data compiled by the U.S. Geological Survey (USGS) indicate that approximately 17 ft of degradation and scour took place in the vicinity of Hunter Road between 1970 and 1980. Width-depth ratios within the 6-mi reach decreased approximately 50 percent over the period.

Bed-level lowering of this magnitude creates an unstable, overheightened bank profile. Continual attack by flow at the toe of the bank can undercut and remove the support for the top part of the bank causing "slab failure" (Thorne and others, 1981). Other types of failure are enhanced by piping and the development of tension cracks at the top of the bank, which allows water to drain down into the bank mass and reduce shear strength. Seepage through a vertical bank and the development of pipes, particularly in loess material, can activate deep-seated rotational failures on the upper bank. Additionally, loess banks may fail near their toe when saturation leads to a loss of shear strength (Thorne and others, 1981). This type of failure is termed "pop-out." Deep-seated rotational failures appear to be the most common mechanisms for upper-bank widening along Cane Creek. Pop-out failures along the low-water bank, slab failures, and small tear-shaped debris-avalanche scars along the vertical face have also been observed.

Examination of specific cross sections compiled by the USGS indicates that roughly 40 ft of bank widening has occurred in the nonscoured reaches of Cane Creek during the 10 years (1970-80) following channelization. Similar accounts of mass bank failure in loess material by the above processes are described by Lohnes and Handy (1968), Bradford and Piest (1977), and Thorne and others (1981).

METHOD OF ANALYSES

Channel Geometry

Geometric characteristics of the Cane Creek channel, such as width, depth, bank height, and bank angle, were obtained from cross sections surveyed by the USGS, SCS, and Tennessee Department of Transportation (TDOT) for 1968, 1970, 1980, 1983, and 1984. Geometric changes between 1968 and 1970 represent those changes imposed by human modifications, whereas changes between 1970 and 1983 are due to channel adjustment processes. The width-depth ratio was used to delineate changes in channel geometry and stability conditions with time. A trend reversal in the W/D data with time can suggest a change from degradation to aggradation or vice versa.

Channel top widths were compared for successive measurements to obtain an average rate of bank widening. Rates calculated in this manner represent a 10-year period of channel adjustment (1970–80). Bank heights, vertical face heights, and bank slope are used in conjunction with soil-mechanics information to calculate critical bank height (H_c), which represents the height of the bank above which failure can be expected. The relation between soil mechanical properties and H_c is discussed in detail in the section on soil mechanics.

The angle attained by failed blocks of soil mass represents a temporary angle of stability (Carson and Kirkby, 1972). This angle, referred to as the "slough-line angle," is used to determine short-term (10–20 years) bank widening by projecting this slope to its intersection with the top of the bank (flood-plain level).

Geobotany

Trees growing on unstable bank surfaces along Cane Creek near Hunter Road show the effects of active bank caving in their stem morphology, anatomy, and ages. Bank failures along unstable reaches may kill, tilt, or scar existing woody plants, and they create fresh surfaces upon which plants may become established. Scars and sprouts from tilted parental stems yield accurate (within 1 year, often to the season) dates of bank failure (Sigafoos, 1964).

Eccentric growth, resulting in anomalous tree-ring series, occurs when the stem is inclined. This type of growth is easily determined from cross sections where concentric ring formation abruptly shifts to the eccentric because ring width is greater in the upslope direction than it is downslope. Eccentric ring patterns yield highly accurate dates, usually to the season, of tilting. Dating of stems that have established on disturbed surfaces yields minimum ages for the surfaces. Trees growing below top banks can indicate rates of degradation or aggradation through measurement of the thickness of sediment burial, or exhumation, from the root collar, which is established at the ground surface during germination.

Cross sections or cores were taken from about 30 trees along a reach of Cane Creek in the vicinity of Hunter Road. Three sites were selected for intensive geobotanical study on this reach: (1) about 300 ft upstream of the scoured area at the bridge site, (2) about 300 ft downstream of the scoured area at the bridge site, and (3) at the confluence of a tributary with Cane Creek, about 200 ft downstream of the old bridge (fig. 2).

Geobotanical study at each site included the identification of trees affected by bank failure, core or cross section removal from affected trees, measurement of widths of the failure block, and interpretation of vegetative-geomorphic relations. Additionally, saplings growing on slough lines and shelves were dated, and thickness of fill sediments above root collar was measured. Location, species, age, and condition of woody vegetation were noted in relation to the various geomorphic surfaces on which they were found: that is, top-bank, vertical face, upper bank, slough line, and shelf (fig. 3).

Soil Mechanics

Soil-mechanics data, including particle-size distribution, Atterberg limits, and calculated values of the

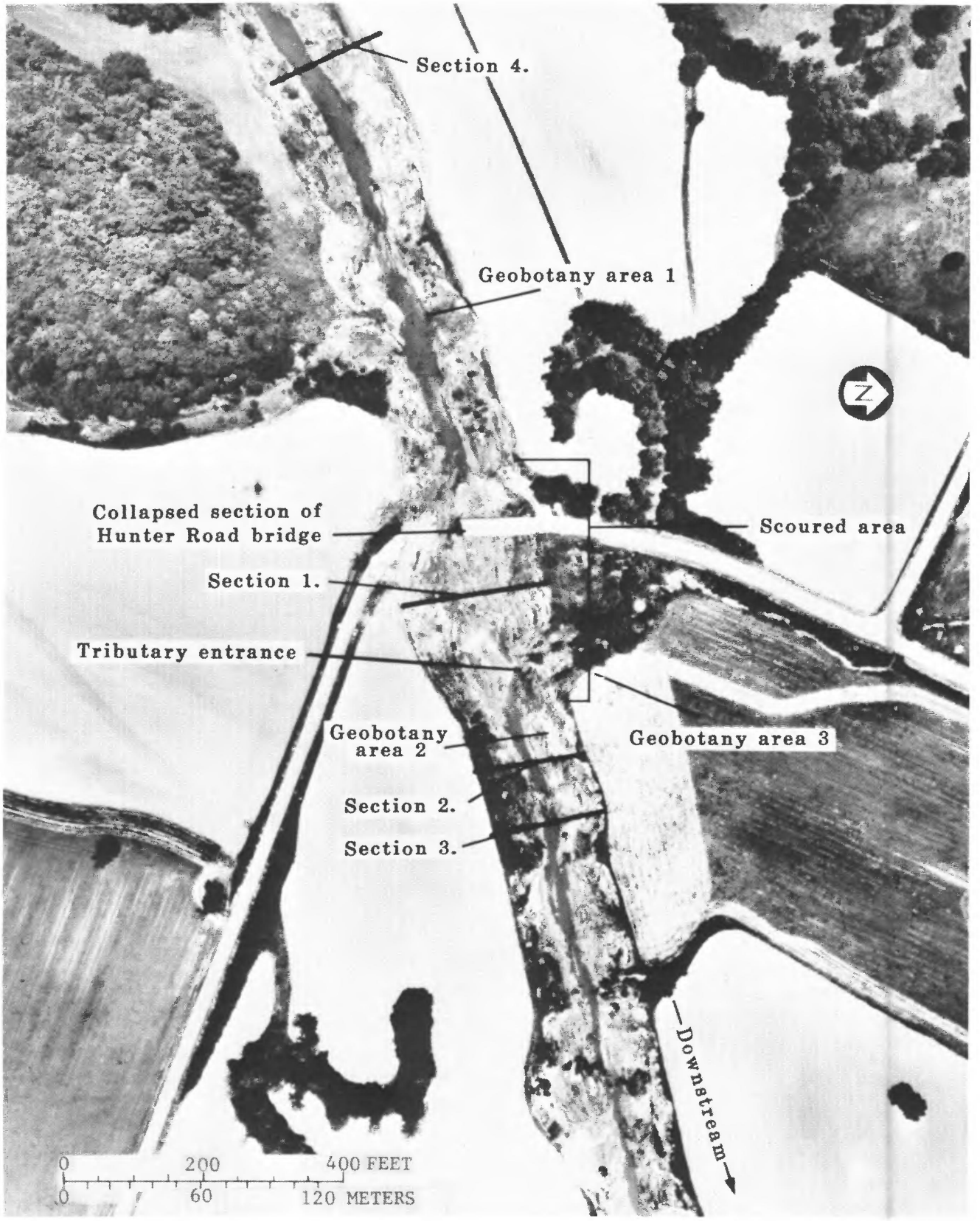

Figure 2. Aerial photograph of scoured area showing surveyed cross sections and sites of geobotanical study, Cane Creek, Lauderdale County, Tenn., June 1983. Photograph by Tennessee Department of Transportation.

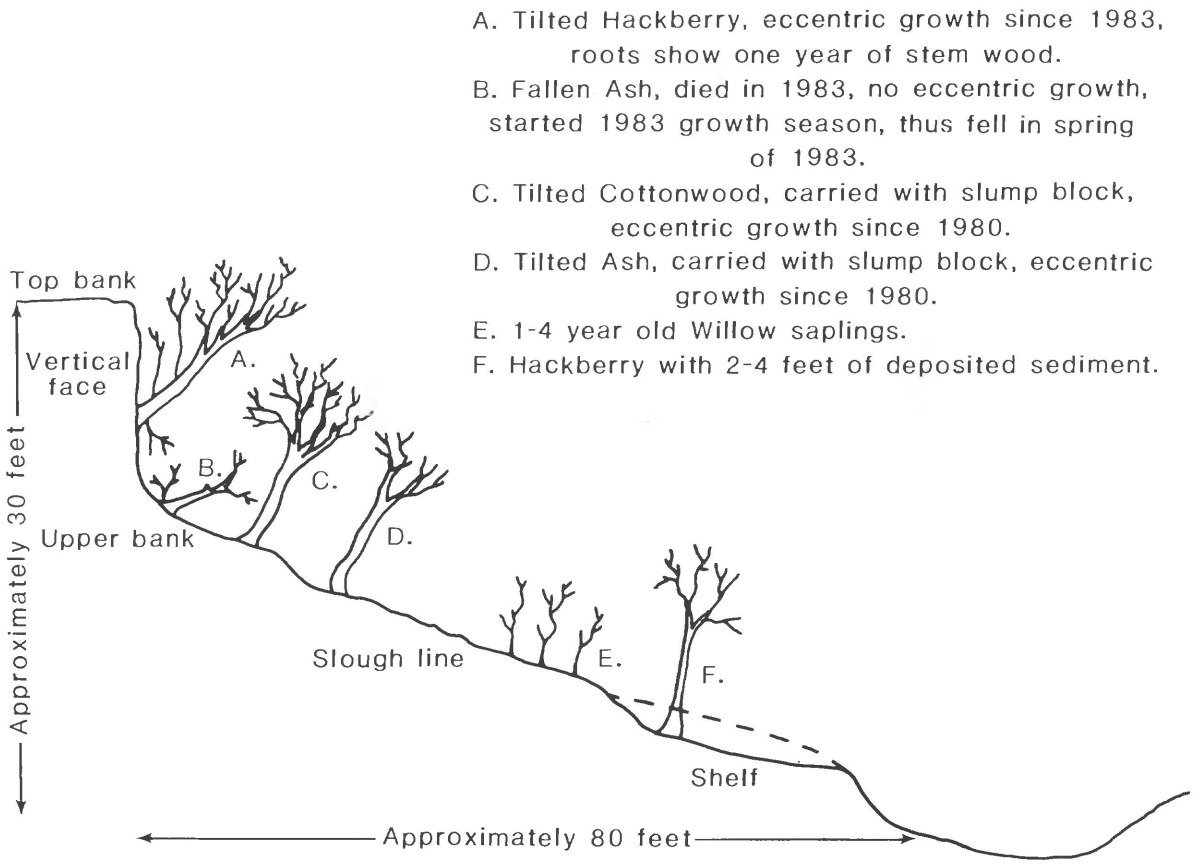

Figure 3. Generalized bank section of Cane Creek in the vicinity of Hunter Road, Lauderdale County, Tenn., showing geomorphic and vegetal characteristics.

angle of internal friction, cohesion, and bulk density, were used with slope stability analyses to calculate critical bank heights (H_c) and to conceptualize thresholds of bank stability.

The theoretical basis for the slope-stability equations used in this paper is presented in detail by Lohnes and Handy (1968), Carson and Kirkby (1972), and Thorne and others (1981) and is not repeated here. However, some discussion of their use in this study is required, owing to complexities inherent in stream channel banks that are not adequately dealt with in the literature.

Standard slope-stability equations are based on surfaces having uniform gradients. The bank slopes in the vicinity of Hunter Road, however, contain several segments (fig. 3) and therefore cannot be characterized by a single angle. Compound slopes such as these pose particular problems in slope-stability analysis. Description and analysis of these slopes as being entirely vertical would result in underestimation of H_c because the slopes, except for the vertical face, are not vertical. Conversely, use of an average bank angle would result in gross overestimation of H_c because the significance of the vertical segment could be vastly reduced. Observed failed banks along Cane Creek suggest that initial detachment of the bank is enhanced by piping and tension crack development along the vertical section of the bank, followed by rotational failure.

The stability equation (Lohnes and Handy, 1968) for a vertical bank was used to obtain a first approximation of H_c. It is as follows:

$$H_c = \frac{4c}{\gamma} \tan (45 + \Phi/2) \ , \qquad (1)$$

where H_c is critical bank height, in feet,
c is cohesion of the bank material, in pound-force per square foot,
γ is the unit weight of the bank material, in pound-force per cubic foot, and
Φ is the angle of internal friction of the bank material, in degrees.

Both c and Φ are defined in terms of the plasticity index and are derived from templates developed by the SCS (Frank Cousins, SCS, written commun., 1984). These data were fit to the following equations:

$$\Phi = 34.54e^{-0.0520\,(PI)} \text{ and} \quad (2)$$

$$c = 1.93 + 0.1444\,(PI)\ , \quad (3)$$

where PI is the plasticity index and
e is the natural log
(r^2 is 0.94 and 0.95 for equations 2 and 3, respectively).

Values calculated for Φ and c in equations 2 and 3 are similar to those Lohnes and Handy (1968) obtained for loess in the Cane Creek basin. Plasticity index data were obtained from samples taken along Cane Creek in 1983 and 1984 by the USGS and at the Hunter Road site by TDOT in early 1984. Shear-strength properties approximate those reported by Grissinger and others (1981). The mean value used here for γ of 97.7 (lbs/ft^3) was recorded by Lohnes and Handy (1968) for samples taken in the loess of the Cane Creek basin.

As discussed earlier, the development of piping and tension cracks at the top of the bank increases the bank's susceptibility to failure, can initiate rotational failure, and effectively reduces critical bank height. A modified equation, therefore, was used to account for the initial detachment of the bank from the flood plain, which allows water to seep into the bank mass and further reduce shear strength. The depth of tension cracking rarely exceeds one-half of the bank height (Terzaghi and Peck, 1948) and can be estimated in the field from the height of vertical failure planes (Thorne and others, 1981). These factors were accounted for by adjusting estimates of H_c according to the formula for vertical failure (after Lohnes and Handy, 1968):

$$H_c' = \frac{4c}{\gamma} \tan\,(45+\Phi/2) - Z\ , \quad (4)$$

where H_c' is critical bank height adjusted for depth of tension cracks and
Z is the depth of tension cracking, in feet.

Values of H_c reported in this study are calculated by using equation 1 but cannot represent the total height of the bank. Because most banks in the study reach are vertical near their tops, relative stability of the bank is defined in terms of those vertical sections. If H_c' is greater than the observed vertical face, the bank is considered relatively stable in terms of failure; if the reverse is true, then the bank is at risk of failing.

DISCUSSION OF RESULTS

Channel Degradation and Aggradation

According to available channel-geometry data, degradation on the main stem of Cane Creek apparently has stopped. The channel is now experiencing a phase of aggradation. This is significant in terms of bank stability because bank heights are no longer being increased through incision, and the bank toe experiences a net accumulation of material rather than a depletion (Andrews, 1982). This reversal was inferred by comparing cross sections taken in 1980 by the SCS and ones taken in 1983 by the USGS. Bed elevations were higher in 1983 than in 1980, and numerous cross sections show the development of a U-shaped bottom, indicative of depositional conditions. Furthermore, a trend of decreasing W/D from 1970 to 1980 (indicating downcutting) had been reversed by 1983, suggesting that incision has ceased although widening remains prevalent.

Headward-progressing degradation, however, is still evident in the tributaries. Figure 4 shows a profile of a tributary that enters Cane Creek on its left bank roughly 200 ft downstream of Hunter Road. Field inspection in February 1984 indicates that significant deepening has occurred and that banks are still widening. Knickpoints were observed close to the mouth and roughly 300 ft upstream where headward erosion has cut into different materials along Hunter Road. Channel banks upstream of this point on the tributary are relatively stable with established vegetation, convex bank slopes, and a top-bank width of 16 ft. Areas downstream that have been overheightened as a response to the deepening of Cane Creek are actively widening. Top-bank widths from the mouth to the upper knickpoint were on the order of 45 ft in February 1984. Twenty feet of additional widening from the mouth to about 50 ft upstream and obliteration of the lower knickpoint were observed when the site was revisited in March 1984 following a substantial rainfall.

Channel Widening

The channelization that took place in 1970 stimulated increased erosion in the uplands and valley flats through gully development. The bed and banks of the main stem and the tributaries also began to erode. From 1970 to 1980 stream power in Cane Creek apparently was sufficient to transport this material out of the watershed and into the Hatchie River. By 1980, W/D values in the study reach approached a mean of 4.50 following roughly 17 ft of degradation and scour between 1970 and 1980.

Rates of channel widening on Cane Creek based on 1970 and 1980 top width data are approximately 4 ft/yr. Widening in the scoured section of the channel just

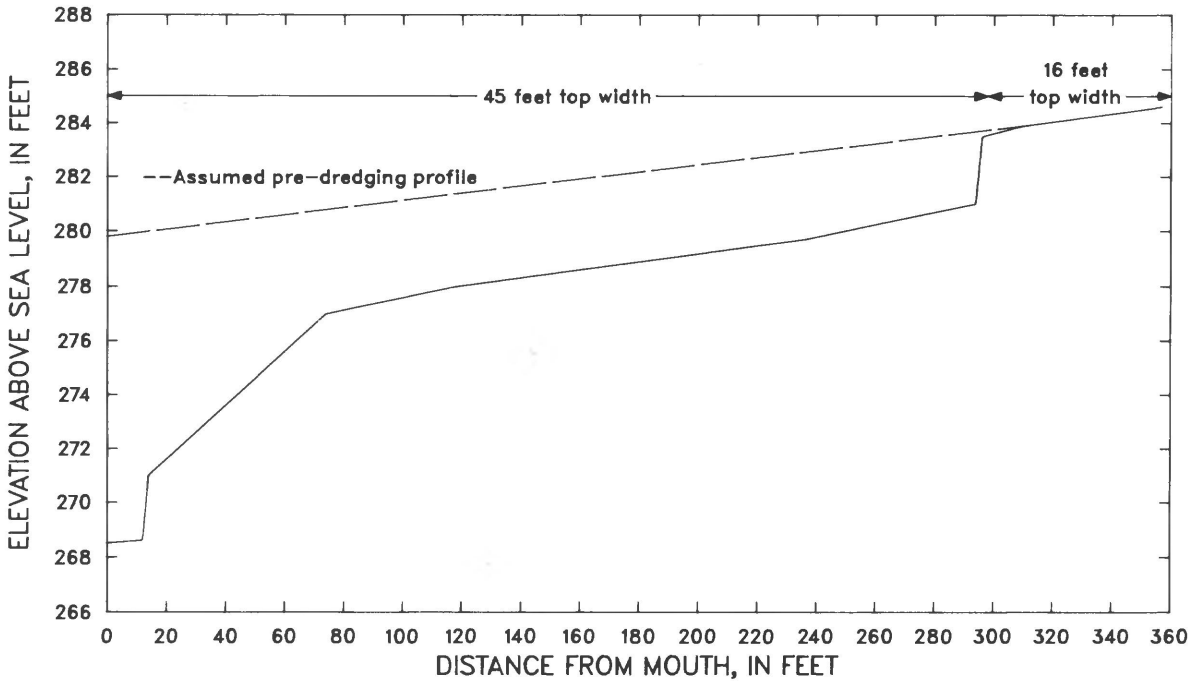

Figure 4. Profile of tributary 200 ft downstream from Hunter Road, Cane Creek, Lauderdale County, Tenn., February 1984.

downstream of the bridge (fig. 2, section 1) at Hunter Road between 1970 and 1980 was similar to that of other reaches of Cane Creek. The estimated 100 ft of widening that occurred at section 1 between 1980 and 1983 was a function of adjustment and localized hydraulic processes in the channel (fig. 5). Upstream bank failures caused by overheightening resulted in the toppling of many trees that were transported downstream. Some of these became trapped on the left upstream side of the Hunter Road bridge, causing blockage, deflection of flow, and accelerated undercutting on the opposite bank. This eventually led to the collapse of at least a 20-ft-wide section of the right bank and contributed to the failure of the bridge during the high flows of April 1983.

The Cane Creek channel in the vicinity of the Hunter Road bridge is characterized by significant lateral instability and maintains the potential for a lengthy period of adjustment. Piping holes 1 ft in diameter are common along the top bank and further reduce bank stability. Channel-top width at the bridge site (section 1) averages 220 ft compared with an average of roughly 160 ft in the nonscoured sections upstream and downstream from the bridge (fig. 2). This 160-ft top width represents the greatest nonscoured channel width throughout Cane Creek. Widening of this magnitude is assumed to be caused by the deflection of flow by the debris on the left upstream side of the bridge towards the right bank. The deflected flow in turn developed into a wave traversing laterally from bank to bank in the downstream direction. If the wave is viewed as a meandering high-flow thalweg, the area where this flow impinges upon a bank is similar to the area of an outside meander bend or cutbank where both the elevation of the flow and the shear stress are greatest. Greater bank erosion occurs at these locations (scoured sections) and is further shown by the uniform pattern of scalloped banks in the downstream direction (fig. 6). We believe that this over-widening will occur in addition to the average widening rate of 4 ft/yr and will migrate some distance downstream, further enlarging the channel by upper bank failure.

Estimates of Channel Widening

Estimates of short-term (10–20 years) widening are obtained from projection of the slough line (fig. 3). Analysis of the four cross sections in the study reach indicate the development of the slough-line angle at roughly 20° to the horizontal. This angle is believed to represent temporary stability of the lower bank sections. The oldest trees dated on this surface in the nonscoured area are from 3 to 4 years old (E, in fig. 3). This age coincides with the onset of aggradation as determined from channel surveys, and, with it, greater stability at the toe of the bank. Thus, an interdisciplinary check confirms the initial renewal of bank stability.

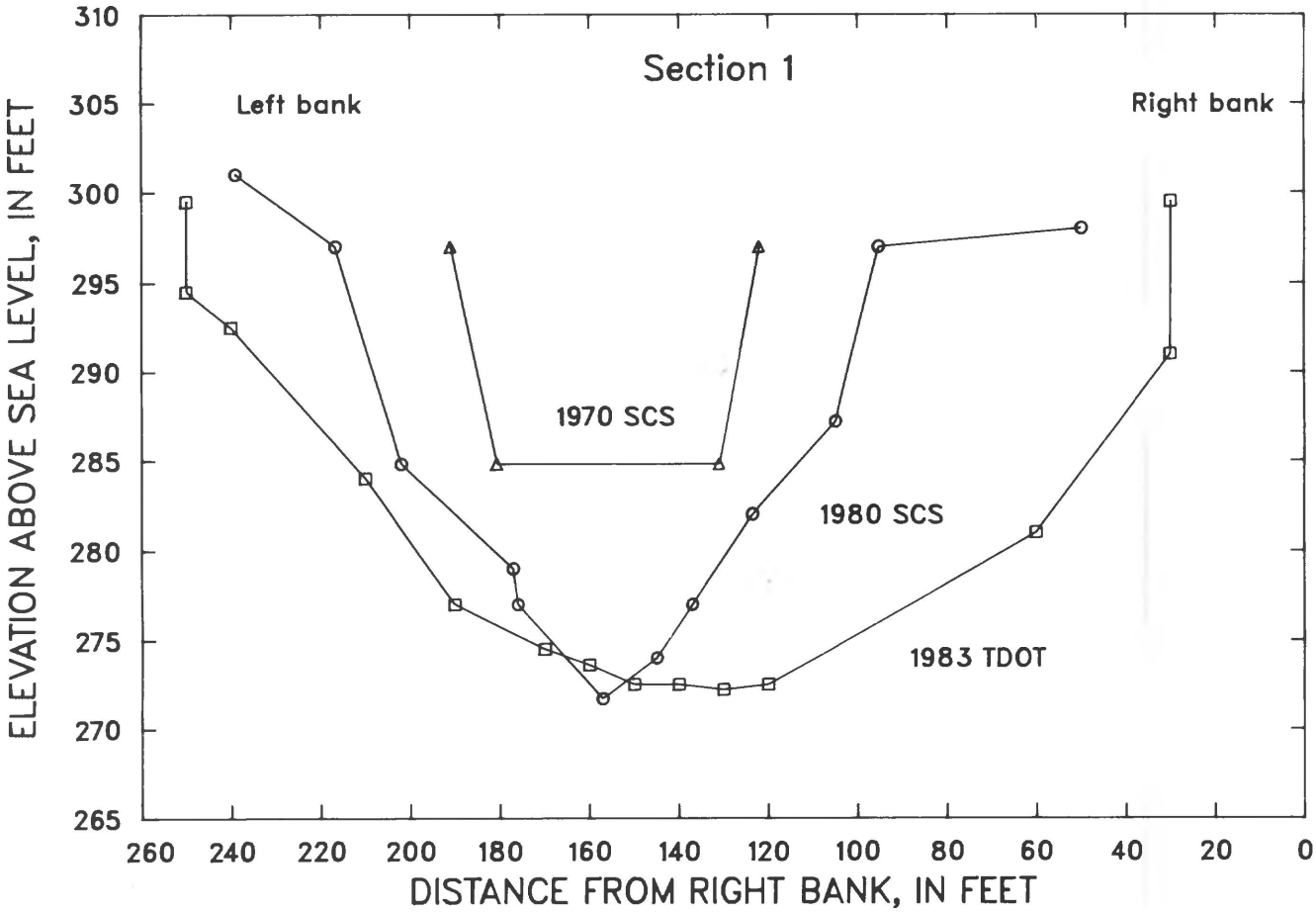

Figure 5. Changes in Cane Creek channel 100 ft downstream from Hunter Road, Lauderdale County, Tenn., 1970–83.

A bank cross section representative of worst case conditions shows that by extending the slough line to top bank elevation, additional widening at section 3 (fig. 2) could be more than 40 ft (fig. 7). This section is representative of locations in the reach where tension cracks are numerous and vertical bank faces 10 ft or greater are common. Apparently the tension cracks will become vertical faces after failure, and the depths of the tension cracks are related to the height of the subsequent vertical bank faces. In the nonscoured area represented by sections 2 and 4 (fig. 2), the slough-line angle indicates the potential for 20 ft of bank widening (figs. 8, 9). A cross section taken in February 1984 within the scoured area (section 1, fig. 2) indicates the potential for roughly 6 ft of widening on the left bank (fig. 10). When the top widths of the cross sections in figures 5 and 10 are compared (1983 and 1984), a 7-ft failure on the left bank can be inferred.

Figure 6. Scalloped bank conditions in the vicinity of Hunter Road, Cane Creek, Lauderdale County, Tenn.; view is downstream. Photograph by U.S. Geological Survey, March 1983.

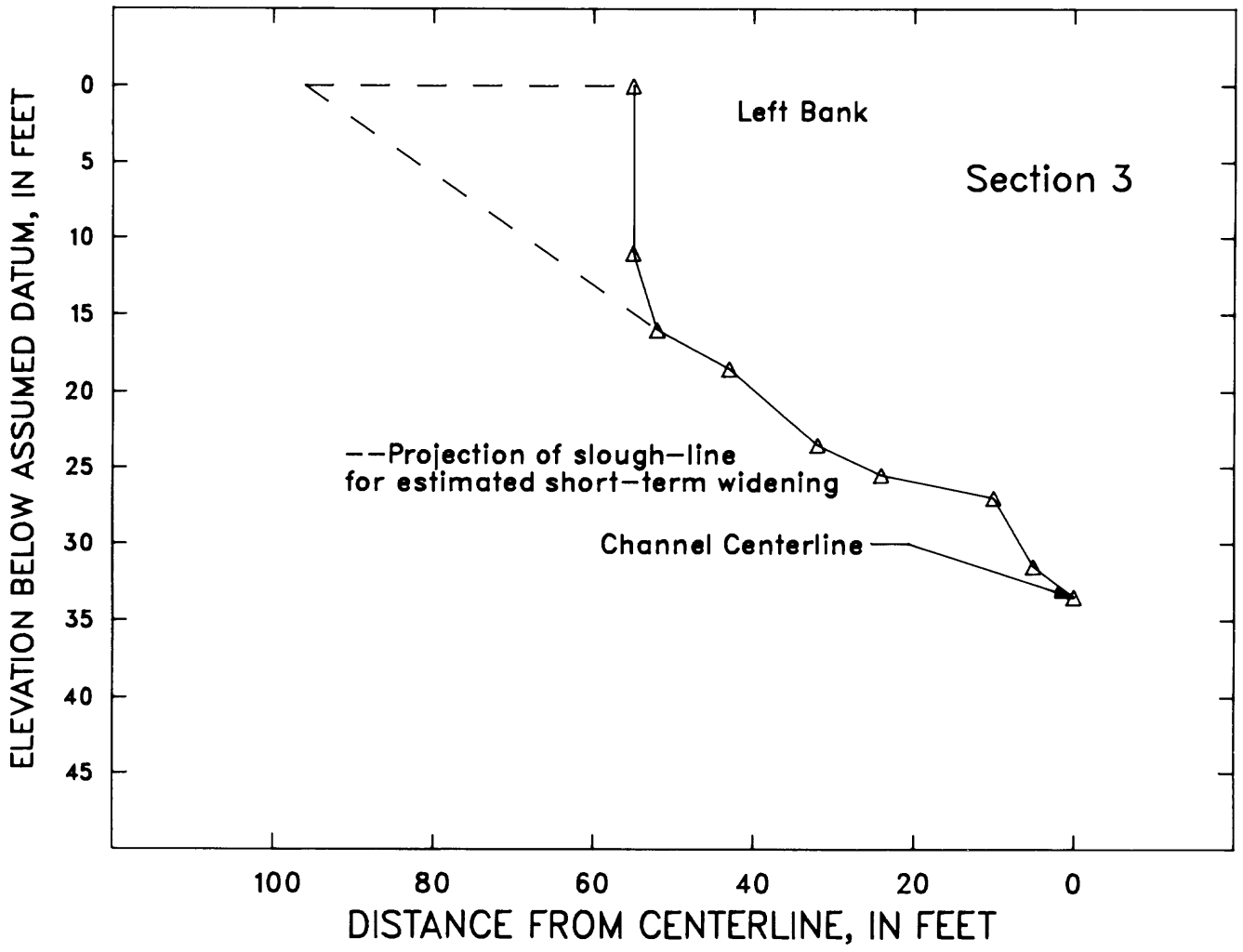

Figure 7. Bank profile of Cane Creek representative of worst case conditions in the study reach, 440 ft downstream from Hunter Road, Lauderdale County, Tenn., 1984.

Bank Failure Recurrence

Tree-ring analysis indicates three episodes of bank failure on the tributary (fig. 1) and the main stem of Cane Creek between 1977 and 1983. Thus, the rate of occurrence for bank failure on a particular bank could be 0.5 times per year. Combining this rate with a mean slump block width of 7.5 ft yields a rate of bank retreat of almost 4 ft/yr through the reach. This rate is in general agreement with the morphologic data detailed earlier. The removal of dead and damaged trees during the extremely high water of March 1975 (U.S. Army Corps of Engineers, 1977) perhaps obscured evidence of slumping prior to 1975. Additionally, it should be noted that botanical evidence of previous slumping (or any geomorphic event) tends to be obscured with time and by succeeding events.

Widening at a rate of roughly 4 ft/yr likely will continue until the vertical faces become gentler sloping, are somewhat rounded, and approach the slough-line angle. Predominating hillslope processes will produce a linear to convex upper bank shape, which is considered more stable. Moving upslope in the nonscoured areas, the ages of saplings on the slough line progressively decrease from 4 years halfway up the slough line to 1 year near the base of the upper bank. Vegetation establishing on the slough line should encroach upon the upper bank as it flattens in accordance with the slough-line angle, thus adding to the stability of the Cane Creek banks. The location, depth of sediment accumulation over the root zones, and ages of saplings (1–4 years) on the slough line indicate that short-term widening to the slough-line angle could take at least 8 more years. However, destructive

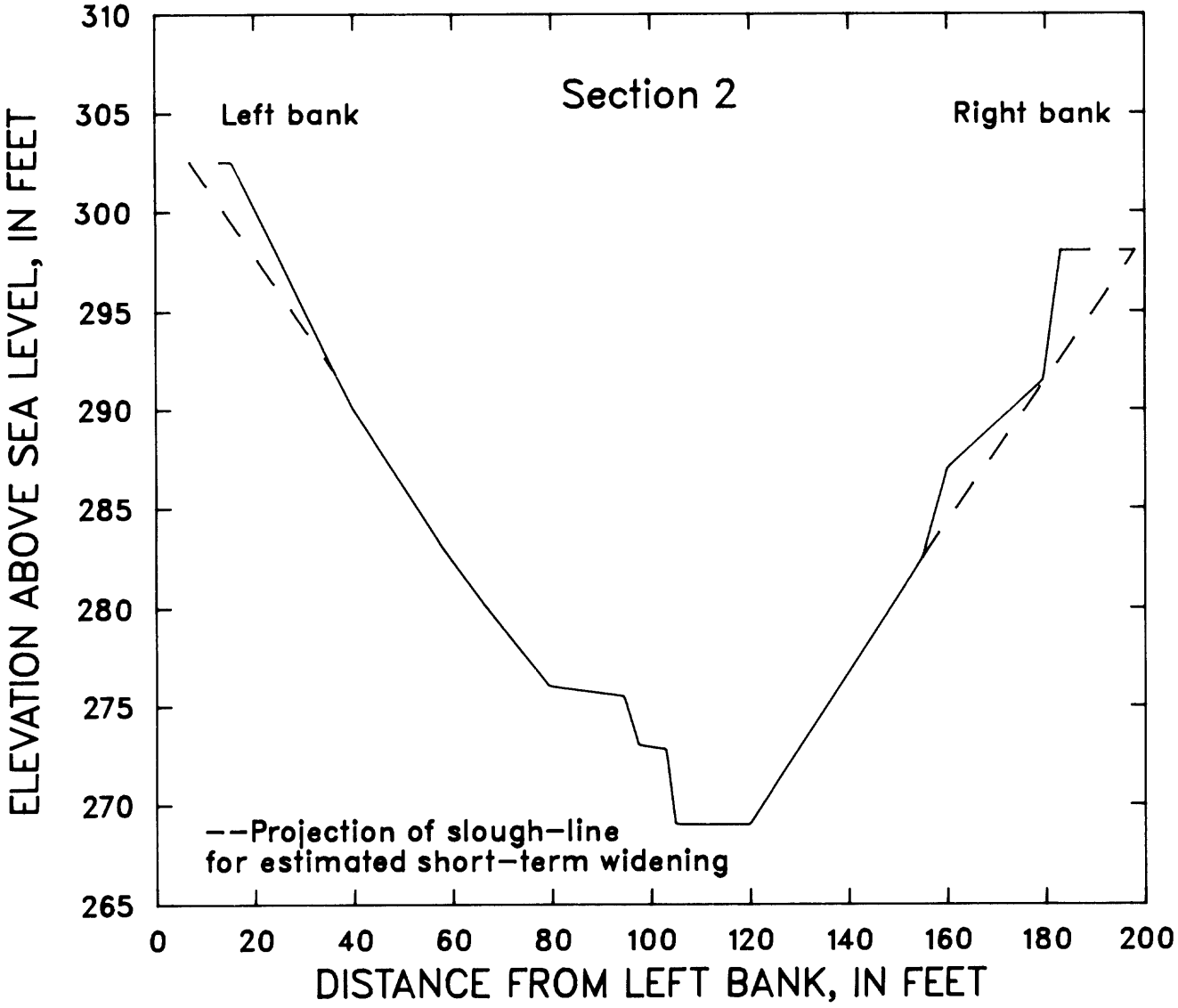

Figure 8. Channel cross section showing expected bank widening in nonscoured area, 350 ft downstream of Hunter Road, Cane Creek, Lauderdale County, Tenn., 1983.

flooding and changes in channel-bed level will certainly affect this rate. A phase of deposition in the channel and on the shelf (2–4 ft of sediment on channel-edge tree root collars) suggests aggrading conditions. As aggradation continues, toe attack is reduced, vegetation is established, bank slopes are flattened, and increasingly stable bank conditions are developed.

Tree-ring analysis at each of the three geobotany sites (fig. 2) indicated three periods of active bank failure, during the springs of 1978, 1980, and 1983. Additional widening occurred in the spring of 1984 with some failed top-bank surfaces measuring 60 ft long by 10 ft wide. A summary of dated bank failures with the types of botanical evidence by site and year is given in table 1.

No trees on top banks or below were older than 12 years owing to the clearing and dredging operations 13 years ago. Areas of greatest damage to banks and riparian vegetation coincide with outside bends of the high-flow thalweg in the current channel configuration. Areas with more complete vegetal cover coincide with inside bends (future locations of point bars). However, banks on both inside and outside bends show evidence of slab failure and usually have vertical faces just below top bank. Downstream sides of scallops in banks have little established vegetation and many fallen trees, whereas upstream sides of scallops have 1- to 4-year-old saplings established on the slough line (fig. 3). Isolated patches of trees, which have 2 to 4 ft of sediment deposited above

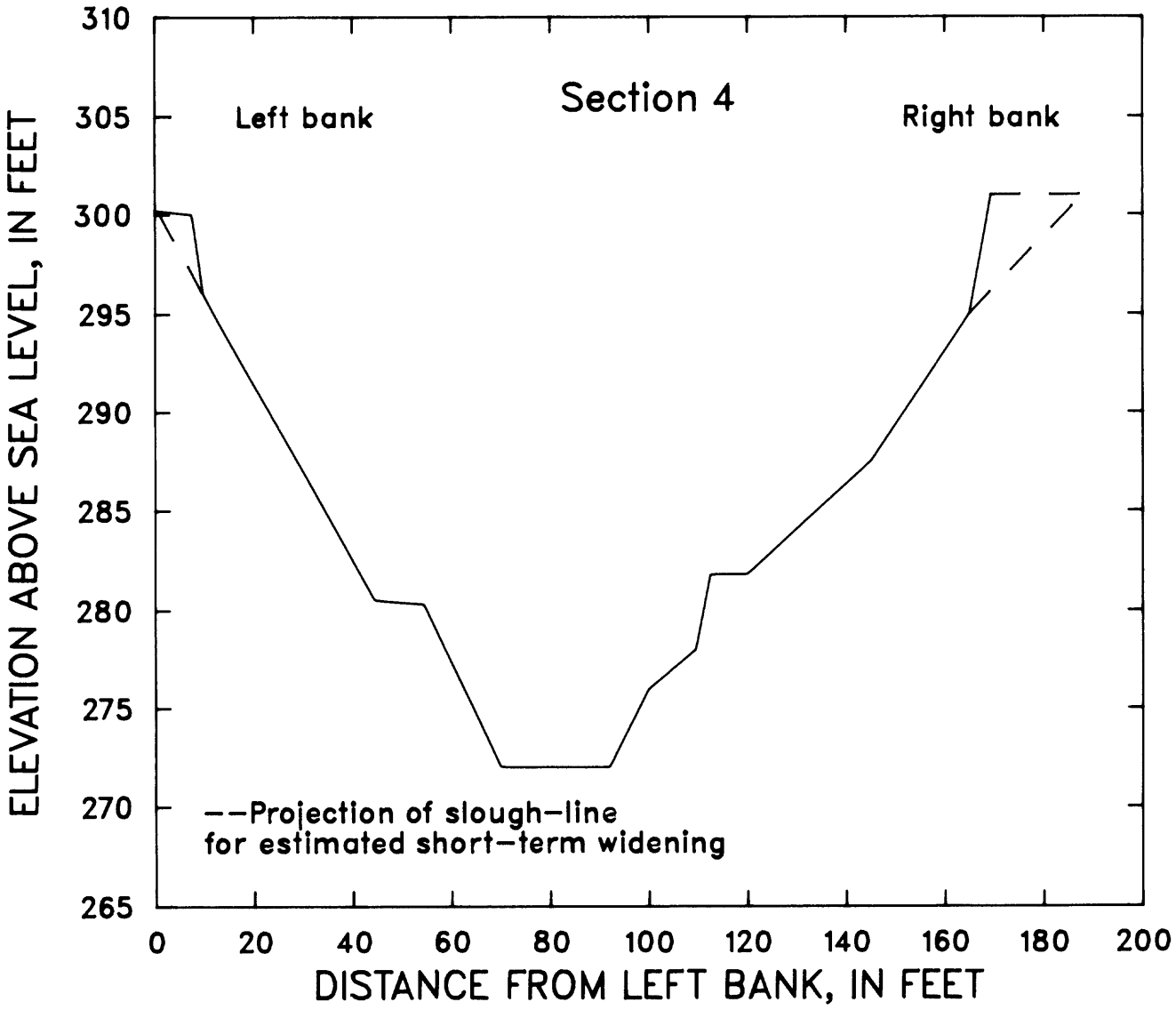

Figure 9. Channel cross section showing expected bank widening in nonscoured area, 700 ft upstream of Hunter Road, Cane Creek, Lauderdale County, Tenn., 1983.

their root collars and are in generally poor condition, occur on shelves (fig. 3) particularly on the upstream sides of scallops.

Failed blocks on the upper bank ranged between 3 and 12 ft in width with a mean width of about 7.5 ft. This width coincides with the distance of present piping holes from the top edge of the banks. Slump blocks on the slough line have been disintegrated by stream action, low-angle slides, and creep. Relative stability has allowed some vegetation to be established. In contrast, active failures of upper bank sections allow little vegetation to be established. The most active sloughing occurs on the scalloped banks through initial weakening by piping and tension crack development along the vertical face, followed by deep-seated rotational failure on the upper bank (fig. 3). Catalysts for these rotational failures are lubrication and increased pore-water pressure along previous slab-failure planes.

Short-term widening estimates listed in table 2 are representative of bank failure on one side of the channel only. By applying the estimated minimum widening rate of 4 ft/yr to the totals, widening at a given location in the scoured area could continue for another 20 years if a failure occurred every other year. Depending on opposite bank conditions, total channel widening could approach 60 ft in the scoured section.

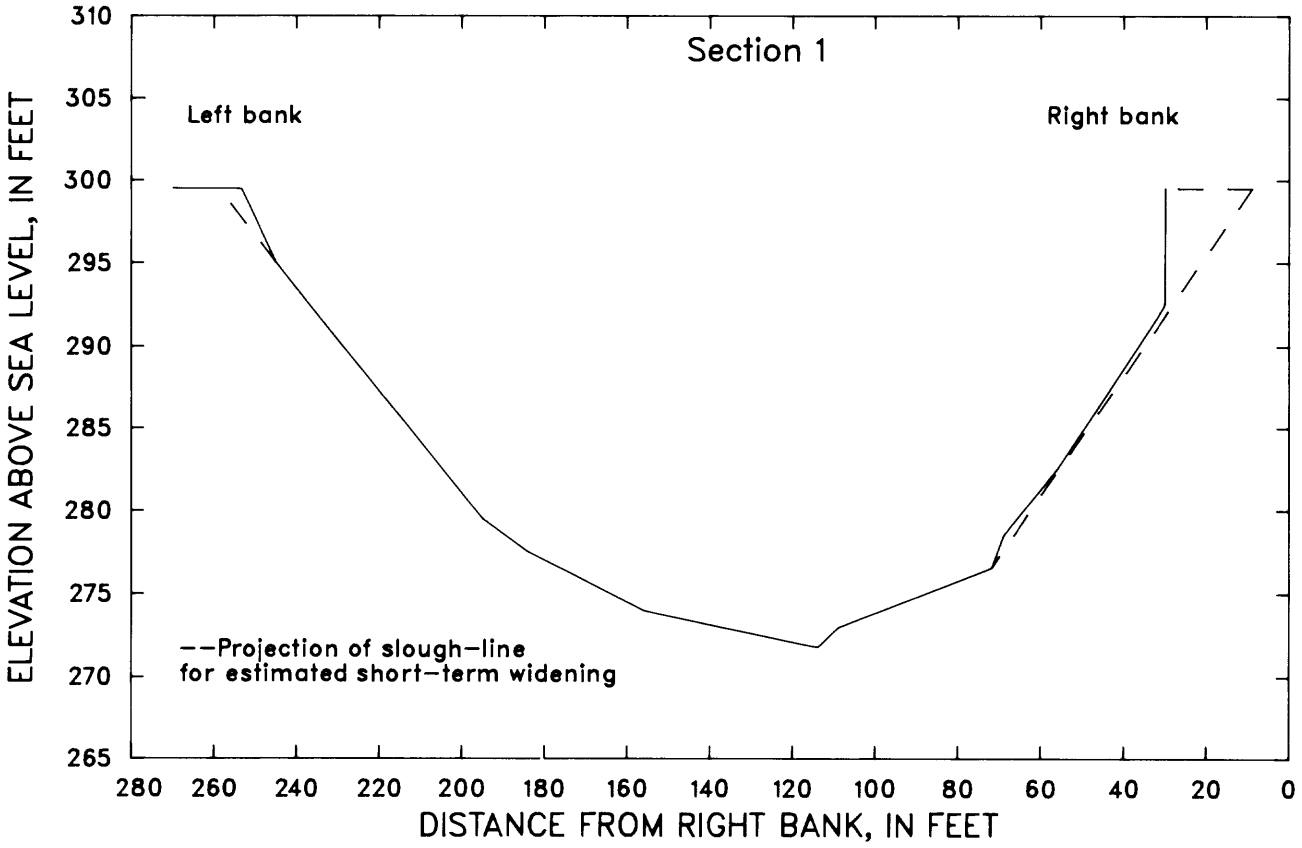

Figure 10. Channel cross section 100 ft downstream of Hunter Road, Cane Creek, Lauderdale County, Tenn., 1984.

Bank Slope Development

Bank slope development observed in the field and reported here appears to be similar to the three-step conceptual model presented by Skempton (1953) and by Carson and Kirkby (1972). According to their sequence of events, bank angles initially approximate the angle of internal friction through stream downcutting and shallow surface slides. The second step involves the onset of slab failures and "deep-seated slips" (Carson and Kirkby, 1972, p. 179) on the upper banks because of imposed bank heights greater than H_c and slope reduction by stream action on the slough line. These processes reduce bank angles greatly near the top of the bank and more subtly along the slough line (fig. 3). The third step is marked by the end of downcutting, the start of flood-plain development, and further flattening by shallow slides and continued stream action.

We believe that the Hunter Road reach has recently entered step 3, and a new flood plain of lower elevation than the former one is being formed. As Cane Creek passed from stage 1 through stage 2, it is believed that the slough line flattened from 26° (mean ϕ) to 20°. As aggradation replaced degradation around 1980–81, stream action and low-angle slides effectively reduced the slough-line angle to its present value. Flattening of the slough line should continue as the flood plain develops. Because the width and depth of the channel have been significantly enlarged, sections of the bank including the slough line and the shelf are more frequently inundated and, consequently, have increased moisture content. The contained moisture reduces the shear strength of the material resulting in low-angle slides, which develop inclinations that can be approximated by the following equation (Carson and Kirkby, 1972):

$$\tan \theta = 1/2 \tan \Phi \ , \qquad (5)$$

where θ is the relatively permanent angle of stability and
Φ is as previously defined.

For the study reach, this angle (θ) is calculated to be 14°. The processes involved in the reduction of slope angles along Cane Creek are analogous to those outlined by Lohnes and Handy (1968) for western Iowa loess, although their reported slope values are somewhat higher presumably due to lower moisture content and, therefore, greater shear strength.

Table 1. Summary of dated bank failures along Cane Creek and botanical evidence for failure by site

Site location relative to Hunter Road	Date of bank failure	Botanical evidence
Upstream	1983	Eccentric growth, freshly exposed roots, dead trees, tilt sprouts.
	1980	Eccentric growth, tilt sprouts.
	1978	Eccentric growth.
Downstream	1983	Eccentric growth, freshly exposed roots, tilt sprouts.
	1980	Eccentric growth, tilt sprouts.
	1978	Eccentric growth.
Tributary	1983	Scars, tilt sprouts.
	1980	Tilt sprouts, eccentric growth.
	1978	Exposed roots change to stem wood.

Table 2. Estimated short-term (10–20 yr) amounts of widening along Cane Creek in the vicinity of Hunter Road

[Data are based on extension of 20° slough-line angle to top of bank]

Section	Bank	Location relative to Hunter Road	Estimated widening (ft)
1	Left	100 ft downstream	6
1	Right	100 ft downstream	23
2	Left	350 ft downstream	9
2	Right	350 ft downstream	14
3	Left	440 ft downstream	42
4	Left	700 ft upstream	6
4	Right	700 ft upstream	18

Soil-mechanics data for Cane Creek are summarized in table 3. Values obtained are similar to those reported by Lohnes and Handy (1968) and Grissinger and others (1981) for loess materials. The alluvial material of Cane Creek is predominantly silt. The plasticity index, from which cohesion and the angle of internal friction are derived, is low, ranging from 2 to 10.

Initial approximations of critical bank heights calculated from equation 1 range from approximately 23.0 to 26.6 ft and average 24.6 ft in the vicinity of Hunter Road. Values derived from this equation negate the important role of piping and tension-crack development in determining susceptibility to bank failure. Observed vertical or nearly vertical failure planes used to infer depth of tension cracking can exceed 15 ft in height, with the greatest frequency at roughly 7 ft.

A worst case scenario can be conceptualized by applying the maximum observed depth (15 ft) of tension cracking to the suite of soil-strength properties that represents the weakest material and yields the lowest value of H_c' in equation 4 (Thorne and others, 1981). Forty percent of the Hunter Road soil samples fall in this category and thus result in H_c' values of approximately 8 ft. Relatively uniform slope development to the slough-line angle will continue for some time inasmuch as banks in the vicinity of Hunter Road are greater than 30 ft high. Banks are expected to remain unstable until the height of the bank approaches H_c'.

The use of mean conditions (H_c = 24.6, Z = 7.0) in equation 4 yields values for H_c' of 17.6 ft. Banks observed in the field do not maintain vertical faces of this magnitude yet still show evidence of active sloughing. This could be due to the severely scalloped condition of the channel generated by the deflection of flow. Because of the greatly incised condition of the channel, flows that ordinarily would spread across the flood plain now can undercut below the vertical face, removing support for the bank and keeping it moist. Furthermore, prevalent piping 3 to 15 ft from the bank allows greater seepage into the soil mass, reducing shear strength and, hence, H_c.

SUMMARY AND CONCLUSIONS

Channelization and its effects have led to approximately 17 ft of degradation and 150 ft of widening of Cane Creek at Hunter Road during 1970–83. The principal causes of widening of this magnitude are (1) overheightening of banks beyond critical bank heights by degradation and (2) deflection of flow towards the right bank, caused by entrapped trees from upstream bank failures, that resulted in severely scalloped banks on the outside bends of the high-flow thalweg.

Rates of bank widening in the Cane Creek channel approximate 4 ft/yr, as determined from channel-geometry data and geobotanical evidence. Slab failures from the vertical face occur in blocks 3–12 ft wide, as determined by vegetative evidence and the location of present piping holes and tension cracks. Initial detachment from the bank occurs predominantly through piping and tension crack development. Seepage along these failure planes and saturation of upper bank sections lead to deep-seated rotational failures and hence lower bank slopes. Stream action and low-angle slips work to further flatten the slough line and eventually the upper bank as a temporary stability is established.

Trees growing on these surfaces consistently show eccentric tree-ring growth, indicating slope movement. This movement is most substantial on the upper bank, where failures are intense, and decreases downslope along the slough line towards the channel.

The degradation that began these channel-widening processes abated about 1980–81, and aggradation became the dominant trend on the main stem. This change has

Table 3. Summary of soil and bank property data of Cane Creek

Property	Number of samples	Mean	Standard error of mean
Median particle size (mm)	13	0.0262	0.003
Percent sand	13	6.2	1.36
Percent silt plus clay	13	93.8	1.36
Plasticity index	18	5.6	.687
Angle of internal friction (degrees)	18	26.1	.903
Cohesion (lbs/in^2)	18	2.73	.099
Critical bank height (ft)	18	25.7	.472
Bulk unit weight (lbs/ft^3)*	4	97.7	--

*Obtained from data reported for Lauderdale County loess (Lohnes and Handy, 1968).

been substantiated by channel-geometry data and evidence of trees no more than 3 to 4 years old established on the slough line.

Projection of the slough-line angle (20°) to top bank results in an estimate of additional channel widening by upper bank retreat and flattening. Values obtained by this method range from about 20 ft to greater than 40 ft. Estimates of future channel widening over the short term (10 to 20 years) range from 23 ft to approximately 60 ft. It should be emphasized that the slough-line angle represents temporary stability and that widening will continue, probably at lower rates as a new flood plain develops.

Mean critical bank heights in the study reach were determined to be 24.6 ft if tension cracking were neglected and 17.6 ft if not. A worst case condition established, with the minimum calculated H_c (23.0 ft) and the greatest tension crack depth, yielded a vertical H_c' of approximately 8 ft. This value is in agreement with the apparent trend of continued top-bank retreat and the proposed model of bank slope development along the slough-line angle. The problem of calculating critical bank heights for compound slopes by means of conventional techniques was not solved, and therefore critical bank height refers to the vertical faces only. Nevertheless, the results reported here are meaningful in terms of the stability of the vertical segments of bank slopes where widening occurs.

Shear-strength properties for loess in the Cane Creek basin are very similar to those reported by Lohnes and Handy (1968) and Grissinger and others (1981). Calculated values of cohesion and the angle of internal friction seem to closely approximate those obtained by more conventional laboratory or field methodologies.

REFERENCES CITED

Andrews, E.D., 1982, Bank stability and width adjustment, East Fork River, Wyoming: Water Resources Research, v. 18, no. 4, p. 1184–1192.

Bradford, J.M., and Piest, R.F., 1977, Gully wall stability in loess-derived alluvium: Journal of Soil Science Society of America, v. 41, p. 115–122.

Carson, M.A., and Kirkby, M.J., 1972, Hillslope form and process: London, Cambridge University Press, 475 p.

Grissinger, E.H., Little, W.C., and Murphey, J.B., 1981, Erodibility of streambank materials of low cohesion: American Society of Agricultural Engineering Transactions, v. 24, no. 3, p. 624–630.

Hupp, C.R., 1983, Geo-botanical evidence of Late Quaternary mass wasting in block field areas of Virginia: Earth Surface Processes, v. 8, p. 439–450.

Lohnes, R.A., and Handy, R.L., 1968, Slope angles in friable loess: Journal of Geology, v. 76, no. 3, p. 247–258.

Sigafoos, R.S., 1964, Botanical evidence of floods and floodplain deposition: U.S. Geological Survey Professional Paper 485–A, p. A1–A33.

Skempton, A.W., 1953, Soil mechanics in relation to geology: Yorkshire Geological Society Proceedings, v. 29, p. 33–62.

Terzaghi, Karl, and Peck, R.B., 1948, Soil mechanics in engineering practice: New York, Wiley, 566 p.

Thorne, C.R., Murphey, J.B., and Little, W. C., 1981, Stream channel stability, Appendix D, Bank stability and bank material properties in the bluffline streams of northwest Mississippi: Oxford, Miss., U.S. Department of Agriculture Sedimentation Laboratory, 257 p.

U.S. Army Corps of Engineers, 1977, Flood plain information, Cane Creek and tributaries, vicinity of Ripley, Tennessee: U.S. Army Corps of Engineers, Memphis District, 31 p.

Evaluation of a Suggested Sequence for the Chemical Extraction of Soluble Amorphous Phases from Clays

By Shirley L. Rettig *and* Blair F. Jones

Abstract

Because the separation of soluble amorphous phases of clays is an important aspect of sediment-water interaction, the efficacy of a sequential treatment for their chemical extraction was evaluated. Treatment consisted of extraction by 0.1*M* sodium pyrophosphate, followed by 1*M* hydroxylamine hydrochloride and either sodium acetate or acetic acid, and finally by 0.2*M* ammonium oxalate. Both the dissolved material and the remaining fine particulates were chemically analyzed after each step. Seven samples were chosen to represent a broad spectrum of ultrafine clays from environments of aqueous deposition. Significant amounts of clay mineral components were removed at each step of the extraction sequence. Some changes in the clays can be attributed to ion exchange or loss of intergrade complexes, but dissolution of clay crystallites with or without reprecipitation of amorphous aluminosilicate must also occur.

INTRODUCTION

Separation and chemical characterization of relatively soluble and amorphous phases such as organic material, carbonates, and oxyhydroxides from ultrafine (<0.5 μm material) clays are necessary to evaluate the transport and deposition of contaminants in hydrologic environments. A number of procedures have been proposed for extraction of these phases without significant structural alteration of crystalline silicate. For example, hydrogen peroxide has long been used for the removal of organic matter, but Douglas and Fiessinger (1971) found that unless suitably buffered its use can bring about excessively acid conditions leading to attack of the clay minerals. Sodium hypochlorite has also been suggested for the removal of organic matter (Anderson, 1963), but its high pH may cause oxyhydroxide precipitation of metals from organic complexes. McKeague (1967) used 0.1*M* sodium pyrophosphate ($Na_4P_2O_7$) and indicated that it did not appear to have a significant effect on clay minerals.

In other studies, removal of carbonates has been effected by treatment with 0.25*M* hydrochloric acid (HCl) (Quakernaat, 1968), 1*M* ammonium acetate (Dean and Gorham, 1976), and 0.2*M* ethylene diamine tetraacetic acid (EDTA) (Bodine and Fernalld, 1973).

Perhaps the most ubiquitous amorphous materials, Fe-Mn oxyhydroxides, have been removed by treatment with sodium citrate-dithionite (Mehra and Jackson, 1960), but this treatment can cause structural alteration of clay (Dudas and Harward, 1971). Schwertmann (1959, 1964) proposed the use of 0.2*M* ammonium oxalate [$(NH_4)_2C_2O_4$]. Chester and Hughes (1967) used 1*M* hydroxylamine hydrochloride ($NH_2OH{\cdot}HCl$) and 25 percent acetic acid (HAc) to extract most of the carbonates, Mn oxides, and amorphous iron oxyhydroxides from marine sediments. Lahann (1976) has indicated that these reagents cause little structural alteration of the clay.

In addition to the above, Jones and Bowser (1978) suggested a sequence for mineralogic analysis of fine-grained lacustrine sediments, which consisted of extraction of organic matter with 0.1*M* $Na_4P_2O_7$ followed by removal of carbonates and amorphous oxides with 1*M* $NH_2OH{\cdot}HCl$ and 25 percent v/v HAc. The present study was undertaken in order to evaluate the efficacy of that treatment. For half of the samples, 1*M* $NH_2OH{\cdot}HCl$ was used with 1 percent sodium acetate (NaAc) solution rather than HAc. The resulting solution (pH 4.35) is less likely to attack clay crystallites than is unbuffered HAc (pH 1.2). A third step was added to examine the further effects of 0.2*M* $(NH_4)_2C_2O_4$ extraction.

EXPERIMENTAL METHODOLOGY

The removal of soluble and amorphous phases has usually been evaluated by analysis of the solvent solutions, while little attention has been paid to changes in the composition of the solid residual itself. Because all treatments dissolve at least a small amount of crystalline clay, analysis of the dissolved material can give a distorted picture of the amount of soluble and amorphous phases. In this study, both the dissolved material and the remaining fine particulates were analyzed after each step of the treatment, and an attempt was made to correlate the changes in the composition of the particulate matter with the amounts of dissolved material in the solvent solutions.

Seven samples were chosen to represent a broad spectrum of ultrafine clay from environments of aqueous deposition. Sample AR33 is an andesitic pyroclastic rock from a formerly submerged outcrop near Lake Abert, Oreg. The two U11g samples are ultrafine clay from a borehole in the northern Frenchman Flat area of the Nevada Test Site near Las Vegas, Nev. They are from

depths of more than 300 m, just above and below the water table. The Fairbanks Butte sample is an ultrafine clay-sized material consisting mostly of interstratified stevensite-smectite from the Amargosa Desert in Nevada. It was apparently formed in an alkaline marsh or shallow lake. More detailed descriptions of these samples can be found in Eberl and others (1982). Sample LVCH is from the Long Valley caldera in California and is a smectitic clay of reworked rhyolitic origin. The GSL–5 sample is an ultrafine sediment sample from Great Salt Lake, Utah, and sample PRES V17 is ultrafine sediment from the Potomac River, Md.

The chemical treatment of the ultrafine clay was as follows: six splits of 40–60 mg each were weighed into centrifuge tubes for each clay. A 25-mL portion of 0.1*M* $Na_4P_2O_7$ was added to each tube and all were shaken overnight on a Burrell wrist-action shaker. The next morning they were centrifuged for 1 hour at 30,000 rpm. The solutions were decanted and saved. A 15-mL portion of deionized water was added to each tube, the tubes were shaken for 1 hour and centrifuged for 1 hour, and the solutions were decanted and saved. This washing process was repeated. At this point two samples were dried in their tubes overnight at 90°C and saved for later analysis. The six $Na_4P_2O_7$ solutions and their respective decanted wash solutions were each diluted to 100 mL and saved for later analysis.

Four centrifuge tubes remained. To two of these, 25.0 mL of 1.0*M* $NH_2OH{\cdot}HCl$ and 1.0 percent NaAc were added; 25.0 mL of 1.0*M* $NH_2OH{\cdot}HCl$ and 25 percent HAc were added to the other two. They were shaken overnight, centrifuged, and washed with two 15-mL portions of water as in the first step. One tube of each (that is, one sample treated with NaAc and one treated with HAc) was dried overnight and set aside for analysis.

To each of the remaining two centrifuge tubes (one treated with NaAc and one with HAc), 25 mL of 0.2*M* $(NH_4)_2C_2O_4$ (pH 7.5) were added. The samples were then shaken overnight, centrifuged, and washed as in the previous steps. At this point there were six dried clay samples: two treated with $Na_4P_2O_7$ and one sample for each further step. There were six solution samples from the $Na_4P_2O_7$ treatment, two solutions from $NH_2OH{\cdot}HCl$ and NaAc, two solutions from $NH_2OH{\cdot}HCl$ and HAc, and two solutions from the $(NH_4)_2C_2O_4$ treatment. The process is shown schematically in figure 1.

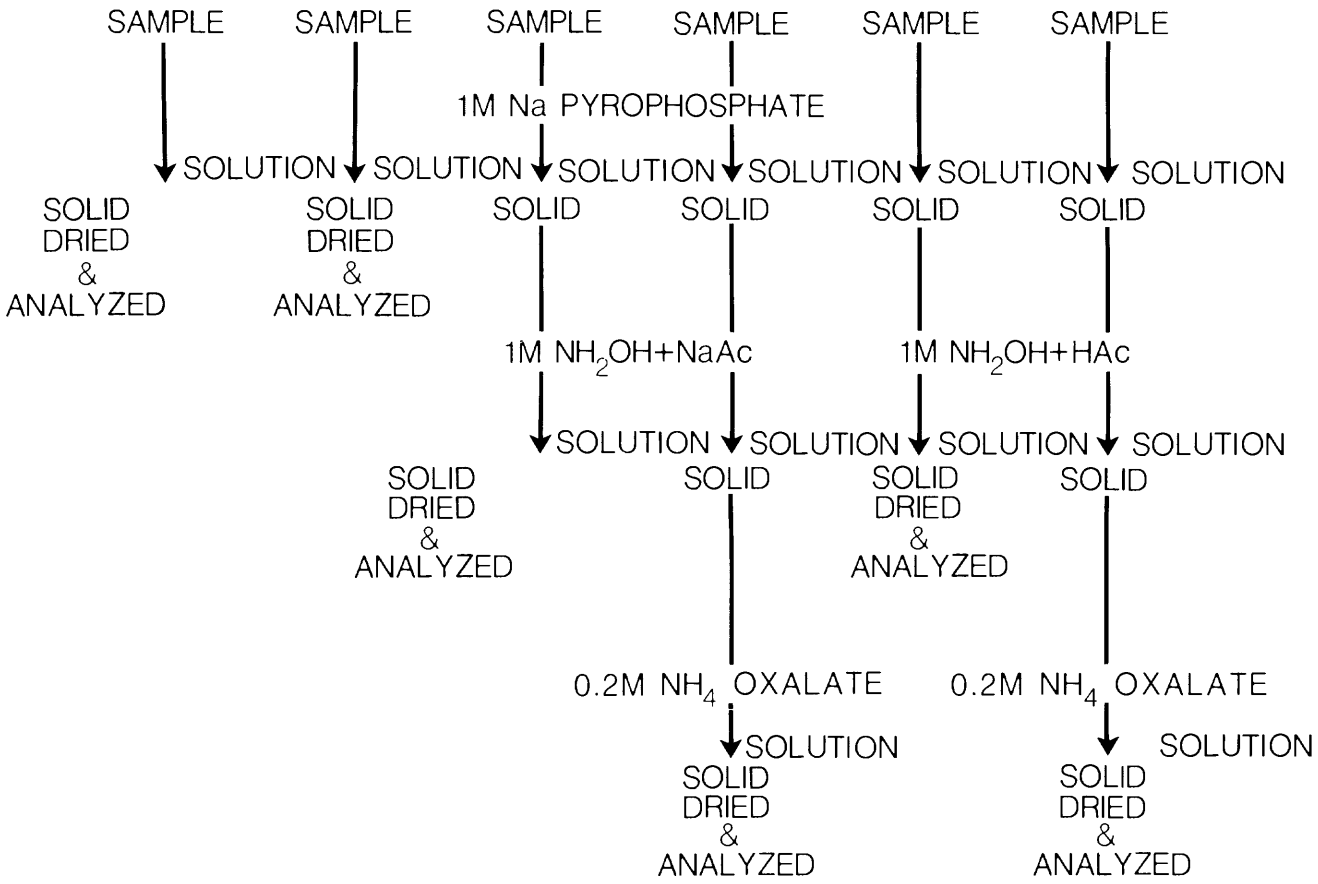

Figure 1. Schematic diagram for sequential treatment of ultrafine (<0.5 μm) sediment.

The dried clay samples were scooped out of the centrifuge tubes, weighed, and fused with 0.2 g of a mixture of lithium borates for 1 hour at 900°C according to the method first proposed by Ingamells (1964) and modified by Shapiro (1975). The resulting glass beads were dissolved overnight in about 50 mL of deionized water and 1 mL of concentrated nitric acid and diluted to 100 mL in volumetric flasks. A further 1/10 dilution was made of the 100-mL solution for use in the silica, aluminum, and iron determinations, and all solutions were transferred immediately to plastic bottles.

Silica was analyzed by the colorimetric ammonium molybdate method, using 5.0 mL of 1*M* HCl, 5.0 mL of 0.1 percent NaF, 5.0 mL of 4.9 percent ammonium molybdate, and 10.0 mL of 17 percent Na_2SO_3. The resulting molybdate blue complex was allowed to stand at least 1 hour before absorption was measured spectrophotometrically at 700 nm. Aluminum was determined colorimetrically with 5.0 mL of 0.05 percent ferron (8-hydroxy, 7-iodo-5-quinoline sulfonic acid), 2.0 mL of 1 percent $NH_2OH{\cdot}HCl$, and 2.0 mL of 35 percent NaAc, and the resulting color complex was measured at 370 nm. Iron was determined colorimetrically at 520 nm after the addition of 1.0 mL of 0.2 percent bipyridine, 2.0 mL of 1 percent $NH_2OH{\cdot}HCl$, and 2.0 mL of 35 percent NaAc. Calcium, magnesium, sodium, and potassium were determined by atomic absorption spectrophotometry. These methods are essentially those described by Skougstad and others (1979).

The solution samples were analyzed for aluminum, iron, magnesium, and potassium by the same methods used for the solid clay samples.

DISCUSSION OF RESULTS

Chemical analyses of the solid samples and dissolved constituents are shown in tables 1 and 2. The analyses of the solid samples have been recalculated on an anhydrous basis by multiplying the sum of the constituent oxides by an appropriate factor to make the total equal to 100 percent. The dissolved constituents were calculated as percent oxide in a hypothetical 40-mg sample.

It was assumed that silica and aluminum oxide are conservative in the solid; that is, any silica and aluminum found in the dissolved phase have come from the dissolution of crystalline aluminosilicate. It was recognized that some aluminum can be in the amorphous iron oxide coatings and that a discrete amorphous silica phase could be present.

The right-hand sides of figures 2 through 8 show cumulative loss or gain of each constituent in the solid samples after each step of the treatment. Each constituent oxide is plotted as the ratio of that oxide to silica and aluminum oxide combined, so that each figure shows the effect of the combined treatments over and above the dissolution of aluminosilicate. Only the results for the $NH_2OH{\cdot}HCl$ and NaAc step in the treatment sequence are plotted because for the solid samples the analyses for the $NH_2OH{\cdot}HCl$ and HAc step were not significantly different. The solid samples are unfortunately subject to problems of inhomogeneity, so that the small quantities of constituents that are dissolved may be obscured by compositional variations between samples. Nevertheless, some general conclusions can be reached from these data.

All the solid samples show a marked increase in sodium content after the $Na_4P_2O_7$ treatment, and much of this increase can be attributed to the exchange of sodium for other ions in the interlayer positions of the clay minerals. The presence of some sodium was no doubt due to incomplete washing of $Na_4P_2O_7$ from the samples, but it was felt necessary to restrict the number of washes in order to minimize aluminosilicate dissolution by H_2O alone.

The calcium loss in the solid samples is greatest after the $Na_4P_2O_7$ treatment, and calcium content remains essentially unchanged at a low level through the subsequent treatments. The loss of calcium is greater in the U11g samples than in the other samples. These observations suggest exchange of sodium for calcium, magnesium, and potassium during the $Na_4P_2O_7$ treatment. Carbonate in the original sediment has been largely removed physically in the fine clay separation.

The left-hand sides of figures 2 through 8 show the amounts of MgO, K_2O, and Fe_2O_3 found in solution after each step of the extraction procedure. They are plotted as the ratio of the constituent oxide to aluminum oxide in solution divided by the ratio of the constituent oxide to aluminum oxide in the untreated solid:

$$\frac{\frac{XO}{Al_2O_3} \text{ in solution}}{\frac{XO}{Al_2O_3} \text{ in untreated solid}}.$$

If all the dissolved aluminum is assumed to have come from the dissolution of crystalline aluminosilicate, then a ratio of 1 represents clay dissolution and a ratio greater than 1 represents removal of MgO, K_2O, and Fe_2O_3 in excess of the amounts involved in clay dissolution. We recognize that aluminum may be present in amorphous iron oxide coatings and that there may be a discrete amorphous silica phase, but in the present study there is no way to distinguish absolutely between aluminum from clay dissolution and that from amorphous phases. Only aluminum, magnesium, iron, and potassium were determined in the solutions because of limited sample size.

Figures 2, 3, 5, and 6 show solution of magnesium and potassium after the $Na_4P_2O_7$ step (step 1) well in excess of amounts expected from clay dissolution, providing further evidence of the exchange of sodium for magnesium and potassium as suggested by the solid samples.

Table 1. Chemical analyses, in percent, of solid samples, recalculated on an anhydrous basis

	SiO_2	Al_2O_3	Fe_2O_3	CaO	MgO	Na_2O
U11g (988.5–989.5 ft)						
Untreated sample (average of 3)	66.93	14.20	5.83	3.32	7.04	.65
After step 1 (average of 2)	66.28	13.65	5.46	.50	8.70	3.76
After step 2a (average of 3)	69.58	15.32	5.38	.30	6.95	.63
After step 3a (average of 3)	69.83	15.36	5.63	.25	6.71	.43
After step 2b (average of 3)	71.95	14.60	4.92	.26	5.94	.45
After step 3b	70.12	15.93	5.41	.26	5.91	.44
U11g (1006.4–1007.5 ft)						
Untreated sample (average of 2)	67.37	12.94	8.02	2.14	6.37	0.74
After step 1 (average of 2)	66.35	15.51	6.48	.59	5.22	3.78
After step 2a	69.71	15.49	6.65	.41	4.99	.89
After step 3a	68.45	16.11	7.31	.33	5.57	.46
After step 2b	71.90	13.70	6.68	.31	4.94	.57
After step 3b	70.70	14.97	6.70	.39	4.52	.61
Fairbanks Butte						
Untreated sample (average of 3)	60.25	10.70	5.74	2.10	15.02	0.66
After step 1 (average of 3)	61.54	12.35	5.45	.32	12.22	1.82
After step 2a	61.97	11.63	5.67	.16	13.74	.36
After step 3a (average of 3)	61.34	13.10	5.77	.15	12.81	.23
After step 2b	65.01	11.68	5.11	.16	11.30	.27
After step 3b (average of 3)	63.00	14.00	5.43	.14	10.30	.23
AR33						
Untreated sample	70.78	16.52	6.19	1.03	3.20	1.11
After step 1 (average of 2)	68.50	16.26	5.94	.49	2.27	5.86
After step 2a	72.94	16.82	6.24	.44	2.08	.73
After step 3a	73.82	16.43	5.63	.62	1.86	.72
After step 2b	75.71	16.04	6.38	.53	1.90	.59
After step 3b	73.49	16.54	6.21	.61	1.79	.53
LVCH						
Untreated sample	63.63	2.11	1.62	1.23	30.14	0.93
After step 1 (average of 2)	61.42	2.51	1.77	.28	30.39	3.31
After step 2a	67.21	2.54	1.53	.17	27.80	.52
After step 3a	67.69	2.27	1.40	.16	28.09	.10
After step 2b	72.11	2.08	1.14	.10	24.24	.06
After step 3b	70.00	2.10	1.16	.14	26.22	.10

Step 1—Treatment with Na pyrophosphate.
Step 2a—Treatment with Na pyrophosphate followed by treatment with $NH_2OH{\cdot}HCl$ and Na acetate.
Step 3a—Treatment with Na pyrophosphate followed by treatment with $NH_2OH{\cdot}HCl$ and Na acetate followed by treatment with NH_4 oxalate.
Step 2b—Treatment with Na pyrophosphate followed by treatment with $NH_2OH{\cdot}HCl$ and acetic acid.
Step 3b—Treatment with Na pyrophosphate followed by treatment with $NH_2OH{\cdot}HCl$ and acetic acid followed by treatment with NH_4 oxalate.

Table 1. Chemical analyses, in percent, of solid samples, recalculated on an anhydrous basis—Continued

	SiO_2	Al_2O_3	Fe_2O_3	CaO	MgO	Na_2O
			PRES V17			
Untreated sample (average of 3)	54.64	24.05	16.03	0.39	1.86	0.33
After step 1 (average of 2)	49.89	28.44	13.90	.02	1.30	2.82
After step 2a	52.22	30.37	12.91	.00	1.48	.38
After step 3a	54.86	28.72	11.49	.07	1.68	.32
After step 2b	53.26	28.95	13.55	.00	1.34	.26
After step 3b (average of 2)	55.08	29.74	10.20	.14	1.73	.31
			GSL–5			
Untreated sample	66.82	17.27	6.84	1.21	4.04	0.78
After step 2a	72.58	12.07	5.86	.65	3.97	1.81
After step 2b	72.76	13.00	5.65	.40	4.48	.54
After step 3a	insufficient sample, not determined					

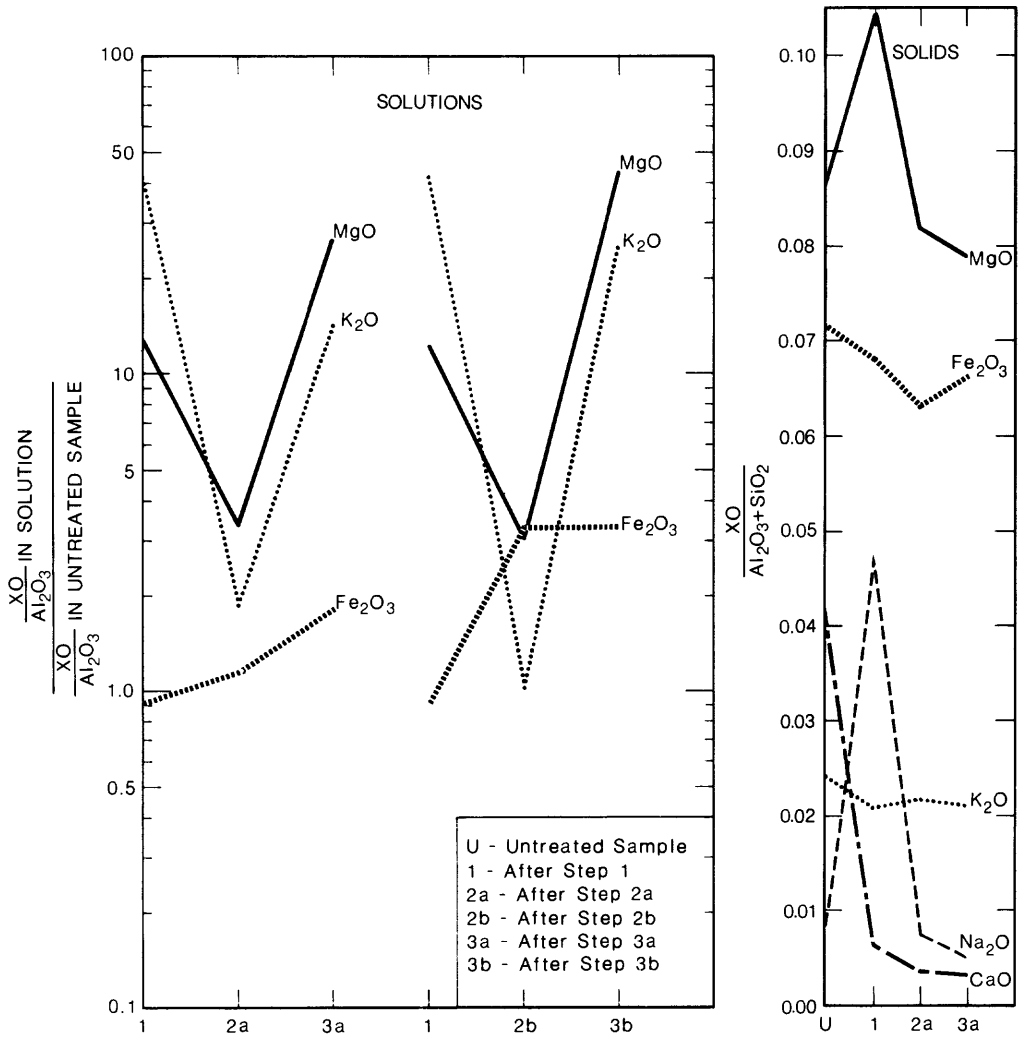

Figure 2. Relative loss or gain of each constituent in solids and solutions, sample U11g (988.5–989.5 ft).

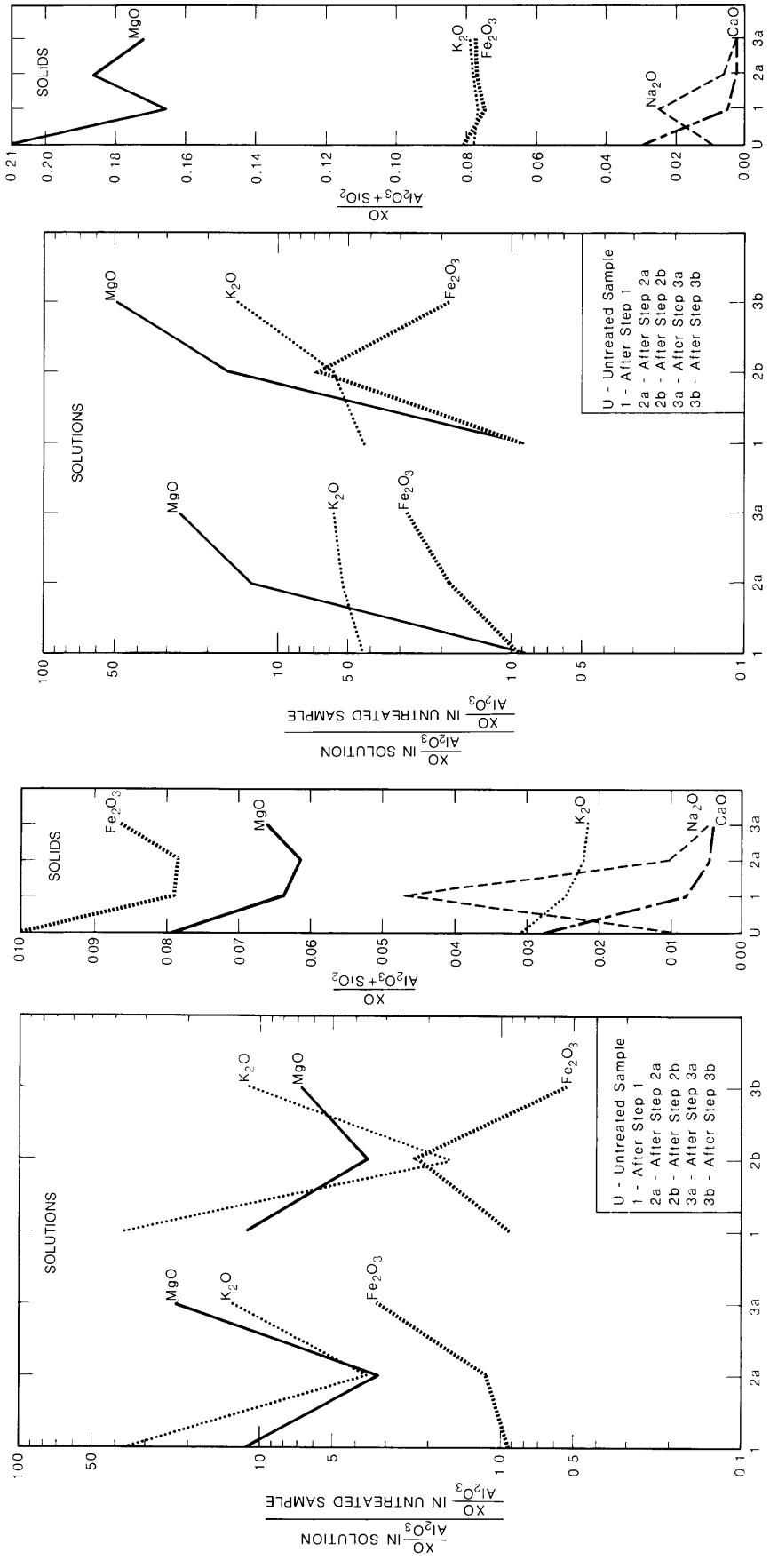

Figure 3. Relative loss or gain of each constituent in solids and solutions, sample U11g (1006.4–1007.5 ft).

Figure 4. Relative loss or gain of each constituent in solids and solutions, Fairbanks Butte sample.

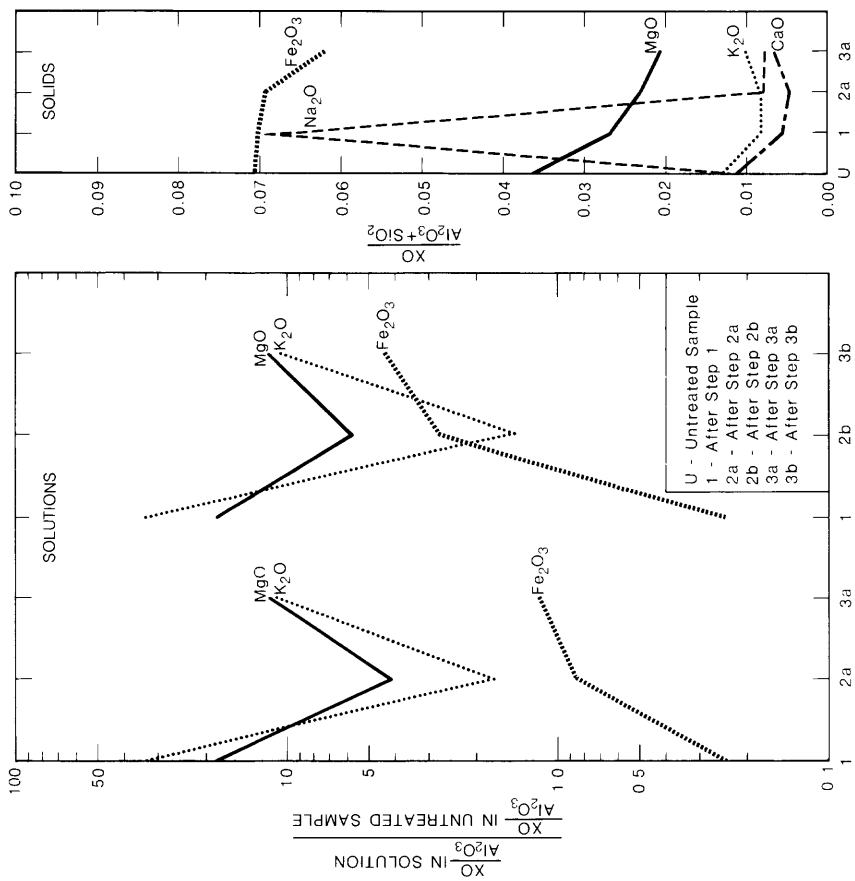

Figure 6. Relative loss or gain of each constituent in solids and solutions, sample AR33.

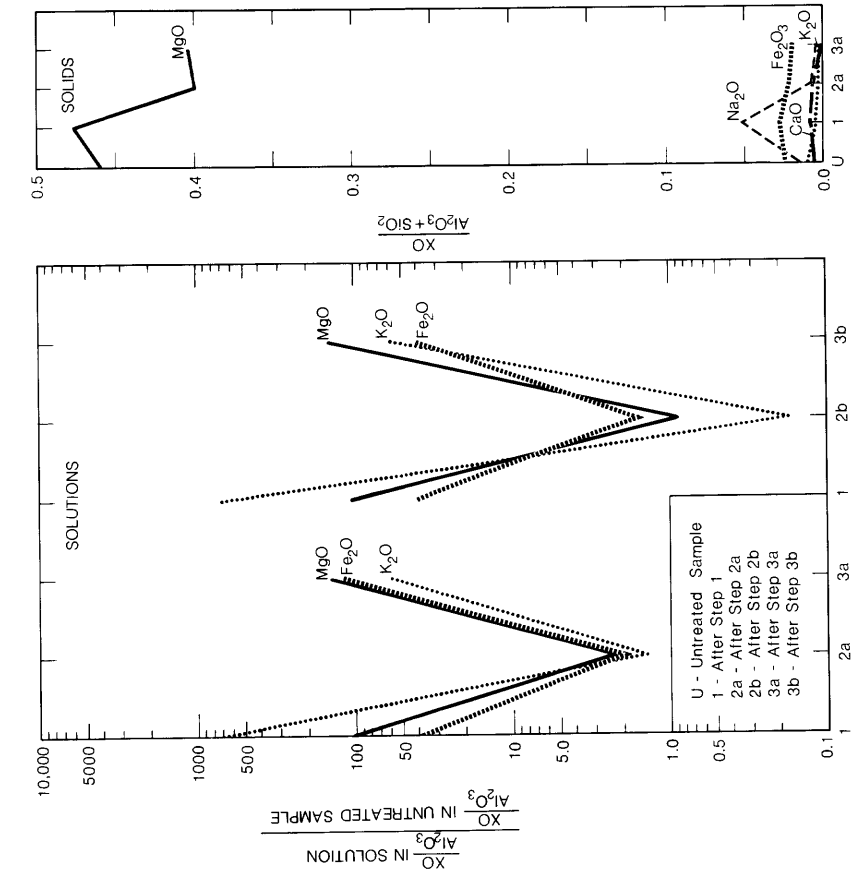

Figure 5. Relative loss or gain of each constituent in solids and solutions, sample LVCH.

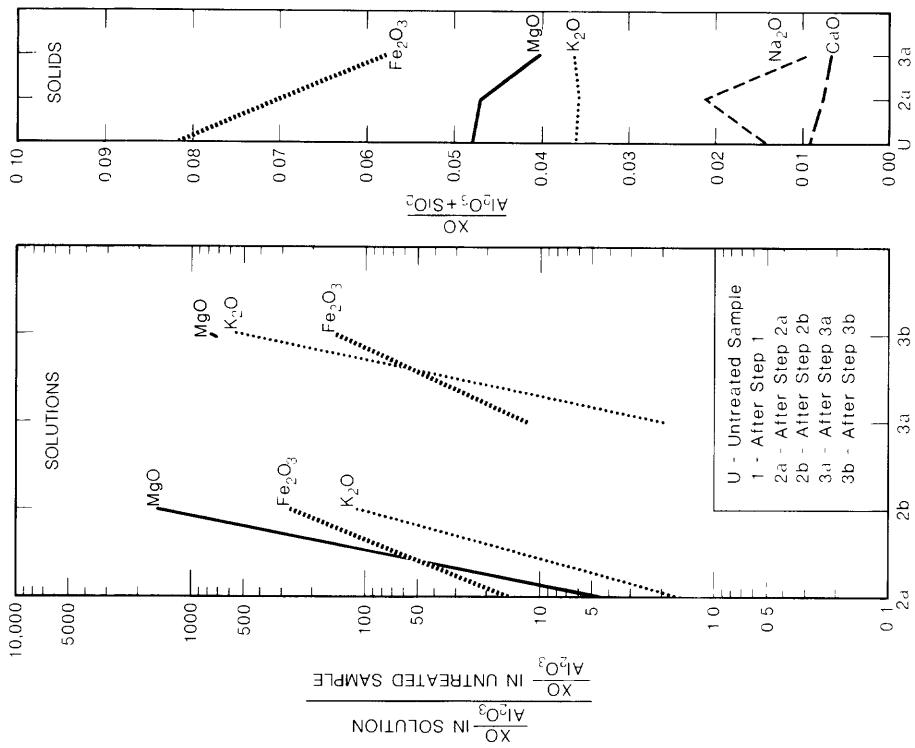

Figure 8. Relative loss or gain of each constituent in solids and solutions, sample GSL–5.

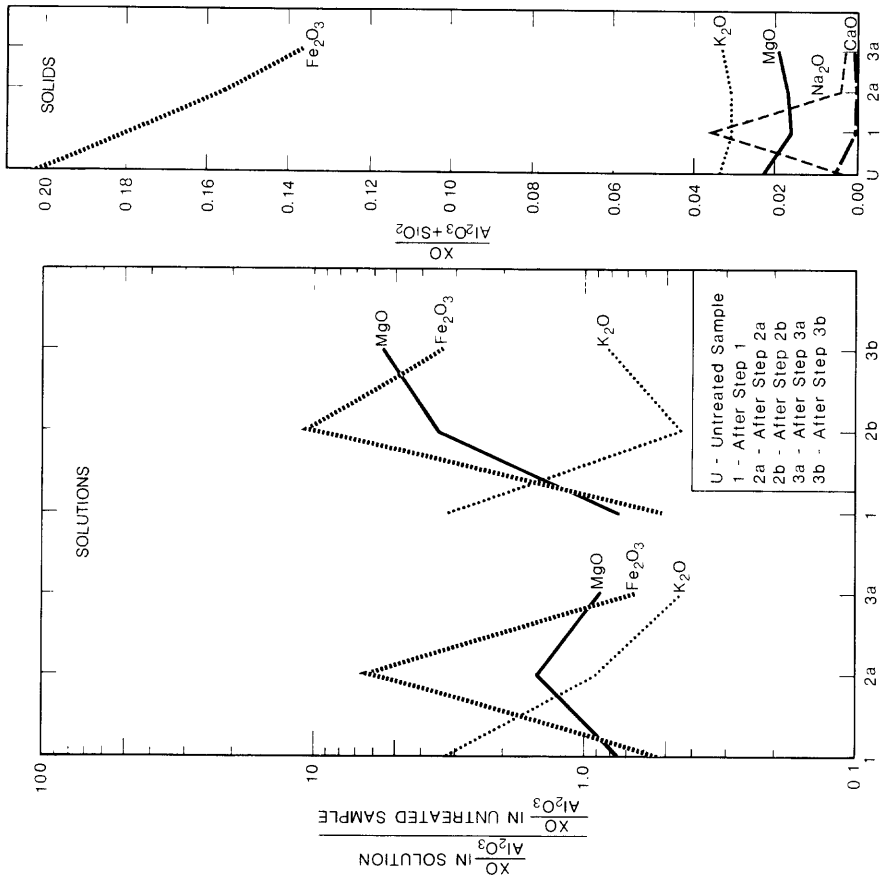

Figure 7. Relative loss or gain of each constituent in solids and solutions, sample PRES V17.

Table 2. Chemical analyses, in percent, of solutions, recalculated on an anhydrous basis for a 40-mg sample
[See table 1 for explanation of steps]

	Al_2O_3	Fe_2O_3	MgO	K_2O
U11g (988.5–989.5 ft)				
After step 1 (average of 6)	0.08	0.03	0.50	0.47
After step 2a (average of 2)	.30	.14	.51	.08
After step 2b (average of 2)	.35	.52	.53	.05
After step 3a	.04	.03	.53	.08
After step 3b	.02	.03	.43	.07
U11g (1006.4–1007.5 ft)				
After step 1 (average of 6)	0.09	0.05	0.50	0.61
After step 2a (average of 2)	.27	.19	.43	.18
After step 2b (average of 2)	.42	.58	.73	.13
After step 3a	.02	.04	.22	.05
After step 3b	.09	.03	.30	.19
Fairbanks Butte				
After step 1 (average of 6)	0.08	0.04	0.10	0.18
After step 2a (average of 2)	.04	.04	.73	.11
After step 2b (average of 2)	.11	.40	2.47	.33
After step 3a	.04	.06	1.49	.12
After step 3b	.04	.04	2.72	.31
AR33				
After step 1 (average of 6)	0.11	0.01	0.38	0.25
After step 2a (average of 2)	.34	.11	.27	.04
After step 2b (average of 2)	.42	.43	.46	.04
After step 3a	.09	.04	.20	.07
After step 3b	.08	.13	.18	.06

Table 2. Chemical analyses, in percent, of solutions, recalculated on an anhydrous basis for a 40-mg sample—Continued

	Al_2O_3	Fe_2O_3	MgO	K_2O
LVCH				
After step 1 (average of 6)	0.00	0.03	1.61	0.12
After step 2a (average of 2)	.04	.06	1.26	.01
After step 2b (average of 2)	.30	.37	3.78	.01
After step 3a	.00	.09	2.06	.01
After step 3b	.00	.09	2.06	.01
PRES V17				
After step 1 (average of 6)	0.17	0.06	0.01	0.06
After step 2a (average of 2)	.42	1.84	.05	.04
After step 2b (average of 2)	.43	3.12	.12	.02
After step 3a	.44	.20	.03	.02
After step 3b	.11	.25	.05	.01
GSL–5				
After step 2a	0.25	1.40	0.28	0.08
After step 2b (average of 2)	.42	2.04	[1]	.15
After step 3a	.00	.11	.36	.02
After step 3b	.00	.06	.17	.10

[1]No measurement.

All samples except the Potomac River sediment (fig. 7), which is composed of relatively insoluble micaceous clays, also showed significant solution of magnesium and potassium after the $(NH_4)_2C_2O_4$ treatment (step 3). These clays are composed primarily of smectites, which have a high magnesium content and are susceptible to further magnesium ion exchange by ammonium. However, most of the potential exchange sites on the clay should already have been filled by sodium as a result of the $Na_4P_2O_7$ treatment, and the possibility of further exchange with the ammonium ion would be limited. We suggest that clay dissolution may be taking place and that silica and aluminum are reprecipitated from the dissolved clay. Evidence for this hypothesis can be found in table 2, which shows that for all samples except the Potomac River sediment the amounts of dissolved aluminum were relatively low, even when significant amounts of magnesium appeared in the $(NH_4)_2C_2O_4$ solutions.

Figures 2, 3, 4, 6, and 8 show a similar pattern of iron removal: little solution after the $Na_4P_2O_7$ step followed by greater removal during the $NH_2OH{\cdot}HCl$ step and the $(NH_4)_2C_2O_4$ step. In most cases the solution of iron is little greater than what would be expected during clay dissolution. This suggests that these samples do not contain much discrete amorphous iron. Figure 5, the Long Valley caldera sample, illustrates a different pattern, but the solution data in table 2 suggest that this anomaly is related to the lack of aluminum extracted during the $Na_4P_2O_7$ step compared with the $(NH_4)_2C_2O_4$ step. In the case of the Potomac River sediment (fig. 7), iron solution is highest after the $NH_2OH{\cdot}HCl$ treatment, a definite indication of the presence of amorphous iron oxides.

Some estimate of the extent of clay dissolution can be obtained from the solution data in table 2. Dissolved aluminum was highest after the $NH_2OH{\cdot}HCl$ treat-

Table 3. Percentage of the sample recovered from the centrifuge tube as a solid after each treatment

[See table 1 for explanation of treatment steps]

Sample	After step 1	After step 2a	After step 3a	After step 2b	After step 3b
U11g (988.5–989.5 ft)	31	29	43	54	53
U11g (1006.4–1007.5 ft)	58	58	53	60	42
Fairbanks Butte	[1]	63	42	56	38
LVCH	37	67	50	68	48
AR33	61	60	47	71	47
PRES V17	82	79	59	71	59

[1]No measurement.

ment for every sample except Fairbanks Butte. The $NH_2OH \cdot HCl$ and HAc dissolved more aluminum and magnesium than $NH_2OH \cdot HCl$ + NaAc, indicating that the more acid treatment is more effective in attacking crystalline aluminosilicates. A greater quantity of iron was also dissolved by the HAc treatment, which suggests that the lower pH is also more effective in removing iron oxides.

Table 3 shows the percentage of the solid samples that was recovered for analysis after each treatment. The values are only semiquantitative, because it was not possible to quantitatively remove the dried precipitates from the centrifuge tubes. Nevertheless, several conclusions can be drawn: (1) about half of the material was lost during the entire extraction process and (2) the Potomac River sample dissolved the least, and the Fairbanks Butte clay dissolved the most. These conclusions are consistent with those drawn from examination of the data for the solids and solutions.

All of these data suggest that clay dissolution and alteration during extraction procedures may be more extensive than has generally been recognized. It seems clear that some clay is being dissolved, but it has not been possible to make an accurate determination of the extent of dissolution. Future work should be directed toward a complete mass balance to determine accurately the amount of clay remaining after each step of an extraction procedure.

In summary, the effects of the sodium pyrophosphate-hydroxylamine-ammonium oxalate extraction procedure are as follows:

Step 1—Sodium pyrophosphate

1. Exchange of sodium for calcium, magnesium, and potassium;
2. some dissolution of clay;
3. some removal of iron oxides.

Step 2—Hydroxylamine and sodium acetate or acetic acid

1. Extraction of amorphous iron and aluminum oxides;
2. greatest clay dissolution of the extraction sequence, greater in the acetic acid medium than in the sodium acetate medium.

Step 3—Ammonium oxalate

1. Exchange of ammonium ion for magnesium and potassium;
2. some dissolution of clay;
3. some removal of iron oxides.

CONCLUSIONS

Comparative analysis of ultrafine (<0.5 μm) clays and solutions associated with chemical treatments to remove organic matter, carbonates, and oxyhydroxides indicates that significant amounts of clay mineral components are removed at each step of a chemical extraction sequence. These losses take place differentially, despite the lack of evidence for structural alteration, and apparently depend closely on the nature of the clay mineral and its environment. Many changes can be attributed to ion exchange or loss of intergrade complexes, but dissolution of complete clay crystallites with or without reprecipitation of amorphous aluminosilicate is also an acceptable hypothesis for particulate weight loss.

REFERENCES CITED

Anderson, J.U., 1963, An improved pretreatment for mineralogical analysis of samples containing organic matter: Clays and Clay Minerals, v. 10, p. 380–388.

Bodine, M.W., Jr., and Fernalld, T.H., 1973, EDTA dissolution of gypsum, anhydrite, and Ca-Mg carbonates: Journal of Sedimentary Petrology, v. 43, p. 1152–1156.

Chester, R., and Hughes, M.J., 1967, A chemical technique for the separation of ferromanganese minerals, carbonate minerals, and adsorbed trace elements from pelagic sediments: Chemical Geology, v. 2, p. 249–262.

Dean, W.E., and Gorham, E., 1976, Major chemical and mineralogical components of profundal surface sediments in Minnesota lakes: Limnology and Oceanography, v. 21, p. 259–284.

Douglas, L.A., and Fiessinger, F., 1971, Degradation of clay minerals by H_2O_2 treatments to oxidize organic matter: Clays and Clay Minerals, v. 19, p. 67–68.

Dudas, M.J., and Harward, M.E., 1971, Effect of dissolution treatment on standard and clay soils: Soil Science Society of America Proceedings, v. 35, p. 134–140.

Eberl, D.D., Jones, B.F., and Khoury, H.R., 1982, Mixed-layer kerolite/stevensite from the Amargosa Desert, Nevada: Clays and Clay Minerals, v. 30, p. 321–326.

Ingamells, C.O., 1964, Rapid chemical analysis of silicate rocks: Talanta, v. 11, p. 665–666.

Jones, B.F., and Bowser, C.J., 1978, The mineralogy and related chemistry of lake sediments, *in* Lerman, A., ed., Lakes: Chemistry, Geology, Physics: New York, Springer-Verlag, p. 179–235.

Lahann, R.W., 1976, The effect of trace metal extraction procedures on clay minerals: Journal of Environmental Science and Health, v. 11, p. 639–662.

McKeague, J.A., 1967, An evaluation of 0.1*M* pyrophosphate and pyrophosphate-dithionite in comparison with oxalate as extractants of the accumulation products in podzols and some other soils: Canadian Journal of Soil Science, v. 47, p. 95–99.

Mehra, O.P., and Jackson, M.L., 1960, Iron oxide removal from soils and clays by dithionite-citrate system buffered with sodium bicarbonate: Clays and Clay Minerals, v. 7, p. 317–327.

Quakernaat, J., 1968, X-ray analyses of clay minerals in some recent fluviatile sediments along the coasts of Central Italy: Publicaties van het Fysisch-Geografisch Laboratorium Universiteit Amsterdam, v. 12, p. 105.

Schwertmann, Udo, 1959, Über die Synthese definierter Bedingungen: Zeitschrift von Anorganische und Allgemeine Chemie, v. 298, p. 337–348.

———1964, Differenzierung der Eisenoxide des Bodens durch Extraction mit Ammoniumoxalat-Lösung: Zeitschrift für Pflantzener-nahrung. Düngung, und Bodenkunde, v. 105, p. 194–202.

Shapiro, Leonard, 1975, Rapid analysis of silicate, carbonate, and phosphate rocks—revised edition: U.S. Geological Survey Bulletin 1401, 76 p.

Skougstad, M.W., Fishman, M.J., Friedman, L.C., Erdmann, D.E., and Duncan, S.S., 1979, Methods for determination of inorganic substances in water and fluvial sediments: U.S. Geological Survey Techniques of Water-Resources Investigations, Book 5, Chapter A1, 626 p.

Comparison of Velocity Interpolation Methods for Computing Open-Channel Discharge

By Janice M. Fulford *and* Vernon B. Sauer

Abstract

The Dutch members of a subcommittee of the International Organization for Standardization have suggested the use of the ratio $V/\sqrt{h}$ to interpolate the horizontal velocity profile from a small number of measured velocities. The velocity profile is computed by assuming that (1) the ratio $V/\sqrt{h}$ varies linearly between measured velocities and (2) the ratio $V/\sqrt{h}$ is constant from the nearest measured velocity to the bank. This method (the ratio interpolation method) and two other discharge computation methods, a modified ratio interpolation method and a linear velocity fit method, were tested on data from the Mississippi and Ohio Rivers and seven smaller rivers in Georgia and South Carolina. Results from all the methods are compared with a "true" discharge computed by the standard mid-section method. Absolute mean error for the methods using all the measured cross section depths with a velocity approximation scheme ranged from 10.2 percent to 1.1 percent. Results from the study indicated that the use of five velocity measurements in a known cross section might be adequate to compute discharges by using the ratio interpolation method or a more simple linear interpolation scheme.

INTRODUCTION

Traditional velocity-area discharge computation methods are simple numerical integration or approximation schemes. The popular mid-section method uses the mid-point rule to numerically integrate discharge across the channel width. Stevens (1908) and Young (1950) reviewed the use of several different numerical integration schemes for computing discharges from field measurements. They concluded that the mid-section method was best when simplicity and accuracy were the criteria for selection. However, the numerous velocity measurements required for standard mid-section computations can be difficult to make, especially for large rivers with intensive navigation. The Dutch members of a subcommittee of the International Organization for Standardization (written commun., 1981) have suggested a velocity-area discharge computation method that requires fewer measured velocities. This method (hereafter called the ratio interpolation method) and two other velocity-area discharge computation methods, (1) a modified version of the ratio interpolation method and (2) a linear velocity fit method, are tested and compared with the mid-section method.

METHODS USED

The three methods tested reduce the number of velocity measurements needed by using different approximation formulas to solve for the velocities between measured values. Additionally, these methods assume that the cross section (depths) of the channel is known.

The *ratio interpolation method* assumes that the ratio $V/\sqrt{h}$, where V is the mean velocity and h is the depth of flow measured at a vertical, is constant or nearly constant for a channel cross section. This ratio, $V/\sqrt{h}$, has the form of a Froude number, $V/\sqrt{gh}$. Its use in approximating a horizontal velocity profile implies that the ratio of kinetic to potential energy is constant throughout the channel section.

To compute discharge by using the ratio interpolation method, the cross section is divided into an arbitrary number of equal-width subsections. For this study 100 subsections were used. The mean velocity for each subsection is then determined by assuming that $V/\sqrt{h}$ varies linearly between verticals where velocities are measured and that $V/\sqrt{h}$ is constant between the bank and the nearest measured velocity. The mean velocity, V_i, for a subsection between two measured velocities is calculated from

$$V_i = (a/L)\cdot V_3\cdot\sqrt{h_i/h_3} + [(L-a)/L]\cdot V_2\cdot\sqrt{h_i/h_2}\ , \qquad (1)$$

where V_3 and V_2 are the measured velocities, L is the distance between verticals where V_3 and V_2 are measured, a is the distance between verticals where V_2 is measured and V_i is computed, and h_3, h_2, and h_i are the known depths at each vertical. Measured velocities are arbitrarily spaced at equal distances across the channel width.

The mean velocity, V_j, for a subsection between the bank and the nearest measured velocity is calculated from

$$V_j = V_1\cdot\sqrt{h_j/h_1}\ , \qquad (2)$$

where V_1 is the measured velocity and h_1 and h_j are the known depths. Figure 1 illustrates the variables used in equations 1 and 2.

Total discharge, Q, is computed from

$$Q = \sum_{k=1}^{100} V_k \cdot h_k \cdot \Delta b \quad , \tag{3}$$

where V_k is the mean velocity and h_k is the depth for the kth subsection, and Δb is the width of the subsection.

The *modified ratio interpolation method* assumes that $V/\sqrt{h}$ decreases linearly to zero at the banks. This modification was tested because the measured values of $V/\sqrt{h}$ tend to decrease toward zero as the banks are approached. The modified ratio interpolation method is computed exactly as the ratio interpolation method is, except that the mean velocity for a subsection between the bank and nearest measured velocity is calculated from

$$V_j = (a/L) \cdot V_1 \cdot \sqrt{h_j/h_1} \quad , \tag{4}$$

where a is the distance measured from the bank to the vertical where V_j is located.

The *linear velocity fit method* assumes that a linear interpolation between measured velocities accurately approximates the velocity distribution in a cross section. The mean velocity, V_i, for a subsection between two measured velocities is calculated from

$$V_i = (a/L) \cdot V_3 + [(L - a)/L] \cdot V_2 \quad . \tag{5}$$

Because velocity is approximately zero at the banks, the mean velocity for a subsection between the bank and the nearest measured velocity is calculated from

$$V_i = (a/L) \cdot V_1 \quad . \tag{6}$$

The total discharge is then computed by using equation 3.

COMPARISON OF METHODS

Sixty-two standard field measurements of discharge were selected to test each of the four methods. The measurement data used in this study are from the Savannah River, Tobesofkee Creek, Coosawatte River, and Chattahoochee River in Georgia; the Little Pee Dee River, Congaree River, and Edisto River in South Carolina; the Mississippi River at Baton Rouge, La., and the Ohio River at Greenup Dam in Kentucky. Data tested were restricted to measurements that did not have obvious pier effects or divided channels. A FORTRAN 77 program was written to perform the computations for the ratio interpolation, modified ratio interpolation, and linear velocity fit methods.

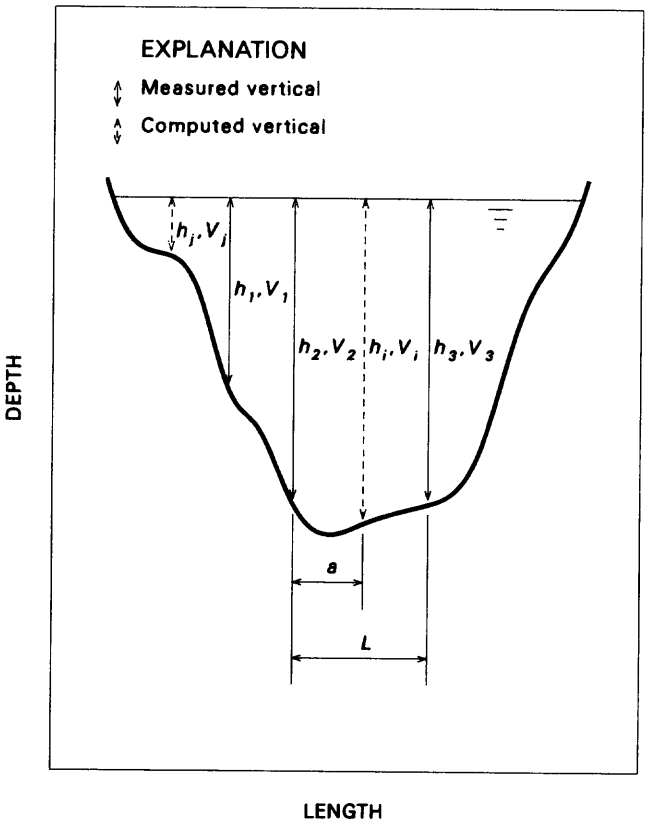

Figure 1. Length and depth variables illustrated.

"True" discharges for comparison were computed by the standard mid-section method using all available observations of depth and velocity in each field measurement. Discharges for the ratio interpolation method and the two other methods were computed using 3, 5, 7, 9, 11, and 13 velocity measurements and were compared with the "true" discharge. Velocities were selected from each field measurement at approximately equal intervals across the channel width. Depths at unmeasured verticals required for the ratio interpolation, modified ratio interpolation, and linear velocity fit methods were linearly interpolated from the measured depths.

Results of the discharge computations are compared with the "true" discharges by computing the error, x, in percent from

$$x = 100 \cdot (Q_d - Q_t)/Q_t \quad , \tag{7}$$

where Q_d is the discharge calculated from the ratio interpolation method (or one of the methods) and Q_t is the "true" discharge. The error calculated by equation 7 is an estimate of the true error. Because the standard mid-section method is an estimate of discharge for natural channels, the "true" discharge used for comparison is not exact.

Mean absolute error, $|\bar{x}|$, mean error, $\bar{x}$, standard deviation of the error, σ, and the root mean square error, $\sqrt{\bar{x}^2 + \sigma^2}$, were computed separately from the discharges computed for the large discharge rivers (Mississippi and Ohio Rivers), the smaller discharge rivers (rivers in Georgia and South Carolina), and the large and smaller discharge rivers combined. Mean error, $\bar{x}$, is an indicator of bias. Error summaries for the tested methods are listed in table 1 and are shown graphically in figures 2 and 3.

The ratio interpolation method, modified ratio interpolation method, and linear velocity fit method have similar absolute errors. For the combined data set, the mean absolute error for the ratio interpolation method and for the modified ratio interpolation method decreases from 8.1 to 1.1 and from 9.4 to 1.4, respectively, when the number of velocity measurements increases from 3 to 13. The "best" or smallest error for the fewest velocity measurements (less than nine) was obtained by using the ratio interpolation method on the large discharge rivers. The mean absolute error declined from 6.3 percent for three velocity measurements to 1.9 percent for seven velocity measurements for the large discharge rivers, an improvement of approximately 2 percent less than for the smaller discharge rivers. The modified ratio interpolation method and the linear velocity fit method also show a smaller error when the data are restricted to the large discharge rivers.

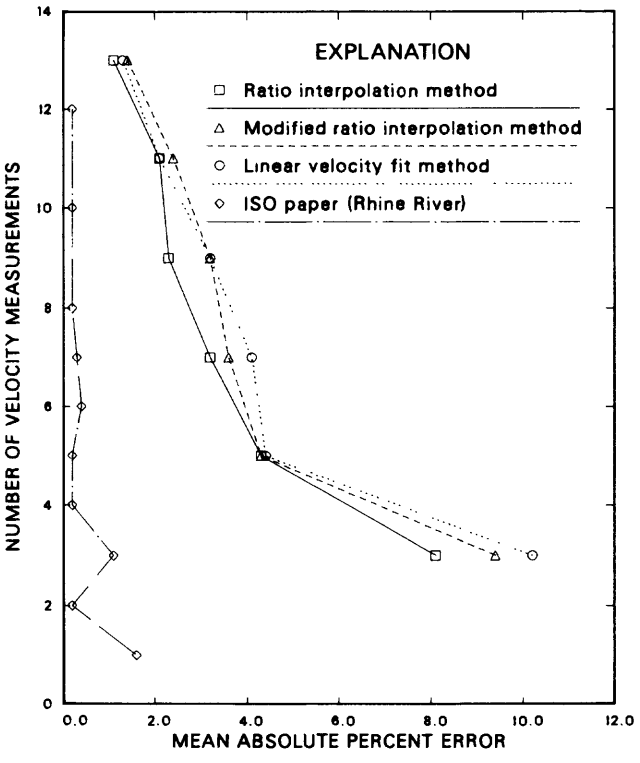

Figure 2. Comparison of mean absolute percent error to number of velocity measurements.

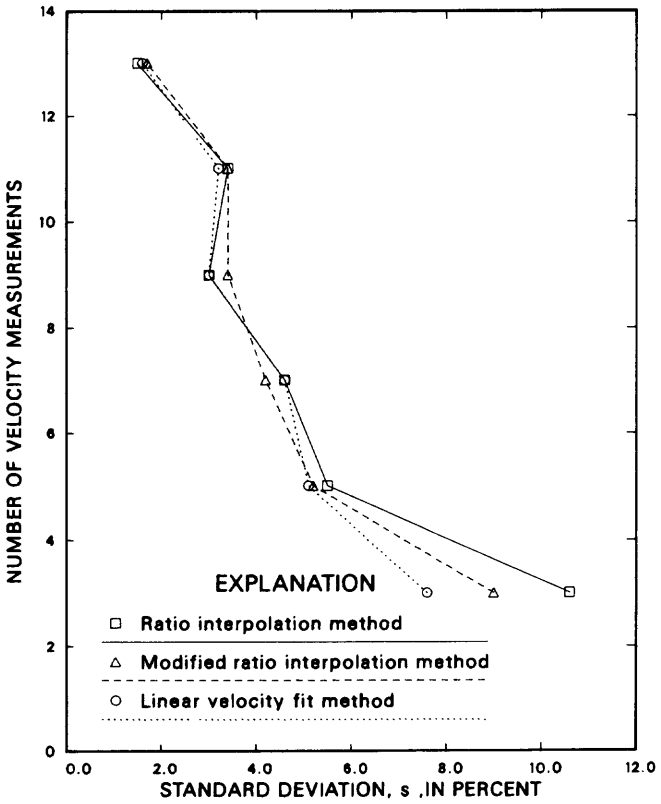

Figure 3. Comparison of standard deviations of mean absolute percent error to number of velocity measurements.

The similar errors computed for the ratio interpolation, modified ratio interpolation, and linear velocity fit are explained when the velocity approximations are compared. All the velocity approximations used by these methods converge to the same velocity when depths are constant. Since most of the discharge for the rivers tested occurred in the center of the channel where depths are nearly constant, the total discharges calculated are similar.

To test the influence of the cross-section depths on error, the standard mid-section method was used on the data set with fewer measurements than is normal practice. Much larger errors resulted from this "reduced" mid-section method. The "reduced" mid-section method and the linear velocity fit method differ computationally only in the approximation of cross-sectional area. Comparisons of these methods show that the relatively small errors computed by the tested methods are largely the result of improved area approximations.

Two of the methods tested, the modified ratio interpolation and the linear velocity fit method, generally underestimate discharges. The mean errors listed in table 1 reflect this negative bias. The ratio interpolation method does not have an obvious bias.

Table 1. Error comparison for the ratio interpolation (RIM), modified ratio interpolation (MRIM), and linear velocity fit (LVFM) methods

[No. meas., number of velocity measurements; Small, smaller discharge rivers (in Georgia and South Carolina); Large, large discharge rivers (Mississippi and Ohio Rivers)]

No. meas.	Method	Maximum and minimum error			Mean error			Mean absolute error			Standard deviation			Root mean square error		
		Small	Large	Both	Small	Large	Both	Small	Large	Both	Small	Large	Both	Small	Large	Both
3	RIM	−33.2/13.7	−3.6/16.2	−33.2/16.2	−5.3	5.7	−0.9	9.2	6.3	8.1	10.8	10.4	10.6	12.0	11.9	10.6
	MRIM	−33.9/12.0	−17.1/3.2	−33.9/12.0	−8.2	−8.0	−8.1	10.0	8.8	9.4	10.4	6.5	9.0	13.3	10.3	12.1
	LVFM	−26.6/4.0	−17.3/3.5	−26.6/4.0	−11.4	−7.9	−9.9	11.6	8.2	10.2	8.4	6.6	7.6	14.2	10.3	12.5
5	RIM	−19.7/13.7	−1.9/8.6	−19.7/13.7	1.5	1.3	1.6	5.5	2.6	4.3	6.8	2.7	5.5	7.0	3.2	5.7
	MRIM	−19.8/9.1	−9.7/0.9	−19.8/9.1	−1.6	−4.1	−2.6	4.2	4.1	4.3	6.1	3.6	5.2	5.5	6.3	5.8
	LVFM	−19.8/8.5	−9.9/1.3	−19.8/8.5	−2.3	−3.6	−2.8	4.9	3.7	4.4	6.1	2.9	5.1	6.6	4.6	5.8
7	RIM	−20.0/11.5	−5.8/5.9	−20.0/11.5	.0	.0	.0	4.1	1.9	3.2	5.7	2.6	4.6	5.7	2.6	4.6
	MRIM	−20.1/6.5	−7.3/4.4	−20.1/6.5	−1.9	−2.9	−2.3	4.0	3.3	3.6	4.9	3.1	4.2	5.3	4.2	5.7
	LVFM	−24.0/7.7	−8.2/3.9	−24.0/7.7	−2.9	−2.7	−2.9	4.6	3.2	4.1	5.6	2.9	4.6	6.3	3.9	5.5
9	RIM	−3.8/9.6	−8.4/6.0	−8.4/9.6	.4	−1.0	−.1	2.3	2.3	2.3	3.1	3.0	3.0	3.1	3.2	3.0
	MRIM	−10.6/5.4	−4.0/4.5	−10.6/5.1	−2.7	−2.2	−2.5	3.2	3.1	3.2	3.1	2.4	3.4	4.1	3.7	3.9
	LVFM	−14.2/2.5	−9.9/4.0	−14.2/4.0	−2.8	−2.9	−2.8	3.2	3.2	3.2	3.2	2.9	3.0	4.2	4.1	4.1
11	RIM	−18.8/7.9	−4.3/5.2	−18.8/7.9	.1	.1	.0	2.5	1.5	2.1	4.1	2.0	3.4	4.1	2.0	3.4
	MRIM	−21.5/3.6	−4.6/4.2	−21.5/4.2	−1.9	−1.1	−1.6	2.4	2.1	2.4	4.0	2.4	3.4	4.4	2.6	3.8
	LVFM	−21.2/2.0	−5.4/3.7	−21.2/3.7	−1.7	−1.3	−1.5	2.3	1.9	2.1	3.8	2.0	3.2	4.2	2.4	3.5
13	RIM	−2.7/3.6	−0.5/4.1	−2.7/4.1	.3	.3	.3	1.2	1.0	1.1	1.5	1.4	1.5	1.5	1.5	1.5
	MRIM	−4.5/2.2	−2.5/3.4	−4.5/3.4	−.8	−.2	−.5	1.6	1.2	1.4	1.7	1.6	1.7	1.9	1.6	1.7
	LVFM	−4.8/1.6	−2.3/3.7	−4.8/3.7	−.8	−.2	−.6	1.3	1.3	1.3	1.6	1.7	1.6	1.7	1.7	1.7

The obvious negative bias in the reduced mid-section method is mainly due to the poor cross-section area approximation used. The negative bias in the modified ratio interpolation and linear velocity fit methods is the result of underestimating the velocities near the bank. These approximations are worst when the distance between the bank and the nearest measured velocity is large. Because the ratio interpolation method results in generally larger estimates of velocity near the bank, it has no obvious bias.

Results of this study differ somewhat from the results presented in the ISO/TC 113 study, "Measurement of Liquid Flow in Open Channels" (Netherlands, International Organization for Standardization, written commun., 1981). Figure 2 shows that the errors presented in the ISO/TC 113 study are much less than those found by this study. Some of this difference may be the result of channel characteristics, uniformity of cross section, velocity distribution, and discharge. The smaller data set used in the ISO/TC 113 study also contributed significantly to the difference in error between the two studies. The ISO/TC 113 paper discussed use of the method at only one location on the upper Rhine River for a single discharge measurement of about 91,000 ft^3/s. Results for two other computations for tidal rivers were illustrated in the appendix of the paper. In comparison, this study investigated 62 different data sets for nine different rivers, and discharges ranged from 1,410,000 ft^3/s to 28 ft^3/s.

Unlike the ISO/TC 113 study, in this study the ratio $V/\sqrt{h}$ was not found to be nearly constant in a channel cross section for all discharge measurements used. Plots of $V/\sqrt{h}$ against channel width (fig. 4) show that, for several different Ohio River discharges, the distribution of the ratio is not constant in the cross section. Several things could cause nonuniform distribution of the ratio, for example meanders of the river channel, nonuniform roughness and conveyance, or manmade structures. The user of these methods should consider factors that create nonuniformity.

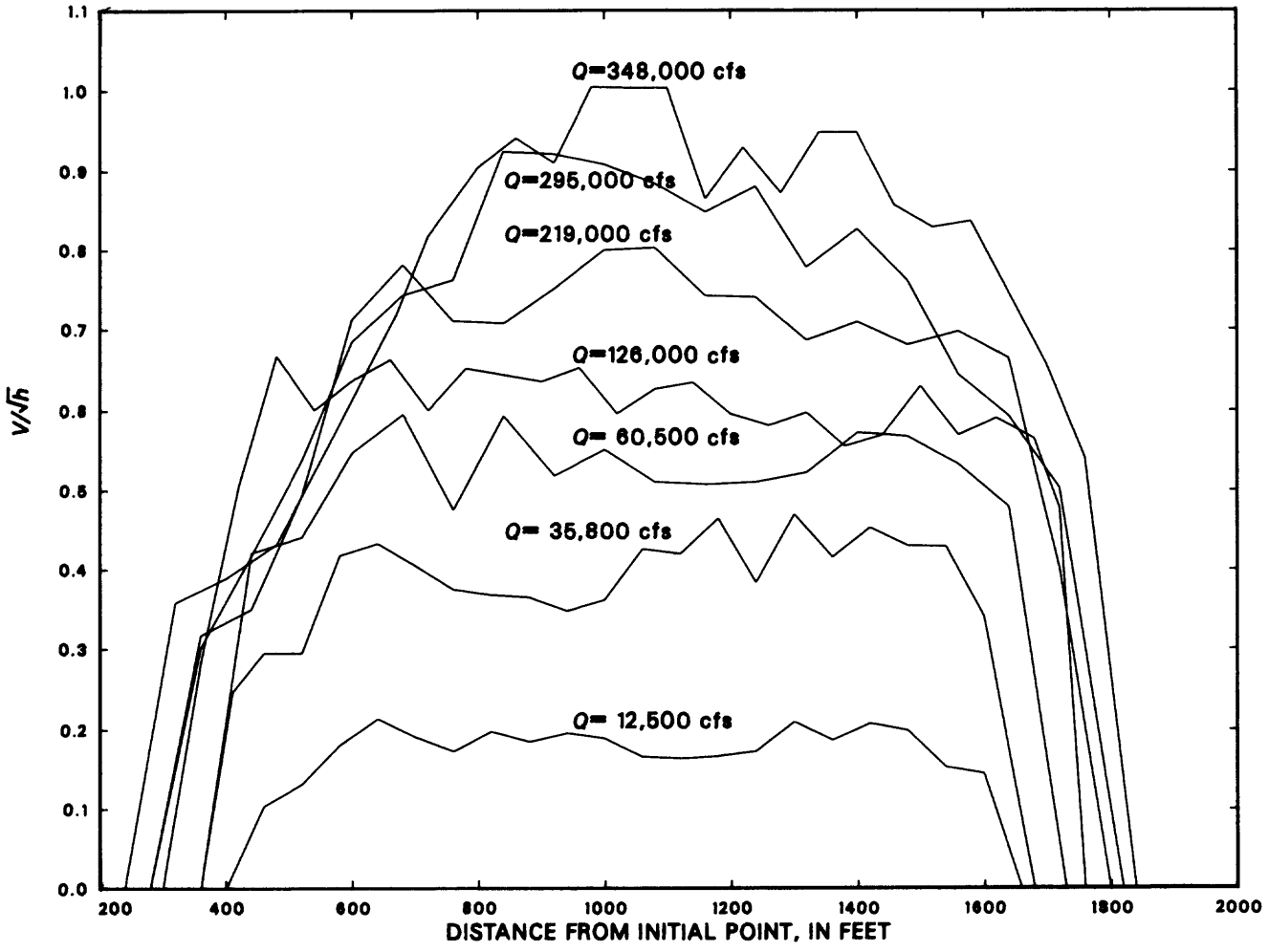

Figure 4. Lateral distribution of $V/\sqrt{h}$ for selected discharge measurements (Q) on the Ohio River at Greenup Dam, Ky.

CONCLUSIONS

The small difference in error between the ratio interpolation method and the linear velocity fit method does not recommend the use of the more complicated ratio interpolation velocity approximation over the linear velocity approximation. Practical application of either method is limited by how much error is acceptable in the discharge calculated. Field use of the methods would require depth soundings, sonic or other, at sufficient points to accurately define the cross section, and velocity measurement in a minimal number of verticals. Caution should be exercised when applying either method at a site without previous discharge measurements because unreliable discharges could be computed for rivers with irregular velocity distributions. Best performance of these methods would be expected for uniform channel sections with regular velocity distributions.

Neither the ratio interpolation method nor the linear velocity fit method is as easy to use as the mid-section method if discharges are computed by hand. If the measurement of fewer velocities is desirable and the cross-section shape is well known, however, then either the ratio interpolation method or the linear velocity fit method will produce reasonable computations of discharge with mean absolute errors of 4.3 and 4.4 percent, respectively, when five measured velocities are used.

REFERENCES CITED

Stevens, J.C., 1908, Comparison of formulas for computation of stream discharge: Engineering News, v. 59, no. 26, p. 682–684.

Young, K.B., 1950, A comparative study of mean-section and mid-section methods for computation of discharge measurements: U.S. Geological Survey Open-File Report, 52 p.

A Preliminary Evaluation of a Discharge Computation Technique That Uses a Small Number of Velocity Observations

By Larry R. Bohman *and* William J. Carswell, Jr.

Abstract

A study was made of a discharge measurement technique for unsteady flow being considered by the International Organization for Standardization. The new technique uses a small number of velocity observations and a measured channel cross section to develop a lateral velocity distribution. The technique was tested using three, five, and seven vertical velocity observations from 25 discharge measurements at five streamflow gaging stations. An average bias of about +2.5 percent indicates that discharge may be overestimated by the new procedure when compared to the standard midsection method. Percent differences ranged from +28.5 to −38.3 and decreased as either the number of velocity observations or discharge increased. A large part of the difference was probably a result of channel-bottom irregularities, pier influence, and extrapolation necessary between the last velocity observation and the bank.

It was determined that the location of velocity observations could probably be optimized to improve the accuracy of the method. The results of this study indicate that further investigation of the technique and its potential as a discharge measurement tool for steady or unsteady flow at large rivers with uniform flow in the vicinity of the measurement section is warranted.

INTRODUCTION

Conventional current-meter discharge measurements frequently are not feasible in tidal rivers or at other sites where flow conditions change rapidly. Often the number of velocity verticals that can be measured simultaneously or within a reasonable time is limited by equipment, personnel, or intensity of river traffic. Even under steady flow conditions, an accurate means of determining discharge with fewer measured verticals would be desirable in terms of safety and time saved.

Usually, however, a reduction in measured velocity data is accompanied by a decrease in the reliability of the computed discharge. A study by Carter and Anderson (1963) indicates that unacceptably large errors result when the midsection method is applied using fewer than the recommended 25 to 30 vertical velocity observations.

Another method that uses limited velocity data, the one-point continuous method, yields highly accurate results, but its adaptability is so limited that its use is restricted to places where the discharge is largely a function of slope and the variation in stage is small (Corbett and others, 1943).

The purpose of this report is to make an evaluation of a measurement technique submitted in 1981 by Dutch members of Subcommittee One of Technical Committee 113 of the International Organization for Standardization. The technique was described in an unpublished document entitled "Computation of Discharge in Velocity-Area Methods" (ISO/TC113/SC1 N345). This document is herein referred to as the "source report" or "source text".

The measurement technique uses a small number of velocity observations and a measured channel cross section to synthesize mean velocities at uniform intervals elsewhere in the cross section. The relations used to generate the velocities were developed empirically from a measurement made on the upper Rhine River near Lobith, West Germany. Discharge is computed by multiplying the synthesized velocities times the subsection areas and summing the results as for conventional discharge measurements. This technique will be referred to as the "interpolation" method or technique in this report.

Twenty-five conventional discharge measurements were selected as a source of cross-sectional geometry and vertical velocity data. Computations were made using three, five, and seven velocity observations with the interpolation method.

DISCHARGE COMPUTATION METHODOLOGY

Two basic procedures used in the computation of discharge are the midsection method and the mean-section method. Both methods involve the summation of the products of subsection areas of the stream cross section and their respective average velocities. In the midsection method, the velocity sample at each vertical is assumed to represent the mean velocity in a rectangular subsection.

The subsection area extends laterally from half the distance to the preceding observation vertical to half the distance to the next, and vertically from the water surface to the sounded depth. In the mean-section method, the velocities and depths at successive verticals are averaged, and each subsection extends laterally from one observation vertical to the next. Subsection discharge is the product of the average of two mean velocities, the average of two depths, and the distance between observation verticals (Rantz and others, 1982). The computation procedure (midsection or mean-section) to be used in the interpolation technique is not made clear in the source report. In this evaluation, the mean-section method is used as the computation procedure for the interpolation technique.

In the interpolation method there may be several subsections between observed verticals or between the banks and the nearest observed vertical. A constant equal to the mean velocity divided by the square root of the depth is computed at each observed vertical. The mean velocity for each intervening subsection is synthesized by first multiplying the constants derived at the observed vertical on either side by the square root of the mean depth at the intervening subsection. These two values are then weighted according to the distances of the subsection from the observed verticals to obtain a final mean velocity for each subsection.

The interpolation method assumes the channel cross section has been measured by weight soundings, echogram, or other survey. A site at which the cross section remains fairly stable for long periods of time would result in even greater time savings, because a survey would not be mandatory with each measurement. The channel reach should be reasonably uniform so that the velocity distribution is not changing. Manmade structures or bends upstream of the measuring section or a bridge opening with a conveyance different from that of the channel would cause channel nonuniformity, which might adversely affect the velocity distribution.

The source text states that a small number of vertical velocity observations should be taken at locations that can be referenced to specific points within the cross section. The locations of these reference verticals should be chosen to give a more or less equal distribution over the channel within the following limits:

$$0.5\,B/n < L < 1.5\,B/n \quad , \tag{1}$$

where B = river width,
n = number of measured verticals, and
L = distance between two measured verticals.

The verticals used in this analysis were arbitrarily chosen within these limits, which are called "L limits" in this report. The only other field information needed is the water-surface elevation during the observation period. The elevation datum must be common to that of the channel geometry.

The first step in computing discharge by the interpolation method is to divide the cross section into several subsections of equal width. The example in the source report had 100 subsections; however, no guidelines for determining the number or width of the subsections were given. In this study a subsection width was arbitrarily chosen for each measurement that would result in 30 to 50 equal-width subsections. For each subsection, the mean depth and mean velocity were calculated. Subsection mean depths were ascertained from the known channel geometry and water-surface elevations. Mean subsection velocities in the interpolation method are related to depth by equations given in the source text. Figure 1 shows a typical channel section; certain variables used in the following equations are depicted.

The method for computing mean subsection velocities between two measured verticals is different from that used between the bank and the first measured vertical. Synthesized mean velocity values for subsections between the bank and the first measured vertical are extrapolated by using the equation

$$\bar{v}_i/h_i^{1/2} = \bar{v}_1/h_1^{1/2} \quad , \tag{2}$$

or rewritten

$$\bar{v}_i = (\bar{v}_1 h_i^{1/2})/h_1^{1/2} \quad , \tag{3}$$

where $\bar{v}_i$ = synthesized mean velocity in subsection i,
h_i = mean depth at subsection i,
$\bar{v}_1$ = mean velocity at the first measured vertical, and
h_1 = depth at first measured vertical.

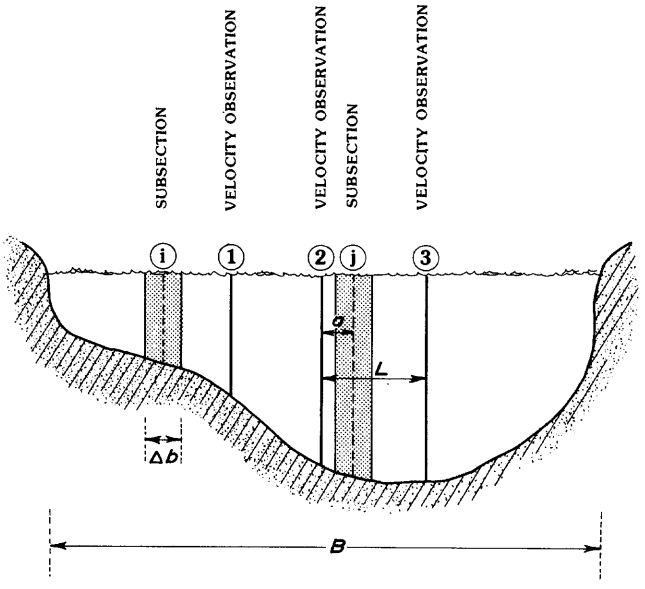

Figure 1. Definition sketch of variables in the interpolation method.

The mean velocity values for subsections that lie between two measured verticals were interpolated by first using equations 4 and 5 at respective verticals. Equations 4 and 5 are identical to equation 3 except that the variable subscripts have been changed to correspond to subsection "j" in figure 1. The resultant mean velocity values were then weighted according to the distance from the subsection to each neighboring measured velocity vertical by using equation 6.

$$\bar{v}_j(2)/h_j^{1/2} = \bar{v}_2/h_2^{1/2} \text{ or } \bar{v}_j(2) = (\bar{v}_2 h_j^{1/2})/h_2^{1/2} \ , \qquad (4)$$

$$\bar{v}_j(3)/h_j^{1/2} = \bar{v}_3/h_3^{1/2} \text{ or } \bar{v}_j(3) = (\bar{v}_3 h_j^{1/2})/h_3^{1/2} \ , \qquad (5)$$

$$\bar{v}_j = (a/L)\bar{v}_j(3) + [(L - a)/L]\ \bar{v}_j(2) \ , \qquad (6)$$

where $\bar{v}_j(2)$ = mean velocity at subsection j as influenced by vertical 2;
h_j = mean depth at subsection j;
$\bar{v}_2$, $\bar{v}_3$ = mean velocities at respective measured verticals;
h_2, h_3 = depths at respective measured verticals;
$\bar{v}_j(3)$ = mean velocity at subsection j as influenced by vertical 3;
$\bar{v}_j$ = weighted mean velocity at subsection j;
a = distance from vertical 2 to center of subsection j; and
L = distance from vertical 2 to vertical 3.

After the mean velocities have been determined, the total discharge can be calculated by

$$Q = \sum_{i=1}^{x} (\bar{v}_i)(h_i)(\Delta b) \ , \qquad (7)$$

where Q = total discharge,
x = number of subsections, and
Δb = equal width of subsections.

Figure 2 depicts the cross section and location of velocity observations used in an example computation shown in table 1 for measurement no. 269, Broad River near Carlisle, S.C.

FIELD DATA USED

Five streamflow gaging stations with drainage areas greater than 2,700 square miles were selected from District files for analysis (fig. 3). The measurements chosen represent a moderate range of discharge at each site. The discharge measurement notes were used as a source of velocity and cross-sectional information. Computations for three, five, and seven verticals were made by using the interpolation method.

In some cases a small percentage of the flow was very shallow or passed through relief bridges. The discharge associated with these occurrences was not included in this study. Pier area was deducted as necessary. The locations of the measured verticals were chosen within the limits prescribed and were not optimized with respect to channel geometry or pier proximity.

DISCUSSION OF RESULTS

A summary of the differences, in percent, between discharges computed by the midsection method and discharge computed by the interpolation method are presented in table 2. Average differences, root mean square error, and bias for all stations combined and all stations combined except the Congaree River Station are given in table 3. Computations are shown in table 3 with and without the Congaree River Station because the differences between discharge calculated using the midsection and the interpolation methods are much greater at this station than at other stations. The large differences shown in table 2 for this station were considered to be a result of the extremely irregular bottom and several deep channels at the measurement cross section.

Two general trends can be seen from tables 2 and 3. The first, as pointed out in the source text, is a tendency for difference and root mean square error to decrease as the number of velocity observations increases. This correlation is not unexpected because as the number of velocity observations increases, the velocity distribution is being defined by actual measurement rather than being estimated with an equation.

Secondly, the bias resulting from this data set seems to indicate that the technique yields discharges that are greater than those derived by using the midsection method. The positive bias may have been a consequence of the computational technique used and is not necessarily inherent in the interpolation technique. A study by Young (1950) concluded that the midsection method is slightly more accurate than the mean-section method used in this evaluation. By using the midsection computational procedure, the apparent bias might have been more or less evident.

Figure 4 compares measured discharge computed by the standard midsection technique with difference, in percent, between midsection and interpolation techniques as shown in table 2 for three, five, and seven velocity verticals. In all three cases the difference is reduced as discharge (and depth) increases. This reduction was probably a result of the increasing stage and discharge reducing the effect of some channel-bottom irregularities. The interpolation method is most accurate in wide, even cross sections and probably should not be applied in channels with shallow overflows or irregular bottoms. At sites with

irregular cross sections, both the area and velocity distribution must be more precisely estimated to obtain reliable results. The subsection areas could be defined more accurately by increasing the number of subsections used for computation. However, this alone would not significantly reduce the error for the interpolation method. The velocity distribution associated with irregular channels is usually highly erratic and must be determined in more detail than for a smooth channel. Increased accuracy in determining the velocity distribution could only be accomplished by increasing the number of measured velocity observations, which would cancel any benefits gained from application of the interpolation method.

Figures 5 and 6 are graphs of cumulative discharge distribution computed by using the midsection and interpolation methods. Figure 5 demonstrates that this technique may not be suitable for those sites where piers greatly influence velocities. Computed and measured lines of cumulative discharge shown in figure 5 are parallel except at or near piers. Although no edge-of-pier verticals were used, several of the velocity observations chosen were probably adversely affected by piers.

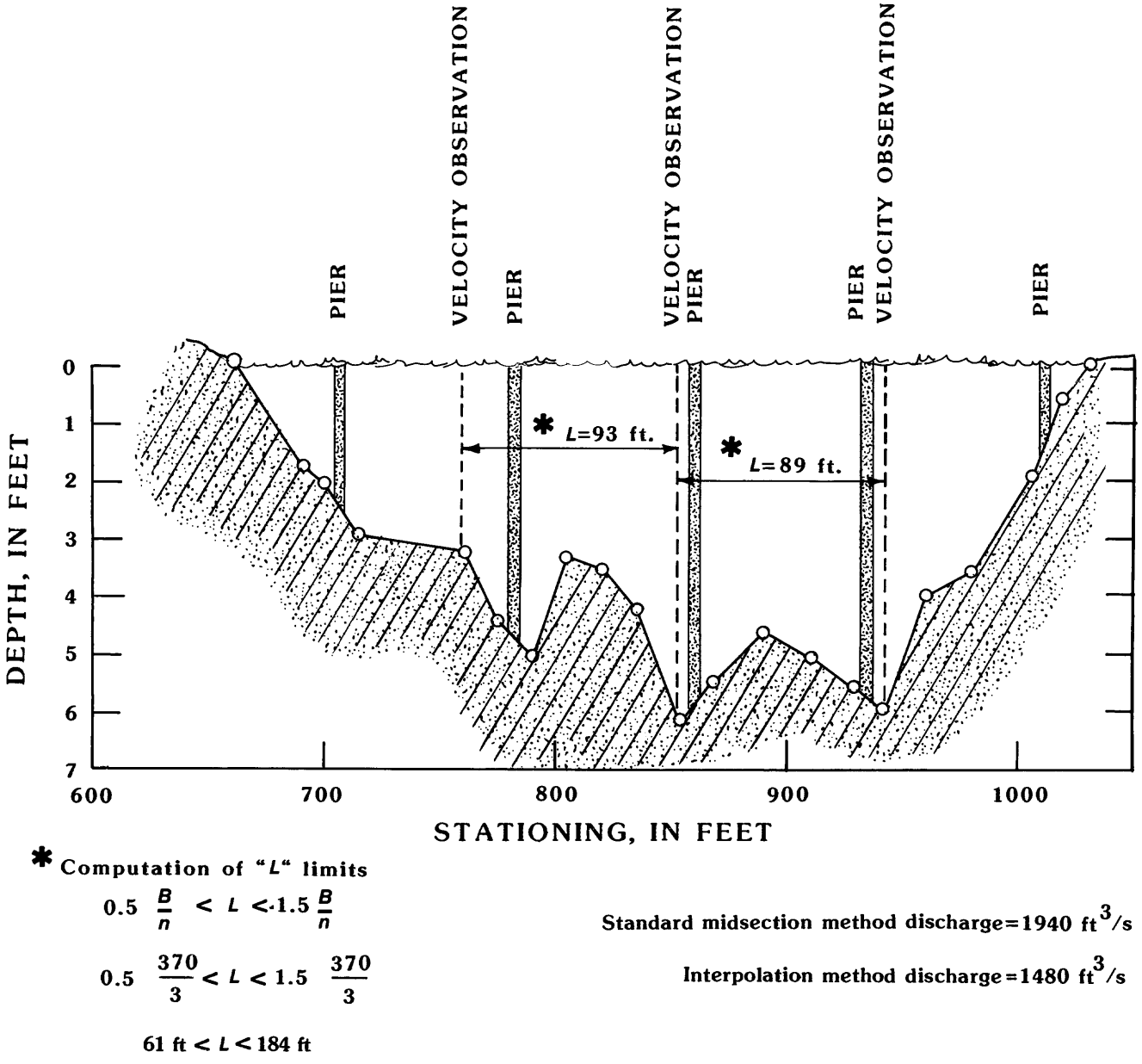

Figure 2. Cross section and location of velocity observations used in example computation, measurement no. 269, Broad River near Carlisle, S.C.

Figure 6 suggests that near the banks discharges computed by the interpolation method deviate from those computed by the standard midsection method. The L limits (see "Discharge Computation Methodology" section) prescribed in the source text to determine distances between reference verticals prohibit placing verticals too

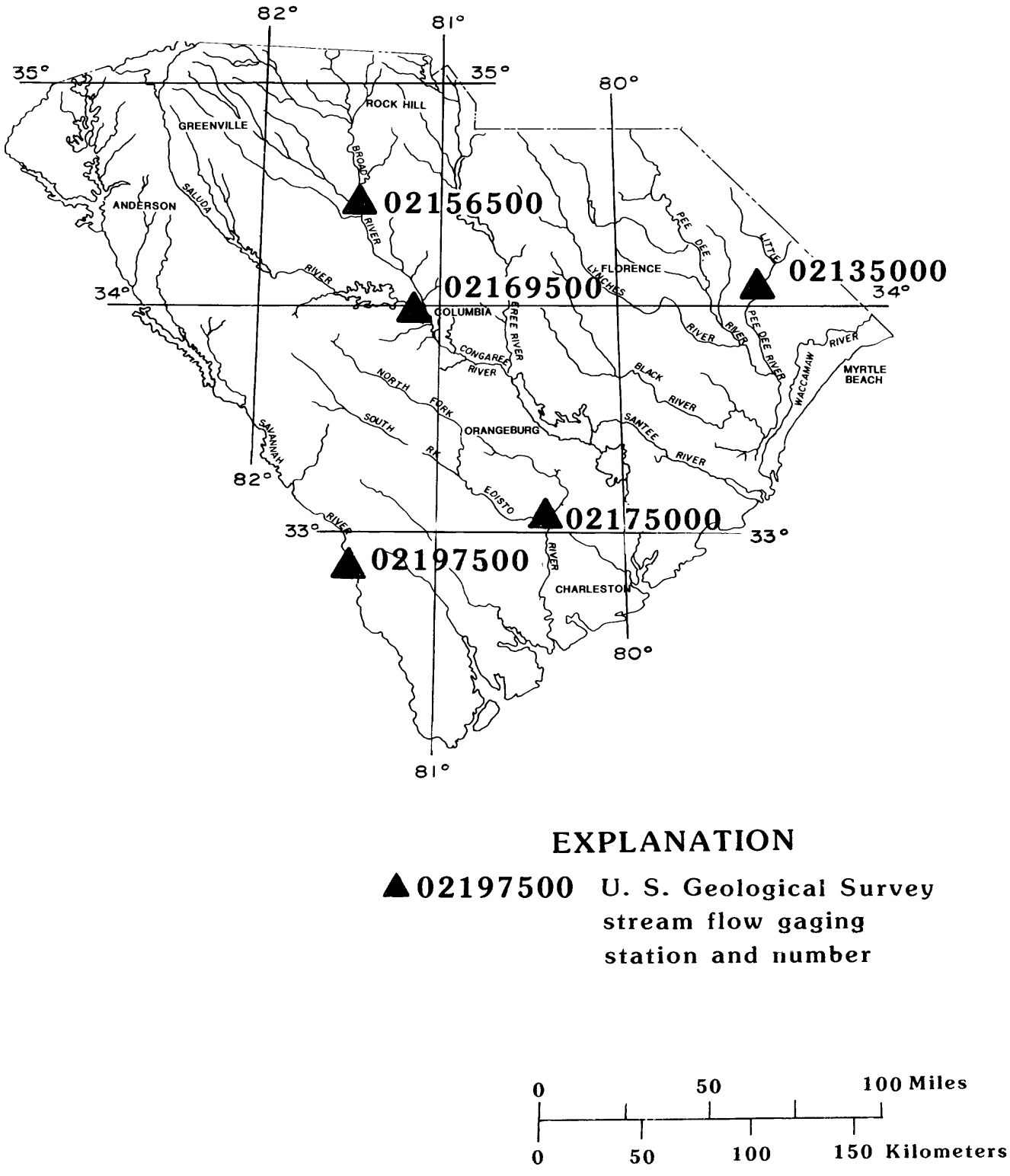

Figure 3. Locations of streamflow gaging stations used in analysis.

Table 1. Example computation using three velocity observations, measurement no. 269, Broad River near Carlisle, South Carolina

[—, no data]

Observed data				Subsection data								
Station (ft)	Mean velocity (ft/s)	Depth (ft)	Velocity depth constant [(ft/s)/ft$^{1/2}$]	Stationing (ft)	Depth (ft)	Mean depth (ft)	Section width (ft)	Weighting factor	Weighting factor	Square root of mean depth (ft$^{1/2}$)	Weighted mean velocity (ft/s)	Discharge (ft^3/s)
				660–670	0.6	0.3	10	—	—	0.55	0.58	2
				670–680	1.1	.8	10	—	—	.89	.94	8
				680–690	1.7	1.4	10	—	—	1.18	1.25	18
				690–700	2.2	2.0	10	—	—	1.41	1.49	30
				700–710	2.7	2.4	10	—	—	1.55	1.64	39
				710–720	3.1	2.9	10	—	—	1.70	1.80	52
				720–730	3.1	3.1	10	—	—	1.76	1.86	58
				730–740	3.2	3.2	10	—	—	1.79	1.90	61
				740–750	3.2	3.2	10	—	—	1.79	1.90	61
760	1.92	3.3	1.06	750–760	3.3	3.2	10	0.00	1.00	1.79	1.90	61
				760–770	4.1	3.7	10	.11	.89	1.92	1.91	71
				770–780	4.3	4.2	10	.21	.79	2.05	1.93	81
				780–790	4.0	4.2	10	.39	.61	2.05	1.72	72
				790–800	3.6	3.8	10	.43	.57	1.95	1.59	60
				800–810	3.5	3.6	10	.54	.46	1.90	1.43	52
				810–820	3.6	3.6	10	.64	.36	1.90	1.32	48
				820–830	4.1	3.8	10	.75	.25	1.95	1.23	47
				830–840	4.8	4.4	10	.86	.14	2.10	1.20	53
				840–850	5.7	5.2	10	.97	.03	2.28	1.16	60
853	1.22	6.2	.49	850–860	5.8	5.8	10	.08	.92	2.41	1.16	67
				860–870	5.4	5.6	10	.19	.81	2.37	1.10	62
				870–880	5.0	5.2	10	.30	.70	2.28	1.03	54
				880–890	4.7	4.8	10	.41	.59	2.19	.96	46
				890–900	4.9	4.8	10	.53	.47	2.19	.92	44
				900–910	5.2	5.0	10	.64	.36	2.24	.91	46
				910–920	5.4	5.3	10	.75	.25	2.30	.90	48
				920–930	5.6	5.5	10	.86	.14	2.34	.88	48
				930–940	5.9	5.8	10	.98	.02	2.41	.87	50
942	.88	6.0	.36	940–950	5.2	5.6	10	—	—	2.37	.85	48
				950–960	4.0	4.6	10	—	—	2.14	.77	35
				960–970	3.8	3.9	10	—	—	1.97	.71	28
				970–980	3.6	3.7	10	—	—	1.92	.69	26
				980–990	2.9	3.2	10	—	—	1.79	.64	20
				990–1000	2.3	2.6	10	—	—	1.61	.58	15
				1000–1010	1.7	2.0	10	—	—	1.41	.51	10
				1010–1020	.7	1.2	10	—	—	1.09	.39	5
				1020–1030	0	9.4	10	—	—	.63	.23	1
Subtotal												1,580
Pier correction												−100
TOTAL												1,480

Table 2. Differences, in percent, between measured and computed discharge for selected measurements at indicated streamflow gaging stations in South Carolina

Station number	Station name	Drainage area (mi^2)	Measurement number	Measured discharge (ft^3/s)	Three verticals		Five verticals		Seven verticals	
					Computed discharge (ft^3/s)	Difference (percent)	Computed discharge (ft^3/s)	Difference (percent)	Computed discharge (ft^3/s)	Difference (percent)
02135000	Little Pee Dee River at Galivants Ferry.	2,790	221	7,120	7,230	+1.5	6,910	−2.9	6,970	−2.1
			226	2,310	2,470	+6.9	2,260	−2.2	2,130	−7.8
			227	6,620	6,250	−5.6	6,770	+2.3	7,260	+9.7
			233	4,290	3,740	−12.8	3,940	−8.2	4,570	+6.5
			240	866	711	−17.9	927	+7.0	760	−12.2
	Average of absolute values of difference					8.9		4.5		7.7
02156500	Broad River near Carlisle	2,790	256	10,700	11,000	+2.8	10,100	−5.6	10,900	+1.9
			269	1,940	1,480	−23.7	2,370	+22.2	2,090	+ 7.7
			272	32,600	35,100	+7.7	35,000	+7.4	31,900	−2.1
			275	20,500	21,900	+6.8	21,800	+6.3	21,900	+6.8
			281	6,050	5,640	−6.8	6,250	+3.3	6,000	−.8
	Average of absolute value of difference					9.6		9.0		3.9
02169500	Congaree River at Columbia	7,850	112	18,000	20,300	+12.8	18,500	+2.8	21,400	+18.9
			125	3,160	4,060	+28.5	2,520	−20.2	1,950	−38.3
			127	12,800	14,400	+12.5	14,800	+15.6	13,000	+1.6
			132	30,100	30,100	.0	32,700	+8.6	34,400	+14.3
			142	5,220	3,280	−37.2	5,020	−3.8	6,290	+20.5
	Average of absolute values of difference					18.2		10.2		18.7
02175000	Edisto River near Givhans	2,730	240	1,650	1,830	+10.9	1,850	+12.1	1,750	+6.1
			281	10,600	11,400	+7.5	11,600	+9.4	11,000	+3.8
			315	983	1,260	+28.2	1,000	+1.7	1,050	+6.8
			324	6,500	7,200	+10.8	6,860	+5.5	6,640	+2.2
			331	3,840	4,360	+13.5	3,900	+1.6	4,200	+9.4
	Average of absolute values of difference					14.2		6.1		5.7
02197500	Savannah River near Millhaven.	8,650	288	17,100	18,100	+5.8	17,000	−.6	17,700	+3.5
			297	10,600	11,200	+5.7	10,900	+2.8	10,700	+.9
			308	21,300	26,000	+22.1	22,900	+7.5	20,600	−3.3
			314	16,100	15,200	−5.6	17,200	+6.8	15,900	+1.2
			326	8,170	7,260	−11.1	7,640	−6.5	8,530	+4.4
	Average of absolute values of difference					10.1		4.8		2.7

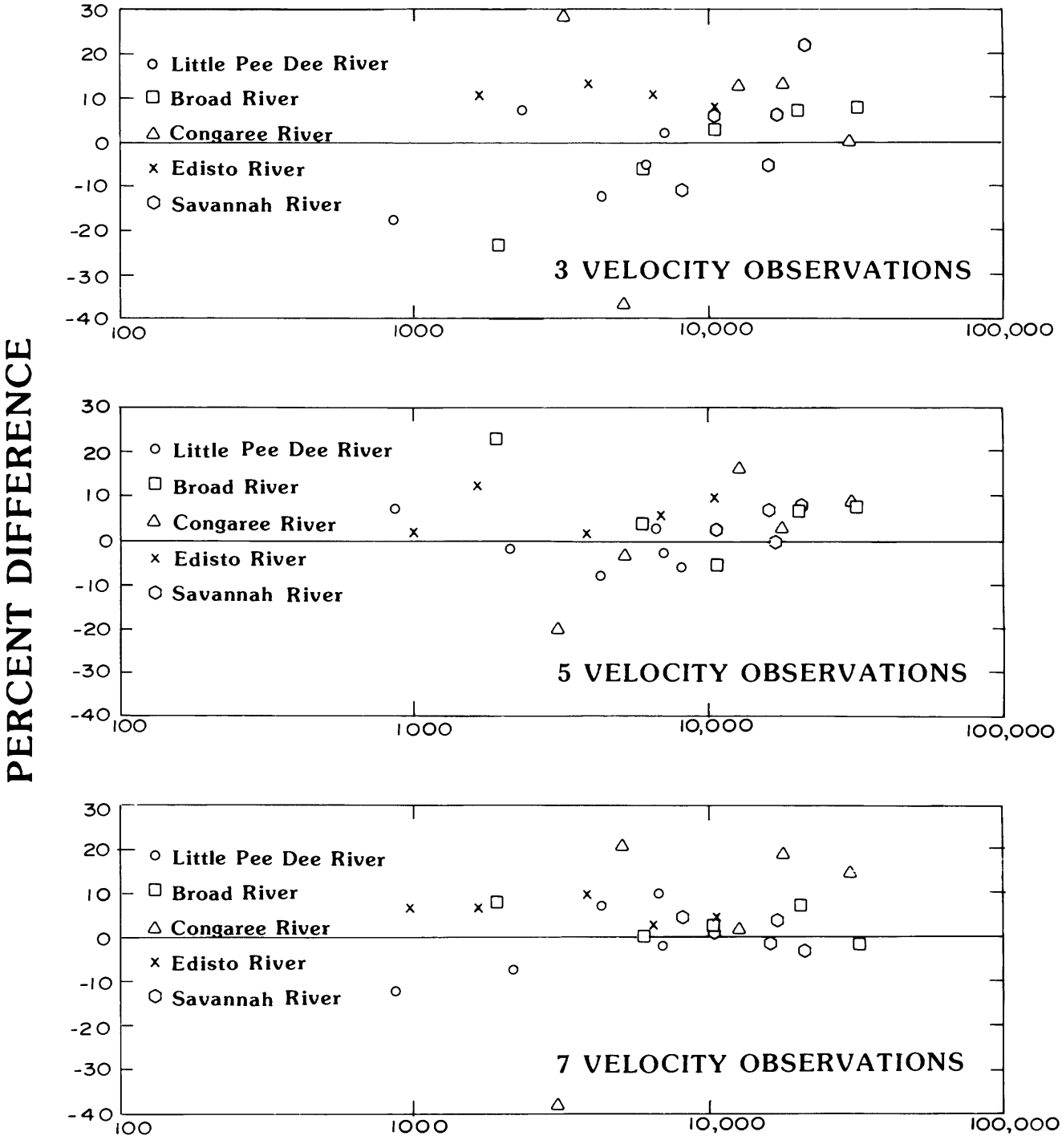

Figure 4. Measured discharge versus percent difference between the midsection and interpolation techniques for three, five, and seven velocity observations.

Table 3. Difference, in percent, root mean square error, and bias between measured and computed discharge for indicated number of verticals at streamflow gaging stations listed in table 2

	Three verticals	Five verticals	Seven verticals
Average percent difference for all stations	12.2	6.9	7.7
Average percent difference for all stations except Congaree River	10.7	6.1	5.0
Root mean square error for all stations	15.5	9.0	11.5
Root mean square error for all stations except Congaree River	13.1	7.9	6.1
Bias for all stations	+2.5	+2.9	+2.3
Bias for all stations except Congaree River	+2.3	+3.5	+2.0

near the water's edge. Because the method extrapolates velocity on a depth-dependent basis from the last velocity vertical to the bank, large errors could occur, especially if the distance was large. When the L limits imposed by the source report were disregarded, and verticals were allowed to be placed nearer the banks, the difference decreased for three out of four measurements, as illustrated in table 4.

SUGGESTIONS FOR FURTHER STUDY

The greatest benefits from application of the interpolation method are realized in wide, tide-affected rivers with uniform channel geometry. However, with additional study, this method may have potential as a discharge measurement technique for any large river where steady or unsteady flow occurs.

The most significant factors affecting the results of this study were the placement and number of the velocity observations. In this test of the interpolation technique, piers and channel geometry were disregarded; that is, the positions of the observed verticals were in no way optimized. Most of the field data used were from bridge sites with piers. Boat measurements made in uniform channel

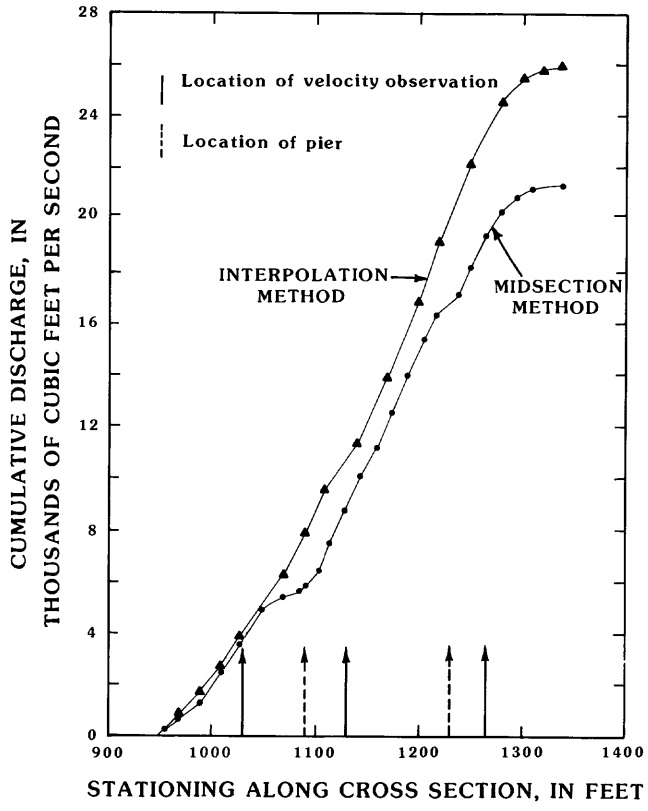

Figure 5. Cumulative discharges calculated by using the midsection method and the interpolation method with three velocity observations from measurement no. 308, Savannah River near Millhaven, S.C.

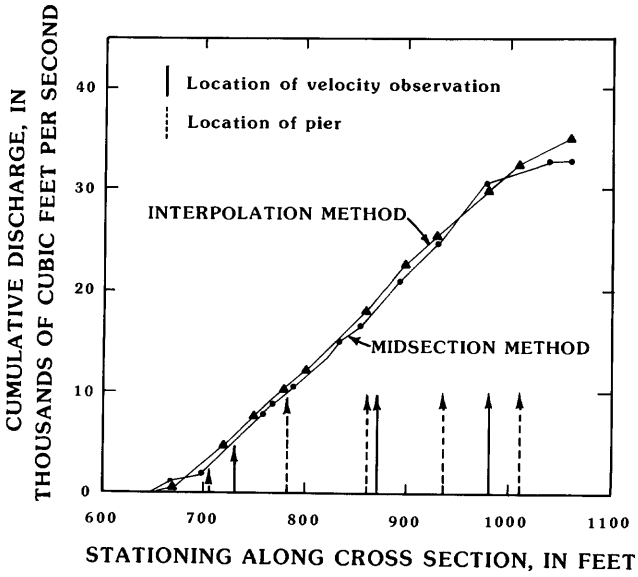

Figure 6. Cumulative discharges calculated by using the midsection method and the interpolation method with three velocity observations from measurement no. 272, Broad River near Carlisle, S.C.

Table 4. Comparison of differences, in percent, in discharge computed within and without *L* limits

Station name and measurement number	Number of verticals	Difference within *L* limits	Difference without *L* limits near banks
Broad River, no. 269	5	+22	+18
Edisto River, no. 240	5	+12	−8
Edisto River, no. 331	7	+9	0
Savannah River, no. 308	5	+8	−13

sections would probably have provided the fairest comparison of methods. Therefore, this analysis might be considered a worst case in which the hydrographer had little or no background in hydraulics. Even so, surprisingly reliable discharges were obtained in several instances, suggesting that optimum positions for the measured velocity observations could be determined, which could significantly increase the accuracy of the interpolation method.

The measurement accuracy might also be improved by varying the location of measured velocity verticals with respect to stage and discharge. The number of measured velocity verticals needed to produce reliable results is obviously a study in diminishing returns. The best number might vary from site to site or between discharges at the same site.

As previously mentioned, an improvement was demonstrated when the *L* limits specified in the source text for the allowable distances between measured verticals were ignored. The velocity at the bank could be estimated by the observer as zero or one half the velocity at the last vertical. With this modification, interpolation between the last observed vertical and the bank, rather than extrapolation from the last observed vertical, might eliminate some of the error near the banks.

SUMMARY

A study was made of an unsteady flow measurement technique being considered by the International Organization for Standardization in which a lateral velocity distribution is developed from a small number of observed velocity verticals. Results from the interpolation method were compared to the midsection method by using 25 conventional current-meter measurements as a source of data on channel geometry, depth, and mean velocity.

The bias in this analysis, about +2.5 percent, indicates that discharges computed by using the interpolation method generally were greater than those obtained by using the standard midsection method. The bias may have been a result of the computation procedure used and is not necessarily intrinsic to the interpolation technique. Differences between the techniques ranged from +28.5 to −38.3 percent and decreased as either the discharge or the number of measured vertical velocity observations increased. The greatest deviations from the midsection method occurred in those subsections close to piers, those between the bank and the first vertical velocity observation, and those that were not uniform or stable. The measurement technique may not be appropriate at discharge measurement sites where highly irregular channel bottoms or shallow depths are prevalent. A decrease in difference usually resulted by ignoring the criterion for the location of reference verticals and placing the verticals nearer to the banks.

Although the interpolation method of discharge computation was developed to facilitate measurements of unsteady flow, it has potential for application at large rivers under steady or unsteady flow conditions where the flow is uniform. Optimization of the number and location of velocity observations with respect to stage or discharge would improve accuracy.

REFERENCES CITED

Carter, R.W., and Anderson, I.E., 1963, Accuracy of current-meter measurements: American Society of Civil Engineers Journal, v. 89, no. HY4, p. 105–115.

Corbett, D.M., and others, 1943, Stream-gaging procedure—A manual for describing methods and practices of the Geological Survey: U.S. Geological Survey Water-Supply Paper 888, p. 42–43.

Rantz, S.E., and others, 1982, Measurement and computation of streamflow, Volume 1. Measurement of stage and discharge: U.S. Geological Survey Water-Supply Paper 2175, p. 80.

Young, K.B., 1950, A comparative study of mean-section and mid-section methods for computation of discharge measurements: U.S. Geological Survey Open-File Report, 52 p.

☆U.S. GOVERNMENT PRINTING OFFICE: 1986-491-405:20113